

**Model Assisted Design of Granular  
Products: Linking Product and Process  
Models for Wet Granulation**



**University of  
Sheffield**

**Peyman Mostafaei**

Department of Chemical and Biological Engineering

University of Sheffield

United Kingdom

November 2023

A thesis submitted in partial fulfilment of the requirements  
for the degree of Doctor of Philosophy

*Supervised by:* Prof. Rachel Smith and Prof. Jim Litster

## Declaration of Authenticity

This thesis contains the research carried out towards achieving the Doctor of Philosophy degree in the Department of Chemical and Biological Engineering at the University of Sheffield. The entirety of the work presented in this thesis is original and solely my own, except where explicitly referenced with proper citations. I confirm that none of the content within this work has been submitted for any other qualification or degree. Additionally, I am well informed and adhere to the University's guidelines regarding the ethical use of materials and avoidance of unfair practices ([www.sheffield.ac.uk/ssid/unfair-means](http://www.sheffield.ac.uk/ssid/unfair-means)).

Name:

---

Signature:

---

Date:

---

## Publication in preparation

- **Mostafaei, P.**, Ahmed, B., Pitt, K, Bala, N., Smith, R.M. A mechanistic model to describe the swelling of disintegrating granules
- **Mostafaei, P.**, Ahmed, B., Pitt, K, Bala, N., Smith, R.M. A mechanistic population balance model to predict the disintegration of granules

## Conference proceedings

- **Mostafaei, P.**, Bala, N., Pitt, K, Smith, R.M. A novel mechanistic model to describe the swelling of disintegrating granules. In PARTEC 2023 (Oral Presentation)
- **Mostafaei, P.**, Bala, N., Pitt, K, Smith, R.M. Model Assisted Design of Granular Products: Linking Process and Product Models for Wet Granulation. In 10th International Granulation Workshop 2023 (Poster Presentation)

## Abstract

Disintegration and dissolution are among the most observed phenomena in granular products. However, in the literature, there is a lack of mathematical mechanistic understanding of disintegrating products specifically for a type of disintegration process known as swelling which can be induced by incorporating swelling agents (also known as disintegrants) into the product formulation. Such a model, designated as a product performance model in the literature, not only would be able to predict the disintegration behaviour of granules but also would be the first and main step to optimize the granulation process based on the desired disintegrating features in the product.

It is important to note that a mechanistic product performance model for the swelling driven disintegration of granules should consider all the mechanisms involved in the process. In this study, a new mechanistic disintegration model has been developed, consisting of two linked sub-models. The first sub-model, also known as the single granule swelling model, considers all the mechanisms involved in the swelling driven disintegration, including liquid imbibition, liquid absorption, swelling and breakage for a single granule. For this model, two different scenarios were considered: The first scenario assumes the primary particles in the granule are mono-sized, while the second scenario considers the size distribution of primary particles. Both scenarios can predict important variables such as granule size and primary particle size within the granule, porosity and saturation. In order to obtain the most important variables and reduce the time for validation and the inverse problem, a global sensitivity analysis was applied to the model. The outcome showed that for both scenarios, initial porosity and diffusivity of disintegrant are the most important parameters while for the distributed scenario, the size distribution of disintegrant also plays an important role. To validate the mono-sized model, a specific type of formulation was chosen to isolate the swelling driven disintegration that focused on the disintegrant content. The validation was performed on two sets of formulation using a specially designed flow cell combined with digital optical microscopy that tracked the size of a single granule during disintegration. Through the validation, it was concluded that the concentration of binder in the solution plays an important role in slowing down the disintegration.

In the second part, a lumped based population balance model was developed based on the mono-sized sub-model developed in the first part. The population balance model considers the growth (due to swelling and also erosion from hydrodynamic forces around the granules) and breakage as the only processes in the model. As with the single granule swelling model, global sensitivity analysis was applied to obtain the most important parameters in the model. It was determined that diffusivity of disintegrant was the single most influential parameter in the model. For the validation, a technique known as focused beam reflectance technique (FBRM) combined with an inverse problem method was utilized to obtain the size distribution of disintegrating granules and the released primary particles. The results showed that the model predicts the behaviour of the disintegration for all formulations, and the degree of disintegration increases as the disintegration time increases. Finally, a series of recommendations has been suggested to increase the accuracy of the model, such as combining the model with more detailed mathematical techniques.

## Acknowledgement

First and foremost, I want to express my deepest appreciation to Professor Rachel Smith and Professor Jim Litster at the University of Sheffield's Particle technology group. Their trust in me and unwavering support over the past four years have been invaluable. I am equally grateful to the postdoctoral researchers, Dr Omid Arjmandi-Tash, Dr Bilal Ahmed, Dr Neeru Bala, Dr. Kunal Pardikar, and Dr Kate Pitt, whose guidances were instrumental throughout my PhD journey.

I extend my utmost gratitude to Dr Stefan Bellinghausen at Siemens and Process Systems Enterprise for his consistent assistance during my doctoral studies. I must also acknowledge the immense help received from Dr Oday Hosein, Mr. Sylwester Mikula, and Mr. Maciej Myszczyński at the Royce Discovery Centre, University of Sheffield, in the past year. Additionally, I am grateful to Dr Daniel Markl, Dr Mithushan Soundaranathan, and their group at the University of Strathclyde for their unwavering support and cooperation.

I would like to express my gratitude to my liaisons at IFRPI, Poul Bach from Novozymes, Michael Brozio, Christophe Grosjean from Syngenta, Sharath (Sri) Kulkarni from DFE Pharma, Joris Salari from Corbion, and Bindhu Gururajan from Novartis, whose support and guidance contributed significantly to my progress. Special thanks to Professor Paul Mort, Professor James N. Michaels and the members of IFPRI for their invaluable advice during my PhD. I am also thankful to Daniel Sieber from DFE Pharma, Vanessa Havenith from Setylose GmbH, Tristan Hessberger and Tobias Heß from Budenheim Fabrik for their kindness and support.

To my friends in the Particle Technology group, Calum, Jed, Victoria, Suruthi, Guo, Georgia, Francesca, Hamza, Faraj, Nabhan, Arun, Kai, Ruihan and Leila. Your kindness and assistance will never be forgotten. Lastly, I extend my gratitude to my friends and relatives in Iran and the United Kingdom for their support over the years, and especially, to my family for their sacrifices. My accomplishment would have happened without you, and I am profoundly grateful to have you in my life.

# Contents

<b>Abstract</b>	<b>iii</b>
<b>Acknowledgement</b>	<b>iv</b>
<b>List of Figures</b>	<b>xiii</b>
<b>List of Tables</b>	<b>xiv</b>
<b>Nomenclature</b>	<b>xv</b>
<b>List of Abbreviations</b>	<b>xxiii</b>
<b>1 Introduction</b>	<b>1</b>
1.1 Research objectives . . . . .	4
1.2 Thesis structure . . . . .	4
<b>2 Literature review</b>	<b>5</b>
2.1 Introduction . . . . .	5
2.2 Mechanisms . . . . .	7
2.2.1 Liquid Penetration (Wicking) . . . . .	9
2.2.2 Swelling . . . . .	10
2.2.3 Strain Recovery (Shape Recovery) . . . . .	12
2.2.4 Dissolution . . . . .	13
2.3 Mechanisms interfering with disintegration . . . . .	16
2.3.1 Erosion . . . . .	16
2.3.1.1 Chemically controlled erosion . . . . .	17
2.3.1.2 Physically controlled erosion . . . . .	18
2.3.2 Heat of Interaction . . . . .	19
2.4 Parameters affecting disintegration . . . . .	19
2.5 Quantifying the disintegration . . . . .	25
2.6 Mathematical Modelling . . . . .	33
2.7 Conclusion . . . . .	43
<b>3 Materials and Methods</b>	<b>44</b>
3.1 Introduction . . . . .	44
3.2 Formulations . . . . .	44

3.3	Experimental methodology . . . . .	45
3.3.1	Powder size distribution measurement . . . . .	45
3.3.2	Granulation experiments . . . . .	45
3.3.3	Sieving analysis . . . . .	46
3.3.4	Density measurement . . . . .	47
3.3.5	Porosity measurement . . . . .	48
3.3.6	Single Granule size measurement during disintegration . . . . .	49
3.3.7	Particle size distribution measurement of disintegrating granules . . . . .	51
<b>4</b>	<b>Single granule swelling model</b>	<b>54</b>
4.1	Introduction . . . . .	54
4.2	Mechanistic Model Development . . . . .	54
4.2.1	Mono-sized single granule swelling model . . . . .	57
4.2.1.1	Liquid Penetration . . . . .	60
4.2.1.1.1	Estimating the change in saturation near the surface of the granule . . . . .	62
4.2.1.2	Liquid absorbance . . . . .	65
4.2.1.3	Swelling . . . . .	67
4.2.1.4	Strength . . . . .	68
4.2.1.4.1	Solid bridges . . . . .	68
4.2.1.4.2	Liquid bridging . . . . .	69
4.2.1.4.3	van der Waals forces . . . . .	69
4.2.1.5	Stress . . . . .	70
4.2.2	Distributed single granule swelling model . . . . .	73
4.3	Global Sensitivity Analysis of the swelling models . . . . .	76
4.3.1	Global Sensitivity Analysis of the mono-sized model . . . . .	78
4.3.1.1	GSA of process parameters . . . . .	81
4.3.1.2	GSA of product parameters . . . . .	82
4.3.1.3	GSA of structural parameters . . . . .	83
4.3.2	Global sensitivity analysis of distributed model . . . . .	84
4.3.2.1	GSA of process parameters . . . . .	87
4.3.2.2	GSA of product parameters . . . . .	91
4.3.2.3	GSA of structural parameters . . . . .	92
4.4	Conclusion . . . . .	93
<b>5</b>	<b>Validation of the single granule swelling model</b>	<b>96</b>
5.1	Introduction . . . . .	96
5.2	Granulation consideration . . . . .	96
5.3	Granulation results . . . . .	97
5.4	Granule size measurement during disintegration . . . . .	98
5.4.1	DCPA granules . . . . .	102
5.4.2	MCC granules made with low binder concentration . . . . .	104
5.4.3	MCC granules made with high binder concentration . . . . .	106
5.5	Conclusion . . . . .	108

<b>6</b>	<b>Development of the population balance model</b>	<b>109</b>
6.1	Introduction . . . . .	109
6.2	Model development . . . . .	109
6.2.1	Population balance equation . . . . .	109
6.2.1.1	Aggregation . . . . .	110
6.2.1.2	Breakage . . . . .	111
6.2.1.3	Growth . . . . .	111
6.2.1.4	Nucleation . . . . .	112
6.2.1.5	Population balance equation: Lumped form . . . . .	112
6.2.2	Population balance modelling of disintegrating granules . . . . .	114
6.2.3	Population balance modelling of the released primary particles . . . . .	117
6.3	Global Sensitivity Analysis of the swelling models . . . . .	118
6.3.1	The GSA of process parameters . . . . .	119
6.3.2	The GSA of structural parameters . . . . .	120
6.4	Conclusion . . . . .	120
<b>7</b>	<b>Validation of the population balance model</b>	<b>122</b>
7.1	Introduction . . . . .	122
7.2	Model validation . . . . .	122
7.2.1	MCC granules with high concentration of HPMC in the binder . . . . .	125
7.2.2	MCC granules with low concentration of HPMC in the binder . . . . .	129
7.2.3	DCPA granules . . . . .	132
7.3	Effect of liquid to solid ratio . . . . .	136
7.4	Conclusion . . . . .	139
<b>8</b>	<b>Conclusions and Recommendations</b>	<b>140</b>
8.1	Conclusions . . . . .	140
8.2	Future works . . . . .	141
	<b>Appendices</b>	<b>159</b>
<b>A</b>	<b>Saturation distribution in a granule</b>	<b>160</b>
<b>B</b>	<b>A PBM model for the hydrodynamic erosion</b>	<b>165</b>

# List of Figures

1.1	Schematic of a typical QbD . . . . .	2
1.2	Schematic of developing the population balance-based disintegration model . . . . .	3
2.1	Drug release process schematic for a tablet (Markl & Zeitler 2017) . . . . .	7
2.2	Cohesion dependency on the molecular weight of a polymer (Myers n.d.) . . . . .	10
2.3	Mechanisms involved in disintegration (Markl & Zeitler 2017) . . . . .	11
2.4	Representation of the: (a) dissolution definition, and (b) particle dissolution in a liquid (Siepmann & Siepmann 2013) . . . . .	14
2.5	Representation of the major steps participating in the dissolution of a solid drug particle in a well-stirred liquid: (a) surface wetting, (b) interparticle solid state bonds rupture, (c) encirclement of the individualized drug units, (d) diffusion of the drug units (atoms, ions or molecules) through the stagnant liquid boundary layer surrounding the drug particle, and (e) convection in the well-stirred bulk fluid (Siepmann & Siepmann 2013) . . . . .	15
2.6	The chart to classify the disintegration mechanism based on excipients properties (Maclean et al. 2021) . . . . .	16
2.7	The polymer erosion process (Sackett & Narasimhan 2011) . . . . .	17
2.8	The parameters affecting the disintegration performance of tablets/granules (Markl & Zeitler 2017) . . . . .	20
2.9	The equipment designed by (Nogami et al. 1967, 1969) to measure the swelling and water uptake of a powder bed . . . . .	26
2.10	The equipment designed by Gissinger & Stamm (1980)(Gissinger and Stamm 1980) to measure the swelling of tablets. A: tablet, E: water penetration, C: transducer, D: recorder . . . . .	26
2.11	The system designed by (Dees 1980) to measure the water uptake, water penetration and swelling of a tablet simultaneously (Markl & Zeitler 2017) . . . . .	27
2.12	The apparatus designed by (Catellani et al. 1989) to measure the swelling force and water uptake of a tablet. A: extensimetric loading cell, B: metallic frame, D: steel cage, G: slide guide, H: steel arm, I: steel bar, L: controlling lever, R: master rack, M: lock, N: precision balance, O: glass container, P = plexiglas lid . . . . .	28
2.13	The device designed by (Bell & Peppas 1996) to measure the swelling behaviour of crosslinked microparticles under load . . . . .	29
2.14	The stub designed by (Jenkins & Donald 1997) to be used in junction with ESEM to measure the liquid penetration . . . . .	30

2.15	The high speed imaging design by (Desai et al. 2012) to measure the swelling of tablets during water penetration . . . . .	31
2.16	An schematic of the setup used by (Wilson et al. 2012) to measure the particles size distribution of disintegrating particles . . . . .	32
2.17	An schematic of the setup used by (Quodbach & Kleinebudde 2014a), utilizing parsum probe to measure the particles size distribution of disintegrating particles . . . . .	33
2.18	An schematic of TPI to study the disintegration of tablets (Markl & Zeitler 2017) . . . . .	34
2.19	An schematic used by (Lenz et al. 2021) to measure the water uptake and swelling of tablet, positioning (left), measurement (right), 1: mechanical clamp (a: open, b: closed), 2: buoyancy body, 3a: tablet holder + filter paper, 3b: tablet holder + filter paper + tablet, 4 valve (a: open, b: closed), 5: balance. . . . .	34
2.20	Presentation of wicking and swelling of fluid in a tablet. The tablet is sealed and held tightly around its circumference. (a) Dry tablet with the initial thickness $\delta_0$ , pore radius $R_{c,0}$ , the porosity $\varepsilon_0$ , and the diameter $W$ . (b) Penetration of liquid through the porous region of tablet with displacement $\Psi$ , swelling $\Delta\delta$ , and the penetration depth $L = \Psi + \Delta\delta$ . $\varepsilon$ and $R_c$ are the porosity and the pore radius of the wetted porous phase, respectively (Markl, Yassin, Wilson, Goodwin, Anderson & Zeitler 2017). . . . .	39
2.21	Overview of time characteristics of flow, absorption and deformation (Sweijen et al. 2020) . . . . .	41
3.1	The size distribution of MCC, DCPA and SSG powders . . . . .	46
3.2	A schematic of the granulator used here, 1) The blade position, 2) Power unit, 3) Binder injection position . . . . .	47
3.3	An schematic of helium pycnometry by (Yang et al. 2017) . . . . .	48
3.4	Schematic representation of the proposed flow cell with its components . . . . .	50
3.5	Schematic representation of the proposed experimental setup for measuring the size of size of an individual granule, adapted from (Soundaranathan et al. 2020) . . . . .	50
3.6	The setup used for measuring the size of granules during disintegration . . . . .	51
3.7	The GUI of the app developed for the image analysis of granules using optical microscopy . . . . .	51
3.8	The flowchart of the image analysis technique used in the developed image analysis app in MATLAB . . . . .	52
3.9	Size measurement of an individual granule using the developed software in MATLAB after (a) 0 minutes, (b) 10 minutes, (c) 15 minutes, (d) 20 minutes . . . . .	52
3.10	A schematic of the back-scattered light and the chord length in a sample hit by a FBRM laser (AutoChem 2016) . . . . .	53
4.1	The schematic of (a) a typical granule with different phases, (b) the assumed granule in this work . . . . .	55
4.2	The processes involving in the disintegration of granules, (a) original granule, (b) liquid penetration in both macro and micro level, (c) liquid absorption, (d) Swelling (and stress build-up) and (e) breakage . . . . .	57

4.3	A diagram of liquid penetration process: a) fully dry granule, b) partly saturated partly dry granule, c) granule with saturated, unsaturated and dry areas, d) partly saturated, partly unsaturated granule, e) fully saturated granule (red: disintegrant, black: excipient, blue: active ingredient) . . . . .	58
4.4	Flowchart of a population balance coupled product model for granule disintegration . . . . .	58
4.5	The calculated values of $\lim_{r_c \rightarrow 1} \frac{\partial \hat{S}}{\partial r_c}$ based on the simulation data obtained from equation (4.26) and the fitted model to those data based on equation (4.28) for $n$ equal to 3 . . . . .	64
4.6	The total effect of all factors on normalized radius in the GSA of mono-sized model . . . . .	81
4.7	The total effect of all factors on porosity in the GSA of mono-sized model . . . . .	81
4.8	The total effect of all factors on normalized porosity in the GSA of mono-sized model . . . . .	82
4.9	The total effect of all factors on stress to strength ratio in the GSA of mono-sized model . . . . .	82
4.10	The total effect of process factors on the responses in the GSA of process parameters of mono-sized model . . . . .	83
4.11	The scatter plot of average normalized radius vs mass fraction of disintegrant in the GSA of process parameters of mono-sized model . . . . .	83
4.12	The scatter plot of average porosity vs initial radius of disintegrant in the GSA of process parameters of mono-sized model . . . . .	84
4.13	The contour plot of the impact of composition and disintegrant size on strength to stress ratio in the GSA of process parameters of mono-sized model . . . . .	84
4.14	The total effect of product factors on the responses in the GSA of product parameters of mono-sized model . . . . .	85
4.15	The scatter plot of average normalized radius vs maximum absorption ratio of disintegrant in the GSA of product parameters of mono-sized model . . . . .	85
4.16	The scatter plot of porosity versus diffusivity of disintegrant in the GSA of product parameters of mono-sized model . . . . .	86
4.17	The contour plot of the impact of initial size of primary particles on strength to stress ratio in the GSA of product parameters of mono-sized model . . . . .	86
4.18	The total effect of structural parameters on the responses in the GSA of structural parameters of mono-sized model . . . . .	87
4.19	The contour plot of the impact of initial porosity and porosity difference at infinite on normalized radius in the GSA of structural parameters of mono-sized model . . . . .	87
4.20	The total effect of all factors on normalized radius in the GSA of distributed single granule swelling model . . . . .	88
4.21	The total effect of all factors on porosity in the GSA of distributed single granule swelling model . . . . .	89
4.22	The total effect of all factors on normalized porosity in the GSA of distributed single granule swelling model . . . . .	89

4.23	The total effect of all factors on stress to strength ratio in the GSA of distributed single granule swelling model . . . . .	90
4.24	The total effect of process factors on the responses in the GSA of process parameters of distributed model . . . . .	90
4.25	The contour plot of the impact of mass fraction and initial average size of disintegrant on normalized radius in the GSA of process parameters of distributed model . . . . .	91
4.26	The scatter plot of normalized radius vs standard deviation of disintegrant in the GSA of process parameters of distributed model . . . . .	91
4.27	The contour plot of stress to strength ratio vs standard deviation of primary particles in the GSA of process parameters of distributed model . . . . .	92
4.28	The total effect of product factors in the GSA of product parameters of distributed model . . . . .	92
4.29	The scatter plot of normalized radius vs diffusivity of disintegrant in the GSA of product parameters of distributed model . . . . .	93
4.30	The scatter plot of porosity vs diffusivity of disintegrant the GSA of product parameters of distributed model . . . . .	93
4.31	The scatter plot of stress to strength ratio vs diffusivity of disintegrant in the GSA of product parameters of distributed model . . . . .	94
4.32	The total effect of structural factors in the GSA of structural parameters of distributed model . . . . .	94
4.33	The scatter plot of normalized porosity vs porosity related exponent in the GSA of structural parameters of distributed model . . . . .	94
4.34	The scatter plot of stress to strength ratio vs strength related exponent in the GSA of structural parameters of distributed model . . . . .	95
5.1	The size distributions of MCC granules with low HPMC binder concentration (5 %w) with different SSG concentration: (a) 0%, (b) 2%, (c) 4%, (d) 6% . .	100
5.2	The size distributions of MCC granules with high HPMC binder concentration (12.5 %w) with different SSG concentration: (a) 0%, (b) 2%, (c) 4%, (d) 6% .	100
5.3	The size distribution of DCPA granules with different SSG and concentration and liquid to solid ratio: (a) 4% SSG and 0.27 L/S, (b) 6% SSG and 0.3 L/S	101
5.4	A diagram showing how to fit the model to the experimental data . . . . .	101
5.5	Granule size as a function of time: Effect of SSG concentration; the standard deviation for experimental results and the fitted data for DCPA based granules during swelling. Image acquisition rate was fixed at 250ms. . . . .	103
5.6	The slope of the first part of swelling data for DCPA granules . . . . .	104
5.7	The size distribution of SSG particles at the beginning and the end of disintegration for both formulations of DCPA . . . . .	104
5.8	Granule size as a function of time: Effect of SSG concentration the standard deviation for experimental results and the fitted data for MCC granules made using 5 %w HPMC binder solution during swelling. Image acquisition rate was fixed at 5s. . . . .	105
5.9	The slope of the first part of swelling data for MCC granules made using 5 %w HPMC binder solution . . . . .	106

5.10	The size distribution of SSG particles at the beginning and the end of disintegration data for MCC granules made of 5 %w HPMC binder solution . . . . .	106
5.11	Granule size as a function of time: Effect of SSG concentration the standard deviation for experimental results and the fitted data for MCC granules made using 12.5 %w HPMC binder solution during swelling. Image acquisition rate was fixed at 10s. . . . .	107
5.12	The slope of the first part of swelling data for MCC granules made using 12.5 %w HPMC binder solution . . . . .	107
5.13	The size distribution of SSG particles at the beginning and the end of disintegration data for MCC granules made of 12.5 %w HPMC binder solution . . . . .	108
6.1	The total effect of all factors on the release profile (Eq. (6.38)) in the GSA of PBM . . . . .	119
6.2	The scatter plot of the release profile (Eq. (6.38)) vs diffusivity of disintegrant in the GSA of PBM . . . . .	120
6.3	The total effect of process factors on the release profile (Eq. (6.38)) in the GSA of PBM . . . . .	120
6.4	The scatter plot of the release profile (Eq. (6.38)) vs diffusivity of disintegrant in the GSA of PBM . . . . .	121
6.5	The total effect of the structural parameters on the release profile (Eq. (6.38)) of the granules in PBM model . . . . .	121
7.1	The profile of total number of particles released during disintegration of granules for MCC granules granulated with 12.5 %w HPMC binder as a function of SSG concentration. The data are normalized for better visualization . . . . .	124
7.2	The experimental and simulation release profile (Eq. (6.38)) of MCC granules granulated with 12.5 %w HPMC binder . . . . .	125
7.3	The release inherent time vs SSG concentration and its estimation for MCC granules granulated with 12.5 %w HPMC binder using linear regression . . . . .	126
7.4	The particle size distribution of disintegrating MCC granules granulated with 12.5 %w HPMC binder at 10 minutes of disintegration . . . . .	127
7.5	$D_{50}$ value of disintegrating MCC granules granulated with 12.5 %w HPMC binder over the course of disintegration . . . . .	127
7.6	The breakage time vs SSG concentration and its estimation for MCC granules granulated with 12.5 %w HPMC binder using a linear regression model . . . . .	129
7.7	The simulated particle size distribution of MCC granules granulated with 12.5 %w HPMC binder at 10 minutes of disintegration . . . . .	129
7.8	The profile of total number of particles released during disintegration of granules for MCC granules granulated with 5 %w HPMC binder as a function of SSG concentration. The data are normalized for better visualization . . . . .	130
7.9	The experimental and simulation release profile (Eq. (6.38)) of MCC granules granulated with 5 %w HPMC binder . . . . .	131
7.10	The particle size distribution of disintegrating MCC granules granulated with 5 %w HPMC binder at 10 minutes of disintegration . . . . .	131
7.11	$D_{50}$ value of disintegrating MCC granules granulated with 5 %w HPMC binder over the course of disintegration . . . . .	132

7.12	The simulated particle size distribution of MCC granules, granulated with 5 %w HPMC binder at 10 minutes of disintegration . . . . .	133
7.13	The profile of total number of particles released during disintegration of granules for DCPA granules. The data are normalized for better visualization . .	133
7.14	The experimental and simulation release profile (Eq. (6.38)) of DCPA granules	134
7.15	The experimental and simulated particle size distribution of disintegrating DCPA granules at 1 minutes of disintegration . . . . .	134
7.16	$D_{50}$ value of disintegrating DCPA granules over the course of disintegration .	135
7.17	The profile of total number of primary particles released during disintegration of MCC granules with different liquid to solid ratio . . . . .	136
7.18	The release profile (Eq. (6.38)) of total number of primary particles released during disintegration of MCC granules with different liquid to solid ratio . . .	137
7.19	The release inherent time vs liquid to solid ratio and its estimation for MCC granules with different liquid to solid ratio . . . . .	138
7.20	The Weibull distribution related exponent vs liquid to solid ratio and its estimation for MCC granules with different liquid to solid ratio . . . . .	138
A.1	The effective saturation profile versus $r_c$ at different times ( $t_c$ ) for $n = 2$ with $\Delta t = 0.01$ and $N_p = 201$ . The computation time was less than 3s. . . . .	164
B.1	The erosion time obtained from FBRM data for each MCC granules made with different SSG loading and binder concentration and its estimation . . . . .	167

# List of Tables

2.1	List of measurement techniques and the measured properties of tablets/granules	35
2.2	Time exponents ( $n$ ) from different capillary imbibition studies (Cai & Yu 2011)	37
3.1	List of materials	45
3.2	The granulation specification for each type of formulation	46
4.1	Equations describing the swelling of individual spherical super absorbent polymers (Sweijen, van Duijn & Hassanizadeh 2017)	66
4.2	The equations needed for solving mono-sized single granule swelling model	72
4.3	The equations needed for solving the distributed single granule swelling model	75
4.4	The factors in global sensitivity analysis of mono-sized model	79
4.5	The values of non-GSA parameters	80
4.6	The list of new and redefined factors in global sensitivity analysis of distributed model	88
5.1	The estimated fitting parameters of initial size distribution of powders used in the granulation using Eq. (5.1). The fitting was obtained using the curve fitting toolbox in MATLAB.	98
5.2	The formulation of the granules and their characteristics	99
5.3	The assumed values of non-fitting parameters	102
5.4	The values of main parameters in the model for each formulation (The fitted parameters are underlined in the table)	103
7.1	The erosion related parameters for each formulation	124
7.2	The Weibull distribution related parameters for each formulation	126
7.3	The breakage time obtained from the fitting the model to release profile (Eq. (6.38)) of FBRM data	128
7.4	The erosion related parameters for MCC granules made with different liquid to solid ratio	137
7.5	The Weibull distribution related parameters for MCC granules made with different liquid to solid ratio	137

# Nomenclature

## Greek symbols

$\alpha$	Wicking related parameter	–
$\beta$	Porosity related exponent, filling angle, coagulation kernel	–, rad, 1/s
$\Delta\varepsilon_\infty$	Porosity difference at infinite	–
$\Delta E_{det}$	Particle layer detachment activation energy	J/mol
$\Delta E_{dif}$	Disintegrated particles into the solvent activation energy	J/mol
$\Delta m$	Mass of granules in sieve	g
$\delta$	Dirac delta function	–
$\eta$	Liquid viscosity	Pa · s
$\eta_w$	Water viscosity	Pa · s
$\gamma, \gamma_{lv}$	Liquid-air surface tension	Pa · m
$\gamma_{ma}$	Surface tension between mercury and air	Pa · m
$\mu$	First moment of density function	–
$\mu$	Average of the log-normal distribution	–
$\mu_{dis}$	Average of the log-normal distribution of disintegrant	–
$\mu_{exc}$	Average of the log-normal distribution of excipient	–
$\omega$	Cumulative pore size (surface) distribution	–
$\phi$	Polar angle	rad
$\psi$	selection function	1/s
$\rho_b$	Binder solution density	kg/m <sup>3</sup>
$\rho_{env}$	Envelope density	kg/m <sup>3</sup>
$\rho_l$	Liquid density	kg/m <sup>3</sup>

$\rho_s$	Skeletal density, Solid density	kg/m <sup>3</sup>
$\sigma$	Standard deviation of the log-normal distribution	—
$\sigma_0$	Residual stress	Pa
$\sigma_{abs}$	Stress produced by the liquid absorption	Pa
$\sigma_{c,0}$	Initial strength of the granule	Pa
$\sigma_c$	Strength of the granule	Pa
$\sigma_{dis}$	Standard deviation of the log-normal distribution of disintegrant	Pa
$\sigma_{exc}$	Standard deviation of the log-normal distribution of excipient	Pa
$\sigma_{sb}$	Strength of the binder (solid) bridge	Pa
$\sigma_{str}$	Internal stress of the tablet	Pa
$\sigma_{str}^{max}$	Maximum internal stress of the tablet	Pa
$\sigma_w$	Stress produced by the liquid penetration	Pa
$\tau$	Tortuosity	—
$\tau_{abs}$	Absorption time characteristic	s
$\tau_b$	Breakage time	s
$\tau_{def}$	Deformation time characteristic	s
$\tau_{flow}$	Unsaturated flow time characteristic	s
$\tau_r$	Release inherent time	s
$\tau_{sat,0}$	Initial imbibition inherent time	s
$\tau_{sat}$	Imbibition inherent time	s
$\tau_s$	Erosion time	s
$\theta$	Contact angle, azimuthal angle	rad
$\varepsilon$	Porosity	—
$\varepsilon_0$	Initial (dry) porosity	—
$\varepsilon_\infty$	Final porosity of the granule	—
$\varepsilon_{sur}$	Surface porosity	—
$\vartheta$	Stress related exponent	—
$\xi$	Variable	—

$\zeta$	Tortuosity	—
<b>Latin symbols</b>		
$\bar{C}$	Normalized cumulative cord length distribution	—
$\bar{P}_l$	Average (gauge) liquid pressure in the granule	Pa
$\bar{R}_{dis,0}$	Disintegrant initial average radius	$\mu\text{m}$
$\bar{R}_{exc,0}$	Excipient initial (average) radius	$\mu\text{m}$
$\bar{R}_{p,0}$	Initial average radius of primary particles in the granule	$\mu\text{m}$
$\bar{R}_p$	Average radius of primary particles in the granule	$\mu\text{m}$
$\bar{V}_p$	Average volume of primary particles	$\mu\text{m}^3$
$\dot{B}$	Birth rate in population balance equation	—
$\dot{B}_{0,nuc}$	Nucleation birth rate	—
$\dot{B}_{agg}$	Birth rate of aggregation in population balance equation	—
$\dot{B}_{bre}$	Birth rate of breakage in population balance equation	—
$\dot{B}_{nuc}$	Birth rate of nucleation in population balance equation	—
$\dot{D}$	Death rate in population balance equation	—
$\dot{D}_{agg}$	Death rate of aggregation in population balance equation	—
$\dot{D}_{bre}$	Death rate of breakage in population balance equation	—
$\hat{m}_{s,thr}$	Normalized threshold load ratio	—
$\hat{m}_s$	Normalized load ratio	—
$\hat{S}$	Effective saturation	—
$\hat{S}_{a,thr}$	Threshold effective saturation	—
$\hat{S}_a$	Average effective saturation in the granule	—
$\bar{M}$	Average of tracer function	—
$\mathbf{G}$	Growth rate	—
$\mathbf{G}_M$	Growth rate of tracer function	—
$\mathbf{M}$	Tracer function	—
$\mathbf{x}, \mathbf{x}', \mathbf{x}_0$	Internal coordinates in population balance equation	—
$A$	Tablet's cross section area, saturation related function	$\mu\text{m}^2, -$

$a$	Fitting parameter, slope in the decrease of capillary radius, average distance between primary particles	$-, \mu\text{m/s}, \mu\text{m}$
$b$	Absorption related constant, fitting parameter	$-$
$c$	Concentration, strength related exponent, fitting. parameter	$-$
$C_b$	Volumetric concentration of the binder	$\text{kg/m}^3$
$C_{con}$	Convective force proportionality contestant	$\text{N}$
$C_{dif}$	Diffusion force proportionality contestant	$\text{N}$
$C_L$	Mass based binder concentration	$-$
$c_s$	Solubility	$-$
$D$	Diffusivity	$\mu\text{m}^2/\text{s}$
$D_{dis}$	Diffusivity of disintegrant	$\mu\text{m}^2/\text{s}$
$d_p$	Pore size	$\mu\text{m}$
$D_s$	Mean diameter of the primary particles	$\mu\text{m}$
$D_v$	Specific diameter of volume-based size distribution	$\mu\text{m}$
$E$	Average operator	$-$
$e$	Eccentricity	$-$
$F$	Disintegration force	$\text{N}$
$f$	Ratio of the area of disintegrant particle covered by the liquid to the total surface area, density function	$-$
$F_0$	Initial disintegration force	$\text{N}$
$F_\infty$	Maximum disintegration force	$\text{N}$
$F_{bin}$	Cohesive force created by solid bridges	$\text{N}$
$F_{cap}$	Capillary force created by liquid bridges	$\text{N}$
$f_m$	Mass-based size frequency	$1/\mu\text{m}$
$f_n$	Number-based size frequency	$1/\mu\text{m}$
$F_t$	Total cohesive force	$\text{N}$
$f_v$	Volume-based size frequency	$1/\mu\text{m}$
$F_{waals}$	Van der Waals force	$\text{N}$
$G$	Swelling rate, Growth rate	$\mu\text{m/s}, -$

<i>Nomenclature</i>		xix
$G_\varepsilon$	Growth rate of porosity	1/s
$G_{n_p}$	Growth rate of primary particles in the granule	1/s
$G_{R_p}$	Growth rate of individual primary particles	$\mu\text{m}/\text{s}$
$G_R$	Growth rate of granules	$\mu\text{m}/\text{s}$
$G_R^{ere}$	Growth rate of granules due to erosion	$\mu\text{m}/\text{s}$
$G_R^{swe}$	Growth rate of granules due to swelling	$\mu\text{m}/\text{s}$
$G_{V_p}$	Growth rate of primary particles in the granule	$\mu\text{m}^3/\text{s}$
$G_{V_s}$	Growth rate of solid phase in the granule	$\mu\text{m}^3/\text{s}$
$G_V$	Volumetric growth term	$\mu\text{m}^3/\text{s}$
$h^*$	Normalized radius in liquid bridge force model	–
$H_{sol-liq}$	Hamaker constant between liquid and solid	J
$K$	Dissolution constant, number of factors in global sensitivity analysis	s, –
$k$	Disintegration force related parameter, cord length probability function, saturation related mass transfer	–
$k_0$	Constant related to Disintegration force related parameter	–
$k_{per}$	Permeability	$\text{m}^2$
$k_{rel}$	Relative permeability	–
$k_{sat}$	Fully saturated permeability	$\text{m}^2$
$k_w$	Water permeability	$\text{m}^2$
$l$	Thickness of a single surface layer of the particles, cord length	$\mu\text{m}$
$L/S$	Liquid to solid ratio	–
$L_0$	Initial length of tablet	$\mu\text{m}$
$L_\infty$	Maximum length of tablet in swelling	$\mu\text{m}$
$L_c$	Penetration depth	$\mu\text{m}$
$L_h$	Pore length	$\mu\text{m}$
$L_{se}$	End to end of pore length	$\mu\text{m}$
$M$	Brooks Corey model exponent	–
$m$	Fitting parameter	–

$m_s$	Solid mass	g
$N$	Number of uncertainty samples	—
$n$	Number based size distribution of pores, the disintegration force related exponent, penetration depth exponent, number-based size distribution	—, $1/\mu\text{m}$
$n_f$	Number-based size distribution of released primary particles	$1/\mu\text{m}$
$n_g$	Number based size distribution of granules	$1/\mu\text{m}$
$N_p$	Number of points in FVM based model	—
$n_p$	Number of primary particles in the granules	—
$N_{tot}$	Total number of particles	—
$N_{tot}^{ere}$	Total number of particles produced by erosion	—
$N_{tot}^{swe}$	Total number of particles produced by swelling	—
$P$	Pressure	Pa
$P_c$	Capillary pressure	Pa
$P_g$	Air pressure	Pa
$P_l$	(Gauge) liquid pressure in the granule	Pa
$P_l^{max}$	Maximum (gauge) liquid pressure in the granule	Pa
$Q$	Volumetric flow rate of liquid penetration	$\text{m}^3$
$q$	Liquid penetration flux	$\mu\text{m}/\text{s}$
$Q^{abs}$	Mass absorption ratio	g/g
$Q^{max}$	Maximum mass absorption ratio	g/g
$Q_{dis}^{max}$	Maximum mass absorption ratio of disintegrant	g/g
$Q_{exc}^{max}$	Maximum mass absorption ratio of excipient	g/g
$Q_{tot}^{abs}$	Total absorption ratio in the granule	g/g
$R$	Granule radius, global gas constant	$\mu\text{m}, \text{J}/\text{mol} \cdot \text{K}$
$r$	Distance from the centre of a granule, radius of primary particles (in a distribution)	—
$R'$	Granule radius	$\mu\text{m}$
$r^*$	Normalized radius in liquid bridge force model	—
$R_0$	Initial granule radius	$\mu\text{m}$

<i>Nomenclature</i>		xxi
$r_0$	Initial radius or primary particle (in a distribution)	—
$R_{c,0}$	Initial (dry) capillary radius	$\mu\text{m}$
$R_c$	Capillary radius	$\mu\text{m}$
$r_c$	Normalized distance from the centre of a granule	$\mu\text{m}$
$R_{dis,0}$	Disintegrant initial radius	$\mu\text{m}$
$R_{exc,0}$	Excipient initial radius	$\mu\text{m}$
$R_h$	Hydraulic radius	$\mu\text{m}$
$R_{min}$	Minimum granule radius	$\mu\text{m}$
$R_{p,0}$	Initial radius of primary particles	$\mu\text{m}$
$R_{p,m}$	Maximum radius of primary particles	$\mu\text{m}$
$R_p$	Radius of primary particles	$\mu\text{m}$
$r_{sb}$	Radius of neck of the bridge	$\mu\text{m}$
$S$	Saturation, Sobol indices	—
$S_0$	Initial saturation	—
$S_a$	Average saturation	—
$S_{max}$	Maximum saturation	—
$S_r$	Residual saturation	—
$S_T$	Total effect Sobol indices	—
$S_w$	Water saturation	—
$T$	Temperature	K
$t, t'$	time	s
$T_g$	Glassy temperatur	K
$U, \mathbf{U}$	Tracer variable	—
$v$	Volume expansion	$\mu\text{m}^3$
$V, V'$	Volume of the granule	$\mu\text{m}^3$
$V_0$	Original volume of the tablet or granule	$\mu\text{m}^3$
$V_1$	Recorded mercury volume at first intrusion stage of mercury porosimetry	$\mu\text{m}^3$
$V_2$	Recorded mercury volume at second intrusion stage of mercury porosimetry	$\mu\text{m}^3$

$V_b$	Volume of the binder	L
$V_l$	Volume of the liquid in the porous phase of the granule	$\mu\text{m}^3$
$V_p$	Volume of the pores in the granule, volume of primary particles	$\mu\text{m}^3$
$V_s$	Volume of the solid in the granule	$\mu\text{m}^3$
$v_s$	Swelling rate	$\mu\text{m}/\text{s}$
$W$	Cumulative size distribution	—
$w$	Mass fraction of primary particles in the granule	—
$w_{dis}$	Disintegrant mass fraction	—
$W_l$	Liquid mass in the porous phase of granules	g
$W_s$	Liquid mass in the porous phase of granules	g
$X$	Factor (in global sensitivity analysis), release profile	—
$x$	Variable, bean size	—, $\mu\text{m}$
$x_l$	Moisture content	—
$x_n$	Number fraction of primary particles in the granule	—
$Y$	Response (in global sensitivity analysis)	—
$z$	Porosity related function in tensile strength model	—

# List of Abbreviations

<b>API</b>	Active pharmaceutical ingredient
<b>BC</b>	Brooks-Corey
<b>BDF</b>	Backward differentiation formula
<b>CCPs</b>	Critical process parameters
<b>CCS</b>	Croscarmellose Sodium
<b>CLD</b>	Chord length distribution
<b>CQAs</b>	Critical quality attributes
<b>DCPA</b>	Dibasic calcium phosphate anhydrous
<b>DEM</b>	Discrete element method
<b>ESEM</b>	Environmental scanning electron microscopy
<b>FBRM</b>	Focused beam reflectance measurement
<b>FDM</b>	Finite difference method
<b>FEM</b>	Finite element method
<b>FVM</b>	Finite volume method
<b>gPROMS</b>	General process modelling system
<b>GSA</b>	Global sensitivity analysis
<b>HPMC</b>	Hydroxypropylmethyl cellulose
<b>IMPES</b>	Implicit pressure and explicit saturation scheme
<b>JEOL</b>	Japan electron optics laboratory
<b>LBM</b>	Lattice boltzmann method
<b>LW</b>	Washburn
<b>MATLAB</b>	MATrix LABoratory

<b>MCC</b>	Microcrystalline cellulose
<b>MPM</b>	Material point method
<b>MRI</b>	Magnetic resonance imaging
<b>NIR</b>	Infra-red imaging
<b>NMR</b>	Nuclear magnetic resonance
<b>ODE</b>	Ordinary differential equation
<b>PBE</b>	Population balance equation
<b>PBM</b>	Population balance modelling
<b>PEG</b>	Poly-ethylene glycol
<b>PFV</b>	Pore finite volume
<b>PGS</b>	Pre-gelatinised starch
<b>PPM</b>	Product performance modelling
<b>PSD</b>	Particle size distribution
<b>PTFE</b>	Polytetrafluoroethylene
<b>PVC</b>	Polyvinyl chloride
<b>PVM</b>	Particle vision and measurement
<b>QbD</b>	Quality by design
<b>RH</b>	Relative humidity
<b>SAPs</b>	Super-absorbent particles
<b>SFV</b>	Spatial filtering velocimetry
<b>SPHs</b>	Super porous hydrogels
<b>SSG</b>	Sodium starch glycolate
<b>TPI</b>	Terahertz pulsed imaging
<b>WLF</b>	Williams-Landel-Ferry
<b>XPVP</b>	Crospovidone

# Chapter 1

## Introduction

Particle technology is a field that delves into the individual characteristics and interactions among solid particles and powders to harness their impact in various particulate processes. This field finds widespread applications across diverse industrial sectors, including but not limited to the chemical, pharmaceutical, food, environmental and industries. Of all the processes used in powder processing, one of the most common processes is wet granulation (Litster 2016).

For many years, wet granulation was viewed as an art, and process design, scale-up and troubleshooting was achieved through extensive, exhaustive and expensive experimentation. While this remains an experimentally heavy operation, significant progress has been made in the development of process models for granulation, which are increasingly being used in industry to reduce the experimental burden and provide guidance for process design. In wet granulation processes, particle size enlargement is performed by adding a liquid binding agent onto the particles in a device like high shear or fluidised bed granulator. The forces, such as viscous or capillary, help the liquid agent bind the particles together, and more permanent bonds are typically formed by subsequent drying or sintering. Granulation is an example of particle design. Formulation parameters (liquid and powder properties) alongside the process variables (type of granulator and the operating parameters) can directly control the desired attributes of the product. Which can include inhalation and explosion risks, improved flow and handling, reduced dustiness, controlled dissolution rates, and increased bulk density. Granulated products usually retain a high degree of the surface area, a property owed to their constituent particles, which is useful for applications requiring high surface area (e.g. rapidly dissolving granules).

Two important questions when it comes to the products obtained from processes such as wet granulation are:

1. How can the product be tailored to deliver the desired the attributes?
2. What is the relationship between these attributes and process parameters?

These questions can be answered to some extent through quality by design (QbD). QbD is a systematic approach used in the pharmaceutical and biotechnology industries, as well as in other sectors such as food and chemical manufacturing, which focuses mainly on the development of products and processes with predefined quality objectives. It involves designing and controlling the quality of a product throughout its entire lifecycle, from research and

development through manufacturing to distribution. In a QbD approach, critical quality attributes (CQAs) of a product are linked to the relevant critical process parameters (CCPs). By understanding these relationships and employing scientific principles, manufacturers can create processes that consistently produce products with the desired quality attributes. The goal of QbD is to reduce variability, enhance product quality, and minimize the potential for defects, ultimately ensuring that the final product meets its intended specifications and is safe and effective (Schlindwein & Gibson 2018).

A crucial consideration when dealing with CQAs is how they can be expressed in mathematical terms, and how they can be linked to CCPs. The solution to the first question lies in the use of a product performance modelling (PPM). The PPM is a mathematical model that leverages product properties to mathematically describe the physical phenomena to which CQAs are linked to. Addressing the second question involves the creation of a mapping model. This model defines how the product parameters used as inputs in the PPM can be described in terms of post-process variables. These models find their foundation in the product's structural characteristics. Nevertheless, this aspect of research has been somewhat neglected in the literature, primarily due to several factors. These include the complexity of the phenomena that the PPM attempts to depict, a limited understanding of how post-process variables can influence the input product parameters of the PPM, and a lack of suitable experimental techniques for measuring CQAs (Markl & Zeitler 2017). Fortunately, there have been significant advances in both computational and experimental techniques over the past two decades, which have substantially alleviated these issues, leading to the recent interest in QbD in powder processing field (Zeitler et al. 2007, Coutant et al. 2010, Markl et al. 2014, Soundaranathan et al. 2023).

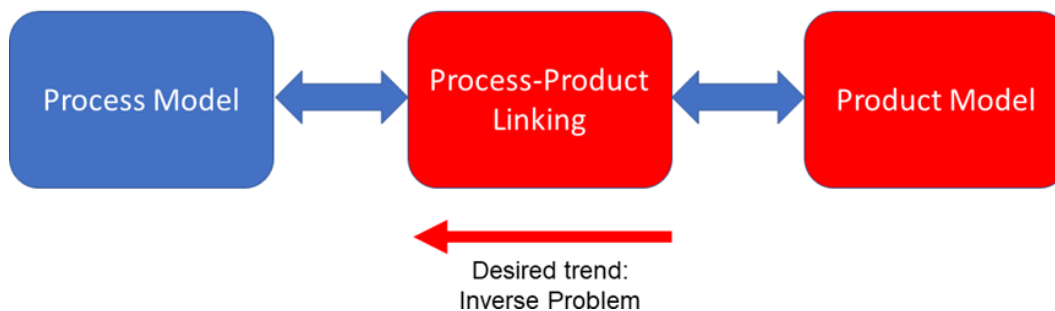


**Figure 1.1:** *Schematic of a typical QbD*

In existing literature, many product performance models are empirical in nature and are typically derived through fitting models or artificial neural networks. These models are undoubtedly valuable, but they present a significant challenge in terms of establishing a direct connection between the fitting parameters and post-process variables. This challenge arises because these parameters are essentially mathematical constructs. Resolving this issue necessitates conducting extensive experimental measurements, which, in practice, can be a time-consuming process that might even span several years. Consequently, there has been a growing interest in mechanistic product performance models (Markl, Yassin, Wilson, Goodwin, Anderson & Zeitler 2017, Soundaranathan et al. 2023). These models are rooted in physical principles, and their parameters can be measured and correlated with post-process variables. This approach has the potential to significantly reduce the time required for ex-

perimental measurements and can also predict variables, such as porosity, for which suitable experimental techniques may not be available. However, it is worth noting that there is a relative scarcity of mechanistic product performance models in the existing literature, particularly when compared to process models.

One of the most highly sought-after CQAs relates to the disintegration properties of products, and the primary reason for this is the frequent occurrence of the disintegration process during product consumption. This is particularly evident in products like tablets, where exposure to the surrounding fluid leads to the breakdown of the tablets into smaller particles. This process results in an increased surface-to-volume ratio, which, in turn, accelerates the dissolution or increases the availability of active pharmaceutical ingredient (API) contained within the granules, allowing for rapid release or bio-availability in the surrounding fluid. Without a doubt, disintegration stands out as the most crucial process in immediate release products, a category where the timely release or availability of the API into the surrounding fluid is of paramount importance.



**Figure 1.2:** *Schematic of developing the population balance-based disintegration model*

In developing these models, it is essential that:

- The outputs of the process model are suitable to act as inputs for the product model.
- There is a strategy to solve inverse problem, where the inputs of the model (CCPs) are obtained from its outputs, here CQAs in Figure 1.1. Inverse problem is mathematically an ill-posed problem where a small change in outputs can lead substantial change in inputs (Gautschi 2004).

It is clear that successfully coupled process and product models need to be developed in tandem. As a research area, the development of complementary and coupled process and product models is in its infancy, and there is no accepted best practice for process-product linking. The connection between the post-process and pre-product parameters is an extremely important element of the process. At least some of the inputs of the product model must be outputs of the process model.

A mechanistic model for granule disintegration should encompass the primary mechanisms occurring at the microscopic level and connect these to macroscopic models. The main mechanisms of disintegration and dissolution are liquid penetration, swelling of particles, in particular disintegrants, and dissolution, including polymer disentanglement as well as small molecule dissolution.

To enable better understanding, each of these processes has been separated and studied in detail. Initially, the processes have been investigated for a typical single granule leading to a model called single granule swelling model. In the next step, a multi-dimensional population balance modelling (PBM) for the disintegration of granule has been developed that includes the swelling and breakage of granules, processes that stem from the disintegration.

## 1.1 Research objectives

The primary aim of this thesis is to build the first mechanistic population balance model for the disintegration of granules where microstructural variables such as porosity or stress are described by measurable attributes such as mass absorption ratio. Conversely, some of these parameters are determined by the (post-process) characteristics of the granules. Specifically, the aim in this thesis is to:

1. Develop, implement and validate a mechanistic swelling model for the disintegration of single granules that could be generalized to tablet swelling.
2. Develop, implement and validate a complementary, mechanistic PBM based product model for swelling driven disintegration of granules.
3. Use novel experimental techniques to measure the disintegration related variables.
4. Develop a framework for future developments of product performance models.

## 1.2 Thesis structure

Chapter 2 provides a critical review of the relevant literature. Chapter 3 outlines the experimental methods and materials used in this thesis. In Chapter 4, a comprehensive explanation of the single granule swelling model is presented, and global sensitivity analysis is employed to identify crucial parameters within the model. Chapter 5 focuses on the validation of this model, utilizing a novel experimental technique. Moving on to Chapter 6, a detailed exploration of the population balance disintegration model is provided. Similar to the single granule swelling model, this chapter identifies the essential parameters of the model. In Chapter 7, the model is subjected to validation. The final chapter encompasses conclusions drawn from the research and offers recommendations for further study and practical applications.

# Chapter 2

## Literature review

### 2.1 Introduction

The primary interest of this research is in the dissolution and disintegration behaviour of granules; however, the majority of dissolution and disintegration research is for tablets and compacts. While the timescales for dissolution and disintegration may vary between granules and tablets, the fundamental mechanisms themselves are identical, and, therefore, the literature on tablet and compact disintegration and dissolution is highly relevant to granule disintegration and dissolution.

Products such as tablets and capsules are the most commonly used method of administering API to a patient orally. Depending on the physical and chemical properties of API, fluid and the materials used in these products, they can either disintegrate rapidly to release the API quickly to the body (immediate release formulations), or based on a modified release profile can take a considerable amount of time to be dissolved in the physiological fluid (modified release) (Uhrich et al. 1999). Immediate release tablets are the most widespread type of such products, they are designed in a way to fully disintegrate and dissolve when they come into contact with physiological fluids in a short period of time, typically less than 10 minutes for most tablets, and in some cases less than a minute (Fu et al. 2004). In the case of modified-release tablets, API may release in a slow, modified manner or the onset time may be delayed so that the API can be carried to the designated areas in the body. Such modification can be either achieved by putting the API into a polymer matrix with a considerable resistance to swelling or dissolution in comparison to API (Uhrich et al. 1999). A (partly) hydrophobic coating that limits the diffusion of the drug out of the tablet can also be used in modified-release tablets (Marucci et al. 2011). Even though it is common to estimate the in-vivo drug performance in the body by establishing an empirical correlations with its release profile in the lab, there are major concerns over such practices leading to an incomplete understanding of the product model (Markl & Zeitler 2017), the concerns are:

1. Explaining the underlying mass transport mechanisms is either very difficult or not possible, especially through a mathematical model.
2. The characteristic parameters of the dosage form are not related to the intrinsic dissolution rate of the drug.

3. The generality of such empirical models limits the ability to predict the effects of change to process parameters or material properties, leading to an incomplete understanding of product and process.

In many cases, the properties of the API, such as its morphology, can lead to processing limitations, for example poor flowability (Carstensen & Chan n.d.) or blending. In most cases the dosage of APIs is low in comparison to the available tablet space and appropriate materials (excipients) are added to contribute volume, or to improve processing (e.g. glidants, lubricants or surfactants) (Davies & Gloor 1972, Jivraj et al. 2000, Sohi et al. 2004, Gohel & Jogani 2005). In some cases, an excipient known as a disintegrant is added to the formulation. These hydrophilic polymers can absorb a considerable amount of fluid in a short period of time, swell and then break up the tablet/agglomerate. This break-up increases the number of smaller particles, which in turn leads to higher amount of available dissolution surface area and eventually an increase in mass transfer of the drug to its surrounding fluid. The synthetic disintegrants such as croscopovidone (XPVP), croscarmellose Sodium (CCS) and sodium starch glycolate (SSG) are commonly used in the pharmaceutical industry (Desai et al. 2016, Quodbach & Kleinebudde 2016). Given that disintegration is a must for immediate-release tablets due to its impact on dissolution rate and through that the therapeutic effect of the drug, the disintegration performance must be assessed using specifically designed disintegration tests.

Depending on the product used, the first step in a disintegration process and subsequent drug release can be either diffusion of compatible fluid into the tablet/agglomerate, or wetting. In the case of diffusion-controlled systems, the solvent diffuses deep into the product, leading to an increasing size in the material, while in for the wetting process, the solvent has to wet the surface immediately and then penetrate into the particle through the pores. In both cases, the compatibility between fluid and particle (especially polymer matrix) and pore structure of the particle are the most influential factors which without the desired drug release or particle size distribution cannot succeed (Figure 2.1).

Even though the disintegration process has a profound impact on the drug release, there is little research focused on understanding and quantifying this essential process through a mechanistic approach. This may be attributed to the complexity of the disintegration process, and difficulty in observing and measuring the process. (Markl & Zeitler 2017) identified a range of challenging problems when trying to understand and quantify the disintegration process of tablets/agglomerates mechanistically:

- i) There are many different types of disintegrating matrices with different formulations, which combined with physical and chemical properties of API, excipients and polymer matrix makes each formulation unique and hard to quantify.
- ii) In some formulations, mechanisms such as dissolution or erosion can interfere with disintegration, leading to a non-linear behaviour over time.
- iii) The process route such as compaction conditions or dry/wet granulation has a significant and complex impact on the tablet/agglomerate properties such as pore size distribution or tensile strength.
- iv) The changes in the physical properties of the excipients and their impact on the disintegration and particle size, distribution and morphology have received less study than the chemical quality and impurity profiles.

- v) Lastly, a quality by design approach may have been very costly to industry, as new developments in both theoretical and experimental areas are likely to have been required.

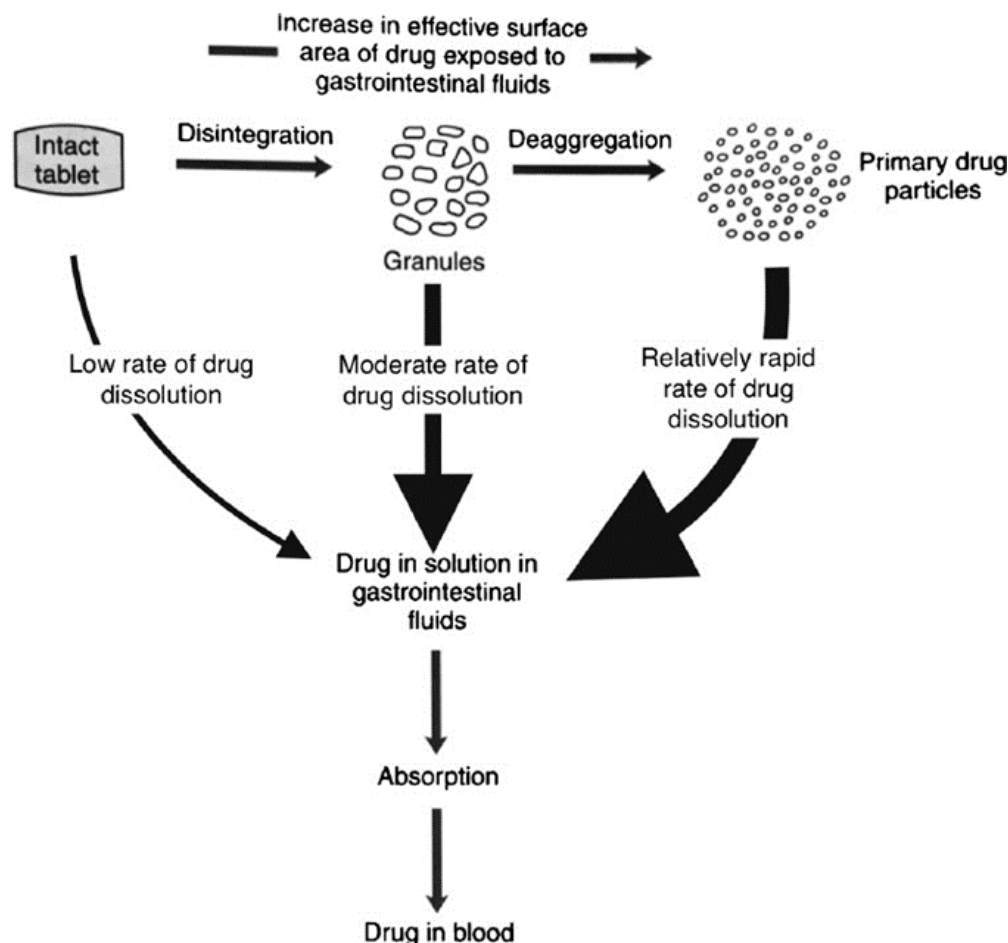


**Figure 2.1:** Drug release process schematic for a tablet (Markl & Zeitler 2017)

There is a lack of reliable characterization tests to monitor and quantify the mechanisms of the disintegration process, and little consensus in standardisation of such tests. These techniques are essential to understand the disintegration process in depth and verify models attempting to explain this process. It is also important to know the capabilities and limitations of experimental tests, and what type of data they can provide. Recent developments in the area of Terahertz Time-Domain Spectroscopy show great promise to monitor and measure real-time changes in a tablet or granule. However at the same time one should know the weaknesses of such technique in comparison to its counterparts such as nuclear magnetic resonance (NMR) (Markl et al. 2018).

## 2.2 Mechanisms

The aim in this section is to review the disintegration and dissolution mechanisms, the techniques to measure and monitor such mechanisms and available models to describe it. Dis-

integration is defined as the break-up of an agglomerate to smaller particles due to internal stress build-up. In many cases this then leads to total dissolution of tablet/agglomerate in the solvent, however there are also non-dissolving systems where the final desired outcome is a suspension. The initial source of the disintegration phenomenon is liquid (solvent) penetration inside the agglomerate, which is the result of affinity between solvent and agglomerate constituents, especially the disintegrant. According to (Nyström et al. 1993), the physical changes happening inside the agglomerate are:

- i. particle rearrangement,
- ii. agglomerate deformation,
- iii. new bonds formation,
- iv. fragmentation.

All these steps, except for particle rearrangement, play significant roles either in breaking/weakening or strengthening the agglomerate. The deformation in the agglomerate can be elastic, plastic or even viscoelastic depending on the materials and the amount of displacement in the agglomerate. Some of these mechanical/rheological behaviours can have significant impact on the drug release mechanism and polymer dissolution (Narasimhan & Peppas 1996, Grassi et al. 2000). Even though inter-particle bonding forces inside the agglomerate are being destroyed, at the same time new bonds are being created too. This will be added to the agglomerates' cohesive force, reinforced by the capillary bridge being created due to liquid capillary force. In other words, the liquid penetration works both in favour of and against the disintegration process. When these inter-particle bonds break-up to reach a limit known as the tensile strength, the agglomerate can no longer maintain its cohesion and instead, undergoes a process known as breakage or fragmentation. This process of breakage continues for smaller agglomerates created from the disintegration process, either until primary aggregates are reached, or agglomerates disappear due to processes such as dissolution. It is worth noting the smaller particles can come together to create a larger particle which is defined as an aggregate (Nichols et al. 2002). This large particle can go through a subsequent process called de-aggregation (Figure 2.1) which has a link not only to forces such as van der Waals or capillary forces but also to electrostatic forces acting and aggregate shape (Kaunisto et al. 2013).

The particles inside an agglomerate can experience different types of binding forces. The most common of them is van der Waals but depending on the constituent materials other forms of inter-molecular forces such as Hydrogen bonds can be present too. Another form of bonding force is mechanical interlocking such as twisting and hooking of constituents inside the agglomerate. Such force happens only when the compaction load is high i.e., in tablets and heavily depends on the shape and surface structure. In other words, more contact surface means higher chance of interlocking happening. For example, if the particles are rounder (close to a spherical shape), the contact level gets lower and so does the probability of mechanical interlocking while in irregular shape particles, twisting and hooking happens often more. Another form of bonding that has a considerable impact on agglomerate strength is entanglements of polymer binders. Molecular structures such as polymers can crawl into each other creating a network of entanglements, due to them having long chains with local freedom of movement. The entanglements in polymeric binders can considerably change the

agglomerate strength, especially if the polymer molecular weight surpasses a critical value (Li et al. 2011) or there is a high level of branching (Qiu et al. 2003). Moreover, according to (Myers n.d.) they have the ability to dissipate stress (Figure 2.2). The fourth type of bonding is known as solid bridges which are contacts at an atomic level and, therefore, act at short distances. These forces mostly happen when particles go through physical or chemical changes such as crystallization or melting. The fifth form of force is capillary force, which is the result of liquid penetration inside the agglomerate. The main cause of the capillary force is the amenable interfacial forces between the solid content and liquid, which can be intensified by smaller pores.

### 2.2.1 Liquid Penetration (Wicking)

The first step in disintegration of porous compacts and the prerequisite for other disintegration mechanisms is the liquid penetration, also known as wicking or imbibition (Nogami et al. 1969, Moreton 2008) where the water penetrates into the pores between particles that form the tablets or large granules. The rate of penetration is determined by a delicate equilibrium between capillary forces due to the wettability of particles in the porous media, viscous forces opposing it, and the disruption of bonds caused by polymer particles making contact with the liquid, thereby diminishing the penetration rate (Shi & Gardner 2000, Schoenmaker et al. 2011). (Kissa 1996) performed a series of experiment on the wicking of fibres. Based on the quantity of liquid and the manner in which the liquid contacts the fabric, wicking processes was categorized into two groups: those from an infinite liquid reservoir (such as immersion) and those from a finite, limited liquid reservoir (involving a single drop wicking into a fabric). Considering fibre-liquid interactions, each of the four wicking processes can further be classified into four categories:

1. Capillary penetration alone.
2. Simultaneous capillary penetration and imbibition by the fibres (liquid diffusion into the fibres).
3. Capillary penetration along with surfactant adsorption on fibres.
4. Simultaneous capillary penetration, imbibition by the fibres, and surfactant adsorption on fibres.

(Curlin 1955) observed that starch filled tablets did not disintegrate in hot water unlike the cold-water case even though the starch shows swelling ability in hot water by itself. He identified capillary force as the main reason behind liquid penetration of starch-based tablets. Liquid can also penetrate through a series of networks created by disintegrant (Shotton & Leonard 1972). Liquid penetration acts to weaken the tablet structure. For example, in the case of water-based liquids such as gastric fluids, water can decrease hydrogen bonds, van der Waals forces and electrostatic bonds, weakening interparticle bonds. However, wicking is the pre-requisite for processes such as shape recovery and swelling, a significant contributor to agglomerate rupture (Figure 2.3) (Curlin 1955). Based on the percolation theory proposed by (Luginbühl & Leuenberger 1994) (Luginbühl and Leuenberger 1994), at a concentration known as the percolation threshold  $C_{per}$  where the disintegrants create the percolating network, disintegration time is at its lowest point while the water uptake and intrinsic dissolution

rate are at their peaks. They added that for the case when the concentration is below the threshold,  $C_{per}$  depends on the cluster size of disintegrants.

(Khan & Rhodes 1975) examined the water-sorption characteristics of four calcium phosphate dibasic dihydrate tablets incorporating disintegrants such as starch, sodium carboxymethyl-cellulose, sodium starch glycolate, and a cation-exchange resin. Their findings revealed that disintegrants with greater water absorption capacity, specifically sodium starch glycolate and cation-exchange resin, demonstrated higher efficiency in most tablet systems. However, (Gissinger & Stamm 1980) after a thorough study on different types of disintegrants, showed that the explanation for disintegration in tablets goes beyond the mere formation of a porous capillary network. Various other factors, including water absorption capacity and swelling degree, must also be taken into consideration to comprehensively understand the disintegration process.

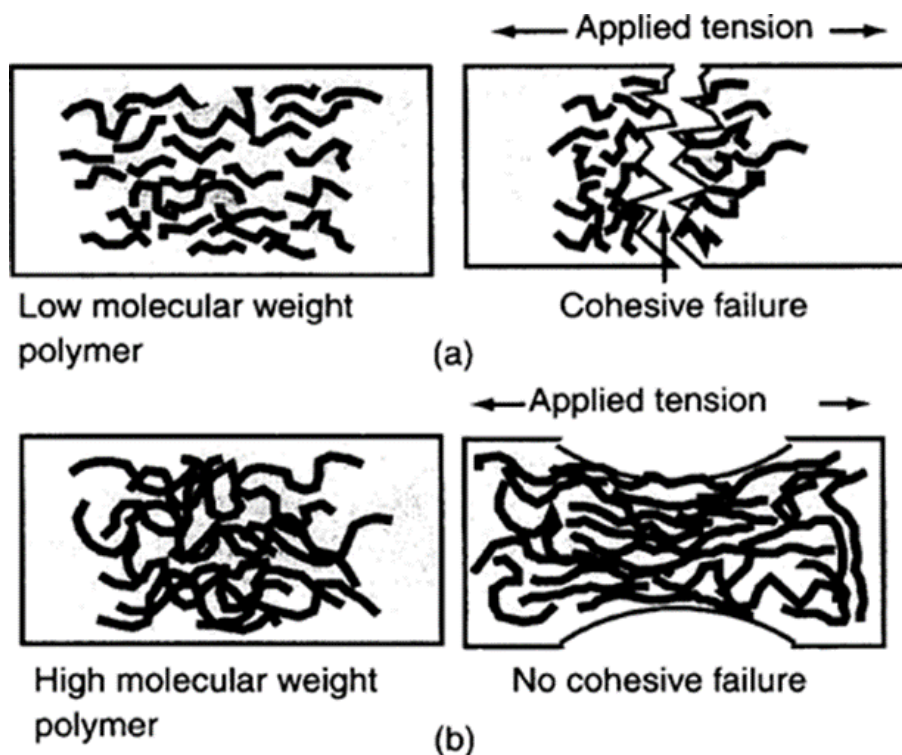
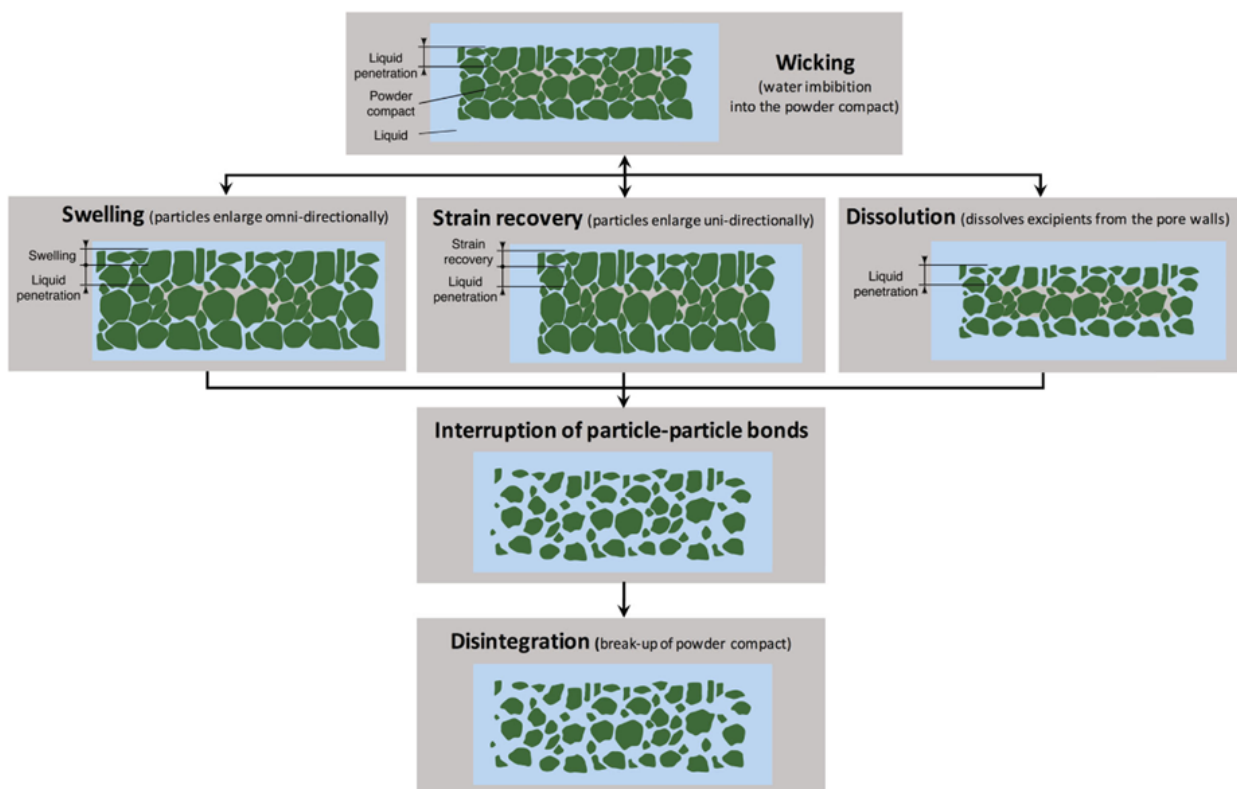


Figure 2.2: Cohesion dependency on the molecular weight of a polymer (Myers n.d.)

### 2.2.2 Swelling

Swelling is the main mechanism behind disintegration of tablets (Patel & Hopponent 1966, El-Barghouthi et al. 2008). In swelling, the polymer matrix or disintegrant within the tablet goes through a fast omni-directional expansion, creating a large deformation that is responsible for the initiation of agglomerate's break-up (Kottke & Rudnic 2002, Quodbach & Kleinebudde 2014b). The main cause of swelling is the fast expansion of disintegrants when they come into contact with the liquid. The liquid can act as a plasticizer improving chain mobility. The polymer chains entangle each other to and reach a lower energy state which causes a volume

increase. If this expansion surpasses the diameter of the pores, a force known as disintegration force acting on the agglomerate would be created. There are several factors affecting the swelling of a disintegrant, but the main ones are degree of crosslinking and chemical structure (Moreton 2008). Another major factor that can have negative effect on the swelling is the porosity (Desai et al. 2016, Bawuah et al. 2023). In a porous agglomerate, due to the existence



**Figure 2.3:** *Mechanisms involved in disintegration (Markl & Zeitler 2017)*

of pores and void spaces, the polymer chains can relax faster which hinders the swelling process, lowering the efficiency of disintegrant. This effect can be in some cases so significant as to halt the disintegration process. The disintegrants can act to resist this impact by absorbing the liquid, and decreasing the porosity, however there is a limit to this absorbance process (Diersch et al. 2010). Therefore, based on earlier discussion and the effect of porosity on liquid penetration, it can be deduced that there is an optimal porosity for a tablet to balance out the mechanical integrity and disintegration rate. As a result, the volume increase has a limited effect on disintegration time. In (List & Muazzam 1979), the effect of increase of volume and disintegration force on disintegration time was investigated. Cross-linked superdisintegrants create a considerable amount of disintegration force while showing limited volume increase. Tablets containing cross-linked superdisintegrants disintegrated faster than tablets that were filled with strongly swelling disintegrants.

(Colombo et al. 1984) suggested that the disintegrating force development rate can also affect the disintegration. They found a relationship between disintegration force and time and concluded from this that the disintegrating force development rate can affect the rapid

disintegration of a matrix. In a following study, (Peppas & Colombo 1989) showed that fluid's force alone is insufficient to disrupt the tablet structure; internal stress generated by swelling is crucial in reducing the force threshold required for the fluid to destroy the porous medium. Even though many studies point at swelling as the main mechanism behind disintegration, several observations contradict such a statement. For example, it was showed that the characteristic swelling time for some polymer disintegrants is longer than the disintegration time of tablets that use these disintegrants. Also, some polymers like crospovidone can disintegrate despite limited swelling ability (List & Muazzam 1979, Thibert & Hancock 1996). According to (Quodbach & Kleinebudde 2016) "failure of tablet disintegration, despite minimal polymer swelling, is possible because only disintegrant particles in the pore walls are initially wetted. When the disintegrant swells only little, the particle will mainly expand into the pore volume".

### 2.2.3 Strain Recovery (Shape Recovery)

Strain recovery is a special behaviour of some polymers that is observed in compact agglomerates such as tablets. If the particles are put under a considerable force, due to crystallization or interlocking of some part of polymer chains, the particles go into a metastable shape with a high energy state (Lendlein & Kelch 2002). Stimulus such as heat or contact with liquids can lead to partial recovery of polymer shape due to bond destruction, which is followed by a heat release. Due to the plasticizing effect of penetrated liquid, polymer chains become mobile, leading to an entropy recovery followed by the shape recovery of the polymer molecules. Therefore, shape recovery is seen as the reversible viscoelastic process of deformation (Patel et al. 2007). It is uni-directional and in the opposite direction of the compression force (Figure 2.3). (Erdoş & Bezegh 1977) investigated the shape recovery of potato starch tablets. They found that compressed agglomerates showed greater volume increase than uncompressed ones, which was in contrast to the findings of (Lowenthal & Burruss 1971) who observed no volume increase for corn-starch tablets. However, a thorough work on verification of strain recovery was done by (Desai et al. 2012). In their work, they investigated the disintegration mechanism of major disintegrants such as crospovidone and microcrystalline cellulose (MCC) by using high-speed video imaging for both compacted and uncompact cases. It was revealed that unlike other disintegrants, XPVP did not show any significant wicking or swelling related activity in both free and compacted states. Instead, the impact of compaction on XPVP and other disintegrants indicated that strain recovery should be the main disintegration mechanism for XPVP. In another study by (Quodbach et al. 2014), further evidence for the shape recovery mechanism of XPVP was found by comparing the expansion behaviour of different disintegrants in tablets utilizing high resolution real-time magnetic resonance imaging (MRI). They assumed that any omni-directional expansion is due to swelling while the uni-directional movements, especially those which are in the opposite direction of compression are caused by strain recovery. Their findings confirmed the work of (Desai et al. 2012) in which XPVP shows a strong uni-directional expansion, in other words shape recovery.

To further investigate the disintegration mechanism of crospovidone, (Quodbach & Kleinebudde 2014b) conducted a similar study to (Quodbach et al. 2014) and used the same premise as before for the uni-directional expansion nature of strain recovery versus omni-directional expansion nature of swelling. Two different scenarios were chosen. In the first scenario, any

expansion in both radial and axial direction of tablets was restricted during water uptake, while in the second one only the axial direction was confined. If the disintegration mechanism was swelling, then despite the axial confinement the tablets should absorb the water and expand in radial direction for the second scenario. If, however the mechanism is shape recovery then the water absorbance should be low and only a minimal expansion should be observed as the direction of compression (axial) has been restricted. They obtained the ratio of absorbed water in partial confinement to water absorbance in complete confinement for all cases and found out that for swelling disintegrants this ratio was more than four, indicating a strong water uptake from the radial direction. For the case of XPVP the ratio was less than two which shows minimal expansion in the radial direction, confirming the role of the shape recovery mechanism of XPVP.

#### 2.2.4 Dissolution

There are other processes which can affect the disintegration considerably. The most important of these are dissolution and erosion. The term dissolution is defined as the mixing of two phases with the formation of one new homogeneous phase (Figure 2.4). At the beginning, the two phases are separated by a clear boundary. As a result of mixing, the boundary starts to disappear, until the starting phases become indistinguishable. Dissolution is the mixing process of the two or more phases intensively at a molecular level, leading to the creation of a new homogeneous phase known as solution. For a polymer matrix agglomerate containing drug, one phase is the agglomerate (all the constituents from the polymer matrix to the drug and other excipients, each having either amorphous or crystalline form), and the other phase is a thermodynamically compatible liquid (which in many cases is a fluid containing water). Based on Figure 2.5, five major physical phenomenon occur during the dissolution process:

- i) Wetting process of the agglomerate surface by the solvent.
- ii) Interparticle solid state bonds, such as van-der Waals forces, hydrogen bonds, electrostatic and covalent forces, rupture in the agglomerate.
- iii) Encirclement of individualized separated units such as atoms, ions or molecules by a shell of water molecules (solvation).
- iv) The diffusion of these individualized units from the surface of the agglomerate into the well-stirred tank through an unstirred layer surrounding the agglomerate known as diffusion boundary layer. (It is important to mention that due to adhesional force, even thoroughly stirred systems have such a layer, the thickness of which is a function of the degree of agitation).
- v) The transfer of the units to the well-stirred part of the system through convection. There may be diffusion in this layer too for solvent molecules and other units thanks to thermal agitation, however because of stirring, the dominant transport process is convection.

Noting that all these processes occur sequentially. Therefore, if one of these steps is much slower than the others, the overall drug dissolution rate can be limited to the slowest mass transport step, leading to quantifying a rather complex phenomenon through a simple mathematical equation. The dissolution rate of a unit, polymer matrix, drug or any other excipient

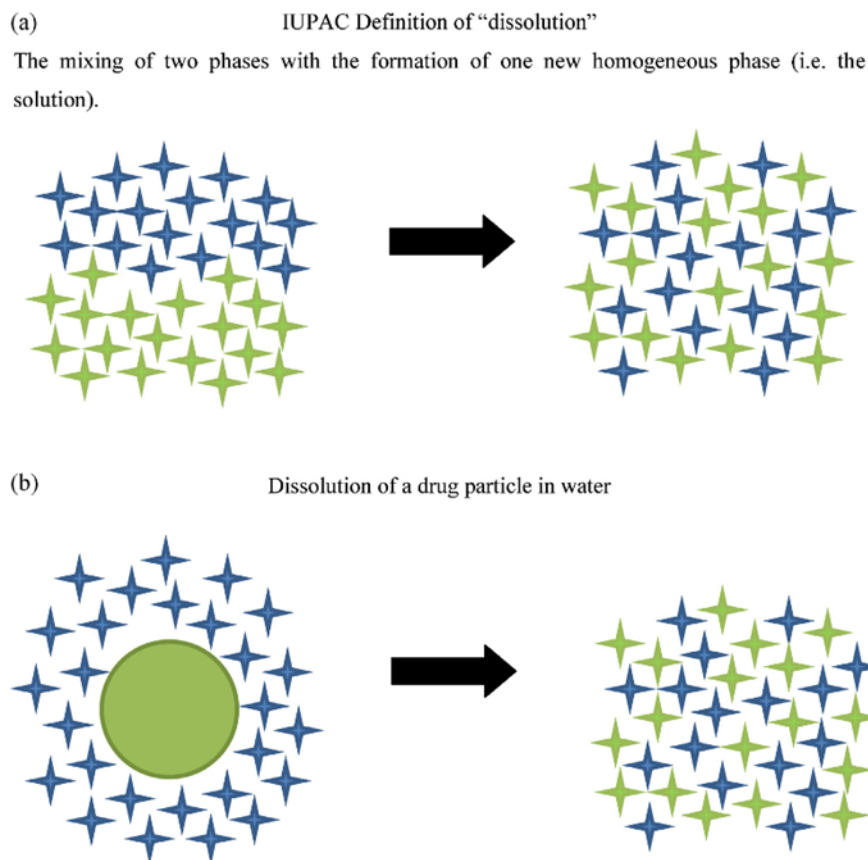


**Figure 2.4:** Representation of the: (a) dissolution definition, and (b) particle dissolution in a liquid (Siepmann & Siepmann 2013)

in a solvent is generally defined as the change of concentration with respect to time, in other words time derivative of concentration:

$$\text{drug dissolution} = \frac{\partial c}{\partial t} \approx K(c_s - c) \quad (2.1)$$

where  $c$  is the concentration (in the surrounding fluid),  $c_s$  is the solubility of the API,  $K$  is a constant and a function of geometry and intrinsic properties of tablets and  $t$  is time. The right side of equation (2.1) is known as Noyes–Whitney equation and is one of the first equation proposed to describe the dissolution rate of an API. According to Figure 2.5, the drug is initially present in the form of solid particles (mainly crystals). Immediately after the agglomerate product (tablet or granule) comes into contact with the liquid, the solvent diffuses into the agglomerate, partially dissolving the drug. Due to mass transfer caused by a concentration gradient, the dissolved drug units diffuse out of the system. As it is evidenced by equation (2.1), the solubility is the highest extent of a drug dissolution. For dissolution to become the dominant mechanism of disintegration, solubility should be high alongside the parameter  $K$  as reported by (Kwan et al. 1957, Florence & Attwood 2015, Quodbach & Kleinebudde 2016, Maclean et al. 2021). The aftermath of the dissolution of a highly soluble material would be a decrease in porosity of the tablet, leading to a significant drop in its

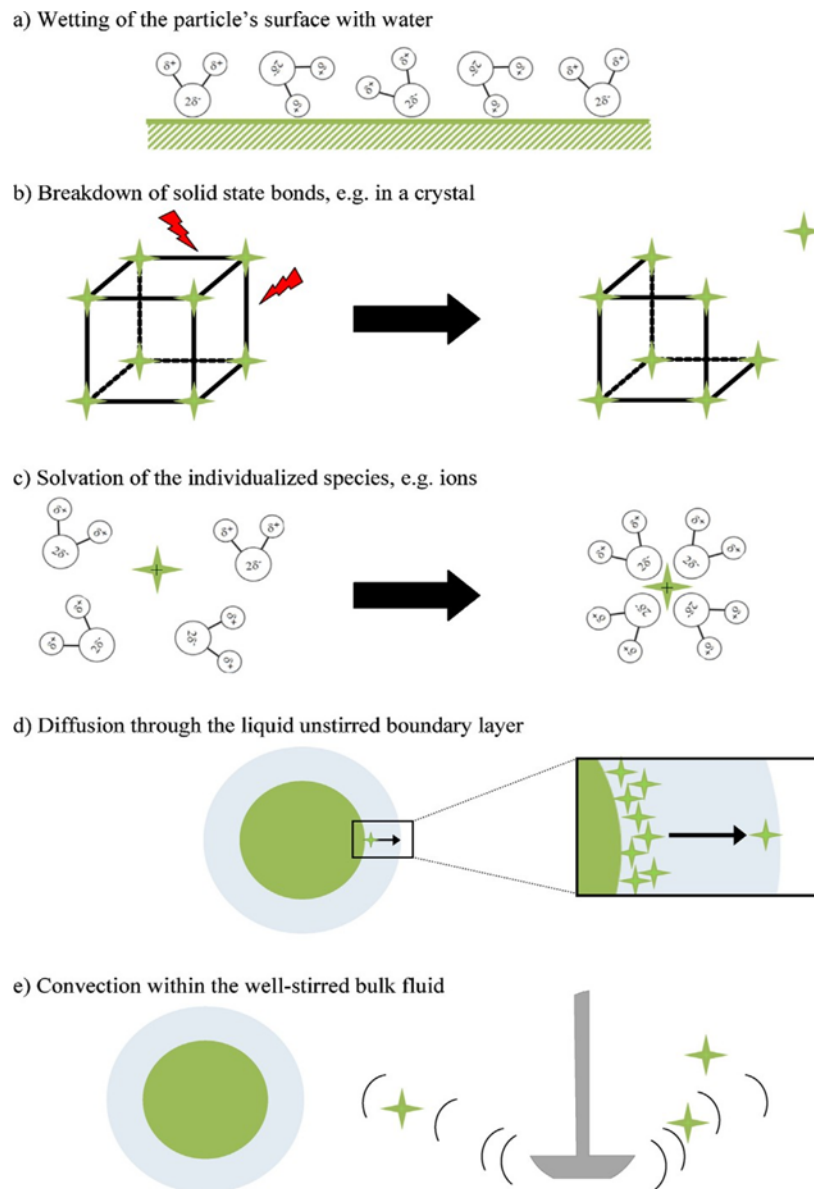


**Figure 2.5:** Representation of the major steps participating in the dissolution of a solid drug particle in a well-stirred liquid: (a) surface wetting, (b) interparticle solid state bonds rupture, (c) encirclement of the individualized drug units, (d) diffusion of the drug units (atoms, ions or molecules) through the stagnant liquid boundary layer surrounding the drug particle, and (e) convection in the well-stirred bulk fluid (Siepmann & Siepmann 2013)

structure stability, so much so that the force exerted by the fluid can disrupt the porous media and break it apart.

In a recent study, (Maclean et al. 2021) tried to determine the disintegration mechanism of a tablet based on the properties of its excipients. Tablets were produced via direct compression, the investigation used four different combinations of excipients: MCC, mannitol, lactose, and dibasic calcium phosphate anhydrous (DCPA). They found that the disinte-

gration mechanism was primarily influenced by the excipient combination. MCC/lactose tablets were identified being controlled by wettability, while for MCC/mannitol tablets the disintegration mechanism was dissolution. In both DCPA-based tablets (MCC/DCPA and lactose/DCPA), swelling dominated the disintegration. Their study led to the creation of a chart, shown in Figure 2.6 that is helpful in identifying the disintegration mechanism. The three main factors in determining the disintegration mechanisms are the component solubility, the dissolution rate of excipients and the wettability of the system. Wettability is determined by a low contact angle and high porosity.

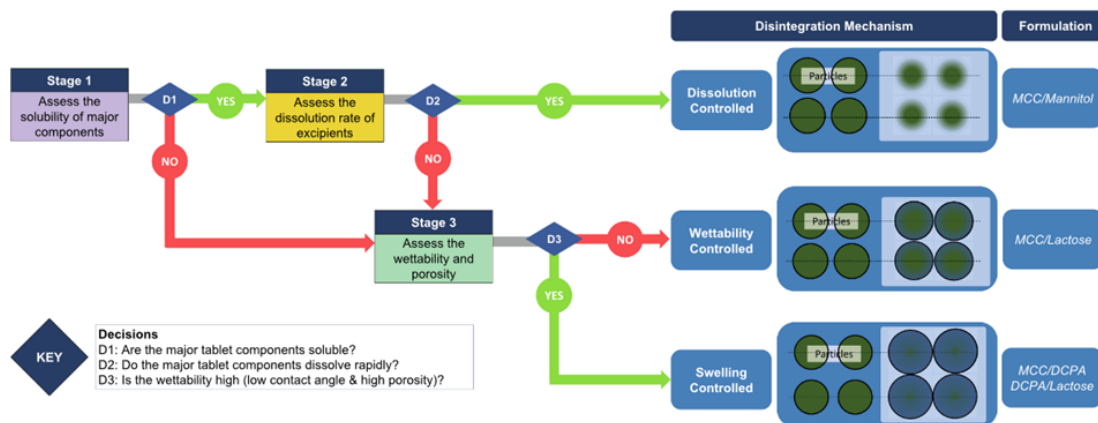


**Figure 2.6:** The chart to classify the disintegration mechanism based on excipients properties (Maclean et al. 2021)

## 2.3 Mechanisms interfering with disintegration

There are mechanisms involved in disintegration of granules; however, they are not the major contributor to the disruption of the media. In sections 2.3.1 and 2.3.2, all these mechanisms are discussed in detail.

### 2.3.1 Erosion

Another important process capable of interfering with disintegration is erosion. As its name applies, the term erosion is a process where the particle erodes due to a stimulus. There does not appear to be a universal definition of erosion. Many reported studies (Siepmann & Göpferich 2001, Kipper & Narasimhan 2005, Sackett & Narasimhan 2011) discuss a chemically oriented process where the polymer due to reactions such as hydrolysis goes through a degradation reaction. On the other hand, other studies (Rwei et al. 1991, Scurati et al. 2005) discuss a physical type of erosion caused by hydrodynamic force imposed by the liquid flow which is more like a wearing phenomenon, leading to the dispersion of particles in the liquid. Chemically controlled erosion can happen at both the surface and in the bulk, while physically controlled erosion only acts on the surface. In sections 2.3.1.1 and 2.3.1.2, chemically controlled erosion and physical controlled erosion are discussed, respectively.

### 2.3.1.1 Chemically controlled erosion

Chemical erosion of polymers has been defined as a combination of degradation, dissolution, and diffusion processes (Sackett & Narasimhan 2011) (Figure 2.6). Degradation refers to the chain scission reaction, which for the case of bio-erodible polymers such as polyesters, poly(orthoesters) or polyamides mostly happens due to hydrolysis (reaction with water). It is appeared that degradation is the main mechanism in the erosion. As polymer chain length decreases the solubility in water increases (Odian 2004) and, therefore, the smaller units (oligomers and monomers) can dissolve easier and faster than the polymer chains they were created from. In the end, the dissolved degradation products, along with released drug, will diffuse into the medium.

Figure 2.7, which is a simplified illustration of polymer erosion, does not consider many other factors affecting the erosion behaviour. For example, before degradation, the polymer must come into contact with water. Therefore, the wetting speed and wicking speed are important factors for surface erosion and bulk erosion respectively. Thus, the agglomerate depth/thickness and the polymer hydrophobicity alongside porosity and pore size distribution can affect the degradation through wetting/wicking. The molecular structure can also play a huge part in erosion behaviour too. For example, many bio-degradable polymers are based on co-polymers that show phase separation behaviour which can make some parts of the polymer chains more accessible to water (Shen et al. 2001, 2002). Even after contact with

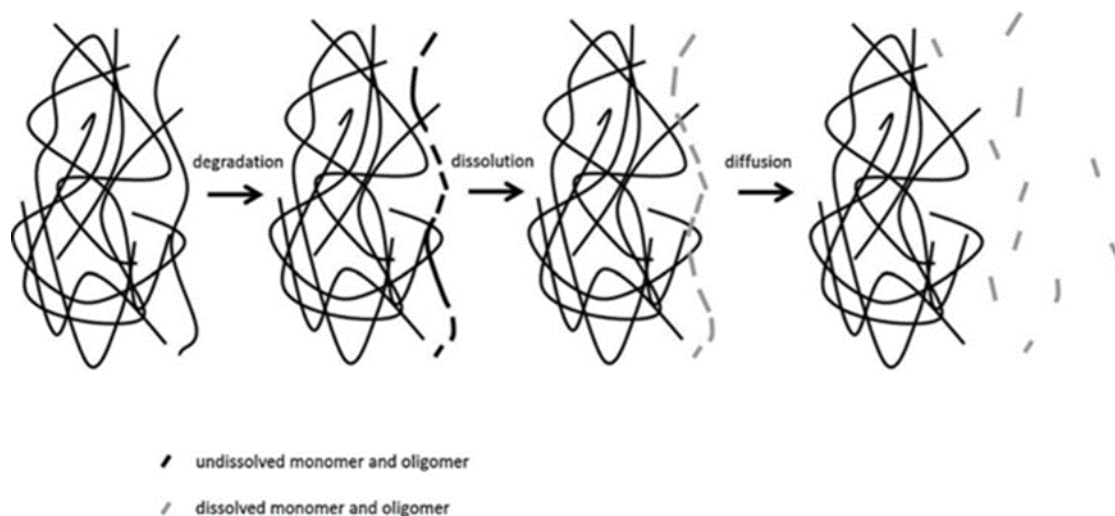


**Figure 2.7:** *The polymer erosion process (Sackett & Narasimhan 2011)*

water, the polymer bonds may not be destroyed at the same time because different monomers have different hydrolysis rates in a co-polymer (Larobina et al. 2002). Additionally, the breaking rate has a strong dependence on the physical state of the polymer. In semi-crystalline polymers, the bonds in amorphous phase break faster than crystalline phase due to the higher chance of water diffusion and subsequent contact. In some cases, the products can affect the hydrolysis. For example, the reaction can increase in some cases where acidic monomer (polyesters or poly(orthoesters)) are produced (Antheunis et al. 2009, 2010). Most bio-erodible polymers are poly-dispersed, meaning the molecular weight distribution of the

products are a function of time. In addition, the bond scission rates can change along the polymer chains, making hydrolysis more complex. The dissolution and diffusion too can change due to interference of chain length as parameters such as molecular weight, pH and temperature can affect both solubility and diffusivity in polymers. In any case, it is evident that erosion consists of a series of processes occurring at different scales simultaneously. The chemical erosion behaviour can be controlled by at least one of these mechanisms in one stage of the process, and the controlling phenomenon may change through the erosion process. In this work, the modelling of this type of erosion would not be discussed as it is not in the interest of this thesis.

### 2.3.1.2 Physically controlled erosion

Unlike chemical erosion, which depends on the polymer chemical structure, the physical erosion can happen in almost any system as long as there is a shear between the particle and the surrounding liquid. In systems with dry agglomerates it has been observed by some researchers (Rwei et al. 1990, 1991, Scurati et al. 2005) that the hydrodynamic forces created by the viscous flow around the agglomerates can lead to phenomenon like erosion (wearing) or even fragmentation, causing dispersion. In erosion, small particles tend to gradually detach from the surface of agglomerates while in the case of fragmentation (rupture), a small number of large particles close to the size of original agglomerate are created due to large hydrodynamic forces on the agglomerate. These shear and normal forces act against the cohesive forces that bind the particles inside the agglomerate together while affecting and being affected by other processes, such as wetting or imbibition at the same time (Scurati et al. 2005). Many factors can change the dispersion behaviour of agglomerates; however, they are mainly categorized as following:

1. Agglomerate properties which in itself is divided to three categories:
  - i) Material properties, such as structure
  - ii) Mechanical properties such as tensile strength (cohesivity) or relation time (spectrum)
  - iii) Overall properties such as particle size distribution or particle shape
2. Liquid properties (e.g viscosity)
3. Hydrodynamic properties, such as the type of flow or flow regime
4. Field properties such as geometry.

Unlike the aerodynamic dispersion, the viscous forces cannot be neglected due to the high viscosity of liquids in comparison to gases. It was found out that a variable dubbed the fragmentation number ( $Fa$ ) (Hansen & Ottino 1996, Ottino et al. 1999) can give an indication to the type of process, i.e. erosion or rupture. The Fragmentation number is defined as the ratio of hydrodynamic stress to cohesivity. For low fragmentation numbers, the stress on agglomerates are too low and therefore an erosion-like behaviour is seen, while for the high values of  $Fa$ , the hydrodynamic stresses are comparable to cohesivity of agglomerate, leading to the its rupture (Rwei et al. 1990, 1991, Scurati et al. 2005). However, other variables such as agglomerate size play an important role in the fragmentation number, which can lead us

to a wide range of behaviours from complete erosion to only rupture. For example, for larger agglomerates the cohesivity is lowered, and rupture is more likely to occur. Particles created from rupture will subsequently go through the same conditions, but due to their different properties they may show different behaviours than their parent particles.

### 2.3.2 Heat of Interaction

When the primary particles comes into contact with liquids such as water, some bonds such as hydrogen bonds can break leading to an energy release in the tablet and an increase in the temperature (Lowenthal 1972). This rise in temperature can expand the air, leading to localized stress in the tablet, helping the disintegration of tablets. It is worth mentioning that this process cannot be the dominant mechanism in the disintegration as the amount of heat generation is not to the extent that it could majorly expand the air and disrupt the structure of the porous media (List & Muazzam 1979). (Lowenthal 1972) argued that if heat generation was a significant mechanism for tablet disintegration, then during compaction and ejection breakage would have occurred, as substantial heat is generated during the compression. (Caramella, Ferrari, Ubaldo, Gazzaniga, LaManna & Colombo 1989) noted that the increase in temperature of the surrounding fluid did not necessarily improve the disintegration process in certain formulations of tablets. Additionally, some disintegrants exhibit endothermic properties (List & Muazzam 1979). Hence, it is imperative to investigate the heat of interaction mechanism thoroughly to determine its extent of influence and assess whether a model could be formulated to elucidate its role in the tablet disintegration process. To this day, no existing literature and research have concluded the heat of interaction as the main mechanism in disintegration.

## 2.4 Parameters affecting disintegration

A series of parameters can affect disintegration efficiency of a tablet which are divided into six different groups:

1. Processing variables which itself has three categories:
  - i) Processing routes: various methods of dry or wet granulation
  - ii) Processing condition: compaction force and speed, storage condition
  - iii) Incorporation of disintegrants: intra- and/or extra-granular
2. Excipients properties: solubility, density, morphology
3. Solvent properties: viscosity, surface tension
4. Porous structure properties: porosity, pore size distribution, tortuosity
5. Solid-liquid properties: wettability (contact angle), chemical affinity (Flory-Huggins parameter)
6. Environmental conditions: temperature, pH.

A schematic of parameters affecting the disintegration is shown in Figure 2.8. As previously stated, wicking is one of the key steps involved in the disintegration process, and in most cases the rate determining step which is determined through an interplay between the cohesive forces between liquid and solid molecules and the viscous forces which acts as adhesive forces among liquid molecules and particle surfaces hindering such movements (Szymkiewicz 2012).

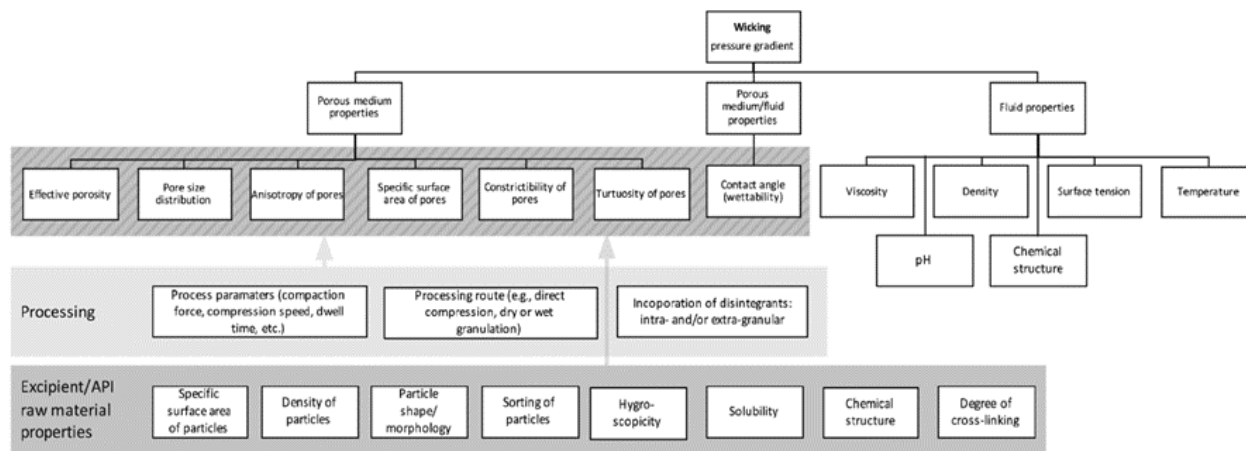


**Figure 2.8:** *The parameters affecting the disintegration performance of tablets/granules (Markl & Zeitler 2017)*

Pore structure plays an important role in liquid penetration and is divided into four main categories: non-porous, micro-porous, macro-porous and super porous. According to (Ganji et al. 2010), the pores is non-porous if its size is in scale of macro-molecular correlation length, between 10 and 100 Å. The polymer chains are densely packed, limiting the movement in the matrix which makes the free volume the only viable option for diffusion into or out of system. The pore size of micro-porous structures is between 100 and 1000 Å (Ganji et al. 2010), and because the pore size are approaching the size of polymer chains and other excipients, the transport mechanism may also include convection alongside diffusion in the solvent filled pores. Macro-porous structures have large pores, usually between 0.1 and 1 µm making the transport mechanism more reliant on convection than diffusion. In 1999, super porous hydrogels (SPHs) were introduced as a new type of water-absorbent polymer systems (Chen et al. 1999, Omidian et al. 2005). The pore size in such system is usually in the scale of several hundred micrometres. Through the connection of most pores inside SPHs, an open channel system would be created acting as a capillary system leading to a rapid wicking into the porous structure reaching the equilibrium state in a matter of a minute (Dorkoosh et al. 2002).

As has been stated repeatedly in the literature, in immediate release tablets, capillary action is the force behind the liquid penetration process (Curlin 1955, Kissa 1996). The easiest way to calculate the wicking and at the same time determine the involved variables is by combining the Hagen-Poiseuille and Young-Laplace equations. In Hagen-Poiseuille equation, the pressure drop is obtained for an incompressible and Newtonian fluid within the laminar flow regime, flowing through a long straight cylindrical pipe of constant cross section

using equation (2.2):

$$\Delta P = \frac{8\eta L_h Q}{\pi R_h^4} \quad (2.2)$$

where  $\Delta P$  is the pressure difference,  $L_h$  is the length,  $\eta$  is the liquid viscosity,  $Q$  is the volumetric flow rate, and  $R_h$  is the hydrodynamic radius. The Young-Laplace equation is obtained from thermodynamic due to surface tension between gas (air), liquid and solid (particles inside the agglomerate) causing a capillary pressure difference which leads to flow of the liquids through narrow walls as described in Eq. (2.3):

$$\Delta P_c = \frac{2\gamma \cos(\theta)}{R_c} \quad (2.3)$$

Here,  $\Delta P_c$  is capillary pressure,  $\theta$  is the contact angle,  $\gamma$  is the surface tension, and  $R_c$  is the capillary radius, different from the hydrodynamic radius. By putting the pressure difference caused by the capillary effect in the left side of Hagen-Poiseuille equation and taking into account factors such as tortuosity  $\tau$  and pore size distribution, the liquid flux through the tablet can be obtained using Eq. (2.4):

$$q = \frac{\pi\gamma \cos(\theta)}{4\eta\tau A} \sum_i \frac{n_i R_{h,i}^4}{R_{c,i} L_{se,i}} \quad (2.4)$$

in which  $n_i$  is the number of pores with hydrodynamic radius  $R_{h,i}$ , the capillary radius  $R_{c,i}$  and  $A$  is the tablet's cross section area. Tortuosity is defined as the ratio of actual length of pore  $L_{h,i}$  to its start to end length  $L_{se,i}$  which is considered constant here. If the effect of surface porosity  $\varepsilon_{sur} (= \sum_i \pi n_i R_{h,i}^2 / A)$  is considered, then:

$$q = \frac{\gamma \cos(\theta) \varepsilon_{sur}}{4\eta\tau} \sum_i \frac{\omega_i R_{h,i}^2}{R_{c,i} L_{se,i}} \quad (2.5)$$

where  $\omega_i$  is the cumulative pore size (surface) distribution. Of all these parameters,  $\gamma$  and  $\eta$  are fluid properties,  $\theta$  which is representative of tablet wettability is a fluid-tablet property and the rest are tablet matrix properties. It has to be noted that tablet properties can be affected by the mechanism of disintegration and indirectly the fluid can affect these properties. In an unsaturated tablet, as the saturation proceeds, the ratio between viscous and capillary forces would increase lowering the wicking volumetric flux. It was reported by (Ganderton & Fraser 1970) through measuring the air permeability and liquid penetration techniques for four different types of tablets, that the capillary force remains relatively constant through the liquid penetration process as the capillary force depends on the dry undisrupted pore system, enhanced by a wettable matrix. They also stated that when a tablet undergoes disruption, there is an enhanced rate of penetration due to the reduction of viscous forces along the disrupted pore system. As the formulations in tablets are pre-determined, the physical property of penetrating fluid cannot be changed and, therefore, the tablet structure can be modified for the specific application.

As it can be seen in Eq. (2.5), a main factor for the wicking flux is porosity which is a representative of the pore structure. A larger porosity leads to a higher flux while a smaller value gives a lower flux. Bi et al. (1999) performed a series of experiments to relate the

tensile strength and disintegration time to control variables such as porosity and parameters representing the characteristics of formulation. They found out that porosity is a big contributor to the disintegration of the tablets. However, the force necessary for the matrix disruption in disintegration decreases with porosity, therefore, there is an optimal range for the porosity where it can induce the disintegrating force while not disrupting the wicking process (Desai et al. 2016). Porosity is a function of the formulation and process conditions such as binder concentration, the elasticity of the powders and granules, compression force and speed (Ganderton & Fraser 1970, Adolfsson & Nyström 1996, Bi et al. 1999, Ruegger & Çelick 2000, Tye et al. 2005, Gabbott et al. 2016, Arndt & Kleinebudde 2018, Arndt et al. 2018).

One of the first experimental approaches to measure air permeability of a tablet was performed by (Lowenthal & Burruss 1971). By measuring the air permeability to size of primary particles using Carman-Kozeny equation, they managed to obtain the mean pore diameter of the pores. This measurement was done for two set of experiments. At the first set, the tablets contained three different disintegrants, with four different concentration and three different compression pressure. The second experiment had four different APIs (aspirin, magnesium Oxide, magnesium trisilicate, and salicylamide), three levels of pressure, and just a disintegrant (corn starch) at the four different concentrations. They concluded that it was challenging to establish broad generalizations concerning the impact of variables on measured parameters due to the complexities and interactions involved. For instance, the effect of disintegrant concentration on mean pore diameter varied depending on the specific APIs, pressure level, and the type of disintegrant. Neither the influence on mean pore diameter nor porosity was identified as the primary mechanism of action for starch and other disintegrants in the disintegration of tablets under the experimental conditions. (Nyström et al. 1993) used a similar approach to obtain the specific surface area of pharmaceutical tablets from air permeability measurements.

However, as it is shown in equation (2.5), porosity alone cannot describe the structure of porous media and other factors such as tortuosity, pore sizes and its distribution are big factors in disintegration. In their study of the flow of Newtonian fluid in a two dimensional porous media, (Koponen et al. 1997) showed that permeabilities can be effectively explained by considering the concept of effective porosity and the precise form of the specific surface area for the definition of parameter such as tortuosity and permeability. They also modified the original form of Carman-Kozeny equation to better describe the flow of fluid in the media. (Berg 2014) though analytical study on Darcy's law showed that variables like tortuosity or constriction factor have directional dependency leading to anisotropic behaviour of the porous media. This shows that extending the method to measure liquid penetration into the powder compact is not straightforward. This challenge arises from the impact of different variables such as tortuosity, pore size and constriction factor influenced by the different mechanisms involved in disintegration, resulted in anisotropic and time dependent permeability.

Many studies hinted at uneven distribution of particles in the tablets, leading to a distribution of density in the tablet. The tablet studies of (Djemai & Sinka 2006) through  $H^1$ NMR imaging indicates that the process condition can affect the density distribution in the granule. Specifically, they showed that geometry of tableting equipment, the friction between the walls and the powders, pressing sequence and initial conditions all have a hand in the change of density in the tablet. This data was corroborated by (Ellison et al. 2008). In their study, they

investigated the impact of lubricant, magnesium stearate, on uniformity of the tablet using infra-red imaging (NIR). It was shown that density has a strong relationship with the friction between the die walls and the powders and the uniformity decreased by decreasing the lubricant level in the tablet. (Patel & Hopponent 1966) study showed that for tablets containing starch grains, disintegration is fastest when there is continuous contact between starch grains in the interparticle spaces, there is limited impact of alterations in the amount of interparticle void on tablet disintegration. However, when the grains are unevenly distributed, the disintegration time increases, and the mode of disintegration undergoes a change. (Smallenbroek et al. 1981) studied the impact of lubricant on the disintegration of tablets containing swelling agents. They found out that the disintegration time decreased as the particle size increased when the formulation was compressed without a lubricant. However, when a lubricant was used, the disintegration time decreased as the particle size of the disintegrant decreased. This was attributed to a reduction in lubricant coverage with an increase in surface area, leading to faster disintegration with finer disintegrant particles. It has been speculated that insoluble fillers have a better impact on disintegration than soluble ones (Desai et al. 2016, Markl & Zeitler 2017). A model was proposed to explain the differences in disintegration due to the impact of fillers Caramella et al. (1988), Caramella, Ferrari, Ubaldo, Gazzaniga, LaManna & Colombo (1989), Caramella, Ferrari, Bonferoni, Ronchi & Colombo (1989), Peppas & Colombo (1989) which led to the proposing of two mechanisms; one is interface-controlled, and the other is diffusion controlled. In the interface-controlled mechanism (e.g. tablets with insoluble fillers), particle detachment from the surface was the rate-controlling mechanism, whereas in diffusion-controlled (e.g. tablets with a soluble matrix), the particle diffusion out of the system is the dominant mechanism. The model established a connection between disintegration force and time through a Weibull-like distribution:

$$\frac{F}{F_{\infty}} = 1 - \exp(-kt^n) \quad (2.6)$$

where  $F$  is the disintegration force,  $t$  is time,  $k$  is an expansion rate constant,  $F_{\infty}$  is the maximum disintegration force and  $n$  is an exponent, the most important parameter in determining the characteristic of disintegration mechanism. Based on this model, for the interface-controlled mechanism,  $n$  is greater than 0.9, while for the diffusion-controlled systems, a small  $n$  was observed. Disintegrants are more effective at breaking up the tablet interfacially at the presence of an insoluble matrix leading to a more efficient disintegration process (Augsburger et al. 2013).

(Yassin, Su, Lin, Gladden & Zeitler 2015) studied the impact of excipients on uni-directional water uptake and swelling of the tablets. In their study they used hydroxypropylmethyl cellulose (HPMC), Eudragit RSPO, and lactose as the excipient. It was shown that upon contact with water, HPMC tablets undergo an initial shrinkage followed by a rapid expansion phase. Examination of the diffusion front in HPMC reveals primarily anomalous diffusion, signifying a blend of both Fickian diffusion and control from polymer disentanglement. Eudragit RSPO has been shown to maintain a stable and unaltered matrix when in contact with water. In contrast, lactose exhibits consistent swelling, particularly just before water penetrates the front face.

(Laity & Cameron 2010) used synchrotron X-ray microtomography to study the disintegration behaviour of tablets made with three different excipients, MCC, HPMC and pregelatinised starch (PGS). The results showed that HPMC and PGS tablets go through a

gel-forming phase decreasing the expansion of the tablets, while MCC tablets experience a rapid swelling phase. While the radius expansion was observed for some tablets, overall, it was negligible compared to the axial expansion (the expansion in opposite direction of compression) which was caused by the relaxation of residual compaction stress. It was shown during the disintegration, the disintegrants release air, leading to an increase in tortuosity and affecting the diffusion kinetics. As stated by (Laity & Cameron 2010), the bubble formation in the tablets alongside the X-ray resolution (Al-Raoush 2002) hinders the method to determine the pore structure.

Another important factor is the method of adding disintegrants to tablets especially in wet granulation process (Shotton & Leonard 1976). Reports indicated that the disintegrants that were incorporated in both extra-granular and intra-granular fractions had the best disintegration efficiency (Lieberman et al. 1989) while in another study, it was found out the disintegration speed was the highest for mixed extra-granular and intra-granular disintegrants in comparison to only extra- or intra-granular phases (Khattab et al. 1993). In another set of studies (Gordon et al. 1990, He et al. 2008), the effect of extra-, mixed and intra-granular phases on dissolution of poorly soluble drug was investigated. The results showed that intra-granular fraction works better in enhancing the dissolution process of such drugs while extra-granular phase provided a better dispersibility. Moreover, the effect of re-compression was studied for both extra- and intra-granular disintegrants. It was shown that for extra-granular disintegrants, the dissolution increases with re-compression. For intra-granular ones, the effect was dependent on the disintegrants. For CCS and XPVP, a decrease in dissolution was seen while the dissolution was increased in sodium starch glycolate.

The sorbed moisture is another factor that has a considerable effect on the functionality of disintegrant. Due to the ability of water to weaken or destroy hydrogen bonds, electrostatic and van der Waals bonds, and the plasticizing effect of water on polymer chains, the mobility of polymer chains increases, leading to an increased compressibility in tablets (Bele & Derle 2012). A methodical analysis on XPVP was performed using dynamic vapour sorption analysis and differential scanning calorimetry on four different powder grades with different particle size. The water uptake, water polymer interactions, and water distribution characteristics were monitored to investigate the effect of sorbed moisture. Because of the plasticizing effect, the glass transition temperature ( $T_g$ ) was reduced with increasing moisture content. No change in other monitored variables, water uptake, water distribution interaction was observed despite the difference in particle size (Saripella et al. 2014*b,a*).

The properties of disintegrants can undergo substantial changes in storage time. Different studies were conducted to investigate these changes. Based on the study by (Marshall et al. 1991), it was determined that the swelling force decreased when the disintegrant, alginic acid, was stored for a year above 30 °C and 75% relative humidity (RH). A thorough study was conducted by (Quodbach & Kleinebudde 2015) to understand the effect of RH (5-97%) and relative density of tablet on the performance of seven different disintegrants with different disintegration mechanisms. It was revealed that the water uptake, disintegration force development and disintegration time were changed significantly by RH when sodium starch glycolate was the disintegrant while other disintegrants were not affected as much by storage condition. The effect of tablet relative densities on disintegrants with swelling as the disintegration mechanism was low, while disintegrants like XPVP with shape recovery as their disintegration mechanism needed a high relative density for quick disintegration.

Solvent related factors can also have a profound impact on the disintegration of agglomerates. Even though many bio-relevant media are water related, they may differ significantly in important variables like viscosity, contact angle or surface tension to the gastric juice (Anwar et al. 2005). (Abbott et al. 1959) speculated that this is due to the influence of the thick, viscous, adhesive mucous, continually produced within the alimentary tract. This means the viscosity of medium can prevent liquid from penetrating deep in the agglomerate, slowing down the wicking process, delaying the disintegration while a lower surface tension leads up to a faster disintegration (Cooper & Brecht 1957, Abbott et al. 1959).

An important physiological related factor that could change the disintegration behaviour is pH of the fluid. The sedimentation volumes of crosslinked starch and cellulose were impacted by acidic pH, while crospovidone and pre-gelatinized starch remained unaffected (Desai et al. 2016). In another study, (Chen et al. 1997) investigated the dissolution behaviour of tablets in neutral and acidic fluid. The result showed that for tablets consisted of acetaminophen and crospovidone, there is significant change in the dissolution while for tablets consisting of acetaminophen, sucrose and CCS, the dissolution was prolonged when the tablet was exposed to the acidic media. They speculated that difference in dissolution time might be due to interaction between the ingredients. As for the environmental parameters, it was found out that some disintegrants could form a gel depending on the temperature when they come into contact with water, slowing down the liquid penetration by filling the pores (Kabiri et al. 2003, Omidian et al. 2007).

## 2.5 Quantifying the disintegration

While most techniques studying disintegration are able to describe the phenomenon, they lack the capability to quantify the disintegration by obtaining the disintegration related variables such as porosity, size or particle size distribution. This would restrict any research on modelling disintegration. One of the first techniques to measure the property of disintegration was done by (Nogami et al. 1969). In the apparatus depicted in Figure 2.9, a specific quantity of powder was compacted in a granulated glass tube with a fine silk cloth at the bottom by mechanical tapping to achieve an equilibrium depth of the bed. Subsequently, the tube and the powder bed were positioned on a moist glass filter plate, and the water intake and swelling of the powder bed were measured at room temperature.

A similar design by (Gissinger & Stamm 1980) was created to measure the swelling and water uptake of a tablet. Additionally, they measured the swelling of tablets composed solely of disintegrants while conducting water uptake measurements, employing a linear inductive transducer (Figure 2.10). To unravel the intricate interactions among various factors in disintegration, (Dees 1980) devised an apparatus capable of simultaneously determining water penetration, water uptake, and swelling (Figure 2.11). The measurement begins by removing the metal foil between the glass filter and the dry tablet sample, initiating the wetting of the tablet. The microbalance is employed to measure the amount of water absorbed by the tablet, while the inductive displacement transducer records the swelling. The equipment uses humidity sensors to determine when the upper tablet face is hit by the water. By assuming that the water moves only in axial direction throughout the tablet and that the swelling effectiveness is consistent across the entire tablet, the penetration depth is then calculated from the swelling.

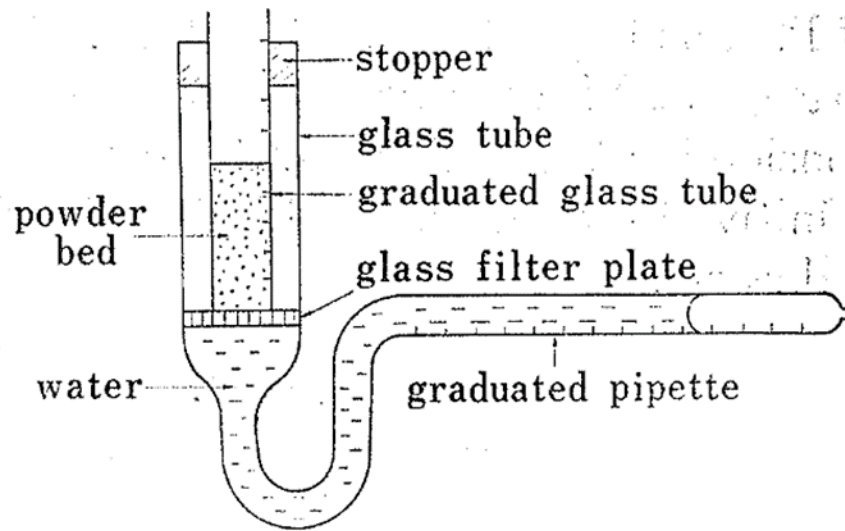


**Figure 2.9:** The equipment designed by (Nogami et al. 1967, 1969) to measure the swelling and water uptake of a powder bed

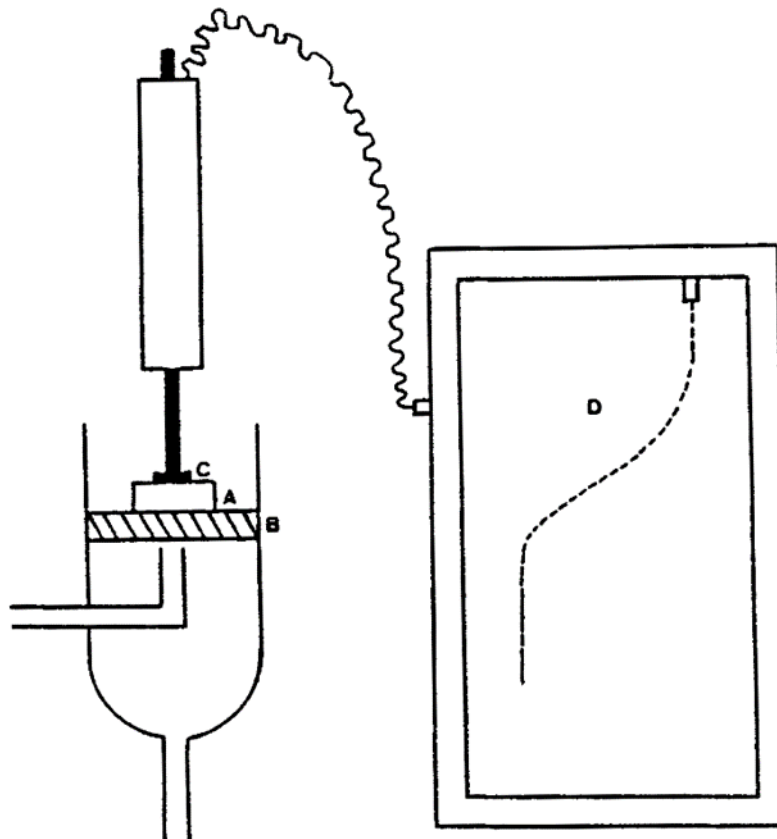


**Figure 2.10:** The equipment designed by Gissinger & Stamm (1980)(Gissinger and Stamm 1980) to measure the swelling of tablets. A: tablet, E: water penetration, C: transducer, D: recorder

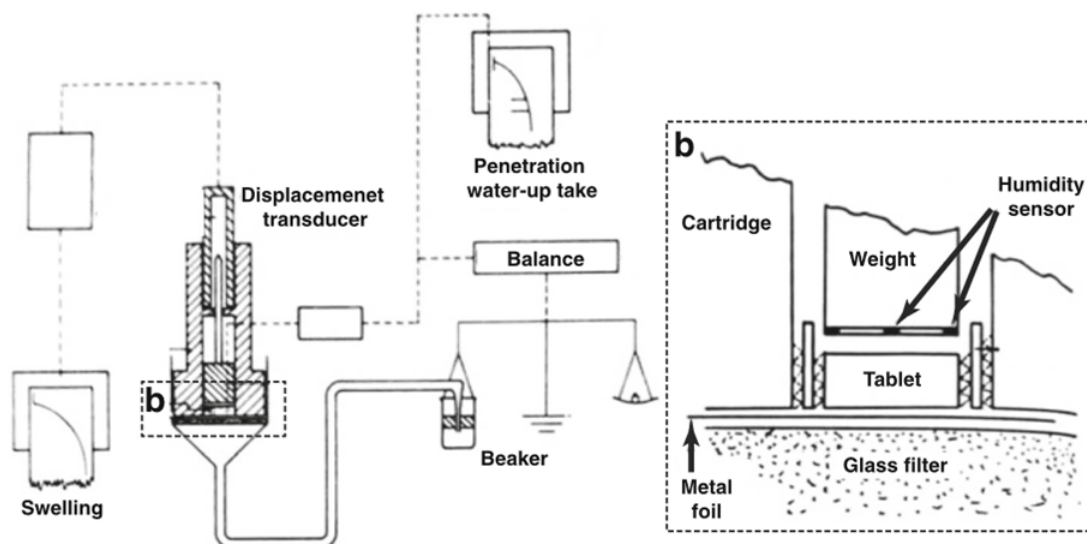


**Figure 2.11:** The system designed by (Dees 1980) to measure the water uptake, water penetration and swelling of a tablet simultaneously (Markl & Zeitler 2017)

(Rudnic et al. 1982) study was one of the first research in disintegration field which used image analysis to obtain the swelling properties of primary particles. In their study, alongside measuring the swelling and water uptake of tablets using the equipment designed by (Nogami et al. 1969). Moreover, the intrinsic swelling rates of individual particles were assessed. The methodology involved observing the wetting and swelling of particles through a microscope and capturing the event with a movie camera. Selected frames, arranged chronologically, were subsequently photo-enlarged. These enlarged photographs were then subjected to image analysis using a computer interfaced with a camera. A series of other works uses the same concept to quantify the swelling properties of primary particles (Gasmi et al. 2015, Soundaranathan et al. 2020). As it will be shown in Chapter 3 and 5, the same concept would be used for measuring the size of single granules during disintegration.

(Catellani et al. 1989) used a new device to measure the force and water uptake of the tablet simultaneously during swelling. The apparatus, shown in Figure 2.12, was an improvement of an earlier design (Colombo et al. 1984). It operates on the principle that a body submerged in a fluid experience an upward force equivalent to the weight of the displaced fluid. The measuring head, immersed at a fixed depth in a water-filled container on a precision balance, displaces a specific volume of water, and the balance indicates the weight of the water displaced. When a tablet is placed in the cage of the measuring head, the balance registers the combined weight of water displaced by both the cage and the tablet. As the tablet fastened to an external arm begins to absorb water, a reduction in weight occurs, reflecting the water absorbed by the tablet. The punch, connected to the extensimetric loading cell and pressing the tablet against the glass disk of the cage, enables the measurement of the force generated during the tablet's water absorption. Consequently, the apparatus can simultaneously gauge water uptake and the disintegration force developed by the tablet. Further studies used the same device to study the impact of medium pH and ionic content of the ingredients (Khare et al. 1992, Am Ende et al. 1995).

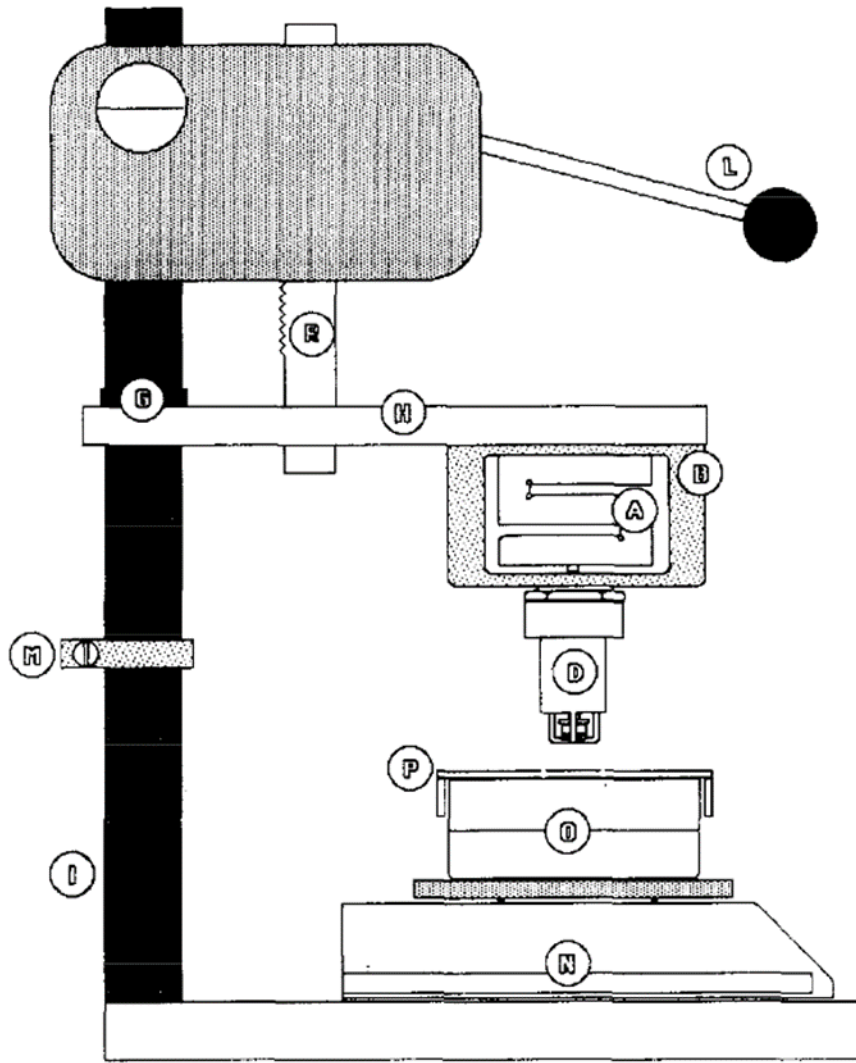


**Figure 2.12:** *The apparatus designed by (Catellani et al. 1989) to measure the swelling force and water uptake of a tablet. A: extensimetric loading cell, B: metallic frame, D: steel cage, G: slide guide, H: steel arm, I: steel bar, L: controlling lever, R: master rack, M: lock, N: precision balance, O: glass container, P = plexiglas lid*

(Bell & Peppas 1996) introduced a novel device for measuring swelling under load. In this experimental setup, microparticles were positioned on the wire mesh at the bottom of the sample holder, ensuring a uniform spread. A Teflon cover was then placed over the sample. Then the sample holder was suspended in a beaker, with the plunger of the device resting on the sample cover and a weight was added to the measuring device, as shown in Figure 2.13. Subsequently, the beaker was filled with saline solution, added through the beaker lip using a syringe. This action resulted in the immersion of the wire mesh portion of the sample in the saline solution. The swelling process commenced upon contact of the saline with the wire mesh. As the polymer microparticles swelled under the applied load, measurements of the

height on the measuring dial were recorded at various time intervals.

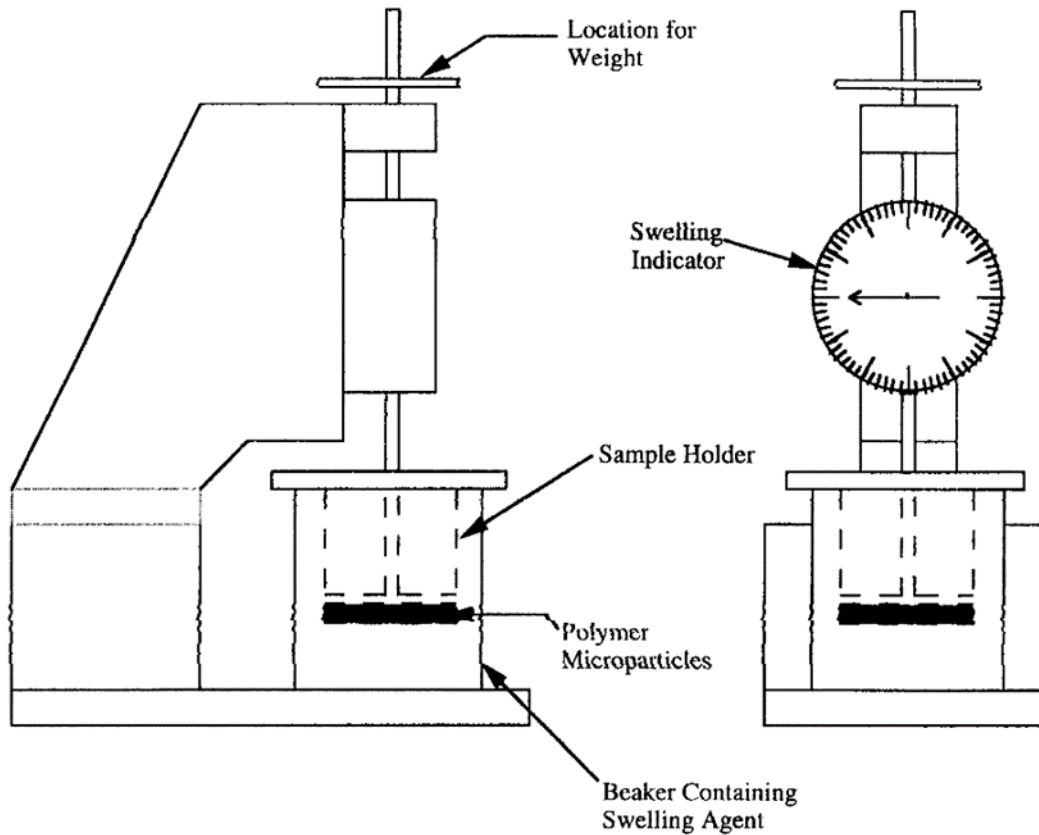


**Figure 2.13:** *The device designed by (Bell & Peppas 1996) to measure the swelling behaviour of crosslinked microparticles under load*

(Jenkins & Donald 1997) developed a new method for observing the transverse swelling of cellulosic fibres in the environmental scanning electron microscopy (ESEM). The presence of liquid water in the ESEM specimen chamber enables the in-situ observation of hydration without requiring coating, freezing, or drying of the sample. The design uses a modified stub (Figure 2.14) based on standard JEOL-style specimen stub design. In this setup, the fibre bundle is threaded multiple times through a hole in the lid of the stub. Cross-sections are exposed using a sharp scalpel, and the lid is then placed over the stub body, keeping the looped fibre lengths suspended in its hollow centre, ensures an effective thermal contact between the stub and cross sections.

(Tritt-Goc & Kowalczyk 2002) were one of the first researchers to use dynamic MRI to study the disintegration behaviour of tablets. They employed a snapshot FLASH (Fast Low Angle Shot) imaging pulse sequence MRI system ( $H^1NMR$ ). The authors estimated disintegration profiles on the basis of the MRI images for different commercial tablets containing paracetamol and for different fluid temperatures in an acidic environment. In later studies by (Tajarobi et al. 2009, Chen et al. 2010, Nott 2010, Uecker et al. 2012, Quodbach et al. 2014), advancements in MRI technology have played a pivotal role. These advancements have enabled the recording of MRI videos with a lower temporal resolution yet a higher spa-

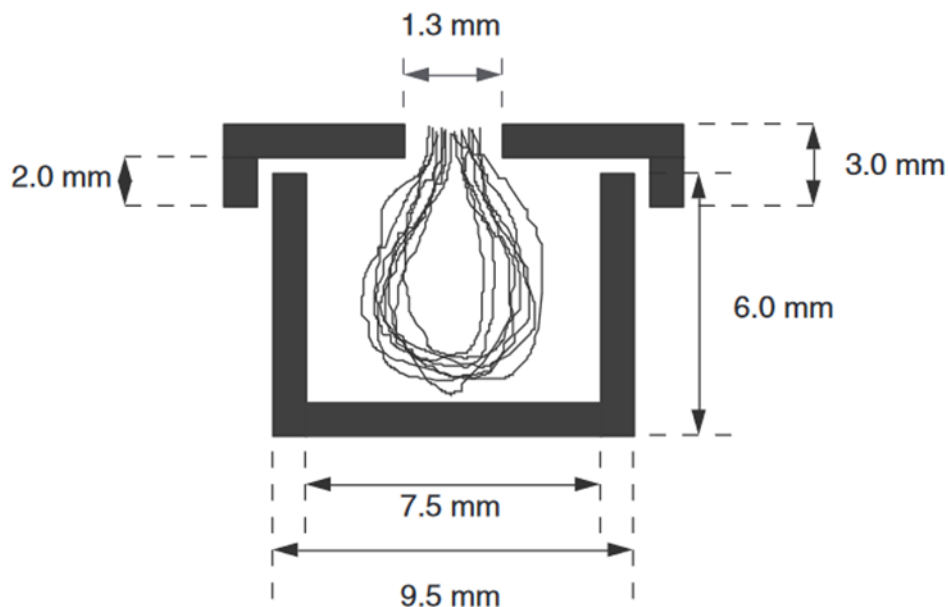


**Figure 2.14:** The stub designed by (Jenkins & Donald 1997) to be used in junction with ESEM to measure the liquid penetration

tial resolution across a more extensive cross-section of tablets. This has facilitated precise measurements of swelling and water penetration in tablets, allowing for the differentiation of disintegration mechanisms among various swelling agents.

(Akseli et al. 2009, 2013, 2017, Sultan et al. 2023) used elastic soundwaves to investigate the mechanical properties of tablets, Young's modulus and shear modulus. They established a relationship between these mechanical properties and the disintegration time of the tablets. These measurements use statistical methods and neural network to estimate the properties of the tablets. It has to be noted that statistical models lack representation of the physical properties of the powder compact, limiting the potential for gaining fundamental insights into disintegration phenomena. However, ultrasound techniques offer intriguing insights into the internal structure of tablets, serving as a potent sensor for in-die measurements during the development of the compaction process (Leskinen et al. 2010).

(Desai et al. 2012) used high speed imaging combined with optical microscopy to measure the changes in size of tablets during water penetration and effect of wetting on disintegrant particles. Figure 2.15 illustrates the experimental arrangement, including an optical microscope equipped with a high-speed video camera and a peristaltic pump. A portion of the compact was positioned on a microscope slide, covered with a cover glass, and observed under microscope. Water was introduced at the side, using the peristaltic pump, and permitted to flow through the compact, positioned between the slide and cover glass. High-speed video recording commenced upon water introduction. Finally, the recorded video was analysed from using the image analysis toolbox in MATLAB. Similar approaches use the same concept to study the swelling of tablets during disintegration (Berardi et al. 2018).

Another aspect of disintegration that has been somewhat neglected is the size distribution of particles created from the disintegration of tablets/granules. The recent advances in techniques to measure the size distribution of particles, has enabled the researchers to obtain

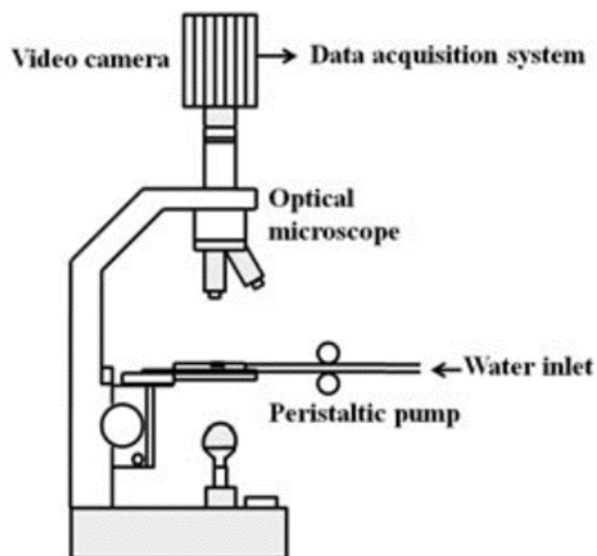


**Figure 2.15:** *The high speed imaging design by (Desai et al. 2012) to measure the swelling of tablets during water penetration*

the particle size distribution (PSD) of particles born during disintegration of tablets. One of the first attempt was by (Coutant et al. 2010). In their study, they used a technique known as focused beam reflectance measurement (FBRM) to measure the chord length distribution (CLD) of disintegrating particles. Information regarding FBRM has been given in Chapter 3 of this thesis as FBRM has been used in this work to measure the particles size distribution of disintegrating granules, the advantages and disadvantages of FBRM have also been discussed in Chapter 3. Another approach to measure PSD of disintegrating particles/granules is using image analysis. In their work, (Wilson et al. 2012) use a device known as QicPic capable of analysing not only size but also shape of the particles. This device has been used repeatedly to measure PSD of dry granules but its usage for measuring the PSD of disintegrating particles is new. A schematic of the setup is shown in Figure 2.16. The QicPic is connected to standard dissolution system via a peristaltic pump. The whole setup is a closed system where the analysed particles would return to the dissolution system. A recent study by (Cardona et al. 2018) uses the same concept to measure the particle size distribution of particles. However, in their study they use a different device known as particle vision and measurement (PVM) V819 probe.

In another study by (Quodbach & Kleinebudde 2014a), a new apparatus known as parsum probe has been used to measure the PSD of disintegrating granules. This device uses spatial filtering velocimetry (SFV). In SFV, the technique computes the chord length using two signals produced when a particle traverses the measurement zone. The first signal is generated as a particle passes through the measurement zone. Subsequently, the particle velocity is calculated based on this data. Parsum probe has found many interests in different fields of particles technology as an inline tool to measure the particle size distribution of particles (Huang et al. 2010, Dieter et al. 2011, da Silva & Taranto 2015). In the setup used to measure particle size distribution of particles (Figure 2.17), a pressurized air-driven double membrane pump was employed to propel the disintegration fluid containing the disintegrating

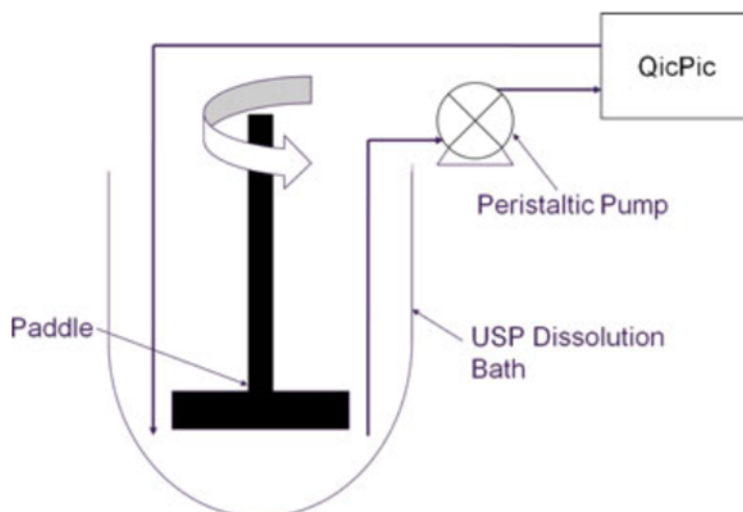


**Figure 2.16:** An schematic of the setup used by (Wilson et al. 2012) to measure the particles size distribution of disintegrating particles

particles through the measurement setup. The high-pressure side of the pump utilized a polytetrafluoroethylene (PTFE) hose, while the low-pressure side utilized a polyvinyl chloride (PVC) hose. A PVC hose was also utilized to link the filter system to the main water reservoir, ensuring proper drainage. The filter system comprised two water-filled vessels: the water from the main reservoir first drained into the initial vessel, where particles would sediment. Subsequently, the water flowed into the second vessel, from where it was drawn up by the pump.

Another novel technique to study the swelling and liquid penetration into a disintegrating tablet is terahertz pulsed imaging (TPI). In TPI (Figure 2.18), brief pulses of radiation are directed at tablet containing excipients that exhibit transparency to terahertz radiation. The reflected echoes are recorded based on their time-of-flight. Due to the tablet matrix's transparency to terahertz radiation, information from both the surface and internal structure of the dosage form can be acquired within the same experiment. The terahertz pulse is capable of traversing the entire tablet, and reflections are detected at every interface where there is a change in refractive index, such as at internal cracks or the liquid front of penetrating liquid. This system produces measurements of liquid penetration depth swelling of tablet alongside detecting the micro cracks caused by swelling (Yassin, Su, Lin, Gladden & Zeitler 2015, Yassin, Goodwin, Anderson, Sibik, Ian Wilson, Gladden & Axel Zeitler 2015). A series of studies tried to use TPI as a non-destructive inline tool to measure the porosity of tablets and investigated the impact of initial porosity of tablets and mass fraction of lubricants on the disintegration of granules (Bawuah et al. 2014, Markl, Wang, Ridgway, Karttunen, Chakraborty, Bawuah, Pääkkönen, Gane, Ketolainen, Peiponen & Zeitler 2017, Bawuah et al. 2023). In the latest study by (Bawuah et al. 2023), it was found that initial porosity has a quadratic relationship with disintegration time, confirming the fact that there is an optimal range for the porosity of tablets.

Recently, a new technique has been introduced to measure the volume and water uptake in tablets (Lenz et al. 2021). A by-product of this measurement is the direct calculation of

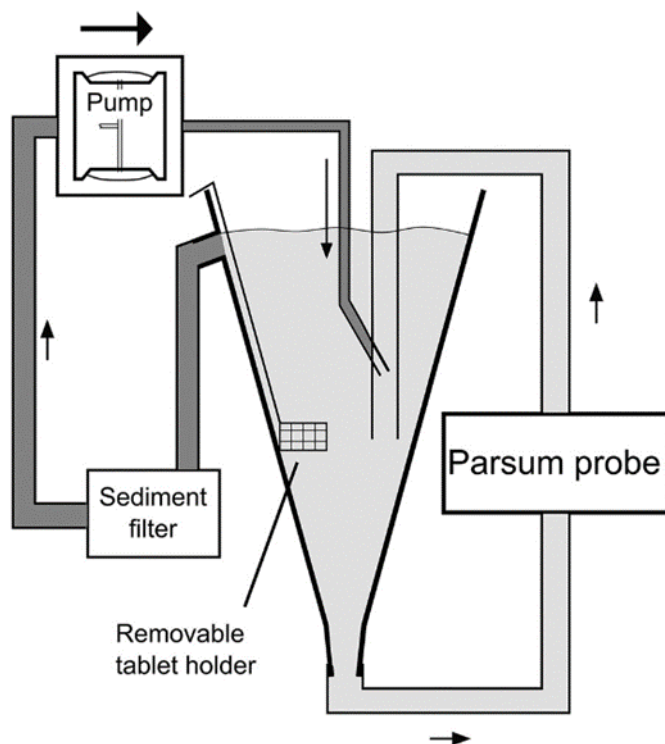


**Figure 2.17:** An schematic of the setup used by (Quodbach & Kleinebudde 2014a), utilizing parsum probe to measure the particles size distribution of disintegrating particles

liquid penetration depth. A schematic of the experimental setup for water uptake and swelling analysis of a tablet is depicted in Figure 2.19. The system includes a water container with inner and outer reservoirs connected by a valve placed on a balance. The tablet holder's self-adjustment at the water surface was achieved using a positioning system based on buoyancy, which remained independent of the actual water level in the container. The buoyancy bodies in the outer reservoir were separated from the tablet holder positioned in the inner reservoir. This technique provided almost the same type of information for the disintegration of granules while being cheaper than techniques like TPI and synchrotron X-ray. At the same time, the post-measurement data processing is easier than many other image analysis-based techniques. In table 2.1, all the aforementioned techniques and the properties they measure are listed.

## 2.6 Mathematical Modelling

In this section, the focus is on mathematical modelling of different mechanistic processes involved in disintegration. As discussed earlier, wicking and swelling are the primary mechanisms of disintegration, however, depending on the porosity, the approach to model each process can differ. In this section, the current state of modelling for these processes is described. In wicking, the liquid penetrates into the agglomerates through their pores, but depending on the size of those pores, the liquid uptake mechanism can be either diffusion or capillary in nature. As is clear in diffusion, due to size of the pores and their porosity, the liquid slowly diffuses into the porous system leading to a gradual liquid increase in the

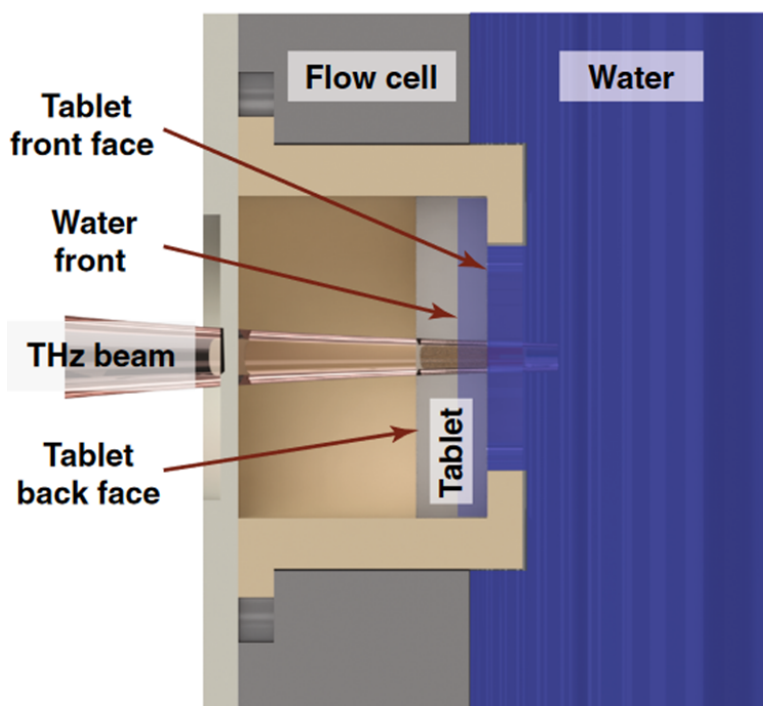


**Figure 2.18:** An schematic of TPI to study the disintegration of tablets (Markl & Zeitler 2017)

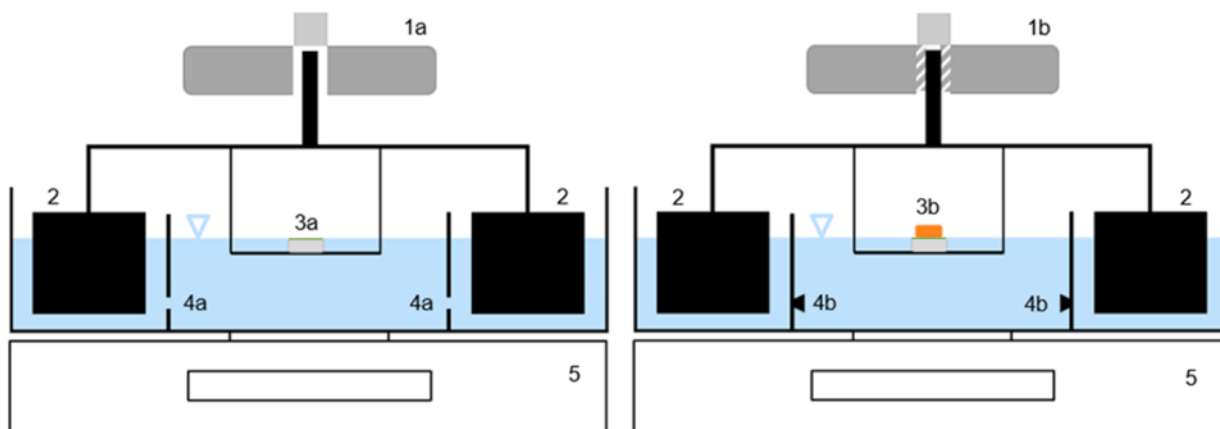


**Figure 2.19:** An schematic used by (Lenz et al. 2021) to measure the water uptake and swelling of tablet, positioning (left), measurement (right), 1: mechanical clamp (a: open, b: closed), 2: buoyancy body, 3a: tablet holder + filter paper, 3b: tablet holder + filter paper + tablet, 4 valve (a: open, b: closed), 5: balance.

agglomerate due to the sudden reaction of disintegrants to the liquid. The modelling of liquid diffusion and liquid uptake will be discussed in Chapter 3. In the case where the capillary force is the main driver for wicking, liquid ascends through the pores via the capillary effect which is due to thermodynamic compatibility of agglomerate and liquid, alongside the surface tension of liquid. The first attempt to model the water uptake was through the Wash-

**Table 2.1:** List of measurement techniques and the measured properties of tablets/granules

Measurement technique	Measured property
Graduated pipette and balance	Liquid uptake and swelling of powder bed
Linear inductive transducer	Swelling of tablets
Microbalance, displacement transducer and humidity sensor	Liquid uptake, liquid penetration and swelling of tablets
Optical microscopy	Swelling of tablets, granules and primary particles, Particle size distribution of granules
Force displacement sensor and balance	Disintegration force and liquid uptake of tablets
Height change measurement	Swelling of tablets
Environmental scanning electron microscopy	Swelling of tablets
Magnetic resonance imaging	Swelling and liquid penetration of tablets
Elastic soundwave measurements	Mechanical properties of tablets
Focused beam reflectance measurement	Particle size distribution of granules
Spatial filtering velocimetry	Particle size distribution of granules
High speed video imaging	Identifying disintegration mechanism
Terahertz pulsed imaging	Liquid penetration, swelling and initial porosity of tablets
Optical microscope and microbalance	Liquid uptake, swelling and liquid penetration of tablets

burn equation. This equation assumes the pore size distribution is mono-sized. Moreover, it suggests that:

$$\frac{dL_c}{dt} = \frac{q}{\varepsilon_{sur}} \quad (2.7)$$

where  $L_c$  is the penetration depth,  $q$  is the liquid penetration flux and  $\varepsilon_{sur}$  is the porosity at the surface of the tablet. In other words, the rate of ascending liquid is the same as liquid penetration rate. therefore, the following equation (2.8) would be obtained:

$$L_c = \frac{R_h}{\tau} \sqrt{\frac{\gamma \cos(\theta)}{2\eta R_c}} t \quad (2.8)$$

in which  $R_h$  is the hydraulic radius,  $R_c$  is the pore size of dry porous media,  $\gamma$  is the air-liquid surface tension,  $\theta$  is the contact angle,  $\eta$  is the liquid viscosity and  $t$  is time. (Handy 1960) tried to obtain the penetration rate of water for porous materials such as rocks. He linked the

penetration of water obtained from Darcy's law to liquid ascension obtained from a piston displacement analogy as shown in Eq.(2.9):

$$q = \frac{2k_w\gamma \cos(\theta)}{\eta_w R_c L_c} = \varepsilon S_w \frac{dL_c}{dt} \quad (2.9)$$

where  $k_w$  is the water permeability,  $\varepsilon$  is (volumetric) porosity,  $\eta_w$  is water viscosity, and  $S_w$  is the water saturation. The result gives us the following equation (2.10):

$$L_c = 2\sqrt{\frac{k_w\gamma \cos(\theta)}{\varepsilon S_w \eta_w R_c} t} \quad (2.10)$$

There are other forms of Washburn equation in the literature (Cai & Yu 2011), but they all consider the water uptake as proportional to square root of time ( $\sqrt{t}$ ). Many researchers have studied this relationship; however, the results show that imbibition of many porous materials does not obey relationships such as the Washburn (LW) equation or Handy's ( $L_c \propto t^{1/2}$ ). For example, (Laughlin & Davies 1961) found that the liquid penetration depth in wool, felt and cotton fabrics in a light grade of lubricating oil does not follow the LW equation. They assumed there is power law relationship between liquid penetration depth and time which can be described in a logarithmic manner:

$$\log(L_c) = \text{const} + n \log(t) \quad (2.11)$$

The experiments showed that time exponent ( $n$ ) varies between 0.41 to 0.5, which showed the materials in this case do not obey from LW equation. Many researchers have investigated such possibilities for other materials, such as paper (Eklund & Salminen 1986, Kwon et al. 1996), cotton and polyester woven fabric (De Boer 1980). Numerical stimulation studies of porous media showed that the capillary imbibition of water is not upheld by LW equation (Dubé et al. 1999, Lam & Horvath 2000). Most values of time exponent ( $n$ ) are found to be less than 0.5, which shows the inability of the LW equation to depict the wicking behaviour in a tri-dimensional porous medium. This deviation mainly stems from neglecting different characteristics of porous structure such as trapping, corner flow or even connection between different pores. The anomalous value of time exponent ( $n < 0.5$ ) suggests that for the cases when the average height increases, the rate of liquid penetration becomes even slower than the models that consider only viscous drag and capillary pressure. As stated by (Lam & Horvath 2000) this phenomenon cannot be explained by initial effects, deformation, gravity, or evaporation. Some studies tried to modify the LW equation by fitting it to experimental data, deriving similar equations with different time exponent. (Delker et al. 1996) found that the experimental data of capillary imbibition of water can be only fitted with a three-parameter model,  $L_c \propto t^n (n < 0.5)$ , over a wide time range for a column of glass beads. (Balankin et al. 2006) did a series of impregnation experiments on paper. They showed in transient regime and the saturation stage precursor film flow and the main bulk impregnation fronts rise proving that  $L_c \propto t^n (n < 0.5)$ . Furthermore, (Brú & Pastor 2006) showed that the average liquid penetration depth follows the same rule as before  $L_c \propto t^n (n < 0.5)$  until pinning occurs. Table 2.2 shows us the works on water imbibition and the obtained time exponent for each one.

According to (Balankin et al. 2006), one of the main reason behind the deviation from LW equation can be attributed to the swelling mechanism. In such mechanism, part of the solid

**Table 2.2:** Time exponents ( $n$ ) from different capillary imbibition studies (Cai & Yu 2011)

Source	Time exponent ( $n$ )	Porous Media
(Laughlin & Davies 1961)	0.41-0.5	fibrous textile
(De Boer 1980)	0.351-0.512 <sup>1</sup> ; 0.407-0.52	cotton fabrics
(Horváth & Stanley 1995)	0.386	filter paper
(Kwon et al. 1996)	0.37	paper towel
(Delker et al. 1996)	0.25	glass beads
(Dubé et al. 1999)	0.49	disordered medium
(Lam & Horvath 2000)	0.382	paper
(Li & Horne 2004)	0.4-0.6	chalk/geysers
(Balankin et al. 2006)	0.41 <sup>3</sup> ; 0.3 <sup>4</sup>	paper
(Brú & Pastor 2006)	0.411	bentonite clay

structure can absorb the liquid that can lead to an expansion creating an internal stress that can change many parameters including porous structure, porosity, saturation, hydrodynamic radius and permeability (Figure 2.20). Such mechanisms can cause complex time-dependency behaviours from the material that can make the modelling considerably harder. (Schuchard & Berg 1991) used a modified form of LW equation to account for the swelling in the porous structure. They assumed the hydrodynamic radius in the wetted area decreases linearly with time with slope  $a$  ( $R_h = R_{h,0} - at$ ), leading to the equation (2.12):

$$L_c = \frac{1}{\tau} \sqrt{\frac{R_{c,0}\gamma \cos(\theta)}{2\eta}} \sqrt{1 - \frac{at}{R_{c,0}} + \frac{a^2 t^2}{3R_{c,0}^2}} \quad (2.12)$$

where  $\tau$  is tortuosity and  $R_{c,0}$  is the pore radius of dry media. (Masoodi & Pillai 2010) developed a new formula by considering swelling for liquid penetration depth and pressure distribution based on combining three equations: Darcy's law, mass conservation in liquid phase and the Young-Laplace equation. They assumed that the liquid absorbance rate is  $-b \frac{\partial \varepsilon}{\partial t}$  where  $b$  is a constant between zero and one and the liquid penetration depth is related to the velocity at the wetted-unwetted interface:

$$\frac{dL_c}{dt} = v|_{u-w-i} / \varepsilon_0 \quad (2.13)$$

in which  $v|_{u-w-i}$  is the velocity at wetted-unwetted interface and  $\varepsilon_0$  is the porosity of unwetted part of agglomerate. Considering all these assumptions led us to the following equation (2.14):

---

<sup>1</sup>Water with surface active agents

<sup>2</sup>Water without surface active agents

<sup>3</sup>Precursor film flow in the transient regime

<sup>4</sup>Main bulk impregnation front in the transient regime and the saturation stage

$$L_c = \left( \frac{4\gamma \cos(\theta)}{\varepsilon_0 \eta R_c} \exp((b-1)\varepsilon(t)/\varepsilon_0) \int_0^t \exp((1-b)\varepsilon(t')/\varepsilon_0) k(t') dt' \right)^{1/2} \quad (2.14)$$

This is a comprehensive equation that can include the aforementioned equations too. For example, in the case of no absorbance ( $b = 0$ ), the porosity remains the same ( $\varepsilon = \varepsilon_0$ ) and the equation turns into Washburn equation. If the complete absorbance ( $b = 1$ ) is considered, then the permeability becomes a time-related variable changing equation (2.14) into a unique form described in Eq. (2.15):

$$L_c = \left( \frac{4\gamma \cos(\theta)}{\varepsilon_0 \eta R_c} \int_0^t k(t') dt' \right)^{1/2} \quad (2.15)$$

(Markl, Yassin, Wilson, Goodwin, Anderson & Zeitler 2017) investigated the changes in size of tablet using the data obtained from TPI experiments. They found out that the swelling is composed of two parts, an initial linear swelling caused by liquid penetration followed by an asymptotic non-linear curve. To model the disintegration of the tablets they assumed that:

- The pore structure can be estimated using cylindrical tubes.
- All the water is being absorbed the swelling media ( $b = 1$ ).
- The permeability is isotropic in the wetted area it can be estimated using modified Carman–Kozeny equation.
- The porosity is uniform throughout the wetted area of the tablet.
- The gravity does not affect liquid penetration.

Based on the first assumptions, they obtained the following Eq. (2.16) between the swelling rate  $G$  and pore radius  $R_c$ :

$$R_c(t) = R_{c,0} - \frac{D_s}{2} \left[ \sqrt[3]{1 + \frac{Gt}{L_0}} - 1 \right] \quad (2.16)$$

in which  $D_s$  is the mean diameter of the primary particles and  $L_0$  is the initial length of tablet. Based on the same assumption, they extracted equation (2.17) to relate porosity to pore radius of the tablet:

$$\frac{\varepsilon(t)}{\varepsilon_0} = \left( \frac{R_c(t)}{R_{c,0}} \right)^2 \quad (2.17)$$

Obtain the swelling rate, the change in size of tablet due to swelling ( $\Delta L$ ) was fitted to the time through modified version of Schott model (Schott 1992*a,b*). Schott model was first introduced for the swelling rate of gelatine and cellulose. He speculated that the liquid penetration and subsequent absorption would lead to plasticization effect that decreases the glassy temperature of the polymers. This phenomenon causes the water uptake and swelling mechanism to change from a linear first order kinetic model to a non-linear second model:

$$\frac{d\Delta L}{dt} = G \left( 1 - \frac{\Delta L}{\Delta L_\infty} \right)^2 \quad (2.18)$$

where  $\Delta L = (L - L_0)$  is the swelling of the polymer and  $\Delta L_\infty$  is its maximum value. Solving this equation based on time, results in following equation (2.19):

$$\Delta L = \frac{Gt}{1 + \frac{Gt}{\Delta L_\infty}} \implies \frac{t}{\Delta L} = \frac{1}{G} + \frac{t}{\Delta L_\infty} \quad (2.19)$$

Schott has recommended to obtain swelling rate and maximum swelling of the tablet by using a linear fit of  $t/\Delta L$  versus time, as described in equation (2.19). They then used equation (2.15) to simulate the swelling of the tablets. The simulation data had good agreement with the experimental data. It is worth mentioning later study by (Lenz et al. 2021) showed that the swelling of tablet does not always obey from Schott model.

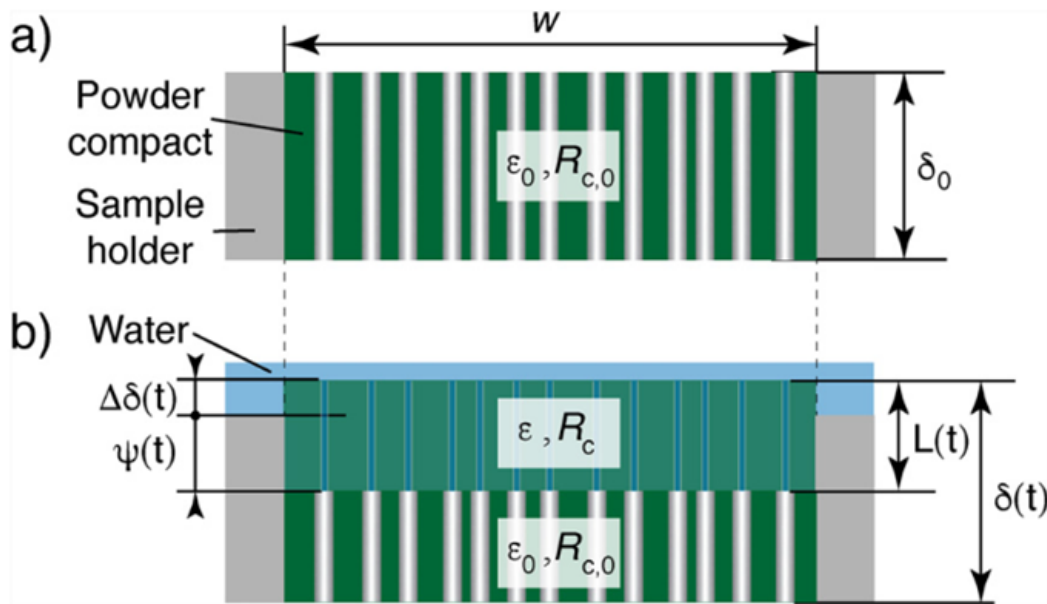


**Figure 2.20:** Presentation of wicking and swelling of fluid in a tablet. The tablet is sealed and held tightly around its circumference. (a) Dry tablet with the initial thickness  $\delta_0$ , pore radius  $R_{c,0}$ , the porosity  $\epsilon_0$ , and the diameter  $W$ . (b) Penetration of liquid through the porous region of tablet with displacement  $\Psi$ , swelling  $\Delta\delta$ , and the penetration depth  $L = \Psi + \Delta\delta$ .  $\epsilon$  and  $R_c$  are the porosity and the pore radius of the wetted porous phase, respectively (Markl, Yassin, Wilson, Goodwin, Anderson & Zeitler 2017).

Discrete element method (DEM) is a powerful tool to capture the swelling behaviour of the tablets. In this technique, the interaction of each particle inside the tablet is considered in the model. Because of this, DEM tends to be very costly computationally. However, it can provide information that cannot be obtained otherwise. In a study by (Sweijen, Chareyre, Hassanizadeh & Karadimitriou 2017), DEM was used alongside pore finite volume (PFV) to model the swelling of a powder bed containing super-absorbent granules. The authors developed a new model to describe the swelling of individual granules. It was found out that the model results agree relatively well with experimental data until 2 minutes and after that time some deviations are seen in the model. Sensitivity analysis on the friction coefficient, shear

modulus, and diffusion coefficient indicates that porosity decreased by lowering the friction coefficient or particle stiffness. The diffusivity does not affect the particle rearrangement and only changes the time to reach equilibrium state. Moreover, to increase the water suction of particles in the bed and subsequently swelling of the bed, fluid must be distributed through the particle bed. In another study by the same authors (Sweijen et al. 2020), grain-scale modelling technique combined with implicit pressure and explicit saturation scheme (IMPES) was utilized to simulate unsaturated flow in deforming and highly swelling granular materials within a powder bed. The results were highly dependent on three-time characteristic parameters: unsaturated flow time characteristic ( $\tau_{flow}$ ) a representative of liquid flow in the bed, absorption time characteristic ( $\tau_{abs}$ ) a criterion of how fast the particles absorb the liquid and deformation time characteristic ( $\tau_{def}$ ) which is an indication of deformation relaxation. They provided a chart (Figure 2.21) that gives an outcome of the flow based the ratio between these parameters. Based on the ratio of these time characteristics, the following scenarios in the powder bed can be identified:

- i.  $\tau_{flow} \ll \tau_{abs}$ : liquid inside the pores can reach equilibrium rapidly, and the dynamic effects of unsaturated flow are short-lived. which suggests the usage of a quasi-static capillarity model for the unsaturated flow.
- ii.  $\tau_{flow} \gg \tau_{abs}$ : liquid exchange among pores is slow, and the swelling rate may be strongly influenced by the lack of water inside the particle packing, leading to suction inside the particles even when saturated.
- iii.  $\tau_{def} \ll \tau_{abs}$ : particle-particle contacts can dissipate their potential energy quickly.
- iv.  $\tau_{def} \gg \tau_{abs}$ : swelling occurs at a faster rate than the dissipation of potential energy of particle contact. Particle movement is limited, and the particle packing tends to clog, resulting in a decrease in porosity.
- v.  $\tau_{flow} \ll \tau_{def}$ : liquid inside the pores can quickly reach equilibrium, and dynamic effects are temporary.
- vi.  $\tau_{flow} \gg \tau_{def}$ : particle contacts can dissipate their energy quickly, and water flow dominates the kinetics of particle movement.

(Braile et al. 2022) used the same approach as (Sweijen, Chareyre, Hassanizadeh & Karadimitriou 2017) to study the impact of super-absorbent particles (SAPs) on the expansion of a fully saturated powder bed composed of only SAPs. They used a first order kinetic model to predict the swelling behaviour of single grains. The DEM model was validated for two different SAPs; rice and MCC (PH102 grade). It was shown that the bed expansion is influenced by the swelling capacity of SAP, its kinetics, and the porosity of the layers of particles. Moreover, the DEM model showed that the expansion increases the segregation of the bed.

All of these studies are important but they are focused only on powder beds and not tablets. (Soundaranathan et al. 2023) was the first to study the structure of a tablet under the swelling force. In their study, they used DEM to simulate both the compression and the disintegration states. For the disintegration, they considered a fully saturated fluid flow. A power law equation was used based on the TPI data of the liquid penetration front. The model

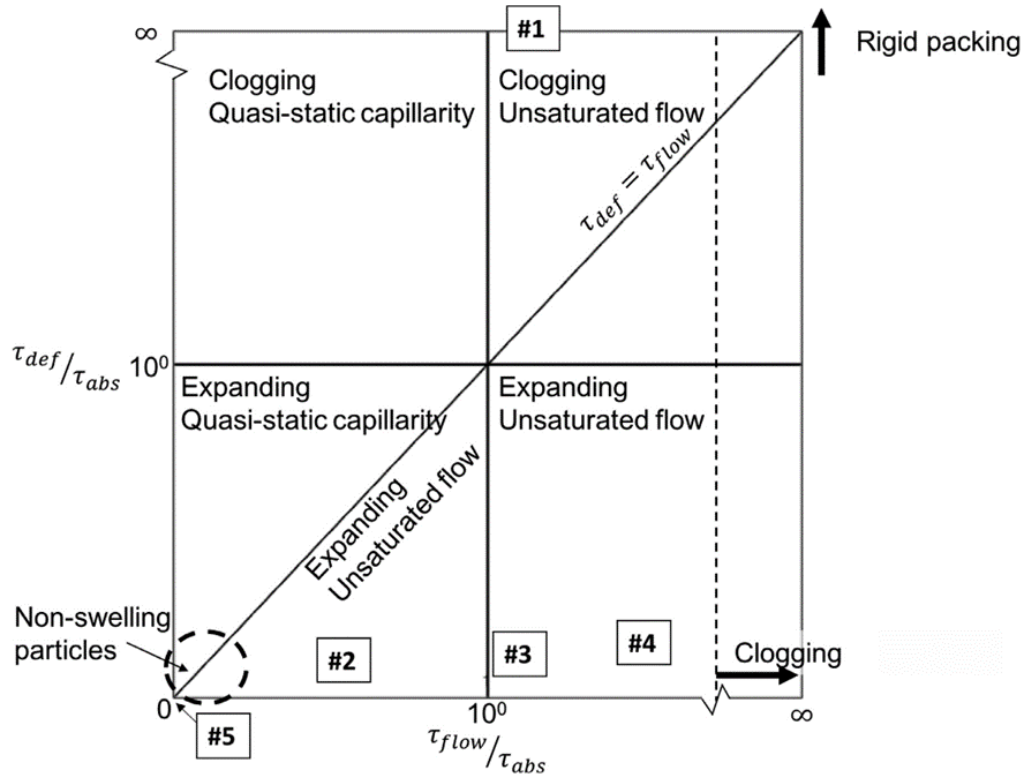


**Figure 2.21:** Overview of time characteristics of flow, absorption and deformation (Sweijen et al. 2020)

considered two different scenarios. One, tablets consisted of only MCC granules (PH101 grade) with different initial porosity and the second scenario considered different levels of CCS disintegrant in the tablet with the same porosity. The experimental and simulation results showed that in all tablets, the porosity increases over time which is in contrast with the results obtained by (Markl, Yassin, Wilson, Goodwin, Anderson & Zeitler 2017). However, the tablets with the lowest porosity in the first scenario and highest disintegrant load in the second scenario, showed the slowest rate of swelling and increase in porosity due to closure of the pores in both wetted and dry volume. Another result was the impact of the growing stress in the wetted area on the porosity of the dry area. This is in contrast to the assumption by (Masoodi & Pillai 2010) where it was considered the porosity of dry area remain constant. This study showed the importance of a tool like DEM for study of the impact of structural parameters and formulation on the swelling mechanism of tablets.

(Caramella et al. 1988) employed a distinct approach to model swelling and the ensuing detachment of particles. They conceptualized the disintegration mechanism as analogous to the phenomenon of nucleation and growth. In their model, the tablet expansion is treated in conjunction with a layer detachment process. Using a theoretical approach, they obtained the following equation (2.20) for the normalized disintegration force  $F(t)/F_\infty$  :

$$\frac{F(t)}{F_\infty} = \frac{1}{V_0} \int_0^t \dot{N}(t') v(t', t) \left(1 - \frac{F(t')}{F_\infty}\right) dt' \quad (2.20)$$

where  $F_\infty$  is the maximum force,  $V_0$  is the original volume of the tablet,  $v(t', t)$  is the expansion of the volume between time  $t'$  and  $t$  and  $\dot{N}$  represents the detachment rate of successive particle layers from the tablet, which occurs due to the separation of bonds as a result of liquid penetration. Equation (2.20) is based on the assumption that volumetric fraction of particles released from the tablet is proportional to the normalized force. They showed that if function  $v(t', t)$  has a power-law relationship with time difference  $t - t'$  and if  $\dot{N}$  has a power law form or has a form of Dirac delta function (the release being spontaneous) with respect to time, then the equation would be reduced to equation (2.6). Based on the nucleation theory of Turnbull-Fischer, they proposed a model to relate the parameter  $k$  (in equation (2.6)) to absolute temperature  $T$  via the activation energies of interfacial detachment of particles,  $\Delta E_{det}$  and diffusion of disintegrated particles into the solvent  $\Delta E_{dif}$ :

$$k = k_0 \exp\left(-\frac{\Delta E_{det}}{RT}\right) \exp\left(-\frac{\Delta E_{dif}}{RT}\right) \quad (2.21)$$

where  $k_0$  is a constant and  $R$  is the global gas constant.  $\Delta E_{dif}$  was obtained using the Williams-Landel-Ferry (WLF) equation (Ferry 1980):

$$\Delta E_{dif} = \frac{17300T}{51.6 + T - T_g} \quad (2.22)$$

where  $T_g$  is the glass transition temperature of the tablets.  $\Delta E_{det}$  can also be formulated in terms of parameters that characterize the tablet dimensions and the thermodynamics of disintegration:

$$\Delta E_{det} = \frac{4l\sigma_e\sigma_s}{\Delta H_m} \frac{T_g}{T - T_g} \quad (2.23)$$

where  $l$  is the thickness of a single surface layer of the particles in the disintegrating tablet, and  $\sigma_s$  and  $\sigma_e$ , are the surface free energies of the side and end planes of the tablet, respectively. it was suggested by (Caramella et al. 1988) to fit the logarithm of  $k$  versus  $T_g/(T(T - T_g))$  to obtain parameter  $(4l\sigma_e\sigma_s)/(\Delta H_m)$ . In a later study, (Peppas & Colombo 1989) used the data obtained from the apparatus designed by (Catellani et al. 1989) to validate their model. In the model, the disintegration force  $F$  has been connected to water uptake  $q$  based on equation (2.24):

$$F = F_0 + C_{dif}\sqrt{q} + C_{conv} q \quad (2.24)$$

in which  $F_0$  is the initial stress of the tablet and the potential change of stresses when pores are filled with the liquid and  $C_{dif}$  and  $C_{conv}$  are diffusive and convective constants. (Peppas & Colombo 1989) speculated that due to nature of diffusion, its contribution to disintegration should be via the square root of water uptake while the convection contribution to the disintegration force is always negative. It was demonstrated that the relationship between force and water uptake was linear before the onset of swelling, at which point the kinetics change. Subsequently, the force becomes a function of the square root of the water quantity. While both (Caramella et al. 1988, Peppas & Colombo 1989) are useful in predicting the disintegration force, it should be mentioned that formation of micro cracks and their propagation through the tablets should be considered to increase the accuracy of the model. So far, the only model to predict the particle size distribution of disintegrating tablet and granules is proposed by (Wilson et al. 2012) which was dissolution limited and used hydrodynamic

erosion as a side process that separates the primary particles from the surface of the granules. They considered all the primary particles in the tablet are mono-dispersed. The model indicates that changes in the dissolution performance can be explained by more fundamental parameters, specifically differences in the initial particle sizes of the dispersed particles and the erosion rates of the tablets.

## 2.7 Conclusion

A thorough literature review was done on the mechanisms involved in disintegration, the factors affecting disintegration, experimental techniques to quantify disintegration and the mathematical models to describe different mechanisms involved. It was shown that while there have been many works on characterisation of tablets, the majority of the works have focused on qualitative descriptions and have fall short of deep understanding of the disintegration process. Thanks to the advances in experimental and computational fields, new techniques have been introduced in the last two decades to describe the disintegration in detail. However, the main issues when it comes to the disintegration are:

1. Impact of different disintegration processes on each other. Unfortunately, in most papers, the formulation are chosen in a way that is very hard to isolate the processes such as swelling or disintegration, something essential to model to validate these processes individually.
2. Limited research on modelling the disintegration of tablets, specifically the swelling driven disintegration, including the impact of stress on the disruption of interparticle bonds and lack of a proper mechanistic macro-level model, capable of predicting swelling, liquid absorption and liquid penetration of tablets and granules all together.
3. Lack of experimental methods on investigating te disintegration of granules. Most introduced methods in section 2.5 focuses on tablets and few have the capability to be used for granules due to geometrical and size limitation.

In the following chapters, it has been tried to tackle some of these issues by:

1. Isolating the swelling driven disintegration using a new formulation that focuses on this process only.
2. Introducing a new macro level mechanistic model for the swelling of single granule swelling model, such as a new liquid imbibition model.
3. Creating a mechanistic population balance model for the swelling that uses the single granule swelling model while considering other processes such as breakage of granules to primary particles.
4. Developing a new experimental method to observe the swelling of single granule to validate the single granule swelling model.

## Chapter 3

# Materials and Methods

### 3.1 Introduction

This chapter addresses the material and method used in this work which includes granulation of the granules, porosity and powder size distribution measurement as part of characterization, and methods to measure disintegration related variables, single granule size measurement and particle size distribution during swelling in order to validate the model.

The granulation and sieving of the processed granules were performed by Postdoctoral researcher Dr Kate E. Pitt, FBRM was performed by Postdoctoral researcher Dr Neeru Bala in conjunction with the postdoctoral researcher based at the University of Strathclyde Dr Bilal Ahmed. The remaining experiments were performed by the author of this thesis.

### 3.2 Formulations

The formulation chosen in this work was based on dispersive granules in which the granules contain excipient, superdisintegrant and binder. Given the focus of this thesis is on swelling based disintegration, no API was included in the formulation to avoid the interference of other mechanisms during disintegration. The excipients chosen for this work were microcrystalline cellulose (MCC) provided by Thermo Scientific and dibasic calcium phosphate anhydrous (DCPA) gifted by Budenheim GmbH. The superdisintegrant was sodium starch glycolate (SSG), a synthetic disintegrant with a high capacity for water absorbance, gifted by DFE Pharma, and the binder was an aqueous solution of a specific grade of hydroxypropylmethyl cellulose (HPMC) known as Pharmacoat 603, a grade recommended with the lowest viscosity in the HPMC grades gifted by SE Tylose GmbH. The reason for selecting this binder was its low dissolution time in water, which avoids the interference of the binder solution in disintegration. A list of the materials have been provided by in Table 3.1.

The binder solution concentration used for MCC granules were 5 %w and 12.5 %w while for DCPA granules the 12.5 %w binder solution was chosen due to fragility of granules produced at lower concentrations. The binder was created using a magnet stirrer. The procedure to create the solution is to pour half of the distilled water into a beaker and then slowly add the binder powder into the mass while the magnet stirrer is kept at high rpm. Then, the rest of the water is added to the beaker. During this process, the HPMC powders would go through gelation in which they create a mass of gel. To avoid this, it is recommended

**Table 3.1:** List of materials

Material	Supplier	Grade	$D_{v,10}(\mu\text{m})$	$D_{v,50}(\mu\text{m})$	$D_{v,90}(\mu\text{m})$	Density( $\text{kg}/\text{m}^3$ )
MCC	Thermo scientific	-	21.5	67.5	150	1560
DCPA	Budenheim GmbH	DI-CAFOS A60	32.3	62.3	108	2830
SSG	DFE Pharma	Primojel	62.1	131	235	1530
HPMC	SE Tylose GmbH	Pharmacoat 603	-	-	-	-

to use manual stirring to break the gels into smaller sizes in order to increase the dissolution as the magnet stirrer may not be able to break the gels. After this process, the beaker was sealed to avoid evaporation.

### 3.3 Experimental methodology

#### 3.3.1 Powder size distribution measurement

To measure the size distribution of the powders, a laser diffraction-based equipment known as malvern mastersizer 3000 was used. This equipment uses laser diffraction and Rayleigh scattering law to determine the size and shape of the particles in a short period time and can obtain the size distribution of granules and powders in a wide size range, between 10 nm up to 3.5 mm. The samples were tested 12 times in a loop to obtain the final size distribution. It is important to note that in laser diffraction-based equipment, the measured type of distribution is a volume-based distribution ( $f_v$ ), which is related to the volume of a powders instead of their number-based distribution ( $f_n$ ). The relationship between volume-based distribution and number-based distribution is (Litster 2016):

$$f_n(x) = \frac{f_v(x)}{x^3} / \int_0^\infty \frac{f_v(x)}{x^3} dx \quad (3.1)$$

To obtain the number-based distribution for the powders, the volume-based distribution of each powder was fitted with a series of log-normal distribution functions through Curve Fitting Toolbox in MATLAB. Then the number-based distribution was obtained using Eq. (3.1). The size distribution of powders are given at 3.1.

#### 3.3.2 Granulation experiments

The granulator used in this thesis was a 3.7L Key International KGS high shear granulator with a three bladed impeller and without any chopper. A diagram of the granulator alongside its specification has been provided in Figure 3.2. To granulate the powders homogeneously, the powders were pre-mixed at 400 rpm in the granulator for 1 minute before adding the binder. The binder was added to the granulator using a peristaltic pump (Watson Marlow

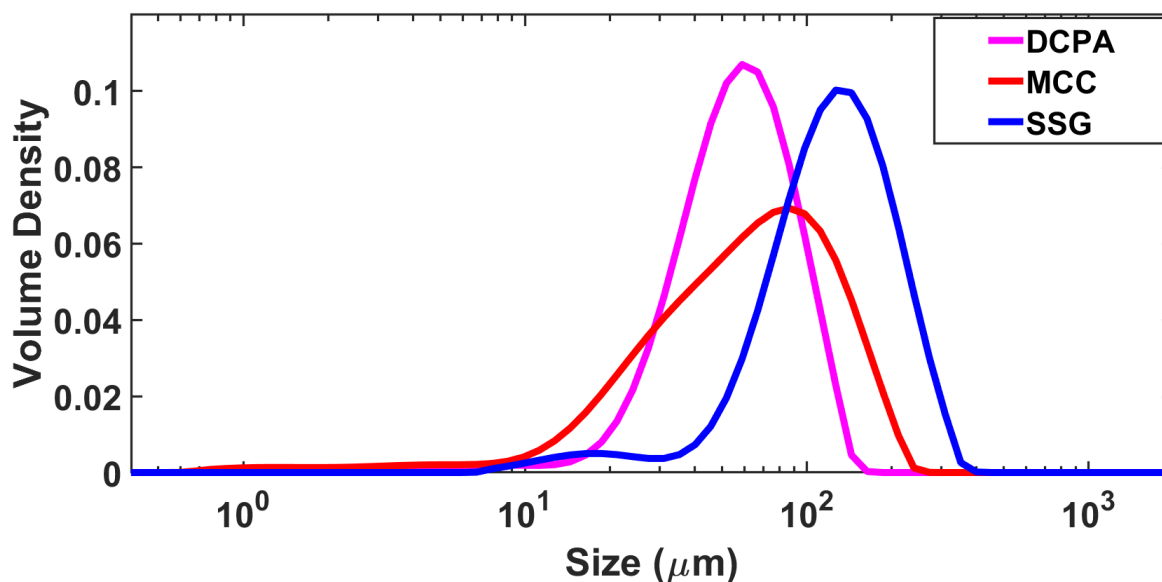


**Figure 3.1:** *The size distribution of MCC, DCPA and SSG powders*

120S). Given two different type of formulation has been used based on two different excipient, the granulation specifications differs such as the filling mass due to different skeletal density of MCC and DCPA. All the important parameters for the two different types of granules are listed in Table 3.2. After the granulation was finished, to dry the granules, they were dried overnight at a temperature of 50 °C prior to analysis.

**Table 3.2:** *The granulation specification for each type of formulation*

Granule type	Filling mass (g)	Impeller speed (rpm)	Massing time (min)	Binder addition time (min)
MCC + SSG + HPMC	500	450	5	3
DCPA + SSG + HPMC	1200	250	10	3

### 3.3.3 Sieving analysis

The dry granule size distribution was obtained using sieve analysis. Due to brittleness of some granules, it was decided to use manual sieving instead of a sieving tower as there is a high chance of granule breakage, changing the particle size distribution. The sieve trays chosen for the analysis were of the following sizes: 5600, 4000, 2800, 2000, 1800, 1400, 1000, 710, 500, 355, 250, 180, 125 and 90  $\mu\text{m}$ . In order to have the small margin of errors in mass measurement, after careful sieving of each sieve, the sample and sieves were weighed together. By subtracting the obtained mass from the weight of the sieves, the mass of the granules in each sieve, designated as  $\Delta m_i$  here, would be obtained. This can lead us to the

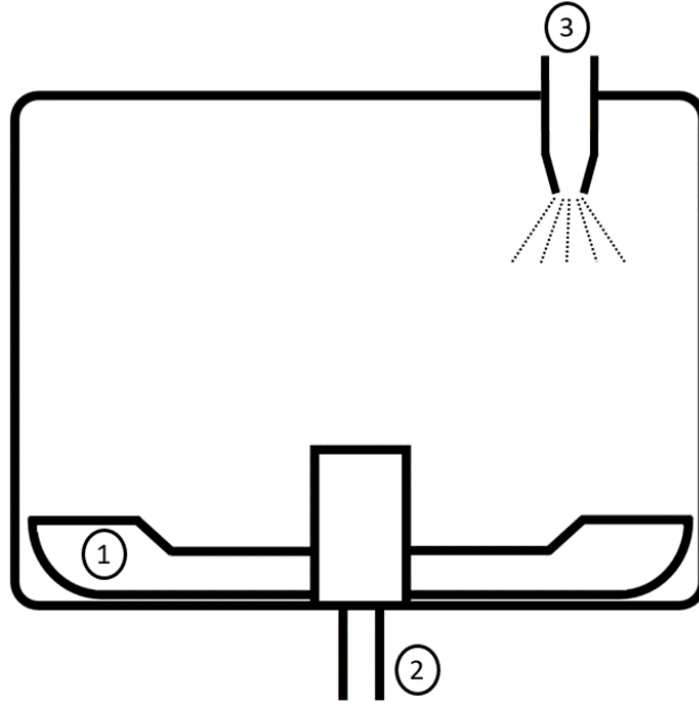


**Figure 3.2:** A schematic of the granulator used here, 1) The blade position, 2) Power unit, 3) Binder injection position

mass frequency ( $f_{m,i}$ ) and log mass frequency ( $f_{m,i}^{log}$ ) of the granules which are defined as following (Litster 2016):

$$\begin{cases} f_{m,i} = \frac{\Delta m_i}{\sum_{i=1}^N \Delta m_i} \frac{1}{x_i - x_{i-1}} \\ f_{m,i}^{log} = \frac{\Delta m_i}{\sum_{i=1}^N \Delta m_i} \frac{1}{\log_{10}\left(\frac{x_i}{x_{i-1}}\right)} \end{cases} \quad (3.2)$$

where  $x_i$  is the sieve tray diameter and  $N$  is the total number of sieves. The cumulative size distribution of  $i^{\text{th}}$  sieve was also obtained using the mass frequencies up to that sieve size:

$$W(< x_i) = \frac{\sum_{j=1}^i \Delta m_j}{\sum_{j=1}^N \Delta m_j} = \sum_{j=1}^i f_{m,j} (x_j - x_{j-1}) = \sum_{j=1}^i f_{m,j}^{log} \log_{10}\left(\frac{x_i}{x_{i-1}}\right) \quad (3.3)$$

To plot the PSD results, the geometric mean diameter of the sieve sizes  $\bar{x}_i (= \sqrt{x_i x_{i-1}})$  was used.

### 3.3.4 Density measurement

The skeletal density was obtained via a helium pycnometry (AccuPyc II Micromeritics) to obtain the true density of porous materials as helium has the capability to go into very small pores. The device consists of a sample chamber and additional sealed chamber (Yang et al. 2017). At the beginning, the sample is weighed. The sample then would be placed in the

sample chamber and the device would be sealed. At the first stage of the measurement with the device, the sample chamber and additional chamber alongside the pipes would be purged of any other gas by opening all the valves and injecting helium into them at ambient pressure and recording the ambient pressure using the pressure transducer, as is shown in Figure 3.3. At the second stage, valves 2 and 3 would close and valve 1 would open and the pressure would be increased with a constant rate until a gauge pressure of 19.5 psig is reached. Then valve 1 would close and the pressure would be recorded. At the third stage, valve 2 would open so that the helium would travel between the sample and additional empty chambers until equilibrium is reached, and then the pressure would be recorded. By using ideal gas law for helium, given it is a noble gas with low molecular weight, the skeletal density of the sample ( $\rho_s$ ) would be:

$$\rho_s = \frac{m_s}{V_s} = \frac{m_s}{V_C + V_A \left\{ 1 + \frac{P_2 - P_{amb}}{P_3 - P_{amb}} \right\}} \quad (3.4)$$

where  $m_s$ ,  $V_s$ ,  $V_C$ ,  $V_A$ ,  $P_{amb}$ ,  $P_2$  and  $P_3$  are the mass of the sample, volume of the solid part of the granules, volume of sample chamber without sample, volume of additional chamber, ambient pressure measured at the end of the first stage, the pressure recorded at the end of second and third stage respectively. This process can be repeated multiple times to increase the certainty of the measurement. The number of cycles chosen here is 5. At the end, the average density and the standard deviation of the density would be reported.

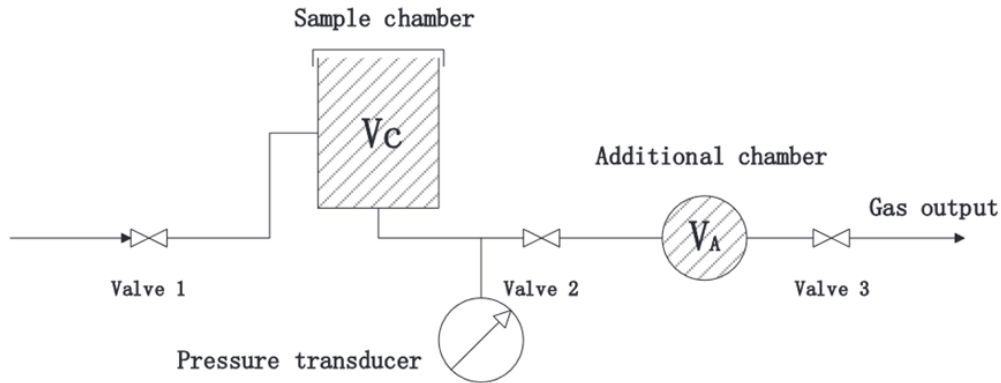


**Figure 3.3:** An schematic of helium pycnometry by (Yang et al. 2017)

### 3.3.5 Porosity measurement

In order to measure the porosity of granules, the envelope density is required. The envelope density can be obtained usually through GeoPyc, a standard method to obtain envelope and bulk density. However, because of irregularity in the granules' shape and their low strength, a more thorough method known as mercury porosimetry was used. Mercury porosimetry is one of the best methods in obtaining porosity and the only technique capable of obtaining pore size distribution and other data such as tortuosity and permeability (Markl et al. 2018). The method works for pores between 2 nm and 300  $\mu\text{m}$  in size which is the widest range among all similar techniques (Schlumberger & Thommes 2021). Mercury is a non-absorbing

fluid with low wettability which is ideal for forced intrusion into porous materials. The measurement of mercury entering pores is achieved using a penetrometer, which is essentially an electrical capacitance dilatometer. These instruments are highly sensitive, capable of measuring changes in mercury volume, with values less than 0.1  $\mu\text{L}$ . The penetrometer itself is comprised of a glass body filled with mercury (an electrical conductor). The stem of the penetrometer operates as a reservoir for mercury and is coated with a metal layer, another conductor. The system therefore can be called a capacitator as two conductors (mercury and metal plate) are separated by the glass body, an insulator. As pressure is applied, it forces the mercury to flow out of the capillary and into the sample. Consequently, the volume of mercury within the capillary decreases, leading to a decrease in capacitance. This reduction in capacitance is directly proportional to the volume of mercury exiting the capillary in response to changes in pressure. The amount of pressure applied ( $P$ ) has an inverse relationship with the pore size in the granule ( $d_p$ ) through the well-known Washburn equation:

$$d_p = -\frac{4\gamma_{ma} \cos(\theta)}{P} \quad (3.5)$$

in which,  $\gamma_{ma}$  is the surface tension between mercury and air and  $\theta$  is the contact angle. Because of this, the measurements in mercury porosimetry are performed in two steps. The first step, known as the low pressure mercury porosimetry is suitable for intrusion into large pores while the second stage, the high pressure is suited for small pores. It is important that low pressure experiment should be done before the high pressure experiment. Furthermore, the amount of volume going into the granule in a specific pore size (or pressure) has a direct relationship with the number of pores with that size in the granule.

To measure the porosity of the granules, first the weight of the penetrometer with and without the sample was measured. Then carefully, the penetrometer was sealed and put in the low pressure part of the equipment. After de-airing, the pressure would slowly increase until it reached 30 psia. After reaching equilibrium, the penetrometer was taken out of the sample and weighed again. Then, the penetrometer was placed in the high-pressure part. First, the sample would be purged from any air left in it and then it would be sealed for the measurement to be started. It is important to note that in the data provided, in the case of these granules, two intrusion sections are seen. It was found out that the first part was related to the intrusion of mercury between the granules and therefore should be omitted out of the measurement in order to obtain the volume penetrated into the granules. The envelope density of the granule ( $\rho_{env}$ ) is:

$$\rho_{env} = \frac{m_s}{V} = \frac{m_s}{V_s + V_p} = \frac{m_s}{V_2 - V_1} \quad (3.6)$$

where  $V$  is the volume of the granules,  $V_s$  is the volume of the solid part of granules,  $V_p$  is the volume of the pores and  $V_1$  and  $V_2$  are the recorded mercury volume at the end of the first and second intrusion. Based on equations (3.4) and (3.6), the porosity would be:

$$\varepsilon = \frac{V_p}{V} = 1 - \frac{V_s}{V} = 1 - \frac{\rho_{env}}{\rho_s} \quad (3.7)$$

### 3.3.6 Single Granule size measurement during disintegration

In swelling driven disintegration of granules, an important phenomenon is the expansion of the granules before breakage. The intention here was to measure this size evolution using

optical based techniques combined with image analysis. This data is then used to calibrate the single granule swelling model, which simulates the size expansion of granules. Given that the granules must be submerged in water in order to study the swelling behaviour, efforts have been made to design an experimental setup that minimizes both the depth of fluid and the thickness of material enclosing the dissolution chamber, while fixing the granule in place. Based on these criteria, a new experimental setup based on a 3D-printed flow cell was designed to perform the measurement (Figure 3.4 and 3.5). This is based on the design first suggested by (Soundaranathan et al. 2020) using an optical microscope to measure the growing size of a disintegrant particle.

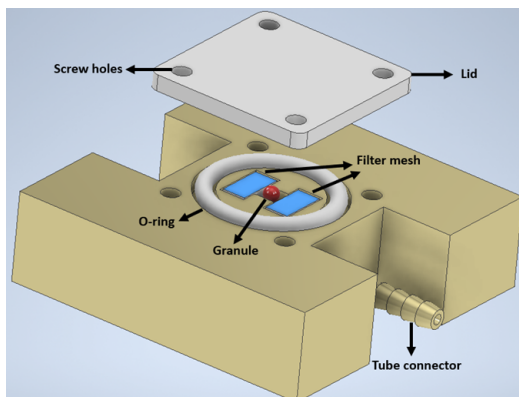


**Figure 3.4:** Schematic representation of the proposed flow cell with its components

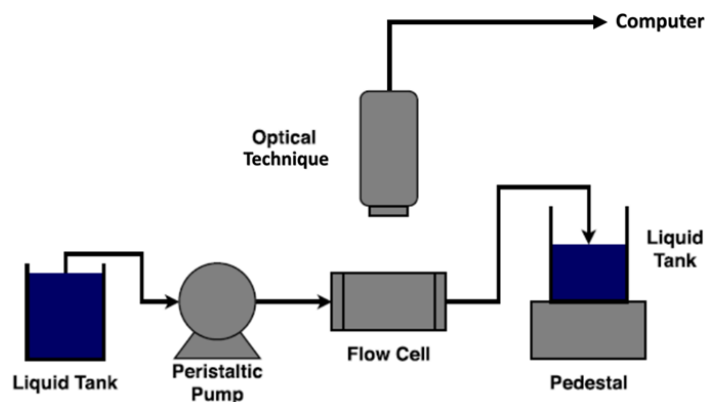


**Figure 3.5:** Schematic representation of the proposed experimental setup for measuring the size of an individual granule, adapted from (Soundaranathan et al. 2020)

The centre of this design is the sample holder area, where the granule was placed. Adjacent to this area are two hollow cubic areas called the mesh area. The main reason behind creating this area is to not let the flow going immediately to the sample. After inserting the granule in the sample holder area and before connecting it to the liquid flow, the flow cell was sealed using an O-ring and a thin transparent Plexiglas lid was fixed on top. This plexiglas has a refractive index close to that of glass. The experimental system for individual granule swelling studies is shown in Figure 3.6. The microscope was situated above the top of the flow cell, which was connected to a computer with image capturing software. Distilled water flow is provided via the peristaltic pump. Following image capturing, the images were analysed to obtain the required properties, mainly the size of the granule. While there are tools available on the market, image analysis is notoriously sensitive to the image capture conditions, and those available softwares which were trialed (e.g. ImageJ, Digimizer) were not suitable for this purpose. Therefore, an image analysis app was developed in MATLAB using its comprehensive image analysis package and the app designer (Figure 3.7). This image analysis app consists of many steps shown schematically in Figure 3.8. Finally, the data would be de-noised using another app created in MATLAB. Inline size measurement of a single granule using this software have been presented in 3.9.

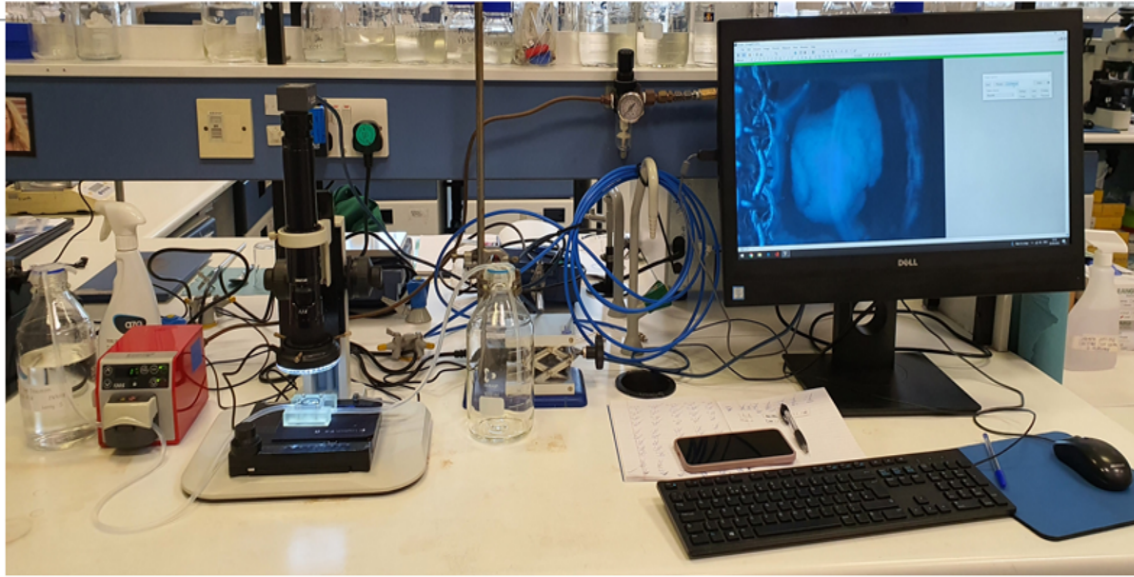


**Figure 3.6:** *The setup used for measuring the size of granules during disintegration*



**Figure 3.7:** *The GUI of the app developed for the image analysis of granules using optical microscopy*

### 3.3.7 Particle size distribution measurement of disintegrating granules

The second part of a disintegration process is breakage of granules to smaller ones. The population balance model developed in this thesis tries to model the particle size of granules during disintegration. However, to validate the model, the evolution of particle size distribu-

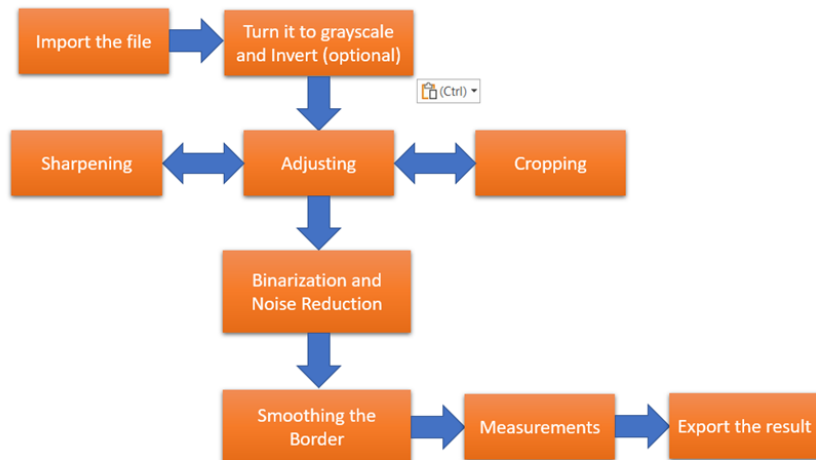


**Figure 3.8:** The flowchart of the image analysis technique used in the developed image analysis app in MATLAB

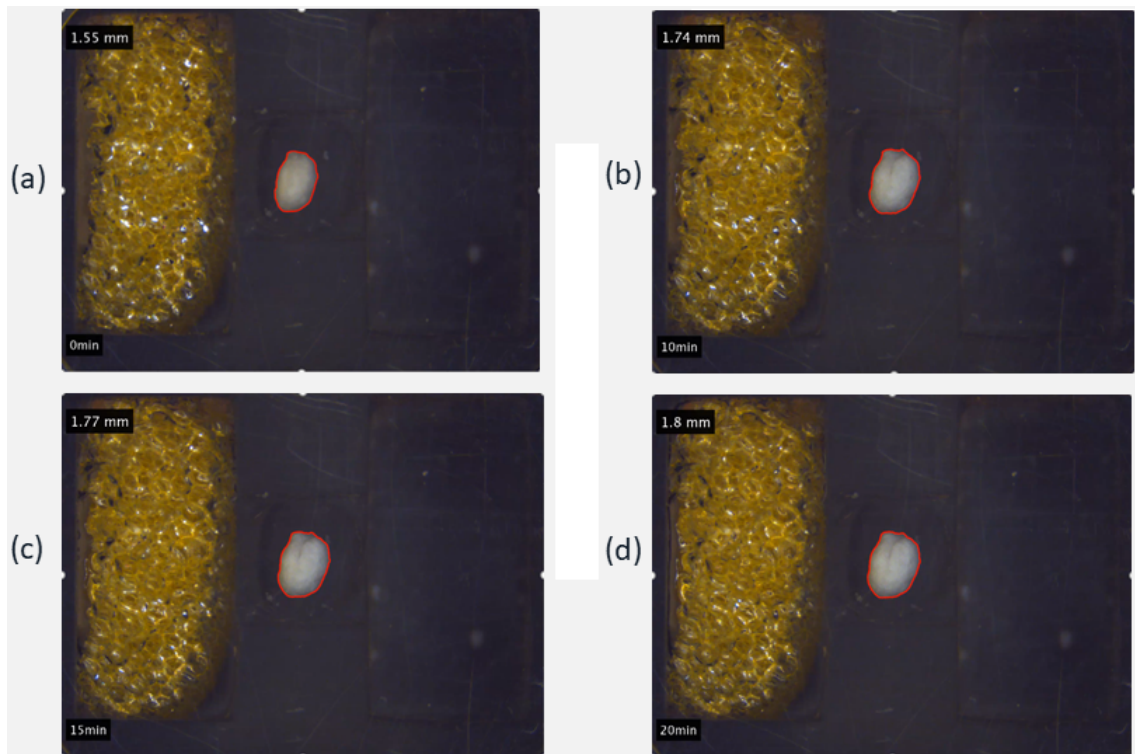


**Figure 3.9:** Size measurement of an individual granule using the developed software in MATLAB after (a) 0 minutes, (b) 10 minutes, (c) 15 minutes, (d) 20 minutes

tion of granules is needed which was done using a rather novel technique known as focused beam reflectance measurement (G400 FBRM probe). This technique employs a laser beam for quick scanning over a confined area. The beam is meticulously focused and transmitted through the sapphire window of the FBRM probe. The focused beam rotates at a constant

high speed, enabling quick scans over the granule solution (with a 1.5 %w in 400 ml at 300 rpm in Optimax) in the confined space. The rapid movement of the scanning beam minimizes the impact of granule motion on the output data. As the beam intercepts the moving granules, a series of back-scattered lights are created which are captured by a stereoscopic optics detector. Then, the system counts the number of back scattered lights. Each scattered light has a pulse time that when multiplied by the scan speed, gives a parameter known as chord length, which is essentially the distance between two sides of the projected granule when the laser has hit it (Figure 3.10). The results of this was a number-based CLD. To obtain the particle size distribution, a link must be established between the size of the granule and its chord length. If it is assumed the shape of the granule is a spheroid<sup>5</sup>, then the following relationship between normalized cumulative cord length distribution ( $\bar{C}$ ) and number-based frequency of the granule  $f_n$  (Brivadis & Sacchelli 2022) can be obtained:

$$\bar{C}(l) = \int_{R_{min}}^{R_{max}} k(l, R) f_n(R) dR \quad (3.8)$$

in which  $l$  is the chord length,  $R$  is the granule diameter and  $k(l, R)$  is a function known as a probability function which represents the likelihood of measuring a chord length shorter than  $l$  when a particle with a radius of  $R$  passes through the sensor and is defined as:

$$k(l, R) = 1 - \int_0^{2\pi} \int_0^\pi \sqrt{\text{MAX}(0, 1 - \left(\frac{l}{2R}\right)^2 \left\{ \frac{\cos^2 \phi}{\cos^2 \theta + e^2 \sin^2 \theta} + \sin^2 \phi \right\})} \frac{\sin \theta}{4\pi} d\theta d\phi \quad (3.9)$$

where  $e$  is the eccentricity of the spheroid. To obtain number-based frequency  $f_n$  from the normalized cumulative chord length distribution, an inverse problem should be performed on Eq. (3.8). In this case, the data was recorded every 30 seconds.

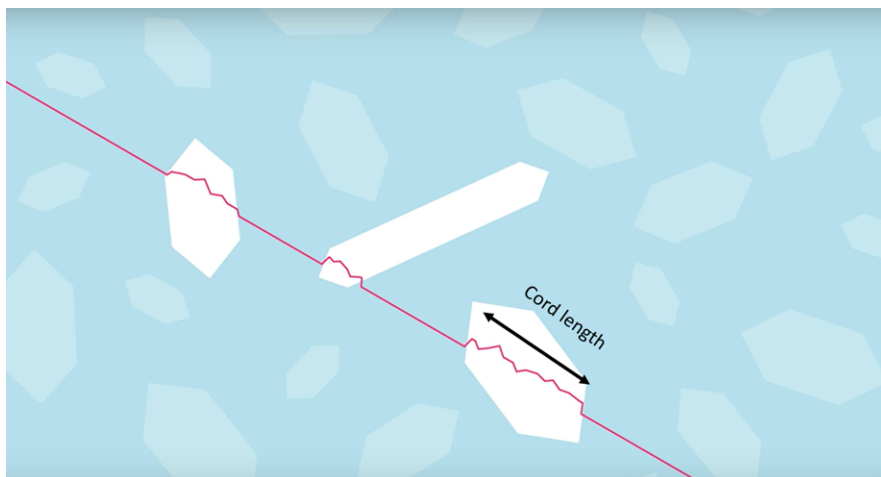


**Figure 3.10:** A schematic of the back-scattered light and the chord length in a sample hit by a FBRM laser (AutoChem 2016)

<sup>5</sup>A spheroid is an ellipsoid (a three-dimensional oval) that is symmetrical along two of its axes.

## Chapter 4

# Single granule swelling model

### 4.1 Introduction

In this chapter, the development of two mechanistic single granule swelling models has been presented. Both models are capable of predicting many attributes of a granule such as porosity, stress and size. The difference between them are the consideration of size distribution for the primary particles. Later a series of global sensitivity analysis were performed on both models to identify the most important parameters and predict their behaviour in the models.

### 4.2 Mechanistic Model Development

A typical granule designed for disintegration consists of many different components: active ingredient, disintegrants, binders and other excipients (shown in Figure 4.1 (a)). Generally, the primary objective behind the formulation of these granules is to fix ingredients in a stable, safe and easy to handle structure when dry, and to then release the active ingredients in a desired fashion on contact with liquids. The primary reason to design disintegrating granules is to increase the available surface area, leading to a faster active ingredient release in the surrounding fluid. Disintegrants are materials which absorb a large amount of water compared to their own weight on exposure to a thermodynamically compatible liquid such as water, and as a result expand and create an internal stress in the granule, eventually leading to disintegration. Another important ingredient in granules is the binder which increases the cohesive strength of the granule and consequently influences the disintegration time. To simplify this model, the modelled granule formulation would be limited to binder, disintegrant and excipient as shown in Figure 4.1 (b).

Like other porous media, the granule consists of at least three phases: the solid phase which itself can be divided into different parts depending on its constituents, the volume of the granule occupied by the penetrating liquid, and the trapped air which is slowly being pushed out of the granule. The penetrating liquid and the trapped air form the free space inside the granule, referred to as the porous phase. The ratio of the solid volume to the total volume of the granule is defined as the porosity ( $\varepsilon$ ) of the granule and is considered uniform throughout the granule through the disintegration process. The granulation process introduces variability in both porosity and primary particle sizes due to the non-uniform distribution of these features. Additionally, disintegrant particles exhibit a range of sizes and

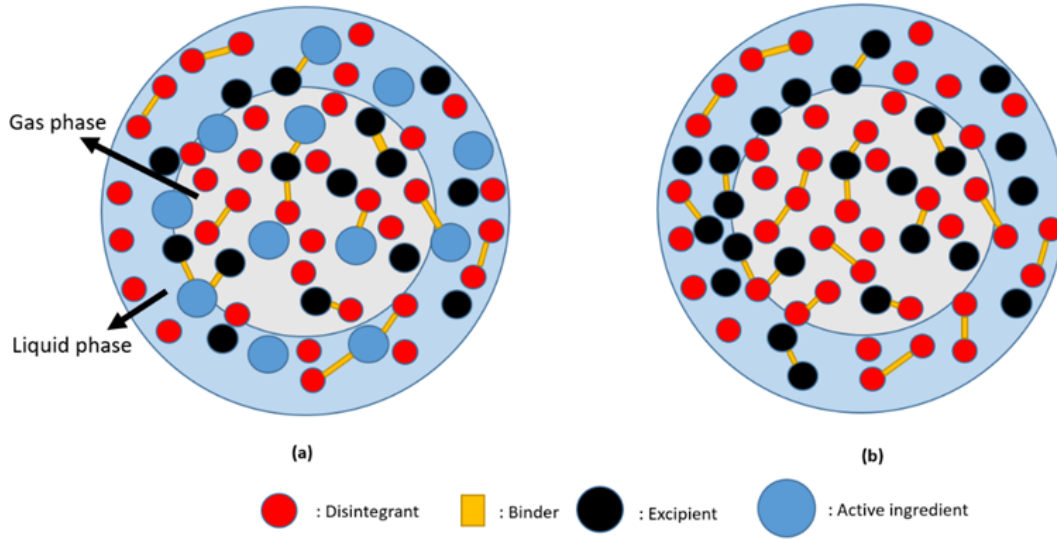


**Figure 4.1:** The schematic of (a) a typical granule with different phases, (b) the assumed granule in this work

they don't all start swelling at the same time. Consequently, one can expect a varied porosity and pore size distribution within the resulting granules. If the size of disintegrant particles ( $V_p$ ) is much smaller than the granule size ( $V$ ), then porosity can be defined by the following Eq. 4.1:

$$\varepsilon = 1 - \sum_i \frac{\partial n_{p,i}}{\partial V} V_{p,i} = 1 - \frac{\partial V_0}{\partial V} \sum_i \frac{\partial n_{p,i}}{\partial V_0} V_{p,i} \quad (4.1)$$

where  $\frac{\partial n_{p,i}}{\partial V}$  and  $\frac{\partial n_{p,i}}{\partial V_0}$  denote the distribution of disintegrant particles in the granule in the current and initial time respectively and  $\frac{\partial V_0}{\partial V}$  is the change of volume due to deformation at local level (inverse of dilation factor).

Another important characteristic parameter is the saturation ( $S$ ) which is defined as the ratio of the liquid volume to the volume of the porous phase within the granule. Just like porosity, in "real" granules this parameter would be expected to have a distribution inside the granule due to direct interference of parameters such as surface tension, contact angle and especially pore size distribution. As it would be discussed later, the saturation has a direct relationship with capillary pressure and as the capillary pressure decreases, the saturation increases. Saturation is typically obtained experimentally through measuring the moisture content, which itself is defined as the mass of the liquid to the initial mass of the solid phase. Unlike most porous media where there is only liquid penetration and no liquid absorbance by the solid phase, in granules containing swelling materials (e.g. disintegrants), the mass of the solid phase increases as a result of liquid absorbance. Therefore, in addition to considering the liquid absorbance by the solid phase (disintegrant particles), the moisture content can be

defined as the following for a granule:

$$x_l = \frac{W_l}{\sum_i W_{s,i}(t=0)} = \frac{\rho_l}{\sum_i \rho_{s,i} w_i} \frac{V}{V_0} \frac{S\varepsilon}{1 - \varepsilon_0} \quad (4.2)$$

where  $x_l$  is the moisture content,  $W_l$  is the mass of liquid in the porous phase,  $W_{s,i}$  is the mass of each constituent of the solid phase,  $\rho_{s,i}$  is the initial density of  $i^{th}$  particles,  $w_i$  is the initial mass fraction of the components in the solid phase,  $\varepsilon_0$  is the initial porosity and  $V$  and  $V_0$  are current and initial volume of the granule. The process of disintegration modelled here is a special case of a phenomenon known as the swelling porous media and is a combination of five different processes which are shown in Figure 4.2:

- i. Liquid penetration (also known as imbibition),
- ii. liquid absorbance,
- iii. swelling,
- iv. stress build-up,
- v. breakage.

The liquid penetration step is the first stage of the overall disintegration process, where the evolving penetration time is shown in Figure 4.3 and is the rate determining process in disintegration (Markl & Zeitler 2017). During liquid penetration, the thermodynamically compatible liquid penetrates into the granule's porous phase as a result of capillary force. The first step of liquid penetration is wetting where the liquid contacts dry solids in the granule. As time progresses, the volume of dry solid shrinks, until no dry primary particles remain inside the granule (Figure 4.3 (d) and (e)). The area containing the liquid where the saturation is increasing is called the unsaturated area (Figure 4.3 (b)-(d)). After a while, within the unsaturated area of the granule, the local saturation reaches its maximum value ( $S_{max}$ ) which leads to the creation of a new third area known as the saturated area (shown from Figure 4.3 (c) onward). As the liquid penetrates into the granule, part of the liquid is absorbed by the disintegrants, leading to an increase in disintegrant particle size and a decrease in the liquid phase volume. As this phenomenon progresses, this can cause the disintegrants to push other particles apart and reduce granule porosity. The swelling of disintegrant particles also leads to a deformation distribution inside the granule which causes granule expansion. All of these processes continue to occur simultaneously until the final state of a granule is reached. This state depends on the size, porosity, saturation and other factors, and can be either:

- i. The stress exceeds the strength of the granule, leading to breakage.
- ii. The case where the granules do not disintegrate as:
  - a) The swelling of disintegrant particles does not create enough stress to break the granule,
  - b) the rise of granule strength due to porosity decrease exceeds the stress increase or,

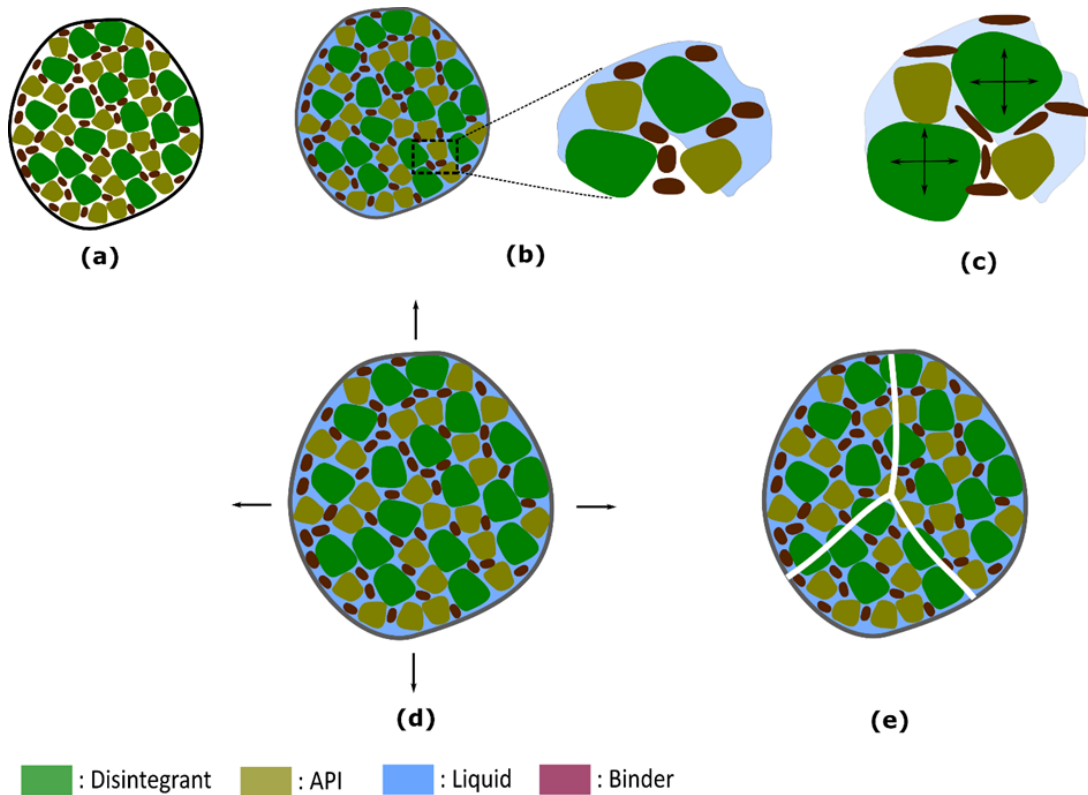


**Figure 4.2:** The processes involving in the disintegration of granules, (a) original granule, (b) liquid penetration in both macro and micro level, (c) liquid absorption, (d) Swelling (and stress build-up) and (e) breakage

- c) the porosity reduction due to rapid swelling at the surface of the granule prevents liquid penetration (effectively forming a slightly swollen granule), hindering internal stress increase and breakup. This essentially stems from the case where the ratio of permeability to porosity approaches zero as porosity approaches zero, leading to a decrease in saturation of the granule and a lack of liquid inside the granule for disintegrant particles to absorb.

The aim of the model is to incorporate all the aforementioned processes together as depicted in Figure 4.4. The model in this work consists of two separate parts. The first part describes the swelling of a single granule until breakage due to stress build-up from swelling. The second part combines this model termed as "single granule model" with a population balance model in order to obtain the particle size distribution of granules over time (Figure 4.4). The unified model is based on the assumption that each granule swells and disintegrates separately, meaning there is no interaction between different granules in the middle of the disintegration process.

#### 4.2.1 Mono-sized single granule swelling model

The mono-sized single granule swelling model is based on the physical phenomenon happening inside a disintegrating granule. The model considers the following assumptions which are

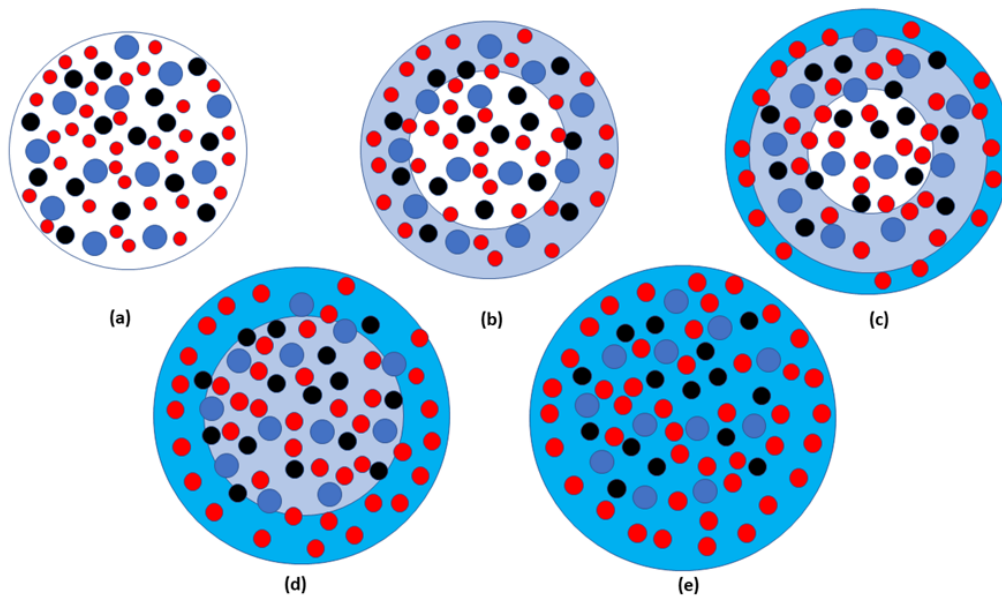


**Figure 4.3:** A diagram of liquid penetration process: a) fully dry granule, b) partly saturated partly dry granule, c) granule with saturated, unsaturated and dry areas, d) partly saturated, partly unsaturated granule, e) fully saturated granule (red: disintegrant, black: excipient, blue: active ingredient)

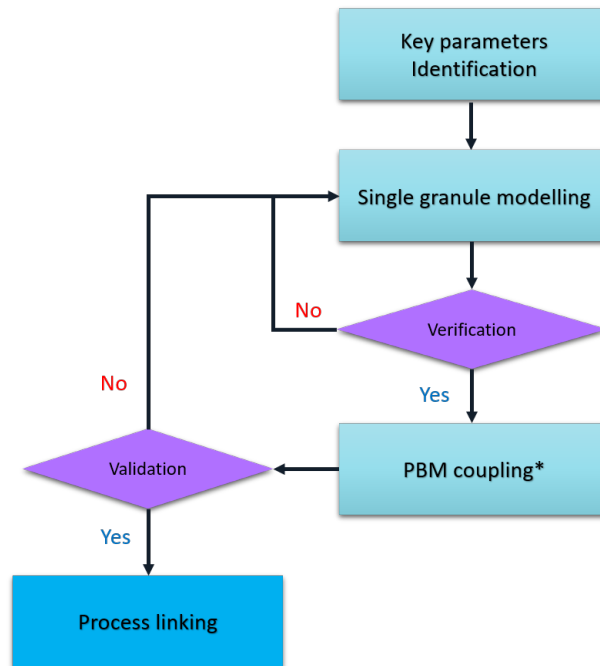


**Figure 4.4:** Flowchart of a population balance coupled product model for granule disintegration

explained in detail later on:

1. The granule comprises a one type of disintegrant, binder, and excipient.

2. Disintegrant and excipient particles alongside the granule are all spherical.
3. Primary particles shape remains constant during the disintegration.
4. Both the disintegrant and excipient particles are mono-sized.
5. The porosity and saturation are uniform throughout the granule and change only with time.
6. The diffusion of liquid into disintegrants can be described by a Fickian-like model.
7. Liquid absorption is uniform throughout the granule and is a function of time only.

The first assumption has been explained before in this chapter and does not need any more explanation. The second and third reason is self-explanatory as in almost all cases in the literature, particles are considered spherical due to simplicity it brings to PBM. The main reason for the fourth assumption is to simplify the model. If there is a distribution, then there is a need for two distributed variables to be solved which at the same time, makes the model harder to be linked with population balance equation model. The fifth assumption is really important as it states there is no (major) gradient of saturation or local porosity inside the granule, thus, these two variables can be considered uniform throughout the granule. The sixth assumption would be explained in more detail later in subsection 4.2.1.2. The seventh assumption in reality is a result of the fifth assumption, because if all primary particles inside the granule have the same situation, same porosity and saturation, then the liquid absorption would be uniform too in the granule. The formula which relates porosity to the local disintegrant particles density and their volume is shown earlier in Eq. (4.1). Assuming the distribution of all component is uniform  $\frac{\partial n_{p,i}}{\partial V} \approx \frac{n_{p,i}}{V}$  and all liquid absorbing particles start swelling at the same time, then the porosity would be uniform through the granule:

$$\varepsilon = 1 - \frac{1}{V} \sum_i n_{p,i} V_{p,i} = 1 - \frac{n_p}{V} \sum_i x_{n,i} V_{p,i} \quad (4.3)$$

where  $V$  is the volume of the granule,  $n_p$  is the total number of primary particles in the granule,  $V_{p,i}$  is the volume of  $i^{th}$  component,  $n_{p,i}$  is the number of  $i^{th}$  component particles in the granule and  $x_{n,i}$  is its number fraction ( $n_{p,i}/n_p$ ). Both  $n_p$  and  $x_{n,i}$  can be obtained via the initial properties of the granule and primary particles:

$$\begin{cases} x_{n,i} = \frac{w_i}{\rho_{s,i} V_{p,i}(0)} / \sum_i \frac{w_i}{\rho_{s,i} V_{p,i}(0)} \\ n_p = (1 - \varepsilon_0) \frac{V_0}{\sum_i x_{n,i} V_{p,i}} \end{cases} \quad (4.4)$$

in which  $V_0$ ,  $\varepsilon_0$ ,  $V_{p,i}(0)$  and  $w_i$  are the initial granule volume, initial granule porosity, initial volume of  $i^{th}$  component particle, and the initial mass fraction of that component in the solid phase. The same uniformity condition holds for saturation too. However, obtaining the saturation in the granule is considerably more complicated than for porosity. The saturation is directly related to a parameter called capillary pressure, through a function called the

retention curve. The capillary pressure is defined as the difference between the gas pressure and liquid pressure ( $P_c = P_g - P_l$ ). However, In most models dealing with porous media, the gas pressure is considered to be zero and therefore  $P_c = -P_l$ . There have been many attempts to establish a connection between liquid pressure and saturation in a mechanistic manner (Joekar-Niasar 2011, Sweijen et al. 2018, 2020) but the majority of such models are complex and computationally time-consuming, and hence not suitable for the model created here. Instead, an empirical power-law model can be used for the retention curve known as Brooks-Corey (BC) model to establish a connection between saturation and the liquid pressure in a porous media (Morel-Seytoux et al. 1996):

$$P_l = P_l^{max}(\varepsilon)\hat{S}^{-M} \quad (4.5)$$

where  $P_l^{max}$  is the maximum liquid pressure,  $M$  is a model related parameter smaller than one directly related to pore size (Morel-Seytoux et al. 1996) and  $\hat{S}$  is the local effective saturation and is defined as:

$$\hat{S} = \frac{S - S_r}{S_{max} - S_r} \quad (4.6)$$

in which  $S_{max}$  and  $S_r$  are known as the maximum and residual saturation. For the case of a granule, the average liquid pressure is preferred to be used in the BC model which is defined as:

$$\bar{P}_l = P_l^{max}\hat{S}_a^{-M} \quad (4.7)$$

where variable  $\hat{S}_a$  is the average saturation in the granule and is described by the following equation (4.8):

$$\hat{S}_a = \frac{3}{R^3} \int_0^R r^2 \hat{S}(r) dr \quad (4.8)$$

in which  $R$  is the radius of the granule. In the following sections, liquid penetration, liquid absorbance, swelling and stress build-up are explained mathematically.

#### 4.2.1.1 Liquid Penetration

The liquid penetration is generally divided into two separate parts: the penetration inside the granule and the penetration at the surface. In the granule, liquid penetration is attributed to the liquid velocity  $v_l$ . This variable can be modelled by using the well-known Darcy's model which relates the liquid velocity  $v_l$  to swelling porosity  $v_s$  and the liquid pressure  $P_l$ :

$$\varepsilon S(v_l - v_s) = -\frac{k_{per}(\varepsilon, \hat{S}, \bar{R}_p)}{\eta} \frac{\partial P_l}{\partial r} \quad (4.9)$$

The parameter  $k_{per}$  is the permeability,  $\eta$  is the liquid viscosity,  $\bar{R}_p = \left(\sqrt[3]{\frac{3}{4\pi} \sum_i x_{n,i} V_{p,i}}\right)$  is the cubic average radius of the particles in the granule and  $r$  is the distance from the centre of the granule. Permeability itself can be divided into two separate parts, the saturated permeability  $k_{sat}$  and the relative permeability  $k_{rel}$ :

$$k_{per}(\varepsilon, \hat{S}, \bar{R}_p) = k_{sat}(\varepsilon, \bar{R}_p)k_{rel}(\hat{S}) \quad (4.10)$$

The saturated permeability depends on the porosity, tortuosity  $\zeta$  and disintegrant particles radius and can be used via Carman-Kozeny equation (Berg 2014):

$$k_{sat}(\varepsilon, \bar{R}_p) = c_k \zeta^2 \frac{\varepsilon^3}{(1 - \varepsilon)^2} \bar{R}_p^2 \quad (4.11)$$

For the relative permeability, many model can be found in the literature (Purcell 1949, Mualem 1976) but the model presented by (Burdine 1953) is used because of its simplicity and mechanistic nature:

$$k_{rel}(\hat{S}) = \hat{S}^l \frac{\int_0^{\hat{S}} P_l^{-2}(\xi) d\xi}{\int_0^1 P_l^{-2}(\xi) d\xi} \quad (4.12)$$

where  $l$  is the model parameter. For the BC model, the relative permeability tends to take a power-law form, just like Brooks-Corey model itself:

$$k_{rel}(\hat{S}) = \hat{S}^{l+2M+1} \quad (4.13)$$

The swelling velocity is directly related to the deformation. Based on the eight assumptions in the model where the deformation occurs only in radial direction within the granule,  $v_s$  can be defined as the following:

$$v_s = \left( \frac{\partial r}{\partial t} \right)_{r_0} = - \left( \frac{\partial r_0}{\partial t} \right)_r / \left( \frac{\partial r_0}{\partial r} \right)_t = \left( \frac{\partial u_r}{\partial t} \right)_r / 1 - \left( \frac{\partial u_r}{\partial r} \right)_t \quad (4.14)$$

in which  $r$  is the location of an arbitrary point inside the granule at time  $t$ ,  $r_0$  is its original position at the start of the expansion and  $u_r = r - r_0$  is the radial displacement. At the same time, it is known from the mass conservation law for the liquid in the porous phase that (Diersch et al. 2010, Bear 2018) that:

$$\frac{\partial}{\partial t}(\varepsilon S) + \frac{\partial}{r^2 \partial r}(r^2 v_l \varepsilon S) = - \sum_i \frac{\partial n_{p,i}}{\partial V} \frac{\partial V_{p,i}}{\partial t} \quad (4.15)$$

The term at the right side denotes the rate of the liquid absorbed by the  $i^{th}$  component in the solid phase per volume. If the equation above is combined with the Darcy's law (Eq. (4.11)), the Lagrangian form of the mass conservation law of liquid in the porous phase can be reached:

$$\frac{\partial}{\partial t}(\varepsilon S) + \frac{\partial}{r^2 \partial r}(r^2 v_s \varepsilon S) = - \frac{\partial}{r^2 \partial r} \left( r^2 \frac{k_{per}(\varepsilon, \hat{S}, \bar{R}_p)}{\eta} \frac{\partial P_l}{\partial r} \right) - \sum_i \frac{\partial n_{p,i}}{\partial V} \frac{\partial V_{p,i}}{\partial t} \quad (4.16)$$

To solve this equation, a constitutive law for the solid phase should be presented. Such a model is capable of explaining the changes in the solid phase based on the exposed stress. By combining the mass conservation law with the constitutive law and the retention curve, variables such as displacement, saturation and porosity profile inside the granule can be obtained. However, the first issue with such model is the lack of a proper constitutive law that can explain the mechanical behaviour of a porous swelling medium such as a granule under internal stress. The second issue is the complexity of solving such equation as the final equation is highly nonlinear making its solution computationally costly compared to a

lumped model. Finally, such a model hinders us to link it to a population balance model for the disintegrating granules. To circumvent this issue, the lumped form of the equation above would be used to obtain the differential equation for the saturation in the granule (by assuming the saturation is uniform throughout the granule). The lumped form can be obtained via integrating the equation (4.16) over the whole granule. In other words:

$$4\pi \int_0^{R(t)} \left\{ \frac{\partial}{\partial t}(\varepsilon S) + \frac{\partial}{r^2 \partial r}(r^2 v_s \varepsilon S) \right\} r^2 dr = -4\pi \int_0^{R(t)} \frac{\partial}{\partial r} \left( r^2 \frac{k_{per}(\varepsilon, \hat{S}, \bar{R}_p)}{\eta} \frac{\partial P_l}{\partial r} \right) dr - \int_0^{R(t)} \frac{1}{4\pi r^2} \sum_i \frac{\partial n_{p,i}}{\partial r} \frac{dV_{p,i}}{dt} 4\pi r^2 dr \quad (4.17)$$

by using the Leibnitz integral rule and considering the boundary condition for capillary pressure at the centre of the granule ( $\lim_{r \rightarrow 0} \frac{\partial P_l}{\partial r} = 0$ ), the lumped form of the mass conservation law for the liquid in the porous phase can be obtained:

$$\frac{d}{dt} \left( \int_0^{R(t)} 4\pi \varepsilon S r^2 dr \right) = -4\pi R^2(t) \lim_{r \rightarrow R(t)} \frac{k_{per}(\varepsilon, \hat{S}, \bar{R}_p)}{\eta} \frac{\partial P_l}{\partial r} - \sum_i n_{p,i} \frac{dV_{p,i}}{dt} \quad (4.18)$$

Due to uniformity assumption of porosity throughout the granule, considering equations (4.6) and (4.13), and assuming that at the surface, the saturation is equal to one ( $S_{max} = 1$  and  $\hat{S} = 1$ ), the equation would reach its final form:

$$\frac{d}{dt}(\varepsilon S_a V(t)) = \frac{d}{dt}(V_l(t)) = 4\pi R^2(t) \frac{M k_{sat}(\varepsilon, \bar{R}_p) P_l^{max}(\varepsilon)}{\eta} \lim_{r \rightarrow R(t)} \frac{\partial \hat{S}}{\partial r} - n_p \sum_i x_{n,i} \frac{dV_{p,i}}{dt} \quad (4.19)$$

In which  $S_a$  is the average saturation in the granule. This equation tells us that the change in liquid in the porous phase is equal to the liquid entered through the surface (the first term at the right side) minus the amount of liquid being absorbed by the solid phase. A major issue with this equation is the first term at the right side containing the boundary condition ( $\lim_{r \rightarrow R(t)} \frac{\partial \hat{S}}{\partial r}$ ). In reality, as discussed earlier, the differential form of the mass conservation law has to be solved to obtain this value but as previously discussed, this method is quite difficult and not the preferred option. To overcome this challenge, it was assumed that the following form exists for the derivative of the saturation at the surface:

$$\lim_{r \rightarrow R(t)} \frac{\partial \hat{S}}{\partial r} = \frac{k(S_a)}{R(t)} (1 - \hat{S}_a) \quad (4.20)$$

where function  $k$  acts as a coefficient and depends on pore size distribution and the retention curve. Equation (4.15) has a striking resemblance to a diffusive mass transfer equation of Fickian nature; however, saturation has replaced the concentration in the equation.

#### 4.2.1.1.1 Estimating the change in saturation near the surface of the granule

As mentioned earlier, the real value of  $\lim_{r \rightarrow R(t)} \frac{\partial \hat{S}}{\partial r}$  can be achieved by combining constitutive law (Eq. (4.16)) with the retention curve (Eq. (4.14)). However, by some assumption it can be estimated this variable if the following set of conditions are met:

1. The imbibition rate would be considerably faster than the absorption rate:

$$-\frac{\partial}{r^2 \partial r} \left( r^2 \frac{k_{per}(\varepsilon, \hat{S}, \bar{R}_p)}{\eta} \frac{\partial P_l}{\partial r} \right) \gg \sum_i \frac{\partial n_{p,i}}{\partial V} \frac{\partial V_{p,i}}{\partial t} \quad (4.21)$$

2. There would no significant change in the porosity and size:

$$\begin{cases} \frac{d\varepsilon}{dt} \approx 0 \implies \varepsilon \approx \varepsilon_0 \\ \frac{dV}{dt} \approx 0 \implies R \approx R_0 \end{cases} \quad (4.22)$$

Based on these assumptions, the differential form of mass conservation law would turn into the following form:

$$\frac{\partial S}{\partial t} = \frac{k_{sat}(\varepsilon_0, \bar{R}_{p,0})}{\varepsilon_0 \eta} \frac{\partial}{r^2 \partial r} \left( -r^2 k_{rel}(\hat{S}) \frac{\partial P_l}{\partial r} \right) \quad (4.23)$$

by considering Eq. (4.5) for the capillary pressure and Eq. (4.13) for the relative permeability, and changing the variable from  $r$  to  $r_c = r/R_0$ , the following differential equation for saturation would be reached:

$$\begin{aligned} \frac{\partial \hat{S}}{\partial t} = \frac{k_{sat}(\varepsilon_0, \bar{R}_{p,0}) P_l^{max}(\varepsilon_0)}{\varepsilon_0 R_0^2 \eta (1 - S_r)} \frac{\partial}{r_c^2 \partial r_c} \left( r_c^2 \hat{S}^n \frac{\partial \hat{S}}{\partial r_c} \right) = \\ \frac{k_{sat}(\varepsilon_0, \bar{R}_{p,0}) P_l^{max}(\varepsilon_0)}{\varepsilon_0 R_0^2 \eta (1 - S_r)(n+1)} \frac{\partial}{r_c^2 \partial r_c} \left( r_c^2 \frac{\partial \hat{S}^{n+1}}{\partial r_c} \right) \end{aligned} \quad (4.24)$$

where  $n$  is equal to  $M + l$ . Another interesting fact about the above equation is that the coefficient for the differential equation at the right side has an time inverse dimension which can be related to a parameter designated as the imbibition inherent time  $\tau_{sat}$ . This parameter tells us how fast the liquid is penetrating into the porous phase and can be representative of the imbibition (when it is compared to the absorption rate) and is proportional to:

$$\tau_{sat} \propto \frac{\varepsilon_0 R_0^2 \eta (1 - S_r)(n+1)}{k_{sat}(\varepsilon_0, \bar{R}_{p,0}) P_l^{max}(\varepsilon_0)} \quad (4.25)$$

If the time would be normalized in Eq. (4.24) based on the coefficient in the right side ( $t_c = \frac{k_{sat}(\varepsilon_0, \bar{R}_{p,0}) P_l^{max}(\varepsilon_0)}{\varepsilon_0 R_0^2 \eta (1 - S_r)(n+1)} t$ ), the final form of the equation would be achieved:

$$\frac{\partial \hat{S}}{\partial t_c} = \frac{\partial}{r_c^2 \partial r_c} \left( r_c^2 \frac{\partial \hat{S}^{n+1}}{\partial r_c} \right) \quad (4.26)$$

the boundary and initial conditions for the equation above are:

$$\begin{cases} \hat{S} = 1, & r_c = 1 \\ \frac{\partial \hat{S}}{\partial r_c} = 0, & r_c = 0 \\ \hat{S} = 0, & t_c = 0 \end{cases} \quad (4.27)$$

Given the equation is nonlinear, then it should be solved numerically. Finite volume method (FVM) was used to solve the equation in MATLAB, as presented in Appendix A. The result showed us that the function has the following form:

$$\lim_{r_c \rightarrow 1} \frac{\partial \hat{S}}{\partial r_c} = \frac{a \hat{S}}{\hat{S} + \alpha} (1 - \hat{S}_a) \quad (4.28)$$

where  $a$  and  $\alpha$  are functions of parameter  $n (= M + l + 1)$ . A typical calculation of  $\lim_{r_c \rightarrow 1} \frac{\partial \hat{S}}{\partial r_c}$  by the differential equation and the fitted model is shown in the Figure 4.5. The model was performed for the values of  $n$  between 0 and 4 and it was found out the model works well in that range as the coefficient of determination ( $R^2$ ) never dropped below 0.98. If Eq. (4.28) was used in Eq. (4.19), the following form of the lumped form of the mass conservation law can be obtained:

$$\frac{d}{dt}(\varepsilon S_a V(t)) = \frac{d}{dt}(V_l(t)) = 4\pi R(t) \frac{a M k_{sat}(\varepsilon, \bar{R}_p) P_l^{max}(\varepsilon)}{\eta} \frac{1 - \hat{S}_a}{\hat{S}_a + \alpha} - n_p \sum_i x_{n,i} \frac{dV_{p,i}}{dt} \quad (4.29)$$

The last step before the obtaining the final form of the mass conservation law of the liquid is

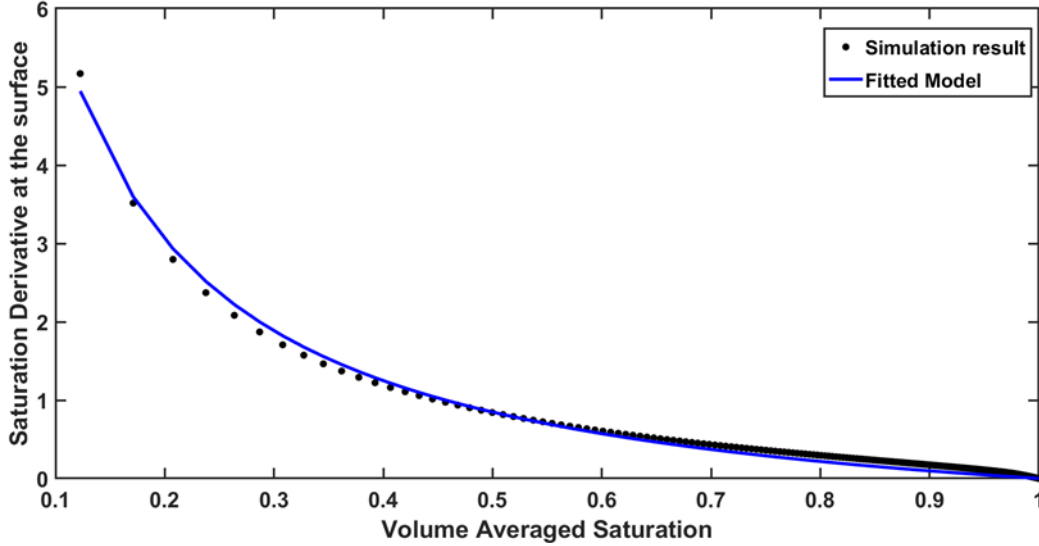


**Figure 4.5:** The calculated values of  $\lim_{r_c \rightarrow 1} \frac{\partial \hat{S}}{\partial r_c}$  based on the simulation data obtained from equation (4.26) and the fitted model to those data based on equation (4.28) for  $n$  equal to 3

to choose proper models for the terms  $P_l^{max}$  and  $k_{sat}$ . As it was described at the beginning of the chapter, one of the widely used models for the saturated permeability is the Carman-Kozeny equation which also has a solid theoretical background. The term intended to be used for  $P_l^{max}$  is based on a theoretical model presented by (Boyle et al. 2005) for the liquid penetration into silica agglomerates:

$$P_l^{max}(\varepsilon) = \frac{3(1 - \varepsilon)\gamma_{lv} \cos \theta}{\varepsilon \bar{R}_p} \quad (4.30)$$

where  $\gamma_{lv}$  is the surface tension between liquid and air and  $\theta$  is the contact angle. By putting both these models into Eq. (4.29), the last form of mass conservation law can be obtained:

$$\frac{d}{dt}(\varepsilon S_a V(t)) = 2\pi R^3(t) \varepsilon \frac{6aM\gamma_{lv}c_k\zeta^2 \cos\theta \bar{R}_p}{\eta R^2(t)} \frac{\varepsilon}{1 - \varepsilon} \frac{1 - \hat{S}_a}{\hat{S}_a + \alpha} - n_p \sum_i x_{n,i} \frac{dV_{p,i}}{dt} \quad (4.31)$$

The main reason for this form is to extract a form that would be easily to use. If the term  $\frac{6aM\gamma_{lv}c_k\zeta^2 \cos\theta \bar{R}_p}{\eta R^2(t)} \frac{1 - \varepsilon}{\varepsilon}$  would be designated as the imbibition inherent time ( $\tau_{sat}$ ), then the final form would be achieved:

$$\frac{d}{dt}(\varepsilon SV(t)) = \frac{3}{2} \frac{\varepsilon V(t)}{\tau_{sat}(\varepsilon, R, \bar{R}_p)} \frac{1 - \hat{S}_a}{\hat{S}_a + \alpha} - n_p \sum_i x_{n,i} \frac{dV_{p,i}}{dt} \quad (4.32)$$

The main reasons in turning equation (4.31) to the form above are:

- To decrease the number of parameters as all the terms can be morphed into one variable.
- To make the comparison between absorption and imbibition easier.
- To make the form simpler, both mathematically and programmatically.

The first reason is quite straightforward. All the parameters in imbibition inherent time, can be morphed into one parameter known as initial imbibition time. In other words:

$$\tau_{sat,0} = \frac{\eta R_0^2}{6aM\gamma_{lv}c_k\zeta^2 \cos\theta \bar{R}_{p,0}} \frac{1 - \varepsilon_0}{\varepsilon_0} \quad (4.33)$$

which after utilizing Eq. (4.4), the imbibition inherent time would turn into:

$$\tau_{sat} = \tau_{sat,0} \frac{R^2}{R_0^2} \frac{\bar{R}_{p,0}}{\bar{R}_p} \frac{1 - \varepsilon}{1 - \varepsilon_0} \frac{\varepsilon_0}{\varepsilon} = \tau_{sat,0} \frac{\bar{R}_{p,0}}{\bar{R}_{p,0}} \frac{\varepsilon_0}{\varepsilon} \sqrt[3]{\frac{1 - \varepsilon}{1 - \varepsilon_0}} \quad (4.34)$$

Based on equations (4.32) and (4.34), the number of needed parameters has been lowered from seven to one ( $\tau_{sat,0}$ ), eliminating many parameters that are needed any more. This can make the fitting to the experimental data much easier as many of those parameters cannot be obtained or it is hard to estimate them. As it will be discussed later, the initial imbibition inherent time can also be compared with an inherent absorption time for the solid components to determine the dominant mechanism in swelling.

#### 4.2.1.2 Liquid absorbance

As mentioned in the model assumptions, the disintegrant particles absorb the liquid through diffusion. There are different models that could describe the absorption of the liquid by the disintegrants however, many of them are quite complex and computationally costly (Hui & Muralidharan 2005, Hong et al. 2008). Instead, a series of model equations, listed in Table 4.1, have been considered which are relatively simpler and predict the volume increase of the disintegrants particles over time as necessary for the model. In the table,  $R_p$  is the size of particle at the current time and  $R_{p,0}$  and  $R_{p,m}$  are its initial and maximum value

**Table 4.1:** Equations describing the swelling of individual spherical super absorbent polymers (Sweijen, van Duijn & Hassanizadeh 2017)

Equations	References
$\frac{R_p}{R_{p,0}} - 1 = \left( \frac{R_{p,m}}{R_{p,0}} - 1 \right) \left( 1 - \exp \left( -\frac{Dt}{R_{p,0}^2} \right) \right)$	(Omidian et al. 1998)
$\frac{dQ^{abs}}{dt} = \frac{\pi^2 D}{R_{p,0}^2} (Q^{max} - Q^{abs})$	(Buchholz et al. 1998)
$\frac{dR_p}{dt} = \frac{D \rho_s}{R_p \rho_l} \frac{Q^{max} - Q^{abs}}{Q^{abs}}$	(Sweijen, Chareyre, Hassanizadeh & Karadimitriou 2017)
$\frac{\partial c_l}{\partial t} = \frac{D}{r^2} \frac{\partial}{\partial r} \left( r^2 \frac{\partial c_l}{\partial r} \right), \frac{d}{dt} \left\{ \int_0^{R_p(t)} r^2 (1 - c_l) dr \right\} = 0$	(Sweijen, van Duijn & Hassanizadeh 2017)

respectively.  $D$  is the diffusivity of the liquid into the disintegrant particles,  $\rho_s$  is the density of dry disintegrant,  $\rho_l$  is the liquid density,  $r$  is the distance from the centre of disintegrant particle and  $c_l$  is the concentration of liquid inside the particle,  $Q^{abs} (= \frac{\rho_l}{\rho_s} (\frac{R_p^3}{R_{p,0}^3} - 1) + 1)$  is the mass absorption ratio of the particles and  $Q^{max}$  is its maximum value. According to (Sweijen, van Duijn & Hassanizadeh 2017), all these models can predict the evolution of polymer gel radius but may give different diffusivities. In this work, the third model in Table 4.1, first proposed by (Sweijen, Chareyre, Hassanizadeh & Karadimitriou 2017), is used. Based on the study done by (Soundaranathan et al. 2020), this model performs well with disintegrants such as MCC, SSG or CCS. However, according to (Diersch et al. 2010) and (Sweijen et al. 2020), the saturation level can affect the diffusion rate, and therefore a new saturation related term should be added to the differential equation. The revised form of third equation in Table 4.1 is:

$$\frac{dR_{p,i}}{dt} = f(\hat{S}_a) \frac{D_i}{R_{p,i}} \frac{\rho_{s,i}}{\rho_l} \frac{Q_i^{max} - Q_i^{abs}}{Q_i^{abs}} \quad (4.35)$$

where  $f(\hat{S}_a)$  is the ratio of the area of disintegrant particle covered by the liquid to the total surface area and is between 0 and 1.  $f(\hat{S}_a)$  is very similar to the single particle coating number  $\phi_p$ , developed for use in fluidised bed granulation (Kariuki et al. 2013). Based on the assumption that the ratio of the filled volume of a pore to its specific surface is related to the pore's radius and that capillary pressure (or the liquid pressure) is proportional to the inverse of pore radius, (Diersch et al. 2010) proposed the following equation for  $f(\hat{S}_a)$ :

$$f(\hat{S}_a) = \frac{\int_0^{\hat{S}_a} P_l(\xi) d\xi}{\int_0^1 P_l(\xi) d\xi} \quad (4.36)$$

which for the Brooks-Corey model, would turn into the following form:

$$f(\hat{S}_a) = \hat{S}_a^{1-M} \quad (4.37)$$

However, as it is theorised by (Sweijen et al. 2018) and reported by (Diersch et al. 2011), the liquid does not sit on top of a primary particle after penetrating in a pore. At first, it fills the edges and corners of a pore and after exceeding a certain saturation threshold, designated here as  $\hat{S}_{thr}$ , the liquid begins to sit on top of the primary particles. Therefore, after normalizing the equation based on this parameter, function  $f(\hat{S}_a)$  would takes its final form:

$$f(\hat{S}_a) = \left( MAX(0, \frac{\hat{S}_a - \hat{S}_{thr}}{1 - \hat{S}_{thr}}) \right)^{1-M} \quad (4.38)$$

It is worth noting that Eq. (4.35) can be written in a similar fashion to Eq. (4.32) which can be done by introducing a parameter known as inherent absorption time which is defined as:

$$\tau_{abs,i} = \frac{R_{p,i}^2}{D} \quad (4.39)$$

and the Eq. (4.39) would turn into:

$$\frac{dR_{p,i}}{dt} = f(\hat{S}_a) \frac{R_{p,i}}{\tau_{abs,i}} \frac{\rho_{s,i}}{\rho_l} \frac{Q_i^{max} - Q_i^{abs}}{Q_i^{abs}} \quad (4.40)$$

The inherent absorption time acts as a criterion for the absorption rate. If it has a high value, the absorption would be slow and if it is low, the absorption would be fast.

#### 4.2.1.3 Swelling

As it is known, the liquid absorbance by primary particles leads to an increase in their volume. This expansion between neighbouring particles can cause stress which in macroscopic scale can lead to deformation in the granule. To know the deformation and its distribution in the granule, there is a need for a model that could relate the stress to the properties of the granule, mainly displacement and porosity. Such a model is called constitutive law of the solid body. Then the stress can be related to the capillary pressure through equation of motion in the solid and to saturation through the mass conservation law of the liquid in the porous phase. However, there are few challenges associated with this type of model. First, there is an inherent problem to connect between constitutive law and fluid motion as one is written mostly in terms of principal stresses and the other one based on its spatial stress. Second, incorporating the model would lead to a very complex set of differential equations that are computationally costly to solve. Moreover, there is a lack of proper constitutive law for granules in the literature. At the same time, such a model introduces many more parameters that are hard to quantify. Furthermore, the model may not be useful for the whole range of deformation, as some granules may show non-linear elastic behaviour while others may show plastic behaviour (Diersch et al. 2011, Braile et al. 2022). Finally, such a model can limit us greatly when trying to expand the single granule swelling model to the population balance model.

To address this issue, (Diersch et al. 2011) have suggested to use an empirical law to relate porosity to a deformation or absorption variable such as dilation factor or mass absorption ratio and that is the approach taken in this work. The equation presented here is based on the type of behaviour simulated in other works such as (Diersch et al. 2011, Braile et al.

2022, Soundaranathan et al. 2023). The model relates the porosity to mass absorption ratio of primary particles in the granule, as shown below:

$$\frac{\varepsilon - \varepsilon_0}{\varepsilon_\infty - \varepsilon_0} = \frac{\varepsilon - \varepsilon_0}{\Delta\varepsilon_\infty} = 1 - (1 - \hat{m}_s)^\beta \quad (4.41)$$

in which,  $\varepsilon_\infty$  is the final porosity,  $\Delta\varepsilon_\infty$  is the difference between final and initial porosity, called porosity difference at infinite,  $\beta$  is a fitting parameter in the model and  $\hat{m}_s$  is a variable known as the normalized load ratio and is defined as:

$$\hat{m}_s = \frac{\sum_i w_i (Q^{abs} - 1)}{\sum_i w_i (Q^{max} - 1)} \quad (4.42)$$

in which  $w_i$  is the initial mass fraction of the  $i^{th}$  primary particles.

#### 4.2.1.4 Strength

Stress and Strength of a granule are the most important criteria in the swelling driven disintegration. This is because as the disintegrant particles start to swell. They push back each other which eventually leads to collapse of the pore wall around them. At the same time, the solid bridges holding the particles together goes through a deformation which eventually leads to its breakage. All these events would lower granule strength (Soundaranathan et al. 2023). At the same time, as the swelling progresses, the particles contact force would increase leading to an increase in internal stress. This process keeps going until the internal stress of the granule exceeds the strength of the granule. This is what designated as the onset of the disintegration process and the release of the primary particles into surrounding fluids.

To model, the strength of the granules, at least three forces should be considered. First, the solid bridge created from the crystallisation of the binder. Second, the liquid bridging from the liquid penetrating inside the granule. Finally, the van der Waals forces between primary particles.

##### 4.2.1.4.1 Solid bridges

The cohesive force created by binders,  $F_{bin}$ , can be described as the following (Bika et al. 2005):

$$F_{bin} = \pi r_{sb}^2 \sigma_{sb} \quad (4.43)$$

where  $\sigma_{sb}$  is the strength of the binder (solid) bridge and  $r_{sb}$  is the radius of neck of the bridge which can be related to liquid to solid mass ratio ( $L/S$ ) and the solid concentration  $C_L$ :

$$\frac{r_{sb}}{R_p} = b \left( \frac{4\pi}{3} C_L \times L/S \right)^c \quad (4.44)$$

Where  $\bar{R}_p$  is the average size of primary particles and parameters  $b$  and  $c$  are fitting parameters depending on the particle-to-particle distance.  $L/S$  and  $C_L$  are also defined as:

$$\begin{cases} L/S = \frac{\rho_b V_b}{\sum_i \rho_{s,i} x_{n,i} V_{p,i}(0)} \\ C_L = \frac{C_b}{\rho_b} \end{cases} \quad (4.45)$$

where  $\rho_b$ ,  $V_b$  and  $C_b$  are the density, volume, and concentration of the binder respectively.

#### 4.2.1.4.2 Liquid bridging

According to (Pierrat & Caram 1997), the force stemming from the liquid bridging comes from two sources. The first is due to the surface tension of the liquid at the liquid-particle contact line and the second one is due to the curvature of the liquid bridge leading to a pressure difference across the surface. The sum of these contributing forces gives the following expression:

$$F_{cap} = 2\pi\gamma\bar{R}_p A(S) \left[ \sin\beta \sin(\beta + \theta) + \frac{\sin\beta}{4} \left( \frac{1}{r^*} - \frac{1}{h^*} \right) \right] \quad (4.46)$$

in which  $\gamma$  is the surface tension,  $\beta$  is the filling angle a variable dependent on the moisture content,  $\theta$  is the contact angle and  $r^*$  and  $h^*$  are the dimensionless radii that are defined as:

$$\begin{cases} r^* = \frac{1 - \cos\beta + \frac{a}{2\bar{R}_p}}{2\cos(\beta + \theta)} \\ h^* = \frac{\sin\beta}{2} + r^* [\sin(\beta + \theta) - 1] \end{cases} \quad (4.47)$$

Parameter  $a$  is the distance between primary particles and  $A$  is a function dependent on saturation and varies between values of 2 and 8 (Pierrat & Caram 1997, Litster 2016).

#### 4.2.1.4.3 van der Waals forces

This force is conventionally weaker than the other two forces but for the sake of accuracy, it is mentioned in this work. According to (Wollborn et al. 2017), the van der Waals force for a granule containing liquid is:

$$F_{waals} = \frac{H_{sol-liq}\bar{R}_p}{12a^2} \left\{ 1 - \left( 1 + (1 - \cos\beta) \frac{\bar{R}_p}{a} \right)^{-2} \right\} \quad (4.48)$$

where  $H_{sol-liq}$  is the Hamaker constant between liquid and solid,  $a$  is the distance between primary particles and  $\beta$  is the filling angle. The total cohesive force is the sum of the mentioned forces:

$$F_t = F_{bin} + F_{cap} + F_{waals} \quad (4.49)$$

While all these models are useful at estimating the strength of the granules but an issue arising from them is their simplistic nature which leads to their deviation from the true values of the strength in the granules. Another issue is the parameters introduced in the model. Some of these parameters are very hard to estimate as isolating the type of force

and measuring the granules strength would be almost impossible, which means there is a necessity for simplification. First, based on the suggestion by (Pierrat & Caram 1997, Bika et al. 2001), it was decided that for the granule strength, an empirical of the following form would be used:

$$\sigma_c = az(\varepsilon)\bar{R}_p^m \quad (4.50)$$

where  $\sigma_c$  is the strength of the granule,  $z(\varepsilon)$  is a porosity dependent function and  $a$  and  $m$  are fitting parameters. For example, from the literature, it is known that function  $z$  can take the form of Rumpf model  $\frac{9(1-\varepsilon)}{8\varepsilon}$  or the Kendall model  $13.3(1-\varepsilon)^4$ . In the case of granules that are dominated by non-dissolving solid bridges, based on the theory proposed by (Bika et al. 2005) at the solid bridges section, parameter  $m$  would be equal  $-6c$ . As the data would show later, the disintegration efficiency of granules is lowered due to the impact of the binder in the granule. Therefore, it was decided to just consider the solid bridging in the granules. As stated by (Rumpf 1962), in large granules, the strength of the granules is dominated by solid bridges. This is supported by experimental observation of disintegration of single granules in this work as there is a significant resistance to breakage in the observation. Based on this assumption, it can be deduced that:

$$\sigma_c = \sigma_{c,0}(L/S, C_L) \frac{z(\varepsilon)}{z(\varepsilon_0)} \left( \frac{\bar{R}_p}{\bar{R}_{p,0}} \right)^m \quad (4.51)$$

where  $\sigma_{c,0}$  is the initial strength of the granule and a function of liquid to solid ratio and binder concentration in the solution. In this work, the Kendall model is used to estimate the strength of the granule as this model considers heterogeneity between particle contact and therefore gives a lower value than Rumpf model which tends to overestimate the granule strength (Pierrat & Caram 1997, Litster 2016).

#### 4.2.1.5 Stress

In a series of paper, (Colombo et al. 1984, Caramella et al. 1988, Colombo et al. 1988, Peppas et al. 1989, Caramella et al. 1990), first empirically and then theoretically, through inventing a new equipment that could measure the stress of swelling tablets, managed to present a robust model for the disintegration force in tablets. It was found that the stress obeys from Avrami model (which was created for the crystallization) and has a cumulative Weibull distribution with respect to time. However, such model, while useful, cannot be used for this case because of its limitation. As it is known, in lumped form of population balance equation, all parameters are averaged in a size interval and therefore the created particles have lower stress than the one predicted from the model. To counter that, the stress should be defined as the function of inherent granule properties such as porosity and mass absorption ratio. To address this, (Peppas & Colombo 1989) proposed a theoretical model for the stress of disintegrating tablets that uses mass absorption instead of time as the input:

$$\sigma_{str} = MAX(0, \sigma_0 + \sigma_w + \sigma_{abs}) \quad (4.52)$$

in which  $\sigma_{str}$  is the internal stress of the tablet,  $\sigma_w$  is a negative stress induced by the wicking into the tablet,  $\sigma_{abs}$  is the positive stress produced by the liquid absorption and  $\sigma_0$  is a term originated from the residual stress. The process of filling the pores and subsequently

compressing the polymer structure results in a wicking stress, that is proportional to the absorbance ratio (total absorption ratio minus 1). This is because it characterizes a convective process. The absorption related stress, due to the diffusive nature of absorption, is proportional to the square root of absorbance ratio. Therefore:

$$\sigma_{str} = MAX(0, C_0 + C_{dif} \left( \sum_i w_i (Q_i^{abs} - 1) \right) + C_{conv} \sqrt{\sum_i w_i (Q_i^{abs} - 1)}) \quad (4.53)$$

where  $C_{conv}$  and  $C_{dif}$  are the proportionality constant for wicking and absorption stresses. If it is assumed the value  $C_0$  is zero, as unlinked tablets, there is almost no residual stress in the granule, then the equation can be reformed to the following form:

$$\sigma_{str} = MAX \left( 0, \sigma_{str}^{max} \left\{ 1 - \left( \frac{\sqrt{\hat{m}_s} - \sqrt{\hat{m}_{s,thr}}}{1 - \sqrt{\hat{m}_{s,thr}}} \right)^2 \right\} \right) \quad (4.54)$$

where  $\sigma_{str}^{max}$  is defined as the maximum stress of the tablet and  $\hat{m}_s$  is the normalized threshold load ratio where the internal stress in tablet starts increasing. Unfortunately, it seems this model cannot show the stress behaviour of the granule accurately, as it is shown in the data provided by them, the stress rises almost linearly at the beginning. In their model, the linearity goes away quickly compared to the data provided. This means the dependency of parameters like  $C_{dif}$  and especially  $C_{conv}$  on the absorbance ratio. To ratify this issue, it is assumed that the stress with respect to time obeys a Weibull distribution, as stated by (Caramella et al. 1988):

$$\sigma_{str} = \sigma_{str}^{max} \left( 1 - \exp(-kt^n) \right) \quad (4.55)$$

where  $k$  and  $n$  are the parameters of the model. If it is assumed that:

$$\ln(1 - \hat{m}_s) \sim -t^n \quad (4.56)$$

by considering the fact that stress has an absorbance ratio threshold to start, the equation (4.56) can be rearranged to this final form:

$$\sigma_{str} = \sigma_{str}^{max} \left( 1 - MAX \left( 0, \frac{\hat{m}_s - \hat{m}_{s,thr}}{1 - \hat{m}_{s,thr}} \right)^\vartheta \right) \quad (4.57)$$

where  $\vartheta$  is a structural parameter. As it can be seen, there is a similarity between equation (4.57) and equation (4.41). This is no coincidence as both these important variables are intertwined and are affected heavily by the medium's microstructure. What matters to us is not just the stress or the strength individually, but rather the ratio between them. This ratio determines when disintegration begins and, as observed later, the rate at which granules break. The ratio then would be :

$$\frac{\sigma_{str}}{\sigma_c} = \frac{\sigma_{str}^{max}}{\sigma_{c,0}(L/S, C_L)} \left( \frac{1 - \varepsilon}{1 - \varepsilon_0} \right)^4 \left( \frac{\bar{R}_p}{\bar{R}_{p,0}} \right)^{6c} \left\{ 1 - MAX \left( 0, \frac{\hat{m}_s - \hat{m}_{s,thr}}{1 - \hat{m}_{s,thr}} \right)^\vartheta \right\} \quad (4.58)$$

Table 4.2 summarises the main equations in mono-disperse single granule swelling model.

**Table 4.2:** The equations needed for solving mono-sized single granule swelling model

Equation	Initial condition
$V = \frac{n_p}{1 - \varepsilon} \sum_i x_{n,i} V_{p,i}$	$R = R_0$
$x_{n,i} = \frac{w_i}{\rho_{s,i} V_{p,i}(0)} / \sum_i \frac{w_i}{\rho_{s,i} V_{p,i}(0)}$	-
$n_p = (1 - \varepsilon_0) \frac{V_0}{\sum_i x_{n,i} V_{p,i}}$	-
$\frac{d}{dt}(\varepsilon S_a V(t)) = \frac{3}{2} \frac{\varepsilon V(t)}{\tau_{sat}(\varepsilon, R, \bar{R}_p)} \frac{1 - \hat{S}}{\hat{S} + \alpha} - n_p \sum_i x_{n,i} \frac{dV_{p,i}}{dt}$	$S_a = 0$
$\tau_{sat} = \tau_{sat,0} \frac{\bar{R}_p}{\bar{R}_{p,0}} \frac{\varepsilon_0}{\varepsilon} \sqrt[3]{\frac{1 - \varepsilon}{1 - \varepsilon_0}}$	-
$\frac{dR_{p,i}}{dt} = f(\hat{S}_a) \frac{D_i}{R_{p,i}} \frac{\rho_{s,i}}{\rho_l} \frac{Q_i^{max} - Q_i^{abs}}{Q_i^{abs}}$	$R_{p,i} = R_{p,i}(0)$
$f(\hat{S}_a) = \left( \text{MAX}(0, \frac{\hat{S}_a - \hat{S}_{thr}}{1 - \hat{S}_{thr}}) \right)^{1-M}$	-
$Q_i^{abs} = \frac{\rho_l}{\rho_{s,i}} \left( \frac{R_{p,i}^3}{R_{p,i}^3(0)} - 1 \right) + 1$	-
$\frac{\varepsilon - \varepsilon_0}{\Delta\varepsilon_\infty} = 1 - (1 - \hat{m}_s)^\beta$	$\varepsilon = \varepsilon_0$
$\hat{m}_s = \frac{\sum_i w_i (Q^{abs} - 1)}{\sum_i w_i (Q^{max} - 1)}$	-
$\frac{\sigma_{str}}{\sigma_c} = \frac{\sigma_{str}^{max}}{\sigma_{c,0}(L/S, C_L)} \left( \frac{1 - \varepsilon}{1 - \varepsilon_0} \right)^4 \left( \frac{\bar{R}_p}{\bar{R}_{p,0}} \right)^{6c} \left\{ 1 - \text{MAX}\left(0, \frac{\hat{m}_s - \hat{m}_{s,thr}}{1 - \hat{m}_{s,thr}}\right)^\vartheta \right\}$	-

### 4.2.2 Distributed single granule swelling model

As it is known, the primary particles of the same type in the granules do not have the same size and in reality, there is a size distribution of primary particles in the granule. Therefore, there is a necessity to consider the distribution in the swelling model of the granule. However, some equations must change to consider the impact of the primary particles size distribution. Moreover, due to liquid absorption the distribution changes which in turn affects the other parameter such as porosity or volumetric averaged radius. Given, the size and distribution are involved, then population balance equation (PBE) shall be used. PBM is discussed in detail in the Chapter 6 but in this chapter, it is mentioned briefly to formulate the change in distribution. PBM deals with changes in particle distribution of a disperse phase when the distribution is a function of variables such as particle size. In general, there are four mechanisms in PBM; breakage, aggregation, growth and nucleation. Of all these mechanisms, the only one happening in swelling of a single granule is growth where particles through liquid absorption, increase their size. Based on this fact, the population balance equation for the primary particles in the granule is:

$$\frac{\partial n_i(r, t)}{\partial t} = -\frac{\partial(G_i(r, t)n_i(r, t))}{\partial r} \quad (4.59)$$

where  $r$ ,  $n_i$  and  $G_i$  are the size variable, density function and growth term of  $i^{th}$  component in the solid phase. The growth term denotes the change in particle size with respect to time ( $\partial r/\partial t$ ). Therefore, the term can be described by the liquid absorption rate in Eq. (4.35):

$$G_i(r, t) = f(\hat{S}_a) \frac{D_i \rho_{s,i}}{r \rho_l} \frac{Q_i^{max} - Q_i^{abs}(r, t)}{Q_i^{abs}(r, t)} \quad (4.60)$$

It has to be noted the mass absorption ratio has to be redefined to consider the impact of the distribution:

$$Q_i^{abs}(r, t) = \frac{\rho_l}{\rho_{s,i}} \left( \frac{r^3}{r_{i,0}^3(r, t)} - 1 \right) + 1 \quad (4.61)$$

The variable  $r_{i,0}(r, t)$  is the initial size of a primary particle of  $i^{th}$  component in the solid phase and is a function of size and time. It is known that:

$$\frac{\partial r_{i,0}}{\partial t} = -\frac{\partial r}{\partial t} \frac{\partial r_{i,0}}{\partial r} \quad (4.62)$$

As it was mentioned before,  $\frac{\partial r}{\partial t}$  is another form of the growth term. Therefore, Eq. (4.62) would change into the following form:

$$\frac{\partial r_{i,0}}{\partial t} = -G_i(r, t) \frac{\partial r_{i,0}}{\partial r} \quad (4.63)$$

It is also worth noting that there is no single value for the volume of primary particle in Eq. (4.4) because the total volume of the primary particles would be:

$$V(1 - \varepsilon) = \sum_i \frac{4\pi}{3} \int_0^\infty r^3 n_i(r, t) dr \quad (4.64)$$

By considering a distribution for the primary particles, an average volume for each type of primary particles alongside the total number of particles and the number fraction can be obtained using the following equation:

$$\left\{ \begin{array}{l} \bar{V}_{p,i} = \frac{4\pi}{3} \int_0^\infty r^3 n_i(r,t) dr / \int_0^\infty n_i(r,t) dr \\ n_p = \sum_i \int_0^\infty n_i(r,t) dr = \sum_i \int_0^\infty n_i(r,0) dr = (1 - \varepsilon_0) \frac{V_0}{\sum_i x_{n,i} \bar{V}_{p,i}} \\ x_n = \frac{1}{n_p} \int_0^\infty n_i(r,0) = \frac{w_i}{\rho_{s,i} \bar{V}_{p,i}(0)} / \sum_i \frac{w_i}{\rho_{s,i} \bar{V}_{p,i}(0)} \end{array} \right. \quad (4.65)$$

Equation (4.65) would turn Eq. (4.64) into the following form of Eq. (4.66):

$$V(1 - \varepsilon) = \sum_i \frac{4\pi}{3} \int_0^\infty r^3 n_i(r,t) dr = \sum_i \bar{V}_{p,i} \int_0^\infty n_i(r,t) dr = n_p \sum_i x_{n,i} \bar{V}_{p,i} \quad (4.66)$$

The equation above has the same form as equation (4.4). The only difference is the average volume has replaced the volume of the primary particle. Also, it is important to mention that Eq. (4.5) applies here too but just like the case with Eq. (4.4), the average volume would replace the volume of primary particles. This is also the case with the definition of cubic averaged radius. The last equation to redefine is equation (4.40). For relating the porosity to mass absorption ratio, a new type of mass absorption ratio that considers the total liquid absorption, this equation needs to be defined. The new absorption ratio in Eq. (4.40) would be:

$$Q_{tot,i}^{abs} = \frac{\rho_l}{\rho_{s,i}} \left( \frac{\int_0^\infty r^3 n_i(r,t) dr}{\int_0^\infty r^3 n_i(r,0) dr} - 1 \right) + 1 = \frac{\rho_l}{\rho_{s,i}} \left( \frac{\bar{V}_{p,i}}{\bar{V}_{p,i}(0)} - 1 \right) + 1 \quad (4.67)$$

The only thing remaining is to replace the mass absorption ratio with this variable in equation (4.40) and for the definition of stress definition is equations(4.57) and (4.58). The last differential equation needed for distributed single granule swelling model is mass conservation law for the liquid in the porous phase (Eq.(4.32)) which needs no adjustment. The requirement to solve this system is the boundary and initial conditions for variables  $n_i$  and  $r_{i,0}$ . For the case of density function, the initial distribution of primary particles in the granule may differ from the pre-process distribution due to the impact of granulation. However, there is no model or experimental method to determine the distribution of primary particles. Therefore, it is assumed the initial distribution of primary particles are the same as their pre-process distributions. At the same time, it is known that initial mass absorption ratio is equal to one. This means the initial value of  $r_{i,0}$  should be equal to  $r$ .

$$\left\{ \begin{array}{l} n_i(r,0) = n_p x_{n,i} f_{n,i}(r) \\ \lim_{r \rightarrow \infty} n_i(r,t) = 0 \\ r_{i,0}(r,0) = r \\ \lim_{r \rightarrow} Q_i^{abs}(r,t) = Q_i^{max} H(\hat{S}_a - \hat{S}_{a,thr}) \end{array} \right. \quad (4.68)$$

**Table 4.3:** The equations needed for solving the distributed single granule swelling model

Equation	Initial condition	Boundary condition
$V = \frac{n_p}{1 - \varepsilon} \sum_i x_{n,i} \bar{V}_{p,i}$	$R = R_0$	-
$x_{n,i} = \frac{w_i}{\rho_{s,i} \bar{V}_{p,i}(0)} / \sum_i \frac{w_i}{\rho_{s,i} \bar{V}_{p,i}(0)}$	-	-
$n_p = (1 - \varepsilon_0) \frac{V_0}{\sum_i x_{n,i} \bar{V}_{p,i}}$	-	-
$\frac{d}{dt}(\varepsilon S_a V(t)) = \frac{3}{2} \frac{\varepsilon V(t)}{\tau_{sat}(\varepsilon, R, \bar{R}_p)} \frac{1 - \hat{S}}{\hat{S} + \alpha} - n_p \sum_i x_{n,i} \frac{dV_{p,i}}{dt}$	$S_a = 0$	-
$\tau_{sat} = \tau_{sat,0} \frac{\bar{R}_p}{\bar{R}_{p,0}} \frac{\varepsilon_0}{\varepsilon} \sqrt[3]{\frac{1 - \varepsilon}{1 - \varepsilon_0}}$	-	-
$\frac{\partial n_i(r, t)}{\partial t} = - \frac{\partial(G_i(r, t)n_i(r, t))}{\partial r}$	$n_i(r, 0) = n_p x_{n,i} f_{n,i}(r)$	$n_i(r \rightarrow \infty, t) = 0$
$G_i(r, t) = f(\hat{S}_a) \frac{D_i}{r} \frac{\rho_{s,i}}{\rho_l} \frac{Q_i^{max} - Q_i^{abs}(r, t)}{Q_i^{abs}(r, t)}$	-	-
$f(\hat{S}_a) = \left( MAX(0, \frac{\hat{S}_a - \hat{S}_{thr}}{1 - \hat{S}_{thr}}) \right)^{1-M}$	-	-
$\frac{\partial r_{i,0}}{\partial t} = -G_i(r, t) \frac{\partial r_{i,0}}{\partial r}$	$r_{i,0}(r, 0) = r$	$Q_i^{abs}(r \rightarrow 0, t) = Q_i^{max} H(\hat{S}_a - \hat{S}_{a,thr})$
$\frac{\varepsilon - \varepsilon_0}{\Delta \varepsilon_\infty} = 1 - (1 - \hat{m}_s)^\beta$	$\varepsilon = \varepsilon_0$	-
$\hat{m}_s = \frac{\sum_i w_i (Q_{tot}^{abs} - 1)}{\sum_i w_i (Q^{max} - 1)}$	-	-
$Q_{tot,i}^{abs} = \frac{\rho_l}{\rho_{s,i}} \left( \frac{\bar{V}_{p,i}}{\bar{V}_{p,i}(0)} - 1 \right) + 1$	-	-
$\frac{\sigma_{str}}{\sigma_c} = \frac{\sigma_{str}^{max}}{\sigma_{c,0}(L/S, C_L)} \left( \frac{1 - \varepsilon}{1 - \varepsilon_0} \right)^4 \left( \frac{\bar{R}_p}{\bar{R}_{p,0}} \right)^{6c} \left\{ 1 - MAX(0, \frac{\hat{m}_s - \hat{m}_{s,thr}}{1 - \hat{m}_{s,thr}})^\vartheta \right\}$	-	-

where  $f_{n,i}$  is the number-based frequency of pre-granulated powders and  $H$  is the step function. The boundary condition for  $r_{i,0}$  is based on Eq. (4.42). Because, as the saturation reaches its threshold, the particles of such sizes instantly expand reaching their maximum absorption ratio. The main equations in the distributed single granule swelling model has been shown in Table 4.3.

### 4.3 Global Sensitivity Analysis of the swelling models

According to (Saltelli 2008), sensitivity analysis is defined as "The study of how uncertainty in the output of a model (numerical or otherwise) can be apportioned to different sources of uncertainty in the model input". Sensitivity analysis is a necessary tool to determine the importance of input parameters in a model. Through this process, the input parameters can be ranked based on their importance. The result of this process is that the focus can be shifted on estimating the parameters with highest impact on the model. There are two types of sensitivity analysis: local and global. In local sensitivity analysis, or nominal sensitivity analysis, only one parameter would be changed while the other parameters would remain constant. Then, the changes in outputs (either through graphical methods or by calculating the derivative of the outputs with respect to the changed input) would be assessed to determine the sensitivity of the output to the input. Unfortunately, as it is addressed by (Christopher Frey & Patil 2002), local sensitivity analysis is only useful for linear model and when utilized for nonlinear model, such as ours, it loses its applicability as the result are restricted to a very narrow range of inputs. In contrast, global sensitivity analysis (GSA) aims to determine the dependency of outputs in the desired range of inputs and not in single points. Based on (Saltelli 2008, Borgonovo & Plischke 2016), global sensitivity analysis methods are categorized as following:

1. Regression based methods
2. Variance based methods
3. Density based methods
4. Transformation invariant methods
5. Surrogate model based methods etc.

Of all these methods, the second one, the variance-based method, was chosen for this work. There are different types of variance based methods in the literature (Zhang et al. 2015). However, one of the best technique in this type of method is Sobol indices which are indices that determine the importance of outputs on the inputs through the variations in the output variables based on the variations in the input parameters (Sobol 2001, Saltelli 2008). Generally, Sobol indices are divided to three categories:

- i. First-Order Sobol Indices  $S_i$ : These indices represent the sensitivity of the model's output to individual input parameters. They are calculated by obtaining from the variance of the conditional expectation of the output with respect to  $i^{th}$  input divided by variance of the outputs:

$$S_i = \frac{\text{VAR}_{X_i}(E_{\mathbf{X}_{\sim i}}(Y|X_i))}{\text{VAR}(Y)} \quad (4.69)$$

These indices represent the contribution of each input to the variance of the output.

- ii. Total-Order Sobol Indices  $S_{Ti}$ : These indices represent the sensitivity of the model's output to individual input parameters while considering the contribution of the input through other parameters. They are calculated by obtaining from the variance of the conditional expectation of the output with respect to all parameter except  $i^{th}$  input divided by variance of the outputs:

$$S_i = \frac{E_{\mathbf{X}_{\sim i}}(\text{VAR}_{X_i}(Y|\mathbf{X}_{\sim i}))}{\text{VAR}(Y)} = 1 - \frac{\text{VAR}_{\mathbf{X}_{\sim i}}(E_{X_i}(Y|\mathbf{X}_{\sim i}))}{\text{VAR}(Y)} \quad (4.70)$$

As it is clear from the definition, these indices are better at determining the impact of a parameter on the outputs.

- iii. Mid order Sobol indices: These indices represent the impact of at least two factors together on the responses. Generally, in most GSAs, these indices are not calculated as they are not needed.

Another issue in sensitivity analysis is the sampling method. In theory, to perform a sensitivity analysis, the number of samples increases exponentially by adding new parameters to the GSA. However, this increases the computation time substantially. To circumvent this issue, Monte-Carlo based sampling method has been suggested which uses randomness to the sampling method, increasing confidence on the data chosen. The advantage of this method over theoretical method is while the parameters can be spread through their ranges at the same time, the number of samples would be decreased substantially, leading to lower computation time. A simple and thorough algorithm of the method by (Saltelli 2008), is presented in the following:

1. Create a sample matrix with  $N \times K$ , where  $N$  is the number of uncertainty samples and  $K$  is the number of factors, designated as  $X_A$  and obtain the response matrix, called  $Y_A$  here.
2. Create another sample matrix with  $N \times K$ , designated as  $X_B$  and obtain the responses. The response of this matrix is called  $Y_B$  here.
3. Create a matrix  $X_{c,i}$  formed by all columns of  $X_B$  except the  $i^{th}$  column, which is taken from  $X_A$  and obtain its responses  $Y_{c,i}$ .
4. Calculate the first order and total order of  $i^{th}$  factor based on the following formulas:

$$S_i = \frac{\left( \frac{1}{N} \sum_{j=1}^N Y_A^{(j)} Y_C^{(j)} \right) - \left( \frac{1}{N} \sum_{j=1}^N Y_A^{(j)} \right)^2}{\left( \frac{1}{N} \sum_{j=1}^N Y_A^{(j)} Y_A^{(j)} \right) - \left( \frac{1}{N} \sum_{j=1}^N Y_A^{(j)} \right)^2} \quad (4.71)$$

and,

$$S_{Ti} = 1 - \frac{\left(\frac{1}{N} \sum_{j=1}^N Y_B^{(j)} Y_C^{(j)}\right) - \left(\frac{1}{N} \sum_{j=1}^N Y_A^{(j)}\right)^2}{\left(\frac{1}{N} \sum_{j=1}^N Y_A^{(j)} Y_A^{(j)}\right) - \left(\frac{1}{N} \sum_{j=1}^N Y_A^{(j)}\right)^2} \quad (4.72)$$

In total the number of simulations to calculate the Sobol indices in this method is  $N \times (K + 2)$  which is far lower than  $N^2$  number of simulations for the brute force method (Saltelli 2008). In the following section, the sensitivity analysis of each swelling model would be presented. The GSA would be done on process parameters and primary particles related parameters separately. In here, GSA was performed using the global sensitivity toolbox in general process modelling system (gPROMS).

### 4.3.1 Global Sensitivity Analysis of the mono-sized model

To perform the sensitivity analysis, some information is needed. First, the global sensitivity analysis was separated to three different categories. In the first category, the impact of process parameters, known as factor in GSA, on three separate variables, known as responses, were tested. In the second category, the intention was to know the effect of the disintegrant and excipient inherent properties on the properties of the granules. Lastly, the effect of structural related factors on the responses investigated. The factors, their type and their ranges has been listed in Table 4.4.

The responses were the average normalized radius, porosity, and stress to strength ratio over 1000 seconds. An additional response, the normalized porosity  $((\varepsilon - \varepsilon_0) / \Delta \varepsilon_\infty)$  was added to estimate the response of all parameters on porosity except initial porosity and porosity difference at infinite. The number of uncertainty scenarios in all GSAs was 1000. The values of other parameters that are not in GSA are listed in Table 4.5. An important note to address is the absence of any saturation related parameters. The main reason is the value of initial inherent imbibition time. In the worst-case scenario, it was estimated that these parameters would not exceed 10s, which is considerably lower than the initial inherent absorption time for the disintegrant, and excipient, leading to low impact of saturation related parameters on this model.

The GSA was first performed on all factors to find the most important parameters, Then the impact of each type of factor on the responses was investigated. Before interpreting the GSA data, the criteria to categorise the parameters shall be addressed. The criteria to determine the impact of each factor based on total effect is not universal however, the same criteria used by (Yeardley et al. 2021) is used here. Based on this criterion, the parameters are divided to three different categories:

1. Low impact parameters (Total Effect < 0.05 ): these parameters do not affect the model and therefore fixed to a reasonable value without affecting the model.
2. Very high impact parameters (Total Effect > 0.3): These parameters are very important. as their impact on the responses are substantial. A thorough plan should be devised to evaluate or controlling these parameters accurately.

**Table 4.4:** The factors in global sensitivity analysis of mono-sized model

Factor	Type	Lower limit	Upper limit	Default value
Initial granule radius ( $R_0$ )	-	300 $\mu\text{m}$	1000 $\mu\text{m}$	500 $\mu\text{m}$
Disintegrant mass fraction ( $w_{dis}$ )	Process	0 g/g	0.1 g/g	0.04 g/g
Disintegrant initial radius ( $R_{dis,0}$ )	Process	40 $\mu\text{m}$	100 $\mu\text{m}$	90 $\mu\text{m}$
Excipient initial radius ( $R_{exc,0}$ )	Process	15 $\mu\text{m}$	60 $\mu\text{m}$	27 $\mu\text{m}$
Liquid to Solid Ratio ( $L/S$ )	Process	0.8 g/g	1.2 g/g	1 g/g
Binder concentration ( $C_L$ )	Process	0.05 g/g	0.125 g/g	0.05 g/g
Maximum absorption ratio of disintegrant ( $Q_{dis}^{max}$ )	Product	5 g/g	10 g/g	10 g/g
Diffusion of disintegrant ( $D_{dis}$ )	Product	5 $\mu\text{m}^2/\text{s}$	500 $\mu\text{m}^2/\text{s}$	100 $\mu\text{m}^2/\text{s}$
Initial porosity ( $\varepsilon_0$ )	Process	0.2	0.6	0.3
Porosity difference ( $\Delta\varepsilon_\infty$ )	Structure	0.05	0.3	0.2
Porosity related exponent ( $\beta$ )	Structure	1	3	2
Stress related exponent ( $\vartheta$ )	Structure	1	3	2
Strength related exponent ( $c$ )	Structure	0.1	0.5	0.326

3. High impact parameters ( $0.3 > \text{Total Effect} > 0.05$ ): These parameters are important to the model but not as to the extent of the very high impact models. While one should be careful on evaluating these parameters, there is freedom to some extent on their evaluations.

The total effect of each factor on the responses has been depicted in Figures 4.6 to 4.9. The result shows us that, the initial size of the primary particles, the composition and structural parameters affect the model heavily, especially in case of stress to strength ratio, which determines the disintegration time. For porosity, the initial porosity and porosity difference at infinite have the most impact which is expected because the relationship between the factors

**Table 4.5:** *The values of non-GSA parameters*

Parameter	Value
Disintegrant density ( $\rho_{dis}$ )	1560 kg/m <sup>3</sup>
Excipient density ( $\rho_{exc}$ )	1530 kg/m <sup>3</sup>
Fluid density ( $\rho_l$ )	1000 kg/m <sup>3</sup>
Maximum absorption ratio of excipient ( $Q_{exc}^{max}$ )	1 g/g
Diffusion of excipient ( $D_{exc}$ )	0 $\mu\text{m}^2/\text{s}$
Residual saturation ( $S_r$ )	0
Threshold saturation ( $S_{thr}$ )	0.1
Initial inherent imbibition time ( $\tau_{sat,0}$ )	10 s
Capillary pressure related exponent ( $M$ )	0.6
Wicking related parameter ( $\alpha$ )	0.02
Normalized threshold load ratio ( $\hat{n}_{s,thr}$ )	0.05
Stress to strain ratio proportionality constant	0.2

and porosity is almost additive, leading to their high impact in GSA. Hence, an additional response was chosen, the normalized porosity to determine the impact of other parameters on the porosity change. By looking at Figure 4.8, it can be seen that the disintegrant diffusivity dominates the response followed by the initial size of the disintegrant which means in this particular case, absorption significantly affects the response. Additional GSAs were performed on different type of factors; process, product and structural factors separately. In the following section, the results are presented.

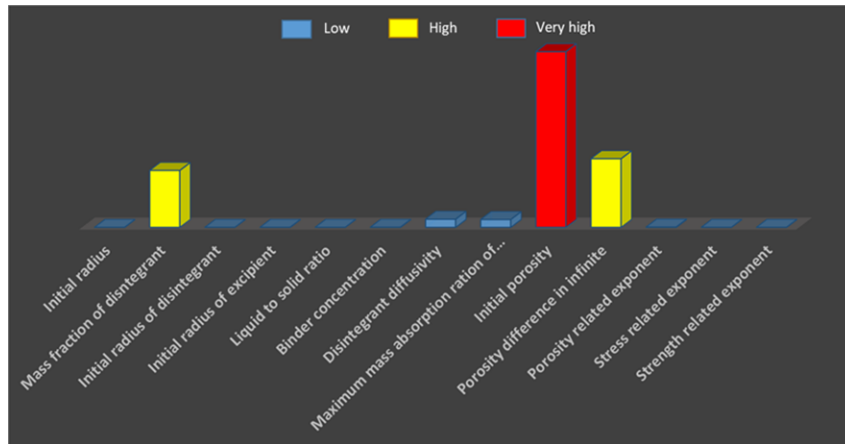


Figure 4.6: The total effect of all factors on normalized radius in the GSA of mono-sized model

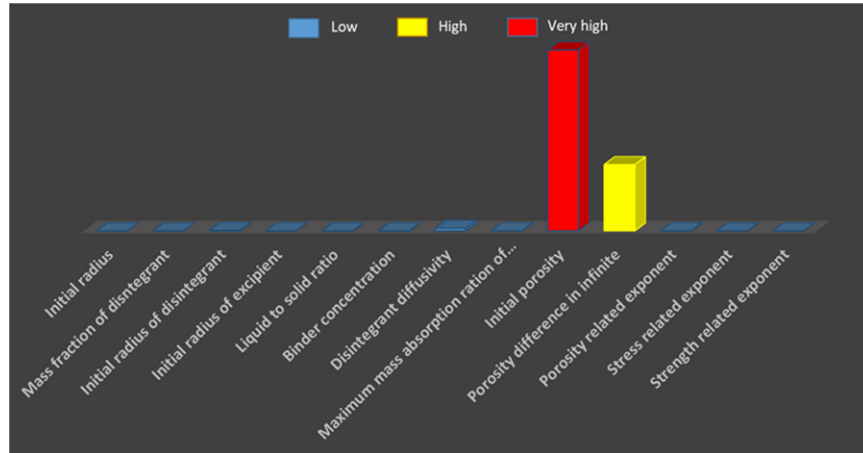
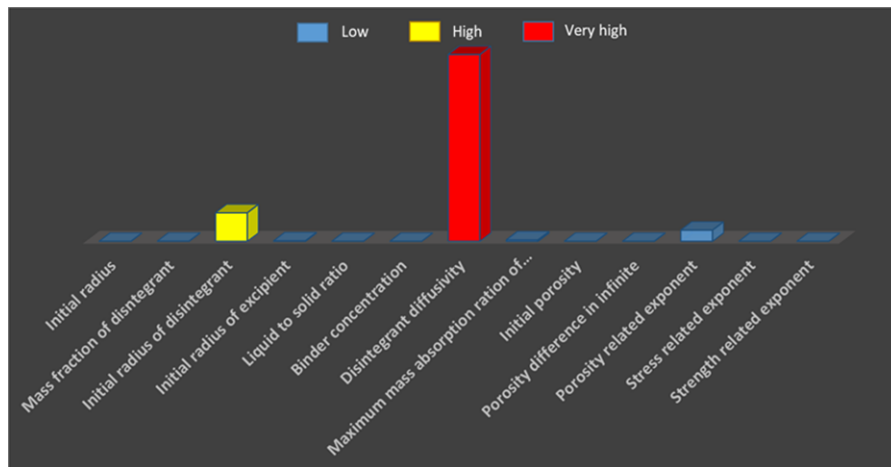


Figure 4.7: The total effect of all factors on porosity in the GSA of mono-sized model

#### 4.3.1.1 GSA of process parameters

In the case of process parameters, the results are shown in Figure 4.10. Clearly, the mass fraction dominates the normalized radius. The scatter plot shown in Figure 4.11, shows an almost linear like behaviour between mass fraction of disintegrant and average of normalized radius, hence its dominating impact on normalized radius. In the case of porosity as the response, the initial radius of disintegrant has the most impact. Like before, an scatter plot was obtained from the GSA results in order to find the relationship between these two variables. A similar linear-like behaviour is seen here which by increasing the initial radius of disintegrant, the porosity decreases. This is because due to decrease in total surface to volume ratio of disintegrant particles, which leads to a reduction in absorption and therefore, the decrease in porosity. For strength to stress ratio, unlike the other two responses, not one factor dominates the response, but the combination of the initial size of primary particles which means the size related term in Eq. (4.51), has the most impact on stress to strength



**Figure 4.8:** *The total effect of all factors on normalized porosity in the GSA of mono-sized model*

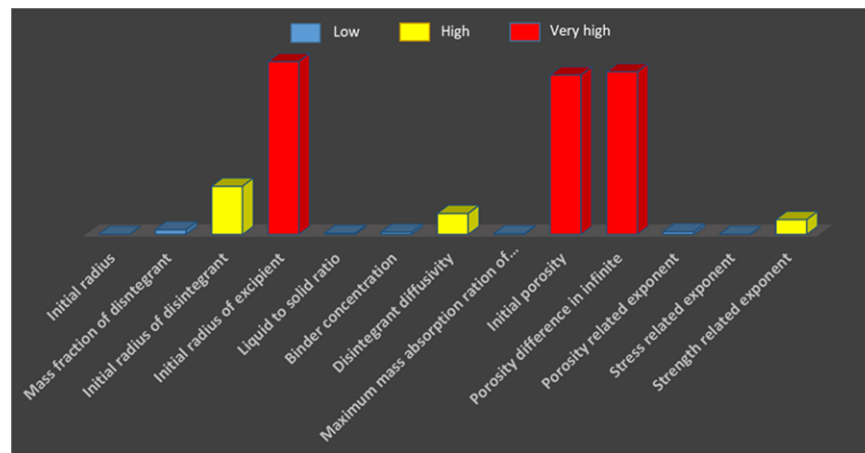


**Figure 4.9:** *The total effect of all factors on stress to strength ratio in the GSA of mono-sized model*

ratio. A contour plot was created from the GSA data to understand the impact of the initial sizes of ingredients on stress to strength ratio. Clearly, by decreasing the size of primary particles, the strength to stress ratio increases which due to the increase in ratio between the average size of primary particles and its initial value. At the same time, smaller particles tend to absorb liquid faster due to higher surface to volume ratio which combined with the increase in their number (if the porosity and size remain the same), leads to a higher absorption ratio in the granule and therefore, an increase in deformation.

#### 4.3.1.2 GSA of product parameters

The sensitivity analysis of product parameters, diffusivity and maximum absorption ratio of primary particles is shown in Figure 4.14. As it is shown, each one of the factors dominates one response while just like the case with process parameters both affect the stress to strength ratio. The result shown in Figure 4.15 shows that the normalized radius increases linearly with initial size, similar to a trend seen in Figures 4.11 and 4.12. In the case of porosity, the

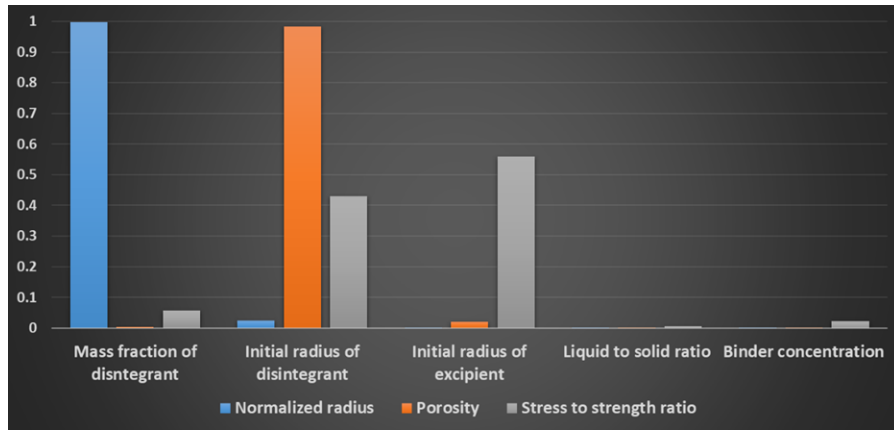


**Figure 4.10:** The total effect of process factors on the responses in the GSA of process parameters of mono-sized model

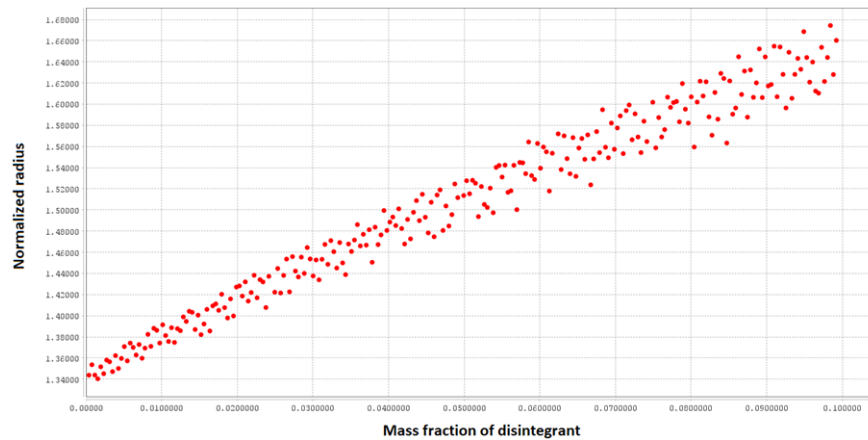
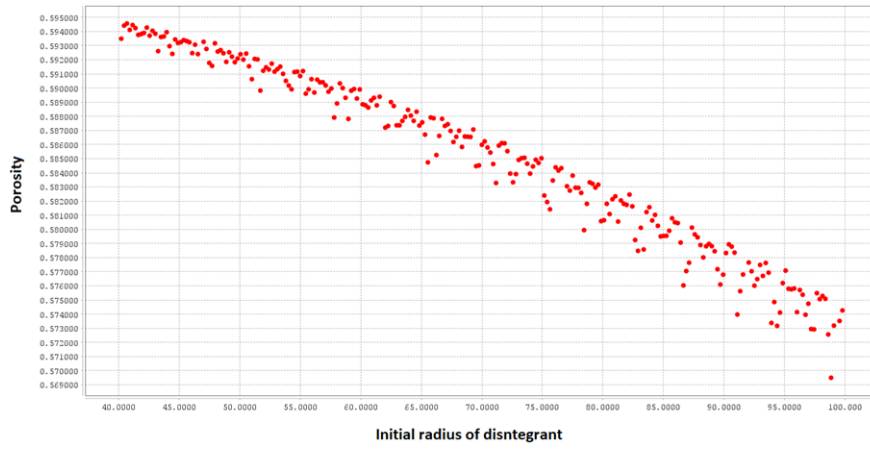


**Figure 4.11:** The scatter plot of average normalized radius vs mass fraction of disintegrant in the GSA of process parameters of mono-sized model

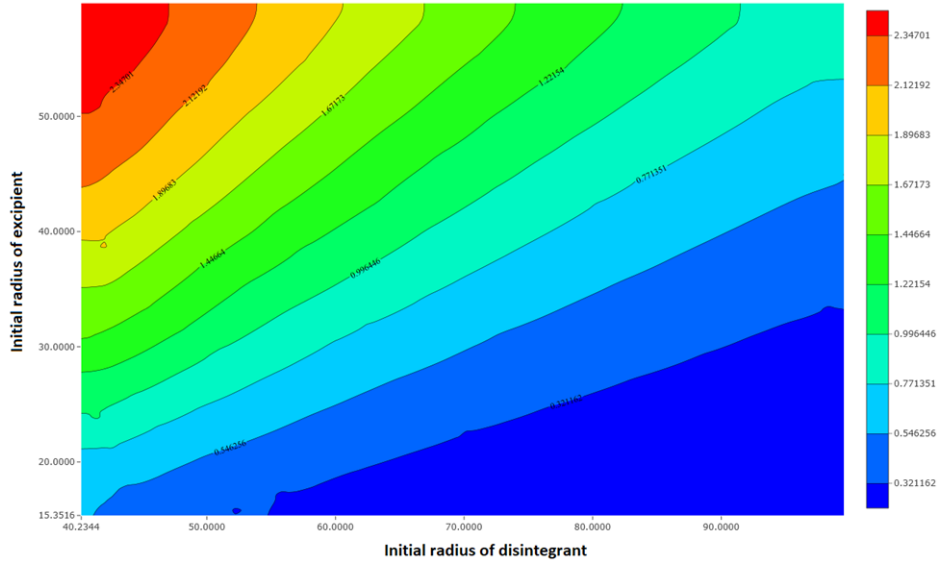
trend is different. Based on the result shown in Figure 4.16, at the beginning, the porosity is low but after a certain threshold, the porosity increases to its final value which shows the impact of absorbance on this variable. Lastly, a contour plot was created to study the impact of both parameters on strength to stress ratio. As it is shown in Figure 4.17, the maximum absorption ratio affects this response more than diffusivity through its impact on the average radius of primary particles.

#### 4.3.1.3 GSA of structural parameters

As it is clear from the results shown in Figure 4.18, initial porosity and porosity difference at infinite are dominating the responses, especially porosity. An additional GSA was performed on these two factors only. The data were then analysed for the impact of porosity only and it was shown the type of behaviour. The data showed that these two parameters have a significant impact on normalized radius while in the case of other responses, the normalized porosity and stress to strength ratio, the impact is negligible. In the contour plot shown in



**Figure 4.12:** The scatter plot of average porosity vs initial radius of disintegrant in the GSA of process parameters of mono-sized model



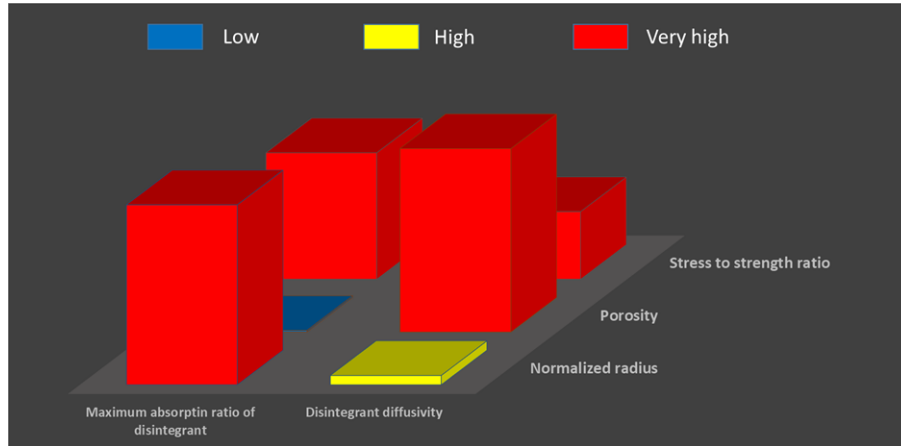
**Figure 4.13:** The contour plot of the impact of composition and disintegrant size on strength to stress ratio in the GSA of process parameters of mono-sized model

Figure 4.19, normalized radius increases as both factors increase. This is due to the impact of porosity in Eq. (4.4).

### 4.3.2 Global sensitivity analysis of distributed model

In the case of distributed model, it was assumed that number-based distribution of primary particles ( $f_{n,i}(r)$ ) has a log-normal distribution. A log normal distribution has the following form:

$$f_{n,i}(r) = \frac{1}{r\sigma_i\sqrt{2\pi}} \exp\left(-\frac{(\ln(r) - \mu_i)^2}{2\sigma_i^2}\right) \quad (4.73)$$



**Figure 4.14:** The total effect of product factors on the responses in the GSA of product parameters of mono-sized model

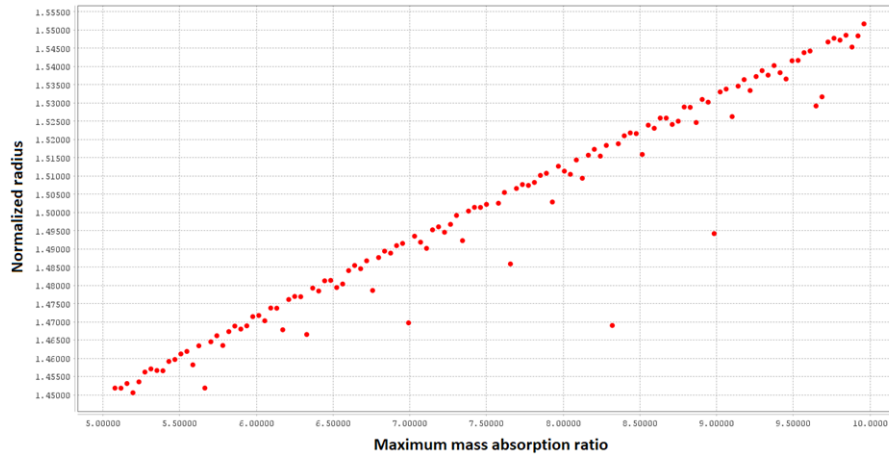


**Figure 4.15:** The scatter plot of average normalized radius vs maximum absorption ratio of disintegrant in the GSA of product parameters of mono-sized model

where  $\mu_i$  and  $\sigma_i$  are the average and standard deviation of the distribution and have the following relationship with the initial average radius of each type of primary particles:

$$f_{n,i}(r) = \ln(\bar{R}_{p,i})(0) - \frac{3}{2}\sigma_i^2 \quad (4.74)$$

which means, in this simulation two new parameters have been added to the GSA, the standard deviation of size distribution of each primary particle. The initial size of primary particles is changed to initial average size of primary particles. All the remaining factors are the same as the ones defined in Table 4.6. The list of redefined and new factors alongside is:

The GSA was done on all parameters and the results are shown in Figure 4.20 to 4.23. As it can be seen, there are striking differences between this model and the mono-sized model. The most important differences are the impact of standard deviation of primary particles in almost all responses alongside their initial sizes, hinting at the high impact of size distribution of primary particles on this model. Just like the case with mono-sized model, initial porosity

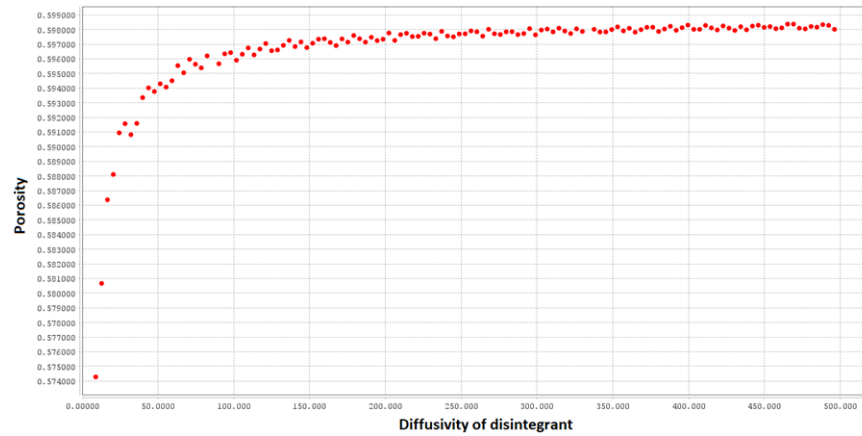


**Figure 4.16:** The scatter plot of porosity versus diffusivity of disintegrant in the GSA of product parameters of mono-sized model

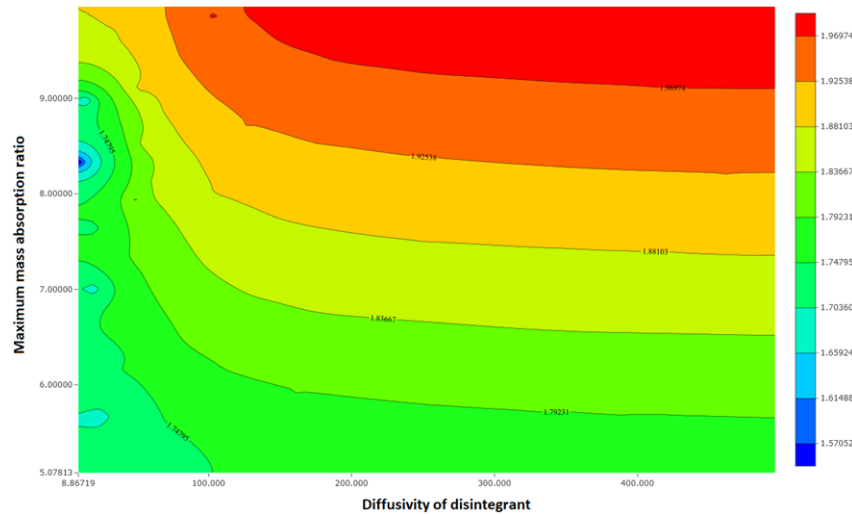


**Figure 4.17:** The contour plot of the impact of initial size of primary particles on strength to stress ratio in the GSA of product parameters of mono-sized model

and porosity difference at infinite dominated the porosity. Therefore, the additional response, the normalized porosity was used to see the impact of other parameters on porosity. The results showed that the size of primary particles have the most impact on the normalized radius (Figure 4.20), which is quite different than mono-sized model where structural factors dominated the response. In the case of normalized porosity (Figure 4.22), the diffusivity is no longer the dominating factor and distribution of primary particles, specifically the standard deviation of disintegrant size distribution, competes with this factor for their impact on normalized porosity. A similar trend can also be seen for stress to strength ratio in Figure 4.23 where particles distribution has an important impact on the response. Furthermore, the standard deviation of disintegrant size distribution has replaced the initial size of excipient here which hints at the higher impact of standard deviation of disintegrant size distribution on the average size of primary particles in the model. In the following sections, the impact

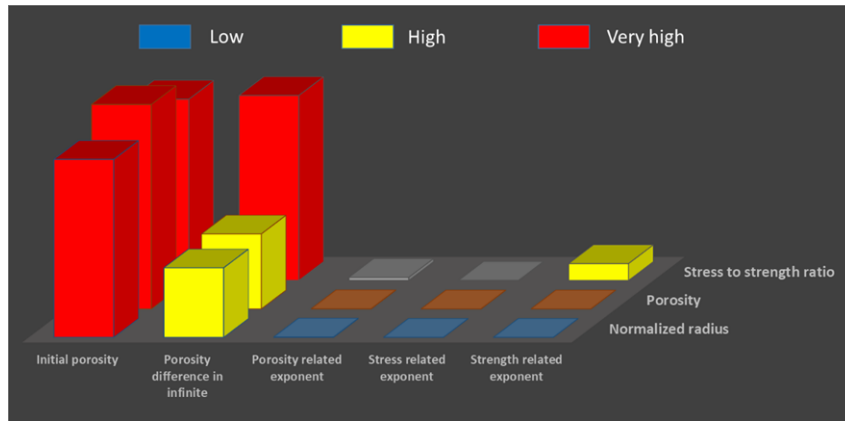


**Figure 4.18:** The total effect of structural parameters on the responses in the GSA of structural parameters of mono-sized model

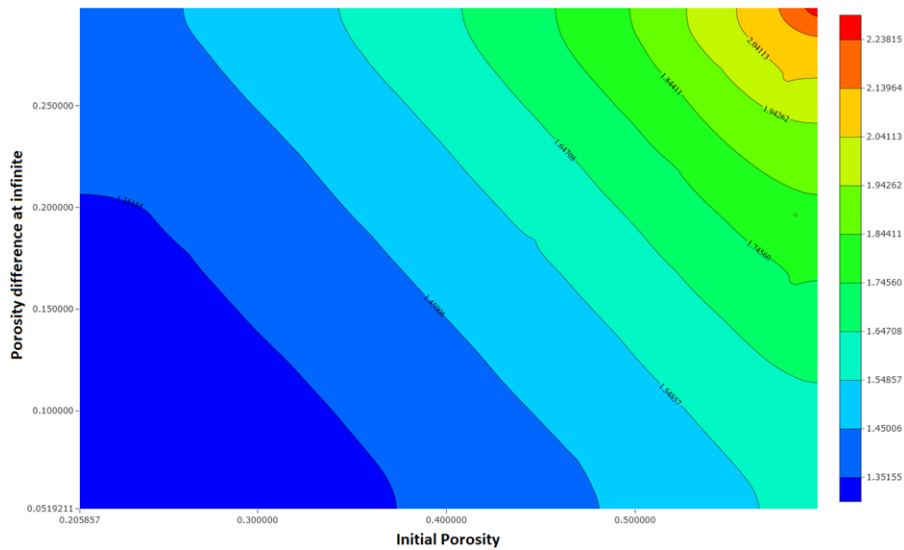


**Figure 4.19:** The contour plot of the impact of initial porosity and porosity difference at infinite on normalized radius in the GSA of structural parameters of mono-sized model

of each type of factor has been studied in detail.

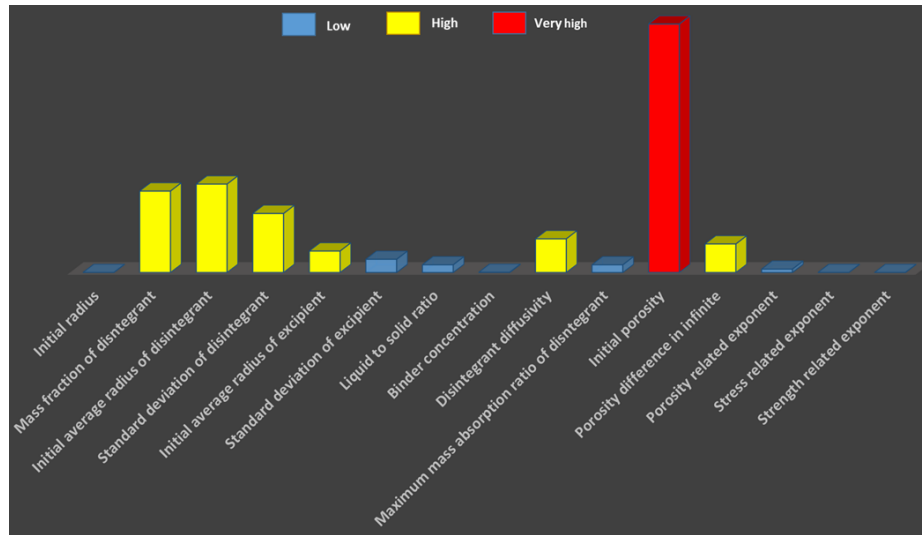
#### 4.3.2.1 GSA of process parameters

A thorough sensitivity analysis was performed on the process parameters. The total effects obtained for each response in Figure 4.24 shows clearly that the mass fraction of disintegrant has the most impact on normalized radius followed by the initial average radius of disintegrant and its standard deviation. In the case of porosity, clearly standard deviation of disintegrant dominates the response, showing that this parameter has the most impact on the size of absorbance rate in the granule. A similar trend is seen for stress to strength ratio, where the size distribution related parameters have the most impact on the response.

Given, the normalized radius showed a different type of behaviour than the other two

**Table 4.6:** The list of new and redefined factors in global sensitivity analysis of distributed model

Factor	Type	Lower limit	Upper limit	Default value
Disintegrant initial average radius ( $\bar{R}_{dis,0}$ )	Process	40 $\mu\text{m}$	100 $\mu\text{m}$	90 $\mu\text{m}$
Standard deviation of disintegrant size distribution ( $\sigma_{dis}$ )	Process	0.5	2	1
Excipient initial average radius ( $\bar{R}_{exc,0}$ )	Process	15 $\mu\text{m}$	60 $\mu\text{m}$	27 $\mu\text{m}$
Standard deviation of excipient size distribution ( $\sigma_{exc}$ )	Process	0.5	2	1

**Figure 4.20:** The total effect of all factors on normalized radius in the GSA of distributed single granule swelling model

responses, an additional GSA was performed on this response with mass fraction of and the initial average size of disintegrant as the response. The contour plot obtained from this GSA, shown in Figure 4.25, gives the type of behaviour expected from these factors, the increase in mass fraction and decrease in size leading to an increase in normalized radius mainly through their impact on absorbance rate.

Because the impact of standard deviation size distribution is not well understood, it was decided to perform a separate GSA on these two factors only. It is important to note that the results from Figure 4.24 indicates that not one factor has an overwhelming impact on

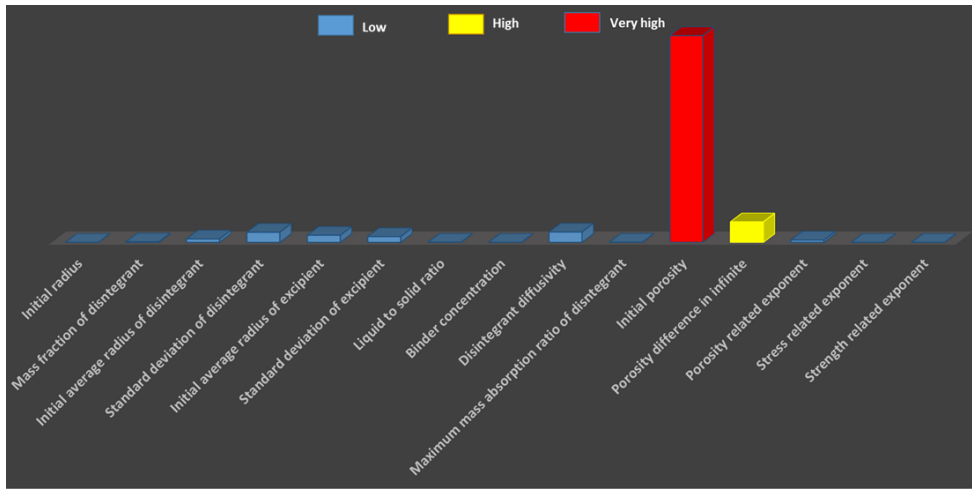


**Figure 4.21:** The total effect of all factors on porosity in the GSA of distributed single granule swelling model

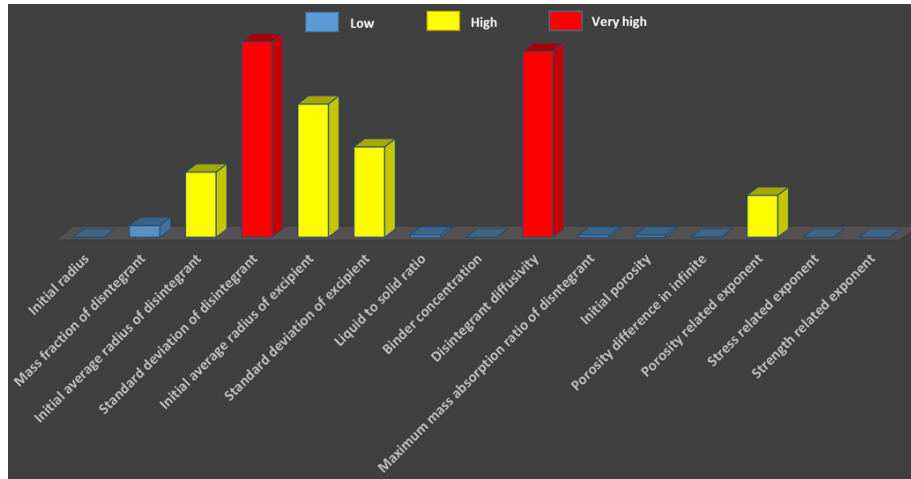


**Figure 4.22:** The total effect of all factors on normalized porosity in the GSA of distributed single granule swelling model

the responses and therefore this GSA could be dependent on values of other parameters in GSA. The GSA results for standard deviation of primary particles showed that only in case of normalized radius that one factor dominates the other and in the case of the other responses, both factors affect the responses.

The scatter plot shown in Figure 4.24 that gives the impact of standard deviation of disintegrant on normalized radius, gives a quite different behaviour than the other scatter plots. Seemingly, by increasing the standard deviation, the normalized radius first decreases to a minimum value and then start increasing. In the first region where the normalized radius drops, the increase in standard deviation given disintegrant particles with larger initial sizes, which can lower the absorbance rate in the granule. However, as the standard deviation gets past a certain point, an increase in disintegrant particles with smaller initial sizes are

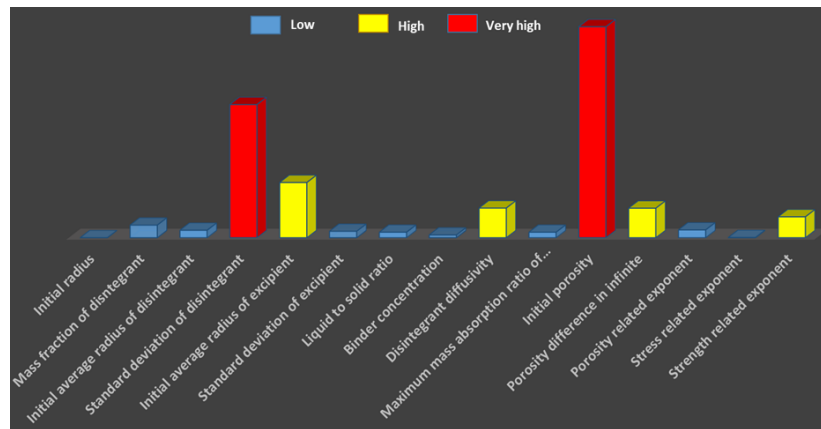


**Figure 4.23:** The total effect of all factors on stress to strength ratio in the GSA of distributed single granule swelling model

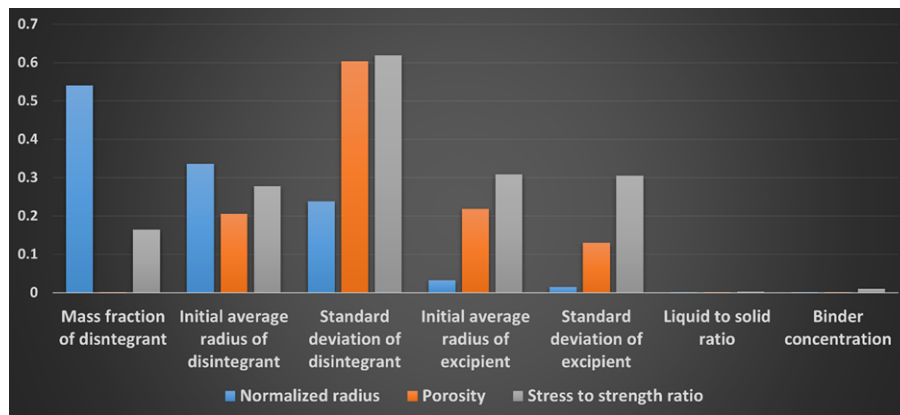


**Figure 4.24:** The total effect of process factors on the responses in the GSA of process parameters of distributed model

seen, which unlike larger particles, absorb the liquid faster and therefore can increasing the swelling rate.

For porosity, the impacts were negligible, given the impact of initial porosity and porosity difference at infinite. However, the trend showed an overall increase in porosity due to increase in standard deviation of disintegrant. Lastly, the stress to strength ratio response was analysed. The results shown in Figure 4.27, show that there is a region where the role of standard deviation is reversed and the standard deviation of disintegrant becomes the main factor at determining the value of stress to strength ratio. This behaviour is mostly because of the impact of average radius of primary particles to its initial value in Eq. (4.58). At low standard deviation of disintegrant, the ratio of average radius of primary particles to its initial value is small and therefore the stress to strength ratio is not affected. However, by increasing it above a certain value, the impact of smaller disintegrant particles increases considerably, leading to an increase in the ratio of average radius of primary particles to its initial value.

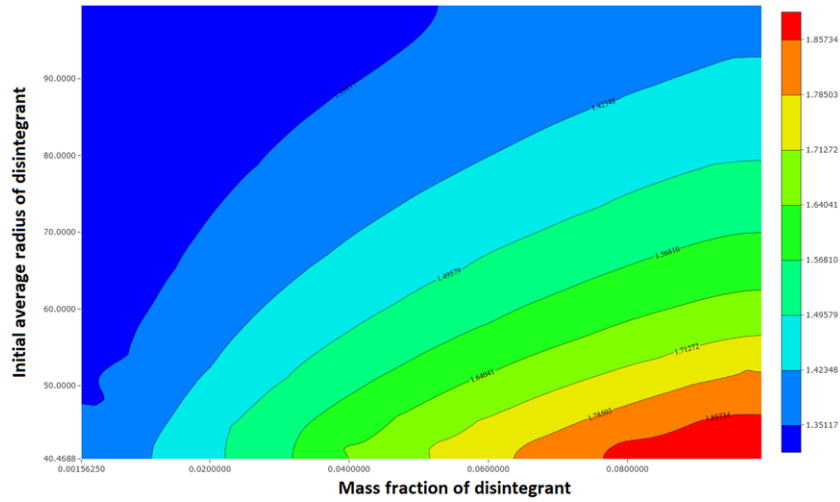


**Figure 4.25:** *The contour plot of the impact of mass fraction and initial average size of disintegrant on normalized radius in the GSA of process parameters of distributed model*

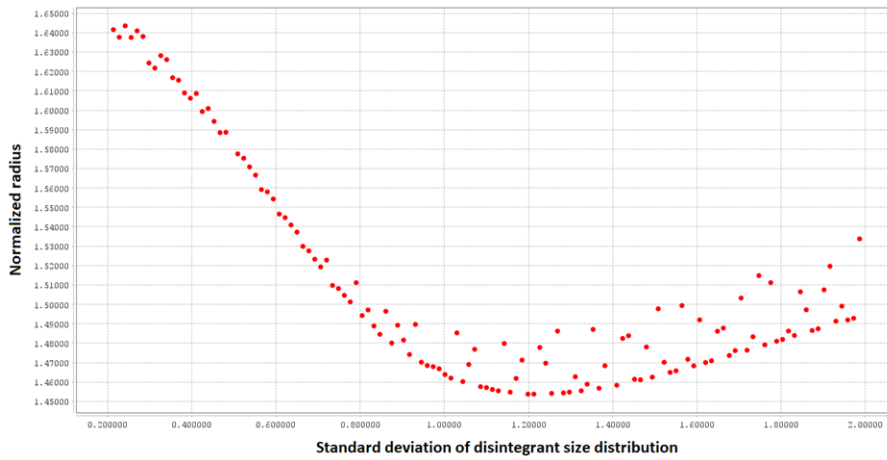


**Figure 4.26:** *The scatter plot of normalized radius vs standard deviation of disintegrant in the GSA of process parameters of distributed model*

### 4.3.2.2 GSA of product parameters

The total effect value obtained from the GSA of product parameters is shown in Figure 4.28. As it can be seen, the diffusivity of disintegrant dominates all responses which is quite different than the results from mono-sized model. The scatter plots obtained from the results are shown in Figure 4.29 to 4.31. For both normalized radius and porosity (Figures 4.29 and 4.30), a similar trend is seen where the increase in diffusivity leads to an increase in absorption rate. In return, a faster absorption rate means a smaller time for the disintegrant particles to reach their maximum absorption and therefore, reaching the final values of both normalized radius and porosity faster. However, this rate is faster for normalized radius due to the impact of absorption rate on size of disintegrant particles in Eq. (4.4). For stress to strength ratio, the trend is almost linear which shows the direct impact of diffusivity on this

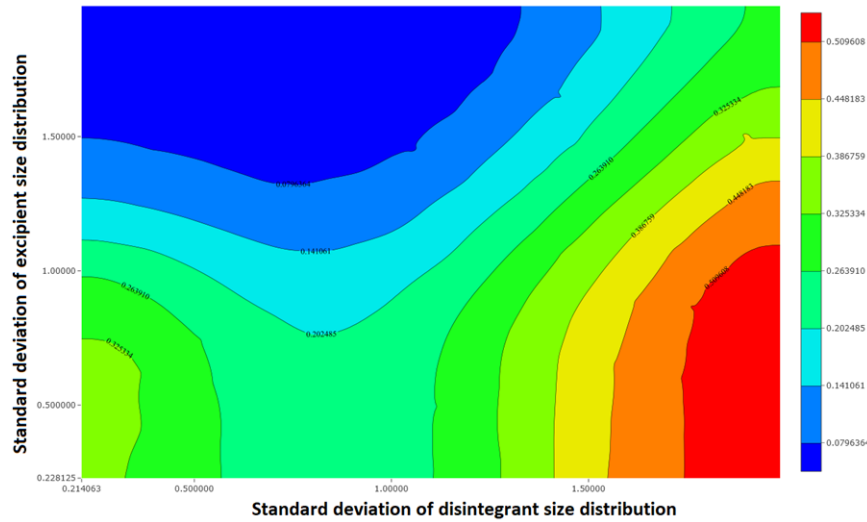


**Figure 4.27:** The contour plot of stress to strength ratio vs standard deviation of primary particles in the GSA of process parameters of distributed model

response.

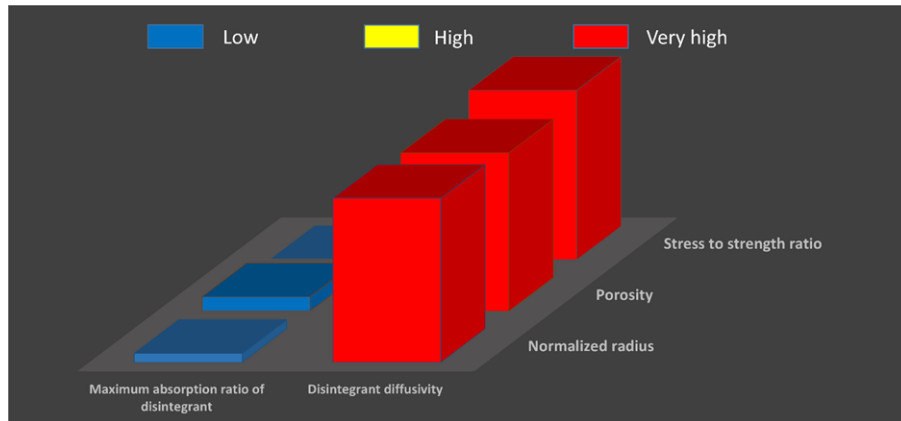


**Figure 4.28:** The total effect of product factors in the GSA of product parameters of distributed model

### 4.3.2.3 GSA of structural parameters

For structural parameters, the normalized porosity was used as the response instead of porosity due to the additive nature between porosity and initial porosity and porosity difference at infinite. The results are shown in Figure 4.32.

For normalized radius, it is obvious that initial porosity is major factor as it has a direct role in determining porosity and therefore can affect the normalized radius through porosity (Eq. (4.4)). For normalized porosity, it is clear from Eq. (4.41) that porosity related exponent dominated the response as evidence by the scatter plot in Figure 4.34 where a linear behaviour is seen between this factor and normalized porosity. A similar reasoning can

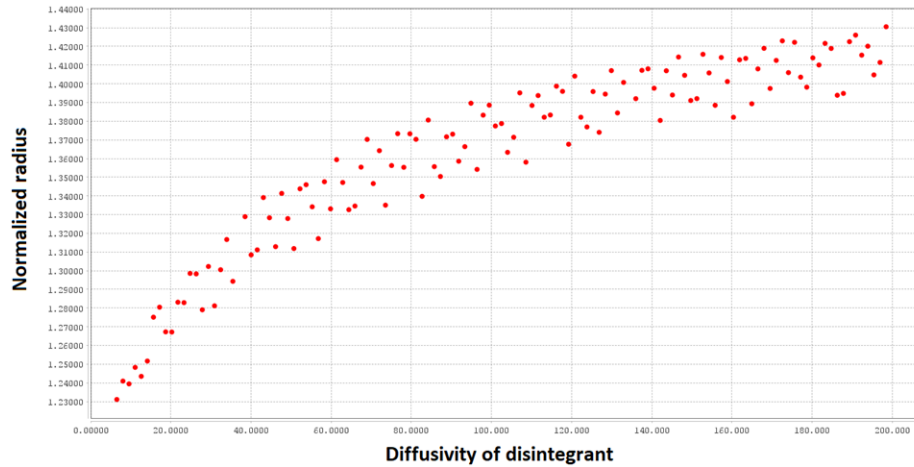


**Figure 4.29:** The scatter plot of normalized radius vs diffusivity of disintegrant in the GSA of product parameters of distributed model

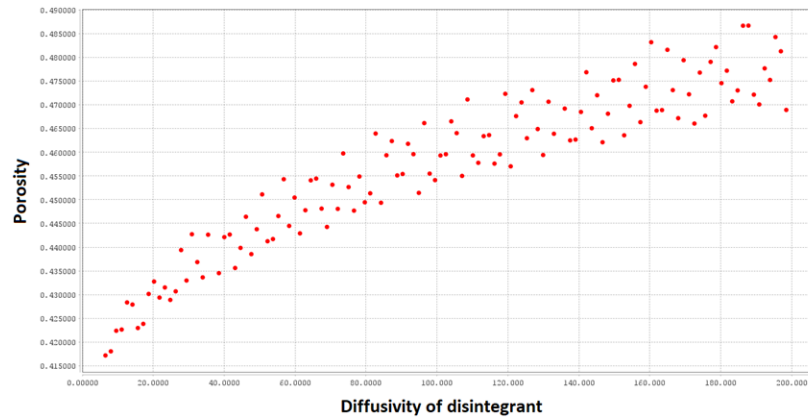


**Figure 4.30:** The scatter plot of porosity vs diffusivity of disintegrant the GSA of product parameters of distributed model

be used for strength related factor on stress to strength ratio. However, it has to mentioned that in stress to strength ratio (Eq. (4.56)), the size related term dominates the response and that is why a similar behaviour is not seen for stress related exponent. The result in Figure 4.34 show a direct relationship between strength related exponent and stress to strength ratio however due to interference of other parameters, the behaviour is linear link.

## 4.4 Conclusion

Two mechanistic models for the swelling of single granules, that consist of excipient, disintegrant and binder, was developed. The first model considers a mono-sized distribution for the primary particles while the second model considers a size distribution for primary particles. In the first part, the main processes in the swelling driven disintegration of granules, were mathematically described including a new mechanistic model for the liquid penetration in

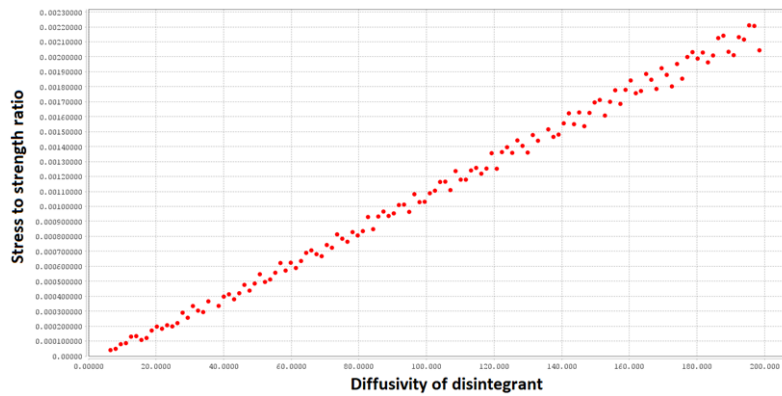


**Figure 4.31:** The scatter plot of stress to strength ratio vs diffusivity of disintegrant in the GSA of product parameters of distributed model

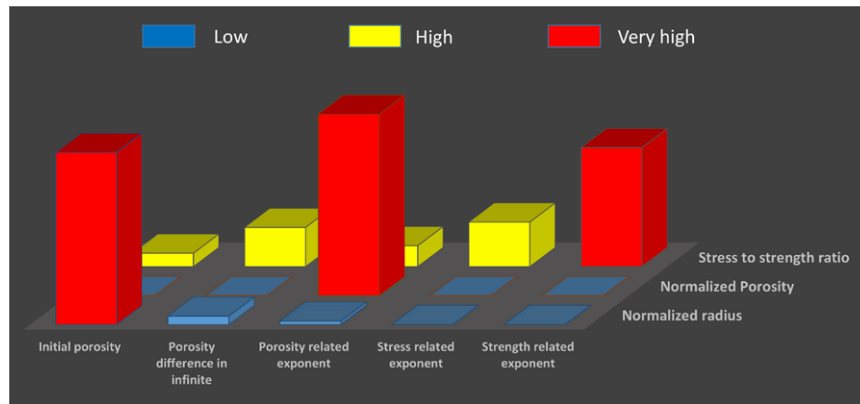


**Figure 4.32:** The total effect of structural factors in the GSA of structural parameters of distributed model

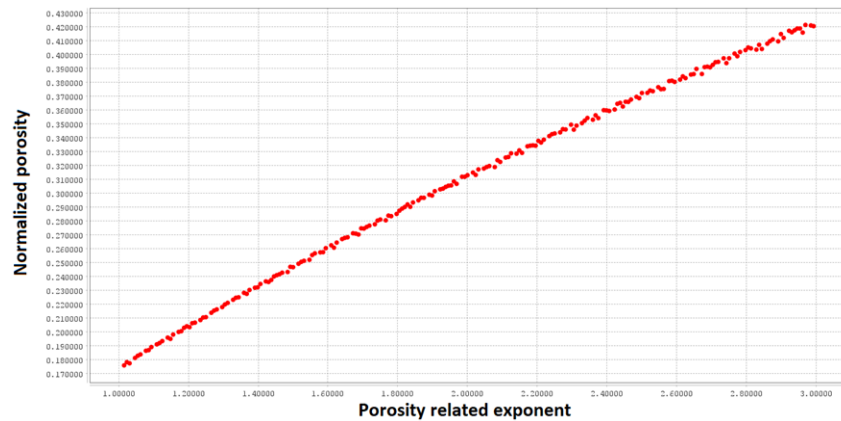


**Figure 4.33:** The scatter plot of normalized porosity vs porosity related exponent in the GSA of structural parameters of distributed model

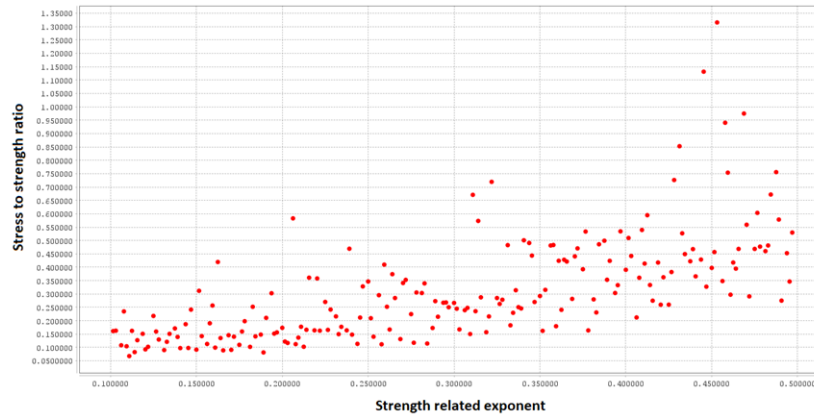


**Figure 4.34:** *The scatter plot of stress to strength ratio vs strength related exponent in the GSA of structural parameters of distributed model*

granules. New simple semi-empirical models were created for the description of stress and porosity based on the absorption ratio, a measurable attribute of a disintegrating granule. Based on an assumption that states solid bridges dominate the granule's strength, a criterion for the disintegration time was defined. In the second section, a series of variance based global sensitivity analyses were performed on both models to identify the important parameters. For the mono-sized model, the structural parameters had the most impact on the model followed by the size and composition of primary particles. In the case of distributed model, the impact was mostly a combination the size of and distribution of primary particles, the inherent property of disintegrant and structural parameters. Between these two models, the distributed model shows potential as the GSA results are similar to what is reported in the literature.

## Chapter 5

# Validation of the single granule swelling model

### 5.1 Introduction

In this chapter, the aim is to validate the single granule swelling model described in the previous chapter. Firstly, the formulations used are discussed. Following this, the granulation results and characterisation of the granules is presented. Then, the size measurement data obtained from the flow cell is discussed. Then using the data in the literature and the flow cell data of the granules, the mono-sized and distributed single granule swelling models are validated.

### 5.2 Granulation consideration

As it is known, during the disintegration of a typical granule, many phenomena can happen simultaneously. However, the aim of this thesis is to model only the swelling driven disintegration of granules. To accomplish this, it is important to isolate this phenomenon from other interfering mechanisms such as erosion or dissolution which means the formulation should not contain any (fast) dissolving material, such as dissolving APIs, and should be strong enough to not be affected by the fluid flow during disintegration. Therefore, the proposed granules can only swell and break leading to the dispersion type of disintegration. The simplest formulation in this case would consist of an excipient, a superdisintegrant which acts as the main factor behind the disintegration, and a binder that has a slow dissolution time in water. It should be noted that the materials should not be hazardous and must be common in industry. Initially, the candidates for the excipient were microcrystalline cellulose (MCC) and dibasic calcium phosphate anhydrous (DCPA). Sodium starch glycolate and CCS were considered for the superdisintegrants, and poly-ethylene glycol (PEG) 4000 and HPMC were considered for the binder material. In the case of the excipient, the preference was DCPA, due to its physical properties. DCPA is an ideal material for the desired granulation process because it is non-dissolving and non-absorbing. However, achieving granulation with DCPA turned out to be an extremely challenging task. The non-absorbing property of DCPA, although initially desirable, presented a significant drawback. It imposed a lower maximum liquid-to-solid ratio compared to MCC. Moreover, even within the allowed liquid-to-solid ratio range,

DCPA either did not granulate successfully or resulted in weak granules. It was only at the highest liquid-to-solid ratio that it was able to produce robust granules. Another excipient candidate, MCC, was not the preferred choice. This was due to its tendency to swell during disintegration. In this context, the swelling of the superdisintegrant is desirable and not the excipient. However, because of its high liquid to solid ratio and its ability to granulate, it was chosen as the excipient in the formulation.

For the superdisintegrant, it was decided to choose SSG instead of CCS. This is because of SSG's high absorption ratio and lower diffusivity together with its omni-directional swelling compared to two-dimensional swelling of CCS (Mohanachandran et al. n.d.). The high absorption ratio of SSG, not only helps in the granulation of DCPA by slightly increasing the maximum liquid to solid ratio but also ensures the material would be less affected by the water in the binder. Finally, HPMC was chosen as the binder. This binder has a much slower dissolution time compared to PEG4000. The physical attributes of all three powders, has previously been presented in Table 3.1. The other considerations for the granulation were:

1. Low level of caking,
2. shape of the granules,
3. lower disintegration time.

Caking is a persisting problem in granulation which continues to present challenges to the industry. An issue with caking is that the existing wet granulation models are not capable modelling this phenomenon properly and, therefore, for process side of the QbD approach to work, caking should be avoided. This was achieved by adjusting the impeller speed, choosing an appropriate grade of binder and adjusting the wet massing time. The model assumes the granules are spherical. Therefore, it is important for the product granules to have a high sphericity. This is why the impeller speed should not be increased beyond a certain point as high impeller speed would deform the granules creating elongated non-spherical granules. The last point is regarding the measurement techniques. Due to the influence of fluid inside the flow cell at the beginning, which leads to rapid granule movement, it is necessary to slow down the disintegration in order to measure the size evolution of the granule in the flow cell.

### 5.3 Granulation results

Given the size distribution is an input for the distributed model, it is necessary to estimate the PSD data mathematically. For this purpose, the data were fit to a series of log-normal distributions in curve fitting toolbox of MATLAB:

$$f_v(x) = \sum_i a_i \exp\left(-\left(\frac{x-b_i}{c_i}\right)^2\right), \quad \sum_i a_i = 1 \quad (5.1)$$

in which  $a_i$ ,  $b_i$  and  $c_i$  are fitting parameters. The distributions are presented in Figure 3.1. MCC and DCPA size distributions are centred around 60  $\mu\text{m}$  with MCC having a wider distribution than DCPA. In the case of SSG, the particles are larger centered around 200  $\mu\text{m}$ . The values of  $D_{v,10}$ ,  $D_{v,50}$  and  $D_{v,90}$  for each powder are reported in Table 3.1. The fitting parameters to estimate the size distribution of each powder has been calculated and given in

**Table 5.1:** The estimated fitting parameters of initial size distribution of powders used in the granulation using Eq. (5.1). The fitting was obtained using the curve fitting toolbox in MATLAB.

Component	$a_i$	$b_i$	$c_i$
SSG	0.8252	4.157	0.684
MCC	0.0123	4.186	0.553
	0.5919	2.473	0.942
DCPA	0.1647	3.918	0.435
	0.0158	4.472	0.281
	0.8207	3.264	0.595

Table 5.1. The formulation variables for the granulation are listed in Table 5.2. Granulations were performed once for most formulation with some formulations repeated again to test the reproducibility of the granulation. The density measurements were performed in triplicate for each formulation, and the porosity measurements were performed in duplicate. From Table 5.2 it can be seen that by increasing SSG concentration, the porosity increases. Figure 5.1 shows the size distribution for MCC granules at low binder concentration (5 %w) at 4 different disintegrant loading while Figures 5.2 is the size distribution of MCC granules with the same disintegrant concentration but higher concentration of HPMC in the binder (12.5 %w). Figure 5.4 gives the size distribution of DCPA granules made with 12.5 %w binder concentration for two different disintegrant loading of 4 and 6%w. From Figure 5.2, it can be seen that for MCC granules, the HPMC concentration affects the size distribution of the granules significantly. This is due to the impact of viscosity on the granules as it is reported by (Rahmanian, Naji, and Ghadiri 2011). Even though, DCPA granules use a high concentration of HPMC in the binder, but the granule size distributions are inclined toward small values which is due to the low liquid to solid ratio used. Also, the reason for different liquid to solid ratios in the case of DCPA is the impact of SSG on the maximum liquid to solid ratio. However, the impact of SSG on the size distribution is not straightforward. For example, in the case of low concentration MCC granules (Figure 5.1), adding SSG to MCC leads to a reduction in size. However, in the case of granules of MCC made with high concentration of binder (Figure 5.2), first the size increases by adding SSG and then it decreases with a higher concentration of SSG in the formulation. Given, the intention here was to granulate strong spherical granules and not investigating the impact of process conditions, the impact of SSG on the granulation was not investigated further.

## 5.4 Granule size measurement during disintegration

For validation, the aim was to fit the model to size data obtained from the flow cell experiments. Given that the granules have different initial sizes and because of the low impact

**Table 5.2:** *The formulation of the granules and their characteristics*

Granule ID	Excipient	Disintegrant concentration (%w)	Liquid to solid ratio	HPMC concentration (%w)	Skeletal density(kg/m <sup>3</sup> )	Porosity	Repeats
D4	DCPA	4	0.27	12.5	2685	0.51	1
D6	DCPA	6	0.3	12.5	2626	0.55	1
ML0	MCC	0	1	5	1514	0.29	1
ML2	MCC	2	1	5	1547	0.32	1
ML4	MCC	4	1	5	1551	0.38	1
ML6	MCC	6	1	5	1544	0.40	1
MH0	MCC	0	1	12.5	1504	0.27	1
MH2	MCC	2	1	12.5	1522	0.29	2
MH4	MCC	4	1	12.5	1515	0.33	2
MH6	MCC	6	1	12.5	1524	0.32	1

of initial size from the GSA results in Chapter 4, the data that were fitted to the model would be normalized radius which is radius at the current time to the initial value. However, before discussing the experimental data and fitting the model to the data, the strategy to fit the model and the necessary parameters to do that will be discussed first. The fitting parameters in this model are diffusivity of MCC, maximum mass absorption ratio of MCC and the porosity difference at infinite ( $\Delta\varepsilon_\infty$ ).

1. Fit the model to experimental data ( $\Delta\varepsilon_\infty$ ) using the values reported for diffusivity and maximum absorption ratio for the disintegrant and excipient.
2. If this is unsuccessful, fit the data by adding diffusivity of disintegrant (or excipient in case of no disintegrant in the granule).
3. If this is unsuccessful, add the maximum absorption ratio to the fitting parameters.

As it will be shown later, the first part of strategy worked very well with DCPA granules. However, for MCC granules, the diffusivity and maximum absorption ratio of ingredients has to be estimated too. For the pure MCC granules, all three parameters had to be estimated using the model. However, in the case of MCC granules with SSG included in them, only the

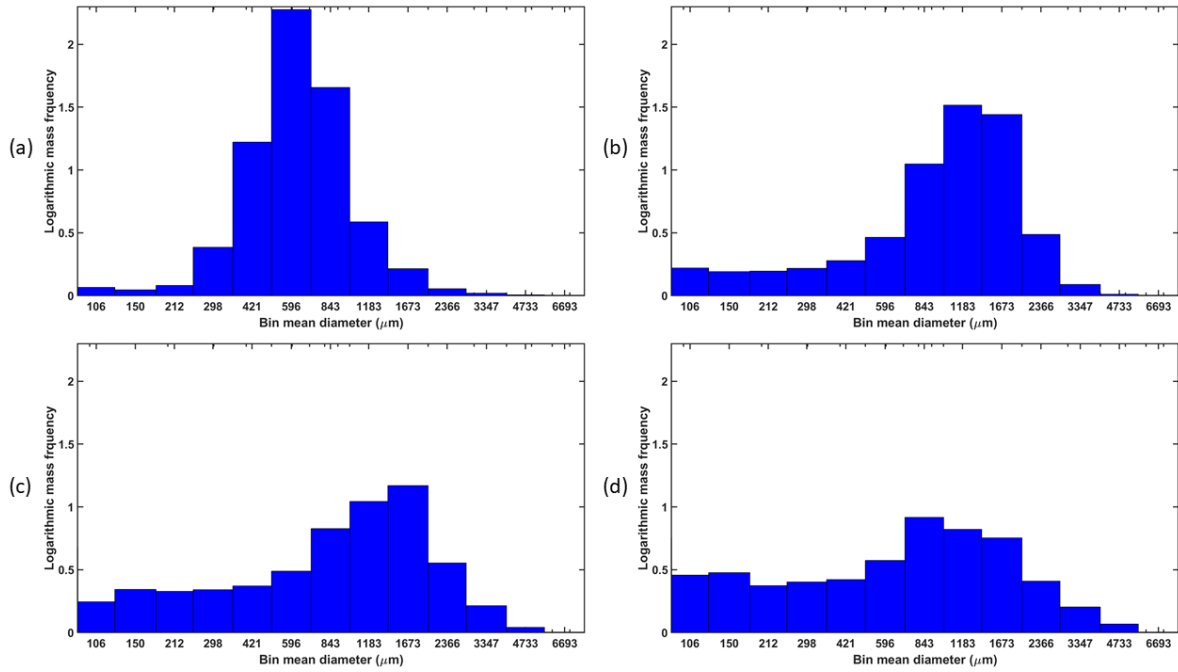


**Figure 5.1:** The size distributions of MCC granules with low HPMC binder concentration (5 %w) with different SSG concentration: (a) 0%, (b) 2%, (c) 4%, (d) 6%

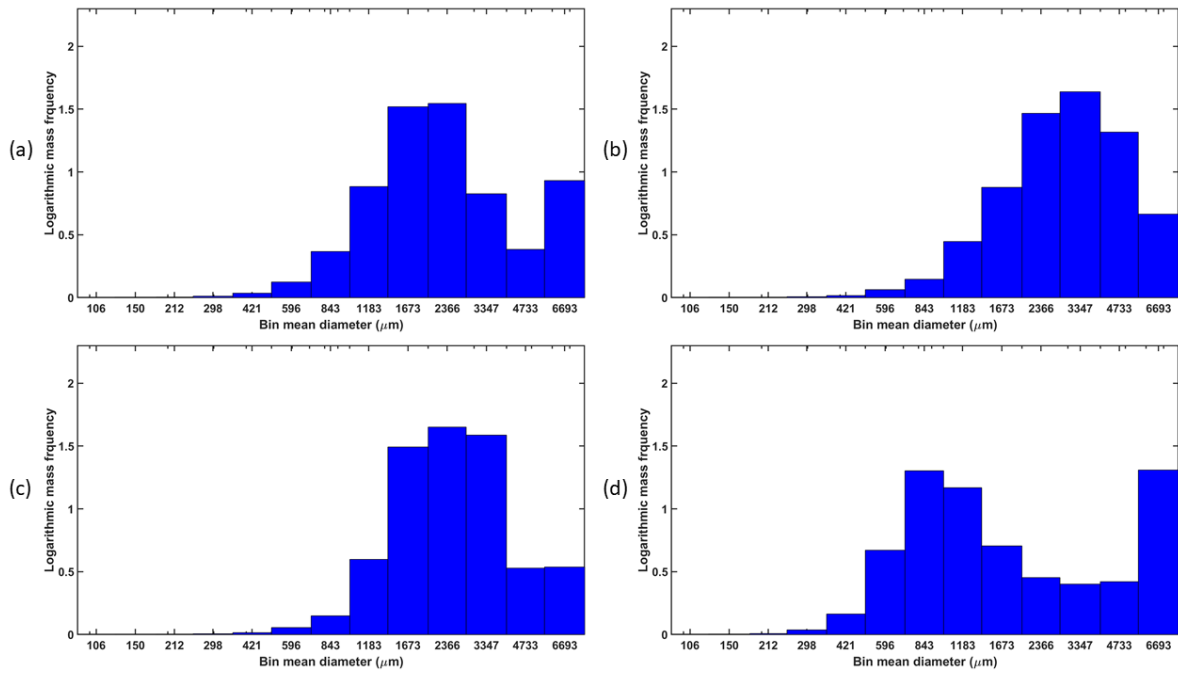


**Figure 5.2:** The size distributions of MCC granules with high HPMC binder concentration (12.5 %w) with different SSG concentration: (a) 0%, (b) 2%, (c) 4%, (d) 6%

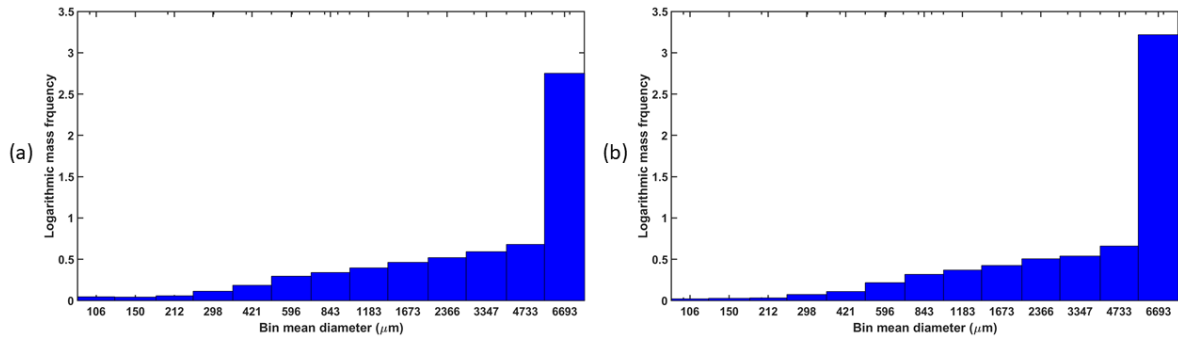


**Figure 5.3:** The size distribution of DCPA granules with different SSG and concentration and liquid to solid ratio: (a) 4% SSG and 0.27 L/S, (b) 6% SSG and 0.3 L/S

diffusivity of SSG had to be estimated as an additional parameter. A flowchart on Figure 5.4 shows the fitting process clearly.

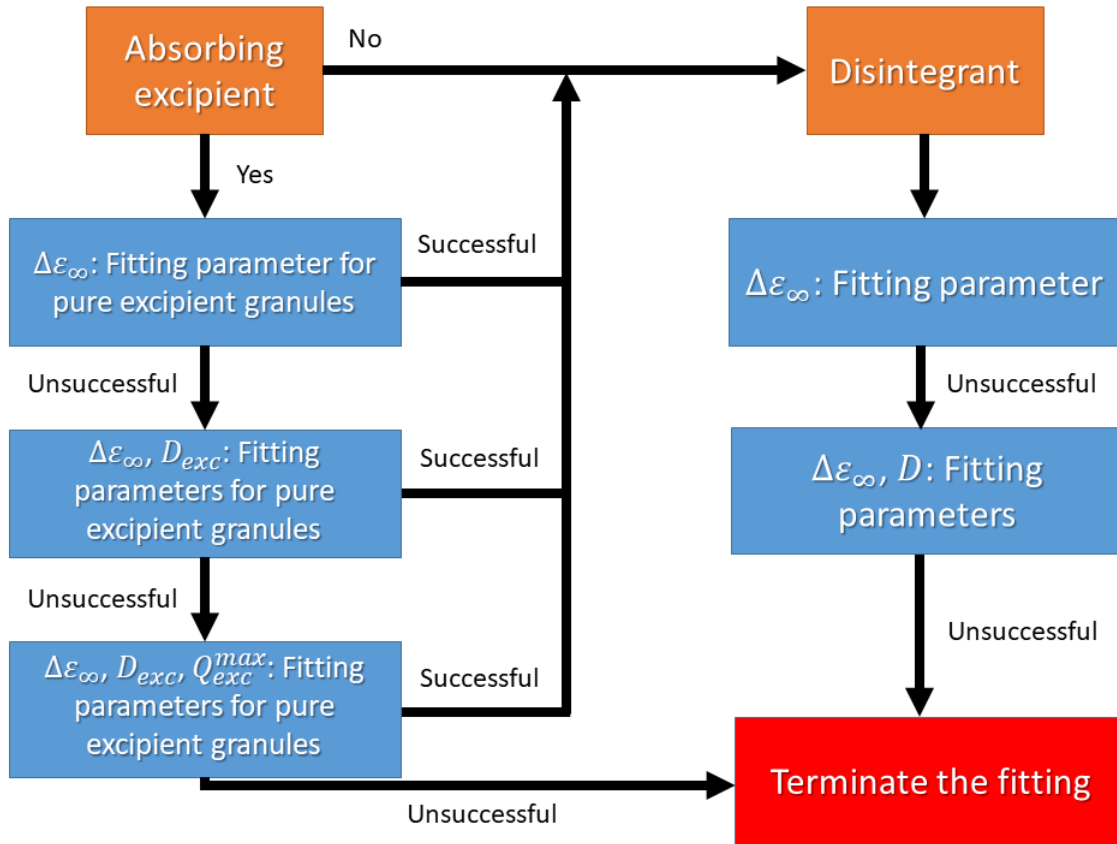


**Figure 5.4:** A diagram showing how to fit the model to the experimental data

The list of assumed parameters and the list of estimated parameters for each formulation are presented in Table 5.3 and 5.4 respectively. The fitted data are underlined in Table 5.4. Note that only the distributed model was used to estimate the parameters of the model. The

fitting was performed by using the trust-region-reflective algorithm of curve fitting toolbox in MATLAB 2022a which utilizes the non-linear least square method to fit the model to the data.

**Table 5.3:** *The assumed values of non-fitting parameters*

Parameter	Value
Disintegrant density ( $\rho_{dis}$ )	1560 kg/m <sup>3</sup>
Fluid density ( $\rho_l$ )	1000 kg/m <sup>3</sup>
Maximum absorption ratio of disintegrant ( $Q_{dis}^{max}$ )	10 g/g
Residual saturation ( $S_r$ )	0
Initial saturation ( $S_0$ )	0
Threshold saturation ( $S_{thr}$ )	0.1
Initial inherent imbibition time ( $\tau_{sat,0}$ )	10 s
Capillary pressure related exponent ( $M$ )	0.6
Wicking related parameter ( $\alpha$ )	0.02
Porosity related exponent ( $\beta$ )	1.2

#### 5.4.1 DCPA granules

The DCPA granule size as a function of time is shown in Figure 5.5 for both experimental and simulation data. The experiments for each formulation carried out in triplicate. By increasing the SSG content of the granule, the swelling rate increases, which is expected. According to (Markl, Yassin, Wilson, Goodwin, Anderson & Zeitler 2017), who studied the disintegration of tablets using terahertz spectroscopy, the first part of the swelling, has a linear like behaviour which is due to wicking. This step is much faster than the next step, which according to (Markl, Yassin, Wilson, Goodwin, Anderson & Zeitler 2017) and (Schott 1992b) obeys a second order kinetic model. Therefore, the slope of the first step can acts as a criterion for swelling. The first part was fitted using a linear model, as shown in Figure 5.6. Clearly, by increasing the SSG content, the granule swells faster leading to a faster disintegration, especially for 6 %w granules, which have a high swelling rate.

The model chosen to fit to the experimental data in this chapter is mono-sized model. This is because of similar results of both models and at the same time because the mono-sized model is the one used in Chapter 6 to develop the population balance model for the disintegration of granules. The model was fitted to the data for both formulations with porosity difference at infinite being the only fitting parameters. As it can be seen from

**Table 5.4:** The values of main parameters in the model for each formulation (The fitted parameters are underlined in the table)

Granule ID (refer to Table 5.2)	$D_{dis}$	$D_{exc}$	$Q_{dis}^{exc}$	$\Delta \varepsilon_{\infty}$	$R^2$
D4	231	0	1	<u>0.26</u>	0.98
D6	231	0	1	<u>0.33</u>	0.94
ML0	-	<u>0.31</u>	<u>1.21</u>	<u>0.05</u>	0.99
ML2	<u>0.8</u>	0.31	1.21	<u>0.05</u>	0.63
ML4	<u>15</u>	0.31	1.21	<u>0.09</u>	0.69
ML6	<u>44</u>	0.31	1.21	<u>0.1</u>	0.88
MH0	-	<u>0.38</u>	<u>1.36</u>	<u>0.04</u>	0.95
MH4	<u>1.2</u>	0.38	1.36	<u>0.05</u>	0.98
MH6	<u>8</u>	0.38	1.36	<u>0.07</u>	0.90

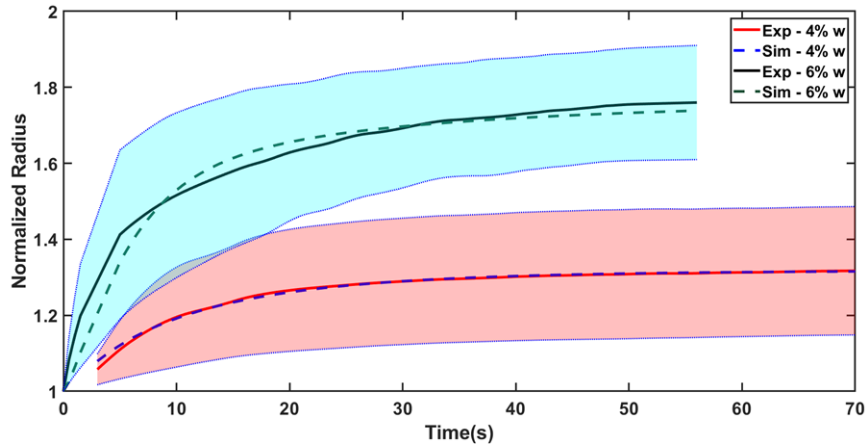
**Figure 5.5:** Granule size as a function of time: Effect of SSG concentration; the standard deviation for experimental results and the fitted data for DCPA based granules during swelling. Image acquisition rate was fixed at 250ms.

Figure 5.5, the model fits to the data very well. Based on obtained data it can be concluded that disintegrant mass fraction has profound effect on granule disintegration performance as it was shown in the GSA of single granule swelling model. Its impact are partly manifested through parameters like porosity difference at infinite, as by increasing mass fraction of SSG, this parameter increases considerably (Table 5.4).

Based on the obtained parameter (porosity difference at infinite), the size distribution of SSG particles inside the granules for each formulation at its final time was modelled using

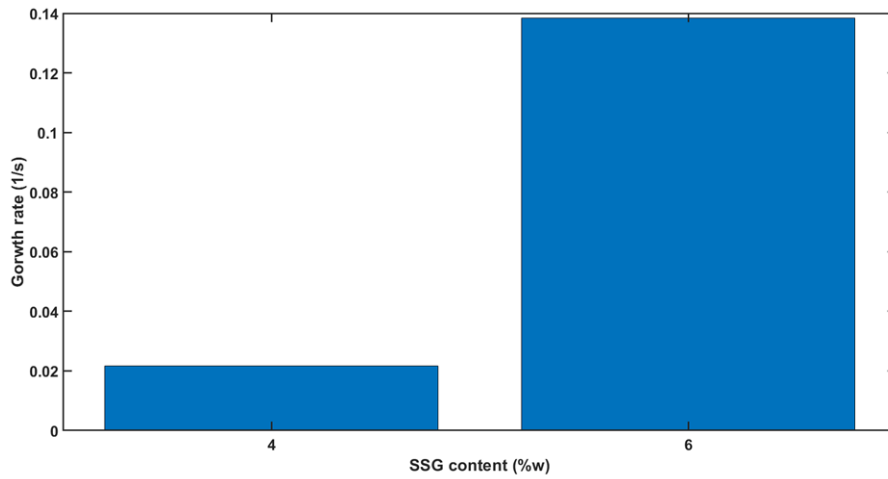


Figure 5.6: The slope of the first part of swelling data for DCPA granules

the distributed single granule swelling model. As it can be seen from Figure 5.7, the final distribution for both data are almost identical, meaning the majority of the SSG particles have reached their maximum absorption ratio.

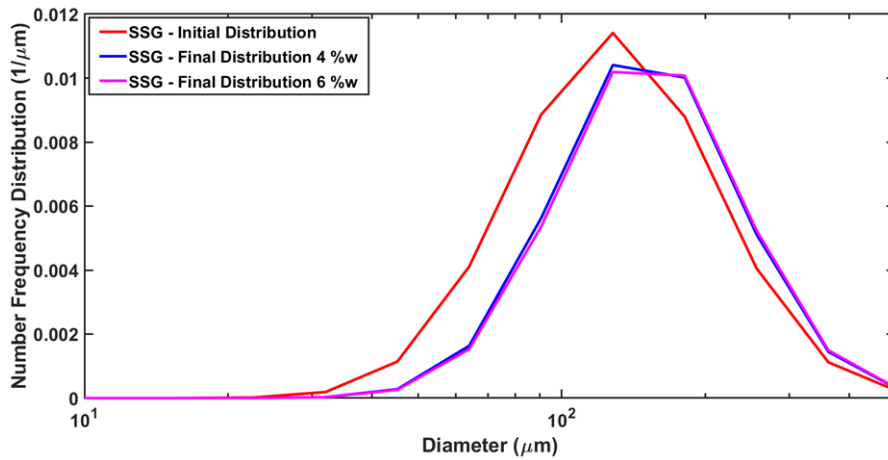


Figure 5.7: The size distribution of SSG particles at the beginning and the end of disintegration for both formulations of DCPA

### 5.4.2 MCC granules made with low binder concentration

The data for MCC granules produced from 5 %w HPMC binder solution is shown in Figure 5.8. Compared to DCPA granules, the swelling of MCC granules is much slower. The growth rate at the wicking part of swelling was calculated and is shown in Figure 5.9. The data clearly shows a much slower growth rate than anticipated. This is mainly to the following reasons:

1. The deactivation of SSG and MCC particles due to the absorbance of water in the

binder during the granulation.

2. The impact of storage and gradual moisture absorbance, as reported by (Quodbach & Kleinebudde 2015).
3. Lastly, the gelling effect of HPMC in the granules. The water absorbance by HPMC can lower its glassy temperature, leading to its expansion and blockage of the pores (Siepmann & Peppas 2012). This is also influenced by the high liquid to solid ratio which leads to more HPMC solid bridges being formed in the granule.

Despite this fact, the impact of disintegrant mass fraction on the swelling rate can clearly be seen, especially in the case of granules made with 6 %w SSG. Because of this slower growth rate, diffusivity had to be added as an additional parameter to the model in order to fit the data. For pure MCC granules, the maximum absorption ratio was also considered as a fitting parameter as in pure excipient granules.

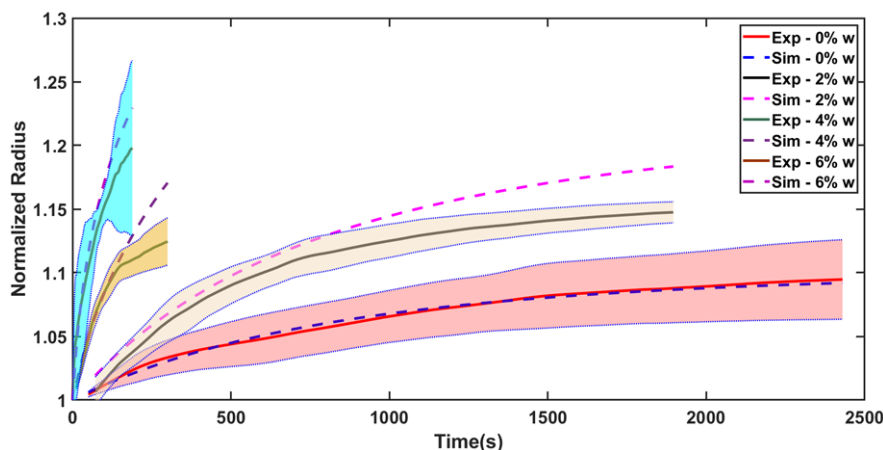


**Figure 5.8:** Granule size as a function of time: Effect of SSG concentration the standard deviation for experimental results and the fitted data for MCC granules made using 5 %w HPMC binder solution during swelling. Image acquisition rate was fixed at 5s.

Following these modifications, a good fit was found. For the granules containing SSG, the model was fitted using the parameters obtained from pure MCC granules as the initial estimate which proved to be a very effective tool to estimate the fitting parameters. For 2 % SSG and 4 % SSG granules, the model is not capable of accurately predict the granule behaviour, while for 6 % SSG granules the confidence in prediction increases, as it shown by R-squared data in Table 5.4. This is mainly due to variability in the granules that go under disintegration. While it is assumed that each granule has the same porosity and disintegrant mass fraction, in reality, the granules have a distribution of porosity and mass fraction which can cause different behaviours in disintegration. This is also influenced by the lack of uniformity inside the granules and the impact of pore size distribution. One major factor that can be deduced from the data is that, while in some cases it may not predict the data accurately for the whole disintegrant mass fraction range, it can predict the behaviour accurately especially the wicking part of the swelling. According to (Markl, Yassin, Wilson, Goodwin, Anderson & Zeitler 2017), this is the most important part of the swelling and most

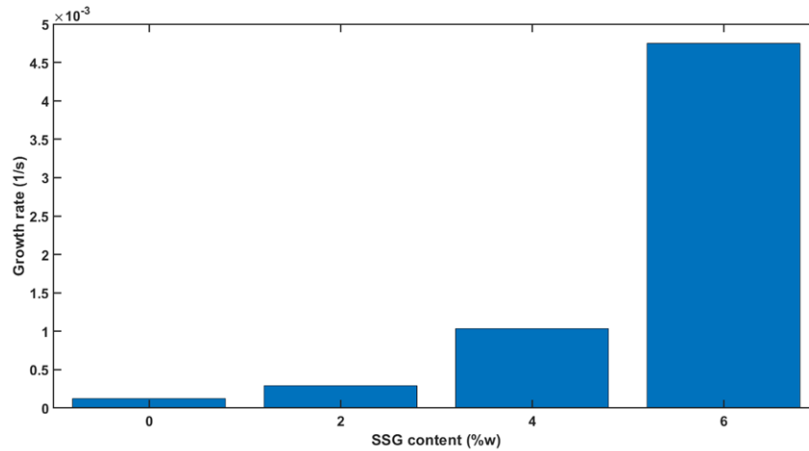


**Figure 5.9:** The slope of the first part of swelling data for MCC granules made using 5 %w HPMC binder solution

disintegration happens in this stage. Furthermore, the data shows clearly the impact of SSG mass fraction on the model through parameters such as SSG diffusivity and to some extent, porosity difference. Based on the obtained fitting parameters, the size distributions of SSG granules at the initial and final moments have been compared for each formulation. From Figure 5.10, the data clearly shows a migration of granules towards the larger sizes. This is due to the increase in diffusivity of SSG, especially in the case of 6 %w granules.

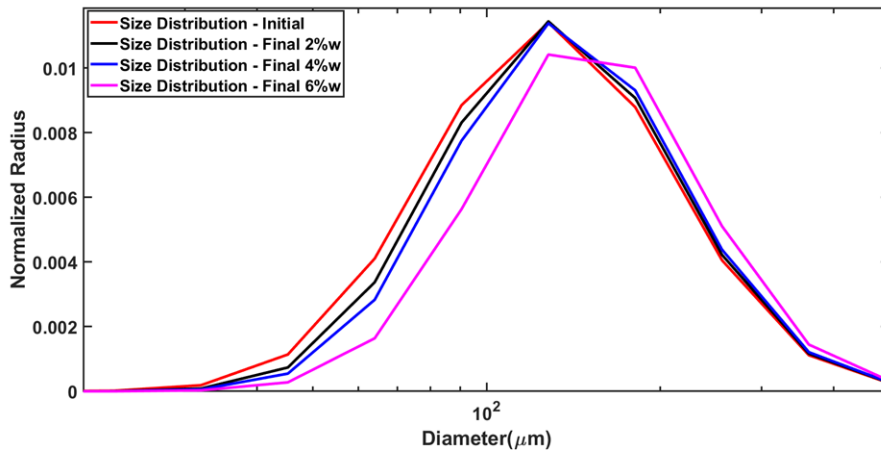
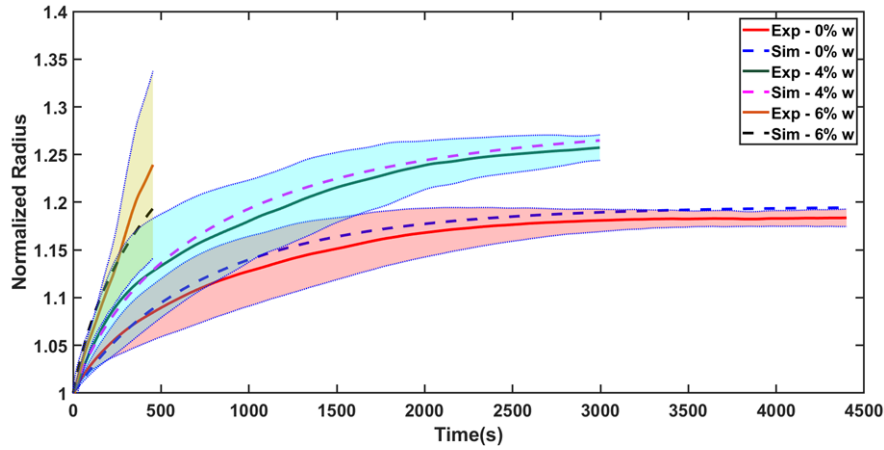


**Figure 5.10:** The size distribution of SSG particles at the beginning and the end of disintegration data for MCC granules made of 5 %w HPMC binder solution

### 5.4.3 MCC granules made with high binder concentration

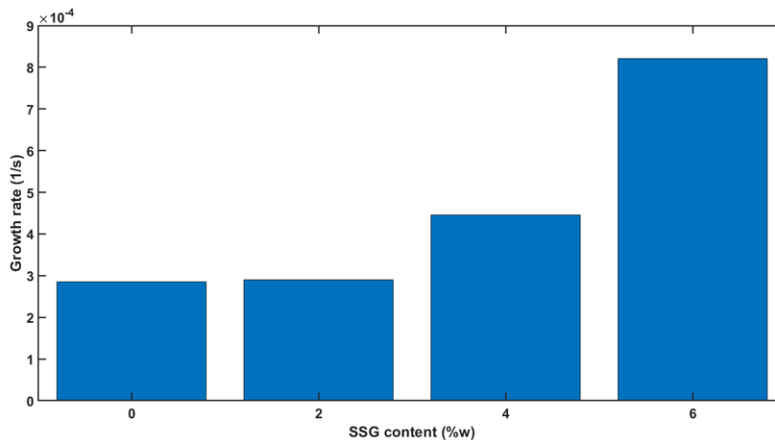
The granule size measurement data, shown in Figure 5.11, clearly shows a slow growth rate, which is even slower than MCC granules with a low concentration of HPMC in the binder. To confirm this, the swelling rate at the wicking part, was obtained. The data, shown in

Figure 5.12, also show the lower impact of SSG disintegrant on the swelling. In the case of MCC with low concentration of HPMC, a big jump is observed between 4 and 6 %w.



**Figure 5.11:** Granule size as a function of time: Effect of SSG concentration the standard deviation for experimental results and the fitted data for MCC granules made using 12.5 %w HPMC binder solution during swelling. Image acquisition rate was fixed at 10s.

While a considerable increase in swelling is seen, the increase is much less than expected. An important note regarding the model and the data obtained here is that the model could not be fitted to the experimental data obtained for 2 % w granules as 2 % w granules showed less swelling capability than pure MCC granules. By taking a look at Figures 5.11 and 5.12, it can be seen that these granules have the same growth rate as pure MCC granules, which is mainly because of the impact of HPMC gelling especially at a high concentration such as used here. Overall, from the experimental data and the fitted parameters in Table 5.4, the same trend can be seen; the increase in diffusivity and porosity difference at infinite by increasing the SSG mass fraction.



**Figure 5.12:** The slope of the first part of swelling data for MCC granules made using 12.5 %w HPMC binder solution

Using the fitted data, the size distributions of SSG particles inside the granules at the end

of the swelling for 4 % and 6 % w granules have been predicted using the distributed single granule swelling model (Figure 5.13). The data shows a slight migration towards larger sizes for 6 % compared to 4 % granules which is mostly due to the increase in diffusivity of the granules.

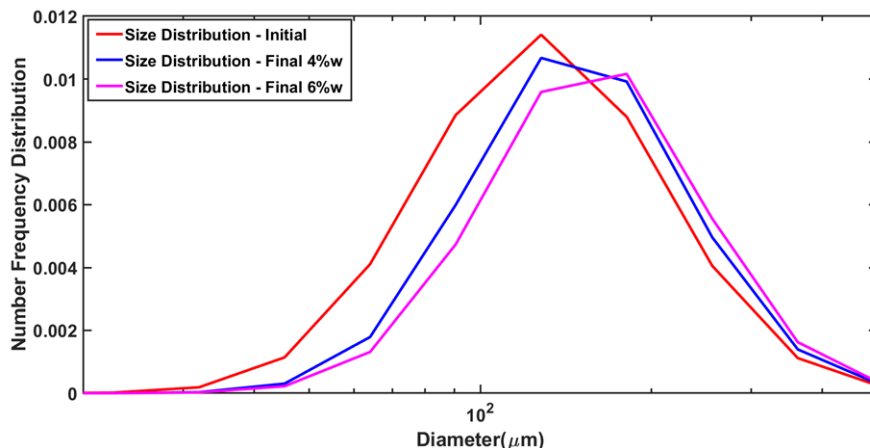


**Figure 5.13:** *The size distribution of SSG particles at the beginning and the end of disintegration data for MCC granules made of 12.5 %w HPMC binder solution*

## 5.5 Conclusion

The mono-sized model presented in Chapter 4 was tested using the data obtained from the specially designed flow cell that measures the size of granules during swelling. The model was fitted to the swelling data obtained from the flow cell. To fit the model into the data, a fitting strategy was suggested. The aim of this strategy was to fit the model to the data using the least number of parameters. The results for MCC granules, with both high and low concentrations of HPMC in the binder solution, showed a very slow swelling rate. This was less than was expected which was due to partial de-activation of disintegrant and excipient particles, the storage impact and mainly the gelling of HPMC binder. The model for the most part predicted the data accurately. However, the model managed to predict the first part of swelling known as wicking stage in all cases. This is an important aspect of the model as most disintegrations would happen at this stage. At the same time, by increasing the binder concentration, the swelling rate decreased which is manifested through the diffusivity of the disintegrant.

The fitted data for DCPA granules shows much improvement. The model was fitted to the data nicely. Simultaneously, the data needed only one fitting parameter to be fitted which clearly shows the strength of the model. Based on the fitting parameters obtained for each granulation, the size distributions of disintegrant particles were predicted using the distributed model developed in Chapter 4. The model predicts the migration of distribution towards the large sizes at the end of swelling by increasing the mass fraction of disintegrants. This research has shown that the model shows a great potential in predicting the behaviour of swelling granules, especially in the case of fast disintegration granules.

## Chapter 6

# Development of the population balance model

### 6.1 Introduction

In this chapter, a new mechanistic population balance model is presented for the disintegration of granules. Justifiable assumptions are applied to simplify the model leading to a set of linear like models for the disintegration. The model uses the terms defined previously for mono-sized single granule swelling model for describing the growth terms in the model. Subsequently, a series of global sensitivity analysis was performed in the model. It was found out that of all the parameters involved in the swelling of granules. the diffusivity of the disintegrant plays the main role in the disintegration behaviour of a population of granules.

### 6.2 Model development

#### 6.2.1 Population balance equation

When dealt with particulate systems, A powerful tool is needed that can quantitatively describe the composition of the system. An equation known as the population balance is a strong tool that has been developed for such purposes. The population balance is a rate equation which gives us the change in number of particles with respect to a given property. It consists of a kinetic expression for each mechanism that involves changing the number of particles. The population balance was introduced as a general equation for particulate systems independently (Hulburt & Katz 1964). It is a powerful tool with uses including:

- Critical evaluation of data to determine controlling mechanisms,
- to predict the mean size and size distribution of product particles,
- optimization and process control,
- facilitate the process of sensitivity analysis which analyses the effect of changes in operating conditions or feed variables on product quality quantitatively.

In most applications there is more than one internal property describing the required properties of the distributions. These properties can be either size (volume or radius), concentration, surface area etc. For a batch system, like the one here, the population balance equation can be written as following:

$$\frac{\partial f(\mathbf{x}, t)}{\partial t} = \nabla \cdot (\mathbf{G}(\mathbf{x}, t)f(\mathbf{x}, t)) + \dot{B}(\mathbf{x}, t) - \dot{D}(\mathbf{x}, t) \quad (6.1)$$

where  $f$  is a parameter known as density function that can determine the number of particle,  $\mathbf{x}$  is the vector of internal properties and  $t$  is time.  $\dot{B}$  is the frequency distribution of the new-born particles with property  $\mathbf{x}$  while  $\dot{D}$  is the death rate frequency distribution. The term  $\mathbf{G}$  is vector function known as the growth term and  $\nabla$  is the gradient operator. There are major processes in population balance modelling are divided to four different categories:

1. Aggregation
2. Breakage
3. Growth
4. Nucleation

In the following sections, each type of process would be discussed in detail.

### 6.2.1.1 Aggregation

Aggregation, agglomeration, coalescence, and flocculation are a family of related rate processes in which several particles join together to form a single larger particle. In its simplest form, only binary coalescence are considered for such processes (think of only two particles or cells combining) which mostly happens in dilute solutions. Binary coalescence involves both a birth term and a death term in the population balance as one larger particle is created (birth) from two small particles (death). The death term of smaller particle depends on the number of collision. If it is assumed the system is completely random (in which the collision rate of particles with sizes  $\mathbf{x}$  and  $\mathbf{x}'$  can be proportional to the number of particles colliding), then it can be assumed that:

$$\text{successful collision rate of } \mathbf{x} \text{ and } \mathbf{x}' \propto f(\mathbf{x}, t)f(\mathbf{x}', t) \quad (6.2)$$

based on this formula, a new function known as aggregation kernel  $\beta$  can be introduce where:

$$\text{successful collision rate of } \mathbf{x} \text{ and } \mathbf{x}' = \beta(\mathbf{x}, \mathbf{x}')f(\mathbf{x}, t)f(\mathbf{x}', t) \quad (6.3)$$

As it can be seen this function acts like a frequency coefficient and depends on both  $\mathbf{x}$  and  $\mathbf{x}'$ . Furthermore, this function is symmetric as the collision rate of  $\mathbf{x}$  with  $\mathbf{x}'$  should be exactly the same when size  $\mathbf{x}'$  collides with  $\mathbf{x}$ . In other words:

$$\beta(\mathbf{x}, \mathbf{x}') = \beta(\mathbf{x}', \mathbf{x}) \quad (6.4)$$

Based on this fact it can be said that a particle with property  $\mathbf{x}$  can be created from smaller particles with size  $\mathbf{x}'$  and  $\mathbf{x} - \mathbf{x}'$  while it can create bigger at the same time with other particles with any possible size. Therefore, the birth and death terms of aggregation is:

$$\begin{cases} \dot{B}_{agg}(\mathbf{x}, t) = \frac{1}{2} \int_0^{\mathbf{x}} \beta(\mathbf{x}', \mathbf{x} - \mathbf{x}') f(\mathbf{x}', t) f(\mathbf{x} - \mathbf{x}', t) d\mathbf{x}' \\ \dot{D}_{agg}(\mathbf{x}, t) = \int_0^{\infty} \beta(\mathbf{x}, \mathbf{x}') f(\mathbf{x}, t) f(\mathbf{x}', t) d\mathbf{x}' \end{cases} \quad (6.5)$$

The reason for coefficient 1/2 in the birth term is the collision rate there is counted twice for each particle. In such processes, the size distribution tends to migrate to larger particle over the time. It is important to know that this process preserve the first moment vector which is defined as:

$$\mu_1(t) = \int_0^{\infty} \mathbf{x} f(\mathbf{x}, t) d\mathbf{x} \quad (6.6)$$

### 6.2.1.2 Breakage

Even though usually processes like crushing and grinding come to mind when the term particle breakage is discussed, but breakage can also occur in many other particulate processes such as granulation and disintegration. Breakage is generally considered as a first-order process in which particle volume is conserved just like the aggregation. In other words, the breakage (death) rate of a particle with property  $\mathbf{x}$  is proportional to its density function. Therefore like the case with aggregation a new proportionality function known as selection function  $\psi$  can be introduced:

$$\dot{D}_{bre}(\mathbf{x}, t) = \psi(\mathbf{x}) f(\mathbf{x}, t) \quad (6.7)$$

However, for the birth term another function should be added. This function should gives us the number of daughter particles with property  $\mathbf{x}$  produced from the mother particle  $\mathbf{x}'$  which is called the breakage function  $b(\mathbf{x}|\mathbf{x}')$  and it can be related to breakage birth term as described in the following equation (6.8)

$$\dot{B}_{bre}(\mathbf{x}, t) = \int_{\mathbf{x}}^{\infty} \psi(\mathbf{x}') b(\mathbf{x}|\mathbf{x}') f(\mathbf{x}', t) d\mathbf{x}' \quad (6.8)$$

It is worth noting due to mass conservation law, just like the aggregation, breakage does not change its first moment. It is important to mention that most important part of the disintegration is particle breakage from the stress build-up due to liquid uptake in the granule. Therefore, in a breakage oriented system such as this, the density function tends to migrate towards the smaller particles over the time as the number of particle is rises due to the nature of the process.

### 6.2.1.3 Growth

In growth process, the small particles are either entering the particulate phase joining the particles in that phase or detach themselves from such particles, leave the particulate phase into the continuous phase. This rate is known as growth term  $\mathbf{G}(\mathbf{x}, t)$  and most happens in a differential manner. As such, the number of particles does not change however there is a gradual particle size migration towards the larger particles region or smaller ones depending

on the type of growth process. For example, in the case of layering in wet granulation and liquid uptake in both disintegration and dissolution that leads up to a swelling, the growth term is positive while in the case of polymer disentanglement/mass transfer in dissolution or erosion, the growth term is negative.

#### 6.2.1.4 Nucleation

Nucleation can be described as any process in which produces new particles are created from continuous phase. In process like wet granulation, this nucleation is from continuous phase while in the case of attrition or physically controlled erosion, it can be from the particulate phase and that is due to the nature of the erosion. In such processes, small particles are gradually detached from the surface of large particle which are known as primary particles/agglomerates and can acts as a nucleation points. Thus, nucleation involves a birth term only. The mathematical expression for nucleation at size  $\mathbf{x}_0$  size is:

$$\dot{B}(\mathbf{x}, t) = \dot{B}_{0,nuc}(t)\delta(\mathbf{x} - \mathbf{x}_0) \quad (6.9)$$

where  $\dot{B}_{0,nuc}$  is a (time dependent) birth term and  $\delta$  is the well-known Dirac delta function. Generally, the main challenges in population balance equation are how to obtain these functions from the physics of the studied phenomenon and the aim in this chapter is to obtain the suitable terms for PBM of disintegration based on its physics.

#### 6.2.1.5 Population balance equation: Lumped form

As it is known in a process like disintegration two major phenomenon happen that can be related to PBM, first is the swelling and the second the breakage of a granules. The process of swelling is a combination of:

- i) Liquid penetration where liquid goes into the porous phase of the granule.
- ii) Liquid absorption where primary particles in the solid phase of the granules absorb the liquid, each type of primary particle with different rate.
- iii) Swelling where the granules expand due to expansion of primary particles.

For the breakage, the process consists of mainly the granule breaking until all particles remaining in the system are primary particles. So, in general, to model disintegration through PBM, a multi-dimensional system consisted of breakage and growth, like equation (6.10), should be considered:

$$\frac{\partial f(\mathbf{x}, t)}{\partial t} = -\nabla \cdot (\mathbf{G}(\mathbf{x}, t)f(\mathbf{x}, t)) + \int_{\mathbf{x}}^{\infty} \psi(\mathbf{x}')b(\mathbf{x}|\mathbf{x}')f(\mathbf{x}', t)d\mathbf{x}' - \psi(\mathbf{x})f(\mathbf{x}, t) \quad (6.10)$$

The occurrence of multidimensional PBMs in the literature is rare due to the difficulty to solve and their complexity. Instead, the researchers have proposed a simpler approach known as tracer approach or lumped-based PBM. In this approach, an additive property of the PBM, mainly volume, is taken as the main internal property and the other parameters are averaged over that main variable. By doing this, the system complexity is reduced whilst still describing the multidimensional nature of the system. (Hounslow et al. 2001) have already developed the lumped form for the breakage. A lumped form of growth was developed using the following assumptions:

- The density function at their limit would be zero like when the volume of the solid phase in a particle is either zero or the same volume of particles.
- The growth function is centred around the average value of the tracer.

By employing these assumptions, the population balance reduces to Eq. (6.11) and (6.11):

$$\frac{\partial n(V, t)}{\partial t} = -\frac{\partial}{\partial V} \left( G_V(V, t)n(V, t) \right) - \psi(V, t)n(V, t) + \int_V^\infty \psi(V', t)b(V|V')n(V', t)dV' \quad (6.11)$$

and,

$$\frac{\partial \mathbf{M}(V, t)}{\partial t} = \mathbf{G}_M(V, t)n(V, t) - \frac{\partial}{\partial V} \left( G_V(V, t)\mathbf{M}(V, t) \right) - \psi(V, t)\mathbf{M}(V, t) + \int_V^\infty \psi(V', t)b(V|V')\frac{V}{V'}\mathbf{M}(V', t)dV' \quad (6.12)$$

where  $V$  is volume,  $n$  is the number-based size distribution,  $G_V$  is the volumetric growth term,  $\mathbf{M}$  is the tracer function and  $\mathbf{G}_M$  is the growth term related to other coordinates in the model. Function  $\mathbf{M}$  is defined in equation (6.13):

$$M_i(V, t) = \int_{\mathbf{0}}^\infty U_i f(\mathbf{U}, V, t)d\mathbf{U}, \quad U_i \neq V \quad (6.13)$$

where  $\mathbf{U}$  is an internal coordinate vector that includes all internal coordinates except the main coordinate in the lumped form of PBE (the volume of granule in here) and can encompass any type of additive variable such as volume of the solid in the granules, number of primary particles, volume of the liquid in the granule and etc. However, there is tendency in the literature towards the reduced form of Eq. (6.12) where instead of function  $\mathbf{M}$ , its average is ( $\bar{\mathbf{M}}(V, t) = \frac{\mathbf{M}(V, t)}{n(V, t)}$ ) is used. By doing this, the size distribution in the tracer equation would disappear from the tracer function and instead variables in the reduced form have more physical meanings such as average volume of solid in the granule or average number of particles. The reduced form of the Eq. (6.12) is shown in Eq. (6.14):

$$\frac{\partial \bar{\mathbf{M}}(V, t)}{\partial t} = \mathbf{G}_{\bar{\mathbf{M}}}(V, t) - G_V(V, t)\frac{\partial \bar{\mathbf{M}}(V, t)}{\partial V} + \int_V^\infty \psi(V', t)b(V|V') \left( \frac{Vn(V', t)}{V'n(V, t)}\bar{\mathbf{M}}(V', t) - \bar{\mathbf{M}}(V, t) \right) dV' \quad (6.14)$$

This form is easier to visualise and to implement in software like gPROMS or MATLAB where utilizing finite difference or finite volume-based techniques are easier. If instead of volume, radius of the granule is taken into account, and considering that  $dR/G_R = dV/G_V$ , the size-based form of lumped form of PBM would be obtained in equations (6.15) and (6.16):

$$\frac{\partial n(R, t)}{\partial t} = -\frac{\partial}{\partial R} \left( G_R(R, t)n(R, t) \right) - \psi(R, t)n(R, t) + \int_R^\infty \psi(R', t)b(R|R')n(R', t)dR' \quad (6.15)$$

and,

$$\begin{aligned} \frac{\partial \bar{\mathbf{M}}(R, t)}{\partial t} = & \mathbf{G}_{\bar{\mathbf{M}}}(R, t) - G_R(R, t) \frac{\partial \bar{\mathbf{M}}(R, t)}{\partial R} \\ & + \int_R^\infty \psi(R', t) b(R|R') \left( \left( \frac{R}{R'} \right)^3 \frac{n(R', t)}{n(R, t)} \bar{\mathbf{M}}(R', t) - \bar{\mathbf{M}}(R, t) \right) dR' \end{aligned} \quad (6.16)$$

For modelling the disintegration process using the mono-sized single granule swelling model, the following assumptions are considered:

1. The granules that go through breakage, directly release their primary particles into the surrounding fluid.
2. There is size threshold after which the breakage is the dominant mechanism in the breakage of granule. Below this value, if there is any aggregate, the dominant mechanism in the breakage would be de-agglomeration.

Regarding the first assumption, as it is known in the disintegration, the large granules go through breakage and release their primary particles. Depending on the formulation and the process, some granules may produce some aggregates too. The aggregates are smaller granules that still have primary particles in them and are produced by granule breakage. This introduces a new level of complexity to the model which is not needed. As it will be shown in chapter 7, the aggregates most likely are not produced or have a very short lifespan and break into primary particles. Therefore, it is assumed that when the granules go through breakage, they straight release their primary particles to the surrounding fluid. The second assumption is very important mainly because mainly swelling happens when a large of number primary particles that are attached together, go through liquid absorbance. This is different to breakage of smaller aggregates that are made of a few primary particles. While these granules may swell, the type of mechanism that break them apart are mostly de-agglomeration (Wilson et al. 2012). Therefore, there is a threshold in size where swelling becomes the dominant disintegrating force.

Combining this assumption with the first one, leads to the conclusion that there are two size distributions in the disintegration: The size distribution of granules and size distribution of released primary particles. Another consequence of this assumption is that no granules can be born from the breakage of larger granules. Instead, all the birth term of the breakage of the granules goes to the released primary particles. In section 6.2.2 and 6.2.3, the population balance model of each of one these size classes.

## 6.2.2 Population balance modelling of disintegrating granules

In this size class, designated as  $R$ , there are other lumped properties that have to be considered in the model which are:

1. The number of primary particles in the granules,  $n_p(R, t)$ ,
2. The total volume of each solid component in the solid phase,  $V_{s,i}(R, t)$ ,
3. The volume of liquid inside the porous phase of the granule,  $V_l(R, t) (= \frac{4\pi}{3} \varepsilon(R, t) S(R, t) R^3)$ .

The changes in the lumped properties described above can be described through Eq. (6.16) while the number-based distribution of granules,  $n_g(R, t)$  can be obtained by using Eq. (6.15). Each one of these equations introduces new terms to the overall population balance model which are:

- $G_R$ , the growth rate of the granule,
- $\psi$ , the selection function of the breakage,
- $G_{n_p}$ , the rate of the number of primary particles,
- $G_{V_{s,i}}$ , the liquid absorbance rate of  $i^{th}$  component in the solid phase,
- $G_{V_l}$ , the liquid penetration rate into the porous phase of granule.

The reason why the breakage probability function is not used here is because of the assumption used earlier where the granules breakage would not produce smaller granules. All these terms, except the selection function, can be obtained from single granule swelling modelling. The value of  $G_{n_p}$ , in a swelling granule is zero because in a swelling granule there is no change in the number of primary particles and thus,

$$G_{n_p}(R, t) = 0 \quad (6.17)$$

In the case of total volume of  $i^{th}$  component in the solid phase,  $V_{s,i}$ , its growth term,  $G_{V_{s,i}}$  is described in equation (6.18) using equation (4.35):

$$\begin{aligned} G_{V_{s,i}}(R, t) = & \text{number of primary particles in the granule} \times \text{number fraction of } i^{th} \\ & \text{component} \times \text{absorbance rate of single granule of } i^{th} \text{ component} = \\ n_p(R, t) \times x_{n,i} \times G_{V_{p,i}}(R, t) = & 4\pi x_{n,i} n_{p,i}(R, t) f(\hat{S}_a(R, t)) D_i R_{p,i}(R, t) \frac{\rho_{s,i} Q_i^{max} - Q_i^{abs}(R, t)}{\rho_l Q_i^{abs}(R, t)} \end{aligned} \quad (6.18)$$

where  $G_{V_{p,i}}(R, t)$  is the absorbance rate of single granule which can be formulated using Eq. (4.35):

$$\begin{aligned} G_{V_{p,i}}(R, t) = 4\pi R_{p,i}^2(R, t) G_{R_{p,i}}(R, t) = \\ 4\pi f(\hat{S}_a(R, t)) D_i R_{p,i}(R, t) \frac{\rho_{s,i} Q_i^{max} - Q_i^{abs}(R, t)}{\rho_l Q_i^{abs}(R, t)} \end{aligned} \quad (6.19)$$

where  $R_{p,i}(R, t)$  is the radius of  $i^{th}$  component in the solid phase of a granule with size  $R$  at time  $t$  and  $G_{R_{p,i}}(R, t)$  is its growth rate which is equal to the right side of Eq. (4.35). The growth term of the volume of liquid inside the porous phase of the granule  $V_l(R, t)$  is formulated in Eq. (6.20) using equations (4.31), (6.18) and (6.19):

$$G_{V_l}(R, t) = 2\pi \frac{\varepsilon(R, t) R^3}{\tau_{sat}(\varepsilon(R, t), R, \bar{R}_p(R, t))} \frac{(1 - S_a(R, t))}{S_a(R, t) + \alpha} - \sum_i G_{V_{s,i}}(R, t) \quad (6.20)$$

and the porosity can be obtained using Eq. (4.41) and (4.42). Lastly, the growth term of the granule  $G_R$ , is shown in Eq. (6.21) using equation (4.4):

$$G_R(R, t) = \frac{R}{3} \left( \frac{G_\varepsilon(R, t)}{1 - \varepsilon(R, t)} + \frac{\sum_i x_{n,i} G_{V_{p,i}}(R, t)}{\sum_i x_{n,i} V_{p,i}(R, t)} \right) \quad (6.21)$$

in which  $V_{p,i}(R, t)$  is the volume of  $i^{\text{th}}$  component in the solid phase and  $G_\varepsilon(R, t)$  is growth rate porosity in the granule and can be obtained through equations (4.41) and (4.42):

$$G_\varepsilon(R, t) = \frac{\Delta\varepsilon_\infty \beta \rho l}{\sum_i x_{n,i} \rho_{s,i} V_{p,i}(0)} \frac{1}{\sum_i w_i (Q_i^{\text{max}} - 1)} (1 - \hat{m}_s)^{\beta-1} \sum_i x_{n,i} G_{V_{p,i}}(R, t) \quad (6.22)$$

Based on the obtained growth terms, and considering there is no birth term from the breakage, the equation for number-based distribution of granules,  $n_g(R, t)$ , would be reduced to Eq. (6.23) using Eq. (6.15):

$$\frac{\partial n_g(R, t)}{\partial t} = -\frac{\partial}{\partial R} (G_R(R, t) n_g(R, t)) - \psi(R, t) n_g(R, t) \quad (6.23)$$

For the total number of primary particles in the granules,  $n_p(R, t)$ , the reduced form of Eq. (6.16), would lead to the following equation (6.24) by considering Eq. (6.17):

$$\frac{\partial n_p(R, t)}{\partial t} = -G_R(R, t) \frac{\partial n_p(R, t)}{\partial R} \quad (6.24)$$

In the case of  $V_{s,i}(R, t)$ , equation (6.16) would be reduced to the following form:

$$\frac{\partial V_{s,i}(R, t)}{\partial t} = -G_R(R, t) \frac{\partial V_{s,i}(R, t)}{\partial R} + G_{V_{s,i}}(R, t) \quad (6.25)$$

However, equation (6.25) can be reduced to rate change of volume of single granule using equations (6.18) and (6.24):

$$\frac{\partial V_{p,i}(R, t)}{\partial t} = -G_R(R, t) \frac{\partial V_{p,i}(R, t)}{\partial R} + G_{V_{p,i}}(R, t) \quad (6.26)$$

This equation can be further simplified to the rate change of radius of primary particles in the granule,  $R_{p,i}(R, t)$ . By considering equation (6.19), the following Eq. (6.27) would be achieved:

$$\frac{\partial R_{p,i}(R, t)}{\partial t} = -G_R(R, t) \frac{\partial R_{p,i}(R, t)}{\partial R} + G_{R_{p,i}}(R, t) \quad (6.27)$$

Lastly, the population balance equation for the volume of liquid inside the porous phase of the granule,  $V_l(R, t)$ , is formulated in equation (6.28):

$$\frac{\partial V_l(R, t)}{\partial t} = -G_R(R, t) \frac{\partial V_l(R, t)}{\partial R} + G_{V_l}(R, t) \quad (6.28)$$

The last term to discuss is the selection function. The selection function is a representative of the breakage rate, and it has a direct relationship with the stress to strength ratio which

acts as a criterion for both disintegration time and breakage rate of the granules. Equation (6.29) shows the mathematical description of the selection function.

$$\psi(R, t) = \frac{1}{\tau_b} \left( \frac{\sigma_{str}}{\sigma_c} \right)_n \quad (6.29)$$

in which  $\tau_b$  is a parameter known as the breakage time and acts as a criterion for the disintegration rate of granules. Parameter  $\left( \frac{\sigma_{str}}{\sigma_c} \right)_n$  is called the normalized stress to strength ratio which from its definition changes between zero and one and is defined in Equation (6.30):

$$\left( \frac{\sigma_{str}}{\sigma_c} \right)_n = \left( \frac{\sigma_{str}}{\sigma_c} \right) / \left( \frac{\sigma_{str}}{\sigma_c} \right)_{max} = \left( \frac{1 - \varepsilon_{max}}{1 - \varepsilon} \right)^4 \left( \frac{\bar{R}_p}{\bar{R}_{p,max}} \right)^{6c} \left\{ 1 - MAX \left( 0, \frac{\hat{m}_s - \hat{m}_{s,thr}}{1 - \hat{m}_{s,thr}} \right)^\vartheta \right\} \quad (6.30)$$

By doing this not only the range of the selection function can be determined but also the dependency of stress to strength ratio to binder concentration and liquid to solid ratio can be removed from the model. The boundary conditions for these equations are summarized in Eq. (6.31):

$$\left\{ \begin{array}{l} \lim_{R \rightarrow \infty} n_g(R, t) = 0 \\ \lim_{R \rightarrow \infty} (n_g(R, t)/R^3) = 0 \\ \lim_{R \rightarrow \infty} R_{p,i}(R, t) = R_{p,i}(0) \\ \lim_{R \rightarrow \infty} S_R(R, t) = 0 \\ R_{p,i}(R, 0) = R_{p,i}(0) \\ n_p(R, t) = (1 - \varepsilon(R, 0)) \frac{R^3}{\sum_i x_{n,i} R_{p,i}^3(0)} \\ S_a(R, 0) = 0 \end{array} \right. \quad (6.31)$$

### 6.2.3 Population balance modelling of the released primary particles

The released primary particles do not undergo any major changes except possibly growth due to liquid absorbance. However, as it will be shown in chapter 7, there is no major growth for primary particles in the released form as most of them have already reached near their maximum absorption ratio before the breakage. Therefore, using Eq. (6.15), the number-based distribution of  $i^{th}$  primary particle in the released form, designated as  $n_{f,i}$ , can be described in equation (6.32):

$$\frac{\partial n_{f,i}}{\partial t} = \int_{R_{min}}^{\infty} \psi(R, t) b_i(r|R) n_g(R, t) dR \quad (6.32)$$

where  $r$  is the size class of released primary particles,  $R_{min}$  is the lowest size that granule undergoes the breakage (considered to be higher than maximum value of size class  $r$ ) and  $b_i$  is the breakage probability function of  $i^{th}$  primary particle.  $b_i(rR)$  is the number of primary

particles of  $i^{\text{th}}$  type with size  $r$  produced from the breakage of a granule with size  $R$  which is obtained in equation (6.33):

$$\begin{aligned} b_i(r|R) &= \text{number of primary particles in the granule} \times \\ &\text{number fraction of } i^{\text{th}} \text{ component} \times \text{frequency number of } i^{\text{th}} \text{ component at size } r \\ &= n_p(R, t) x_{n,i} f_i(R, r, t) \end{aligned} \quad (6.33)$$

in which  $f_i(R, r, t)$  is the number-based frequency of  $i^{\text{th}}$  primary particle in a granule with size  $R$ . Eq. (6.33) transform Eq. (6.32) to its final form, Eq. (6.34):

$$\frac{\partial n_{f,i}}{\partial t} = x_{n,i} \int_{R_{min}}^{\infty} \psi(R, t) b_i(r|R) n_g(R, t) n_p(R, t) f_i(R, r, t) dR \quad (6.34)$$

Obtaining  $f_i(R, r, t)$  in a mono-sized model in the granule is impossible, however, through an assumption, it can be estimated. It is known as that the initial distribution of primary particles can be estimated using a series of log-normal distribution (Fox et al. 2023), described in equation (6.35):

$$f_i(R, r, 0) = \frac{1}{r\sqrt{2\pi}} \sum_j \frac{a_j}{\sigma_j} \exp\left(-\frac{(\ln(r) - \mu_j)^2}{2\sigma_j^2}\right), \quad \sum_j a_j = 1 \quad (6.35)$$

where  $a_j$ ,  $\mu_j$  and  $\sigma_j$  are all parameters. If it is assumed that the overall shape of the distribution of primary particles does not change and the distribution shifts to larger sizes due to liquid absorbance, then  $f_i(R, r, t)$  can be estimated using Eq. (6.36):

$$f_i(R, r, t) = \frac{1}{r\sqrt{2\pi}} \sum_j \frac{a_j}{\sigma_j} \exp\left(-\frac{\left\{\ln(r) - \mu_j - \ln\left(\frac{R_{p,i}(R, t)}{R_{p,i}(0)}\right)\right\}^2}{2\sigma_j^2}\right), \quad \sum_j a_j = 1 \quad (6.36)$$

Eq. (6.36) holds both zeroth moment and third moment, meaning the total number and total volume of solid of  $i^{\text{th}}$  are preserved. The initial and boundary condition are listed in Eq. (6.37):

$$\begin{cases} \lim_{r \rightarrow \infty} n_{f,i}(r, t) = 0 \\ n_{f,i}(r, 0) = 0 \end{cases} \quad (6.37)$$

### 6.3 Global Sensitivity Analysis of the swelling models

Just like the single granule swelling model, a series of GSA were performed on the PBM model to determine the important parameters and their impact on the PBM model. The main response in this model is a parameter known as release profile and is defined as the ratio of the total number of primary particles released at the current time to the total number of primary particles in the granules initially, as stated in equation (6.38):

$$X(t) = \frac{\int_0^{\infty} n_{f,i}(r, t) dr}{\int_{R_{min}}^{\infty} n_g(R, 0) n_p(R, 0) dR} = 1 - \frac{\int_{R_{min}}^{\infty} n_g(R, t) n_p(R, t) dR}{\int_{R_{min}}^{\infty} n_g(R, 0) n_p(R, 0) dR} \quad (6.38)$$

This variable gives us the percentage of the primary particles that have been released due to disintegration and is an important parameter in validating the model experimentally, which is further stated in Chapter 7. The factors for the GSA are the same parameters used in the GSA of mono-sized single granule swelling model (Table 4.4). The breakage time is not considered in the GSA because of its direct relationship with the release profile as direct and additive relationship dominates the responses in variance-based GSA methods. The non-GSA parameters are the same used in GSA of mono-sized single granules swelling model (Table 4.5). The number of uncertainty scenarios were fixed at 500. To obtain the average release profile, the simulation was performed for each sample for 500 s.

The total effect data depicted at Figure 6.1, indicates the dominating impact of disintegrant diffusivity on the release profile which shows the importance of the liquid absorbance on the disintegration of granules. A scatter plot obtained from the GSA data and shown in Figure 6.2, demonstrates the impact of diffusivity on the release profile. As it can be seen, the release profile increases by increasing the diffusivity until a certain point. This is where most of the disintegrant particles have reached their maximum absorption ratio leading to a constant value of the release profile and a high degree of breakage in the granules.

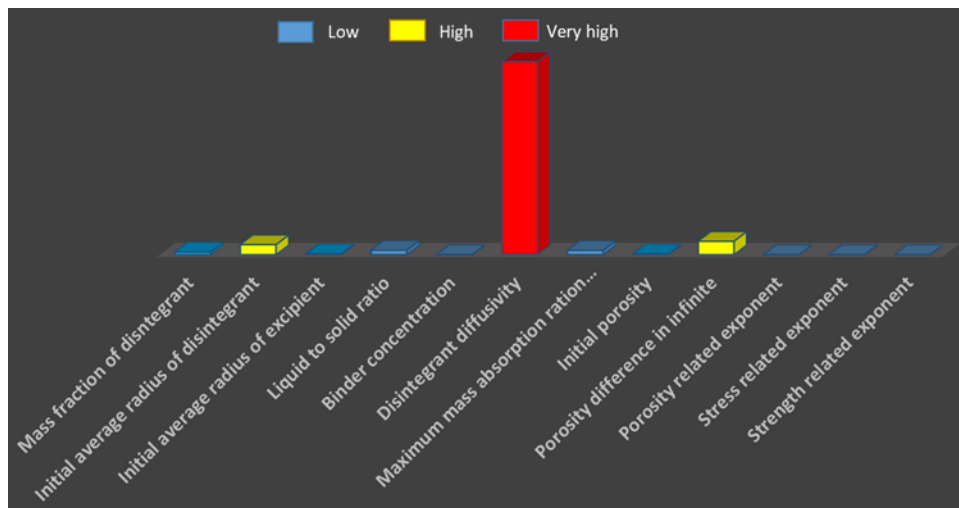


**Figure 6.1:** The total effect of all factors on the release profile (Eq. (6.38)) in the GSA of PBM

### 6.3.1 The GSA of process parameters

The result of the GSA of process parameters on the PBM model, is shown in Figure 6.3. Clearly, the initial radius of disintegrant dominates the response which hints at the impact of liquid absorption on the release profile. Based on the data obtained from the GSA and shown in Figure 6.4, the release profile decreases almost linearly with size, which first indicates the high impact of initial size of disintegrant on the release profile and second, the decrease in the release profile due to decrease in liquid absorbance as a larger disintegrant has a lower surface to volume ratio.

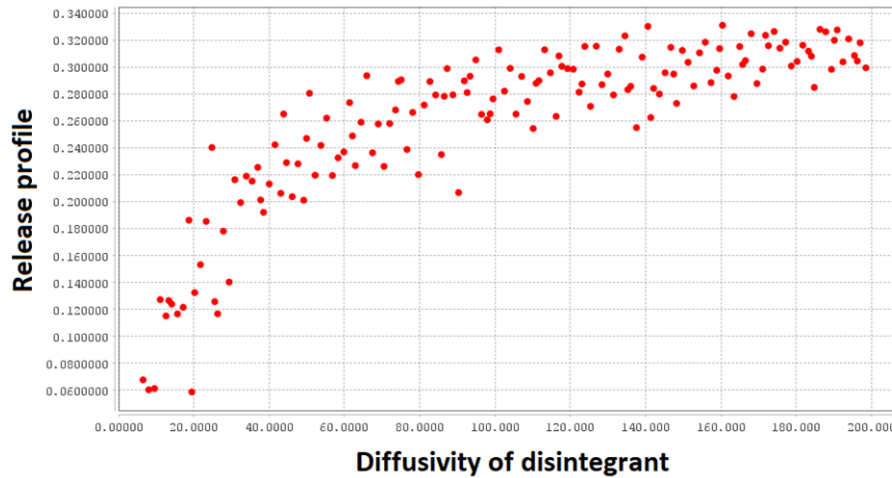


**Figure 6.2:** The scatter plot of the release profile (Eq. (6.38)) vs diffusivity of disintegrant in the GSA of PBM

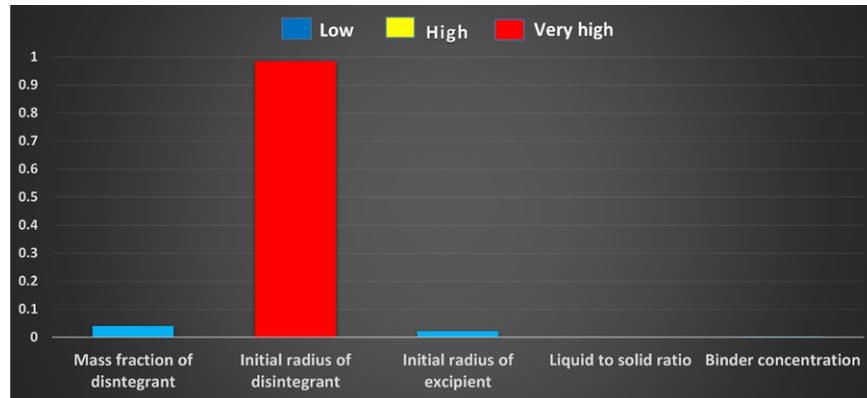


**Figure 6.3:** The total effect of process factors on the release profile (Eq. (6.38)) in the GSA of PBM

### 6.3.2 The GSA of structural parameters

The GSA performed on structural parameters, presented in Figure 6.5, showed that porosity difference at infinite alongside the porosity related exponent had the most impact on the model followed by the impact of had a dominating impact on the release profile, followed by the strength related exponent. This means that all these parameters are affecting the model through the ratio of the average size of primary particles to its initial value in Eq. (4.58).

## 6.4 Conclusion

A new mechanistic model was developed to describe the disintegration of granules. The model utilizes the lumped-based population balance model to track the size distribution of granules and released primary particles. It was assumed the granules release only primary particles into surrounding liquid. Furthermore, there is a size threshold where the swelling becomes the dominant mechanism in disintegration. Through these assumptions, the model

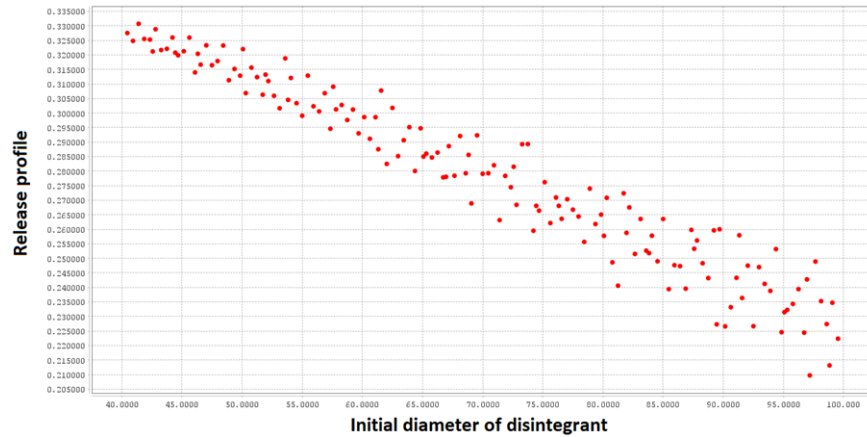


**Figure 6.4:** The scatter plot of the release profile (Eq. (6.38)) vs diffusivity of disintegrant in the GSA of PBM

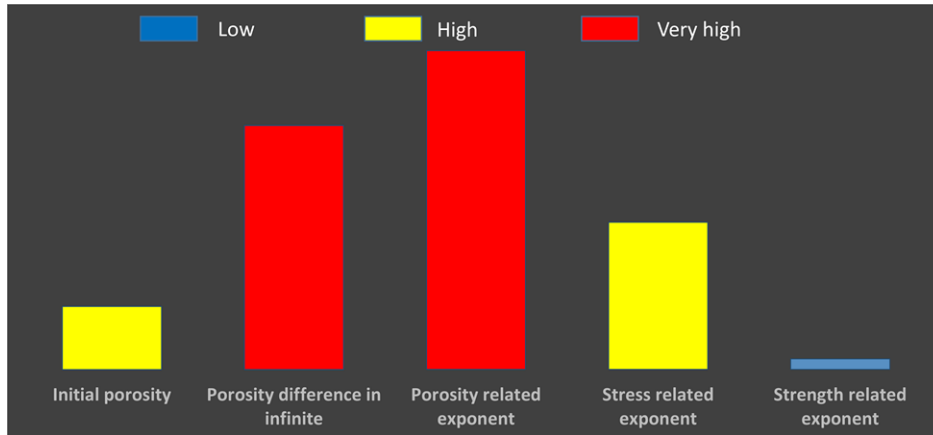


**Figure 6.5:** The total effect of the structural parameters on the release profile (Eq. (6.38)) of the granules in PBM model

was simplified. Then, the growth terms are defined using the mono-sized single granule swelling model. Lastly, a new mechanistic function for the selection function of the breakage was proposed. The GSA results showed the diffusivity of disintegrant have the most impact on the model, followed by porosity difference, initial size of the granules. The impact of each type of parameters were tested on the model. It was shown increasing the initial size of disintegrant leads to a decrease in the release profile rate (Eq. (6.38)). Among structural parameter, porosity difference and porosity related exponent had the most impact, however the result to some extent depends on the value of non-structural parameters which could change the GSA to some extent.

## Chapter 7

# Validation of the population balance model

### 7.1 Introduction

In this chapter, the validation of the population balance model of swelling driven disintegration is discussed. The results obtained from FBRM are used to analyse the breakage profile and the validation of the model. All of the formulations that were tested in the flow cell (Chapter 5) were investigated in the research in this chapter too. The formulations were categorized in three groups:

- MCC granules made with high concentration of HPMC in the binder (12.5 %w) and different concentration of SSG in the granule, ranging from 0 to 6 %w,
- MCC granules created from low concentration of HPMC in the binder (5 %w) and different concentration of SSG in the granule, ranging from 0 to 6 %w,
- DCPA granules made with high concentration of HPMC in the binder (12.5 %w) and two different concentrations of SSG in the granule, 4 and 6 %w,

### 7.2 Model validation

To validate the PBM model developed for the swelling driven disintegration of granules, it is imperative to obtain the size distribution of granules and the released primary particles during disintegration. This task was accomplished using FBRM, something that has rarely been done before as FBRM is mostly used in other fields such as crystallization and its usage in the field of dissolution and disintegration is new (Coutant et al. 2010). FBRM gives the user the number of counts for each chord length, which when combined would lead to total number of particles.

Before discussing the experimental and validation results, it is necessary to talk about the impact of the hydrodynamic forces on the results. As is known, in order to create a high level of homogeneity in the vessel, the fluid is stirred leading to a velocity gradient. This velocity gradient around the granules creates a shear force which can erode the granule surface and release some of primary particles into the vessel. This means the erosion rising

from the hydrodynamic forces can interfere with the experimental results, mainly the number of released primary particles. As will be shown, the data containing the total number of particles has two sections. The first part includes the swelling and the second part, which is almost linear, only contains the impact of erosion. The total number of particle profiles were fitted to a quadratic equation as follows:

$$N_{tot}^{right}(t) = a_1 t^2 + a_2 t + a_3 = N_{tot}^{ero}(t) + a_3 \quad (7.1)$$

where  $a_1$ ,  $a_2$  and  $a_3$  are fitting parameters,  $N_{tot}^{right}(t)$  is the number of particles at the right-side count number vs time and  $N_{tot}^{ero}(t)$  is the total number of counts created by the hydrodynamic forces. To obtain the total number of particles created by swelling, the total number of particles was subtracted by the part obtained from the erosion equation:

$$N_{tot}^{swe}(t) = N_{tot}(t) - N_{tot}^{ero}(t) = N_{tot}(t) + a_1 t^2 - a_2 t \quad (7.2)$$

In which  $N_{tot}(t)$  is the total number of counts at time  $t$  and  $N_{tot}^{swe}(t)$  is the number of counts produced by swelling only. However, the total number of particles created from swelling is susceptible to the initial number of granules which is impossible to determine on this scale. Instead, for fitting of the data, the release profile which is mathematically defined in equation (6.38). The release profile has the following relationship with the total number of particles released by swelling:

$$X(t) = (N_{tot}^{swe}(t) - N_{tot}^{swe}(0)) / (N_{tot}^{swe}(\infty) - N_{tot}^{swe}(0)) \quad (7.3)$$

(Caramella et al. 1988, Colombo et al. 1984) proved experimentally and mathematically that this variable has a direct relationship with the internal stress of the granules, and it obeys from a cumulative Weibull distribution like Eq. (7.4):

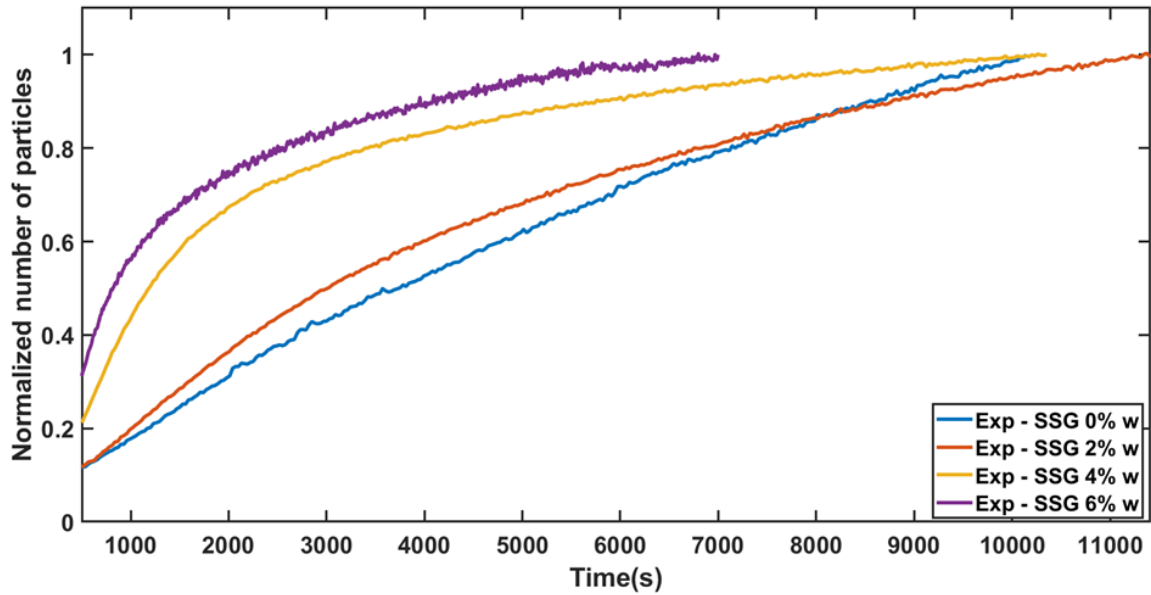
$$X(t) = 1 - \exp(-kt^n) = 1 - \exp\left(-\left(\frac{t}{\tau_r}\right)^n\right) \quad (7.4)$$

where  $t$  is time and parameters  $k$  and  $n$  are coefficient and exponent of the model, unique to each formulation. The parameter  $\tau_r (= k^{-1/n})$  is designated as the release inherent time and it is a criterion for the disintegration rate of granules. As it will be shown in section 7.2.1 onward, the same phenomenon happens here for almost all formulations. All the parameters that are used here are based on the parameters used or obtained in Chapter 5. Just like the single granule swelling model, the PBM model was fitted using a trust region algorithm of curve fitting toolbox of MATLAB. In the following section, the results will be discussed in depth for each type of formulation.

While hydrodynamic erosion is not the focus of this study, due to its involvement in the disintegration validation experiment, a simple mechanistic model for erosion has been presented in Appendix B. An important parameter known as erosion time  $\tau_s$  is introduced which can act as a criteria for the erosion rate of granules and can be obtained from parameters  $a_1$  and  $a_2$ . These parameters are obtained from FBRM experiments for each formulation and are presented in Table 7.1.

**Table 7.1:** The erosion related parameters for each formulation

Granule ID (refer to Table 5.2)	$a_1(1/s^2)$	$a_2(1/s)$	$\tau_s(s)$
D4	-5.27e-6	0.14	39539
D6	-7.29e-6	0.15	31500
ML0	-3.91e-6	0.23	87896
ML2	-5.09e-6	0.28	81311
ML4	-6.095e-6	0.24	59787
ML6	-4.42e-6	0.13	45483
MH0	-3.19e-5	1.08	50646
MH2	-5.29e-5	1.66	47157
MH4	-3.16e-5	0.83	39333
MH6	-1.0-e4	1.54	22515

**Figure 7.1:** The profile of total number of particles released during disintegration of granules for MCC granules granulated with 12.5 %w HPMC binder as a function of SSG concentration. The data are normalized for better visualization

### 7.2.1 MCC granules with high concentration of HPMC in the binder

The total number of particles versus time, obtained from the FBRM experiment for this type of formulation is shown in Figure 7.1. From the data, the erosion related parameters were obtained which alongside other formulations are listed in Table 7.1.

Based on these parameters, the release profile (Eq. (6.38)) for each formulation was obtained and shown in Figure 7.2. It is worth noting that for granules containing 0 %w SSG, swelling profile is minimal, and therefore, the main dispersion mechanism is hydrodynamic erosion.

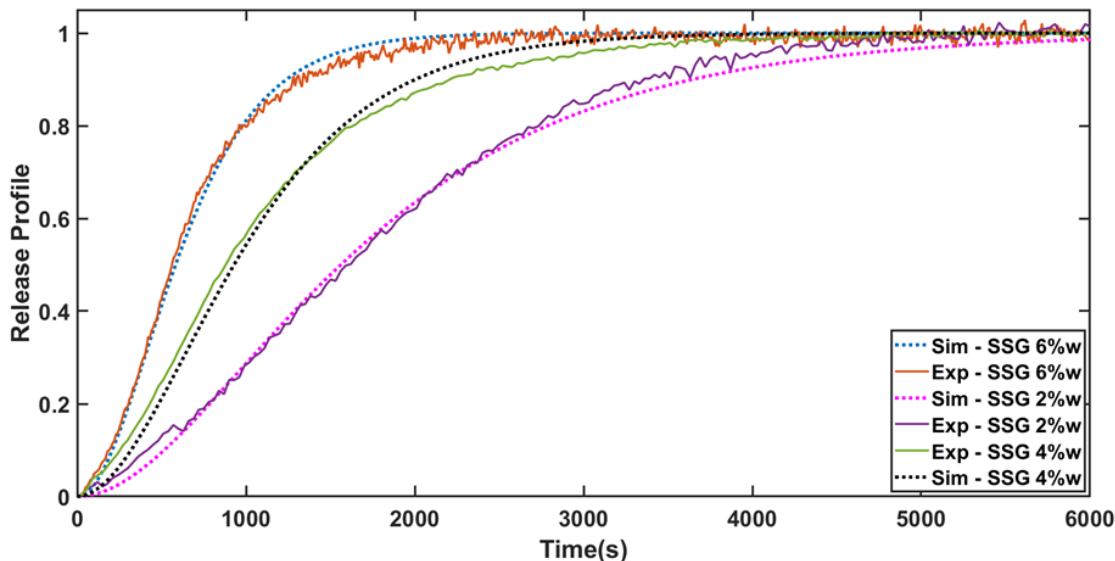


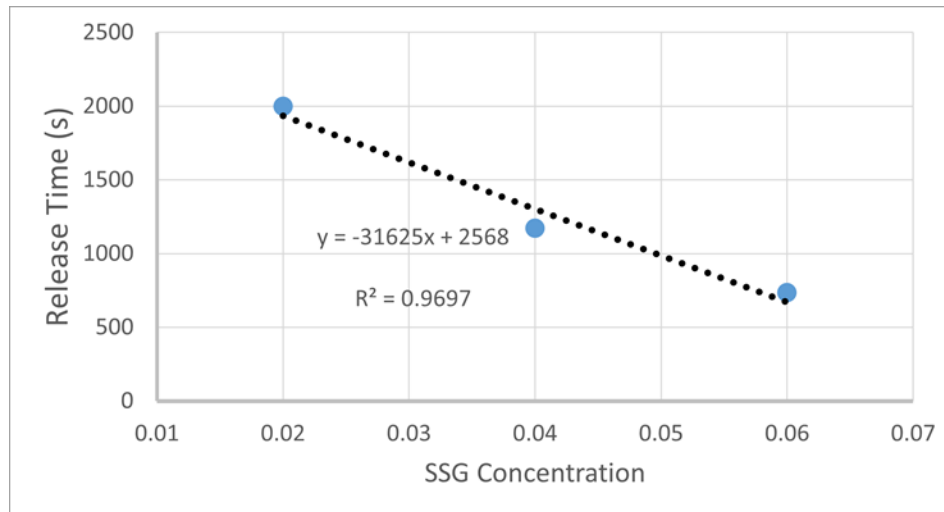
**Figure 7.2:** The experimental and simulation release profile (Eq. (6.38)) of MCC granules granulated with 12.5 %w HPMC binder

Based on these data, the Weibull distribution related parameters were obtained (Table 7.2). Clearly, by increasing the SSG content in the granule, the release rate becomes faster, which clearly shows its impact through the release inherent time ( $\tau_r$ ). From these data, the mechanism behind swelling and the detachment rate of particle layers from the surface can be deduced. By using the theory proposed by (Caramella et al. 1988), the swelling rate obeys from a diffusive nature with volume increasing by square root of time while the detachment rate is constant. The data for release inherent time and their relationship with SSG concentration in the granule are shown in Figure 7.3. The fitting of release inherent time vs SSG concentration can be used to estimate the release time of granules containing other concentrations of SSG with the same type of binder. Before fitting the model to the experimental data, it is important to determine which variable should be the response in the fitting, particle size distribution, release profile or both. To solve this matter, the PSDs of each formulation obtained from the FBRM experiments were tested at a certain time of 10 minutes (Figure 7.4).

As it can be seen from Figure 7.4, there is a decrease in distribution around 1000  $\mu\text{m}$  by increasing the concentration of SSG, while the distribution of particles with lower sizes increases with SSG concentration which is expected as both erosion and swelling produce

**Table 7.2:** The Weibull distribution related parameters for each formulation

Granule ID (refer to Table 5.2)	$\tau_r(s)$	$n$
D4	46	0.32
D6	75	0.6
ML0	-	-
ML2	-	-
ML4	1217	0.76
ML6	397	0.57
MH0	-	-
MH2	2000	1.59
MH4	1174	1.38
MH6	735	1.49

**Figure 7.3:** The release inherent time vs SSG concentration and its estimation for MCC granules granulated with 12.5 %w HPMC binder using linear regression

smaller particles from the granules. However, this shift is mainly focused on the original size distribution of primary particles specifically MCC where the peak of distribution is close to the peak of MCC powder distribution's peak. This would mean that the majority of the created particles from the disintegration are primary particles and not aggregates. The aggregates are smaller sizes than granules and consist of few primary particles. According to (Wilson et al. 2012), the dominating force in breakage of this type of particles is deagglomeration and not swelling. To find out the average number of primary particles for each

formulation, the value of  $D_{50}$  was calculated over the course of disintegration experiment. The obtained data shown in Figure 7.5, clearly show a sudden drop at the beginning of the disintegration experiment to a value which is assumed to be the average size of MCC. At the same time, excipients like MCC or DCPA exhibit low water absorption and maintain their size over time, as evidenced by the maximum absorption ratio determined through the fitting of pure MCC granules in Chapter 5 and the constant value of  $D_{50}$  shown at Figure 7.5.

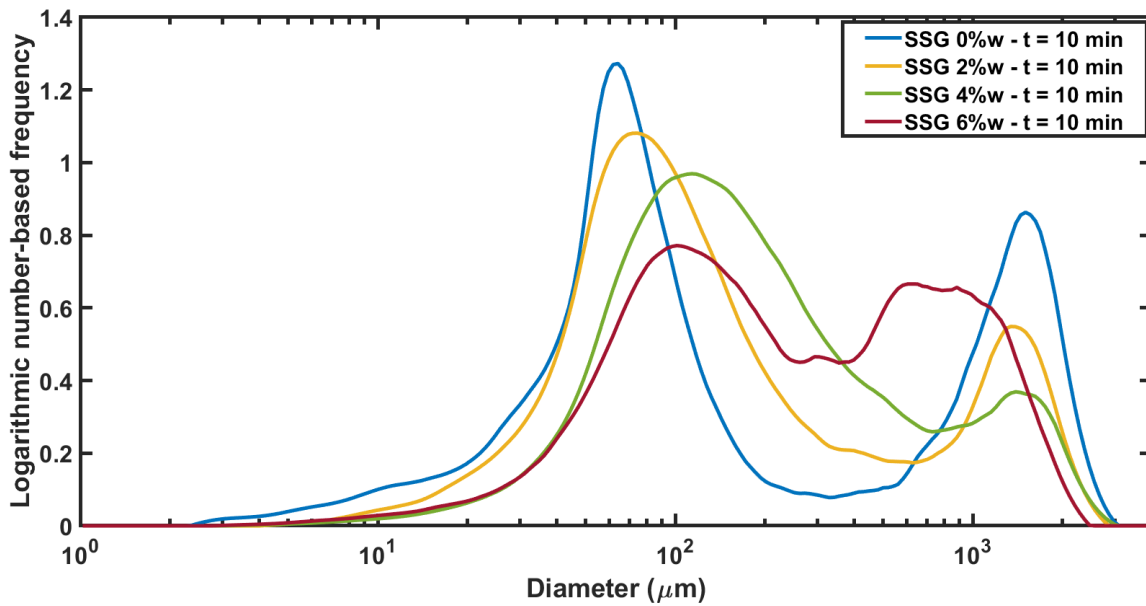


**Figure 7.4:** The particle size distribution of disintegrating MCC granules granulated with 12.5 %w HPMC binder at 10 minutes of disintegration

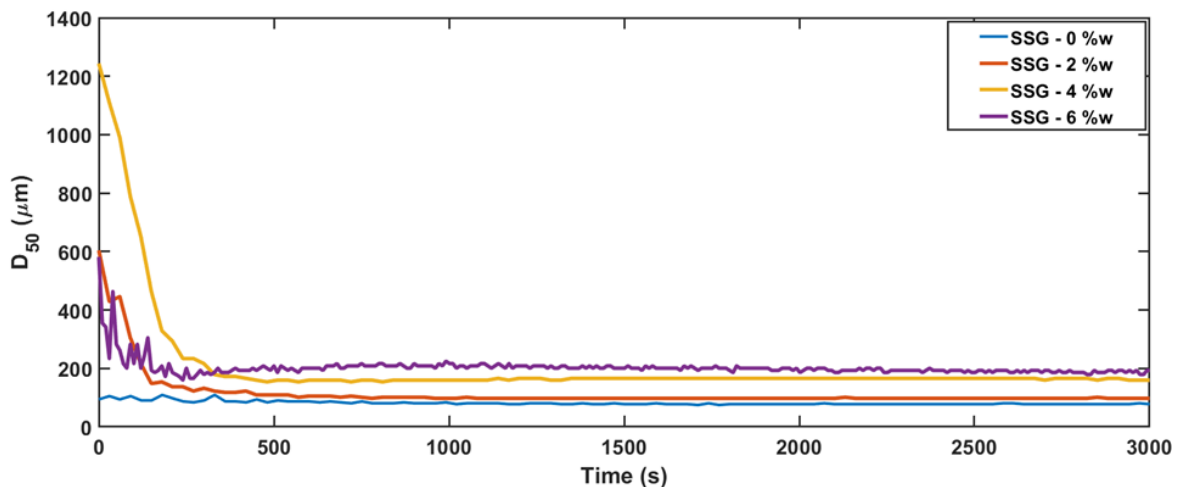


**Figure 7.5:**  $D_{50}$  value of disintegrating MCC granules granulated with 12.5 %w HPMC binder over the course of disintegration

These findings have two significant implications. First, they support the assumption that

granules disintegrate directly into primary particles which is also supported by lower value of distribution between the granules and the primary particles. Second, they suggest that the release profile can be the sole parameter in the model fitting process. Based on this assumption, the model was fitted to the experimental data, which are shown in Figure 7.2 alongside the experimental results and the obtained breakage time is listed in Table 7.3. The

**Table 7.3:** *The breakage time obtained from the fitting the model to release profile (Eq. (6.38)) of FBRM data*

Granule ID (refer to Table 5.2)	$\tau_b(s)$	$R^2$
D4	18	0.21
D6	18	0.67
ML0	-	-
ML2	-	-
ML4	644	0.78
ML6	176	0.68
MH0	-	-
MH2	1113	0.99
MH4	524	0.99
MH6	326	0.99

results agree with the experimental data with a higher level of accuracy for MCC granules made with 12.5%w of HPMC in the binder. In Figure 7.6, the relationship between the breakage time and SSG concentration is shown which can help in linking this parameter to post-process models.

The final topic to address within this section is related to the comparison between the particle size distribution data acquired from experimental measurements and the model. Figure 7.7 presents the simulated logarithmic PSD data at 10 minutes of disintegration for different loadings of SSG made with high concentration of binder. The simulation data predicts a size distribution towards lower sizes with no distribution between primary particles and granules which is due to the assumption that primary particles are directly created from the breakage of granules and no aggregates would be created in the midst of disintegration. This is to some extent in contrast to what is seen in Figure 7.4 where aggregates exist between the granules and primary particles. It is important to highlight that the initial distribution of granules in the simulation differs slightly from the real distribution. The granules selected for the FBRM experiments were specifically obtained from sieves with diameters ranging between 1 and 1.4 mm. In contrast, for the simulation, the initial distribution was configured so that 90% of the granules fell within the 1 to 1.4 mm range, introducing some level of errors to the simulated data. Furthermore, the data presented in Figure 7.5 show an immediate

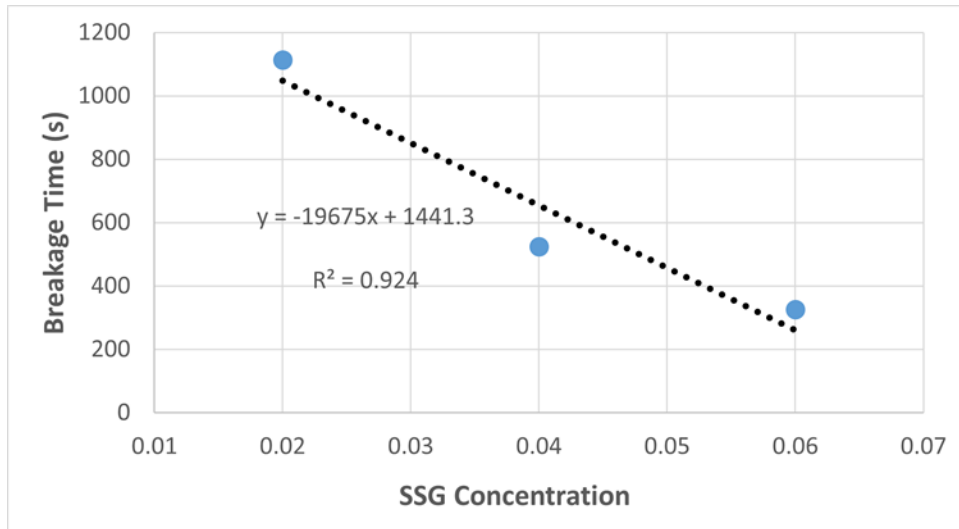


**Figure 7.6:** The breakage time vs SSG concentration and its estimation for MCC granules granulated with 12.5 %w HPMC binder using a linear regression model

decrease in the average size of particles in the disintegration, meaning disintegration occurs immediately, changing the particle size distribution.

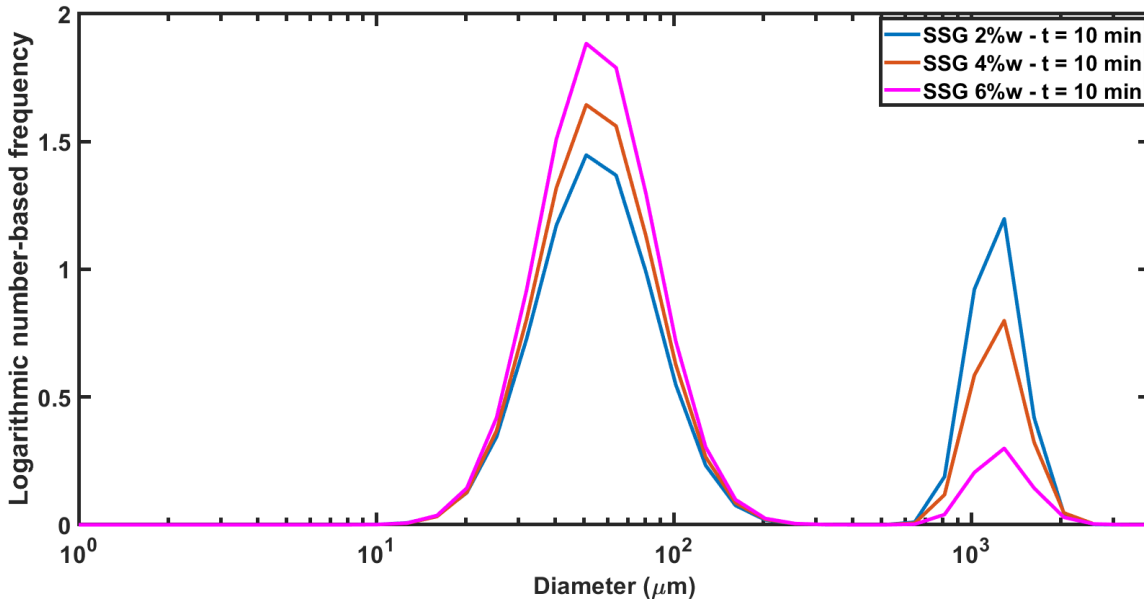


**Figure 7.7:** The simulated particle size distribution of MCC granules granulated with 12.5 %w HPMC binder at 10 minutes of disintegration

### 7.2.2 MCC granules with low concentration of HPMC in the binder

The particle counts data obtained from FBRM technique for MCC granules made of binder with 5 %w of HPMC, along with their release profile, are shown in Figures 7.8 and 7.9

respectively. In contrast to what was observed in Section 7.2.1, here the 2 %w granules do not experience disintegration, just like pure MCC granules. This supports the gelling theory of HPMC in the granule and the observation seen in the flow cell experiments (Section 5.4), leading to its omission from the formulations chosen for simulation. The erosion related parameters were determined (Table 7.1) and then the swelling profile was obtained after omitting the erosion effect. To make sure that there is a high level of breakage for this formulation and the granules breakage directly to primary particles, the experimental PSD at 10 minutes and  $D_{50}$  for each formulation made with low concentration of HPMC was obtained.

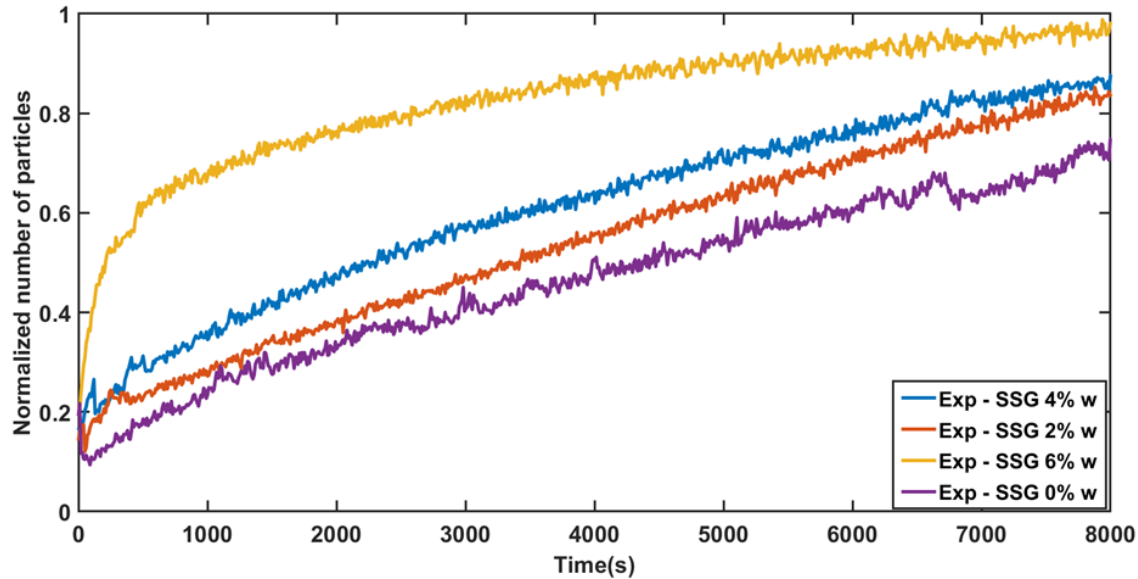


**Figure 7.8:** The profile of total number of particles released during disintegration of granules for MCC granules granulated with 5 %w HPMC binder as a function of SSG concentration. The data are normalized for better visualization

When the PSD of granules in Figure 7.10 and their average size at Figure 7.11 are compared to the PSD and average size of granules made with high concentration of binder (Figure 7.4 and 7.5), it can be deduced that there are fewer granules at larger sizes, indicating a faster disintegration. However the average particle sizes are larger for the granules made with high concentration of binder. This is mainly due to a lower erosion rate for these granules which is attested by a lower value of  $a_2$  in Table 7.1, leading to more aggregates present in this type of MCC formulation compared to their counterparts made with high concentration of HPMC. Just like section 7.2.1, it was assumed that the primary particles are produced through the disintegration of granules and no aggregates are formed during the disintegration.

The obtained release profile (defined in Eq. (6.38)), depicted in Figure 7.9 for 4 %w and 6 % w SSG clearly show a faster disintegration compared to the granules made of 12.5 %w HPMC binder solution, which is in line with the flow cell observations. Both the parameters and Weibull distribution parameters were obtained and listed in Table 7.2. If the same reasoning used in the last section to determine the mechanism behind the expansion and detachment rate would be utilized here, it can be concluded that expansion again follows a diffusion related mechanism while the detachment rate is spontaneous.

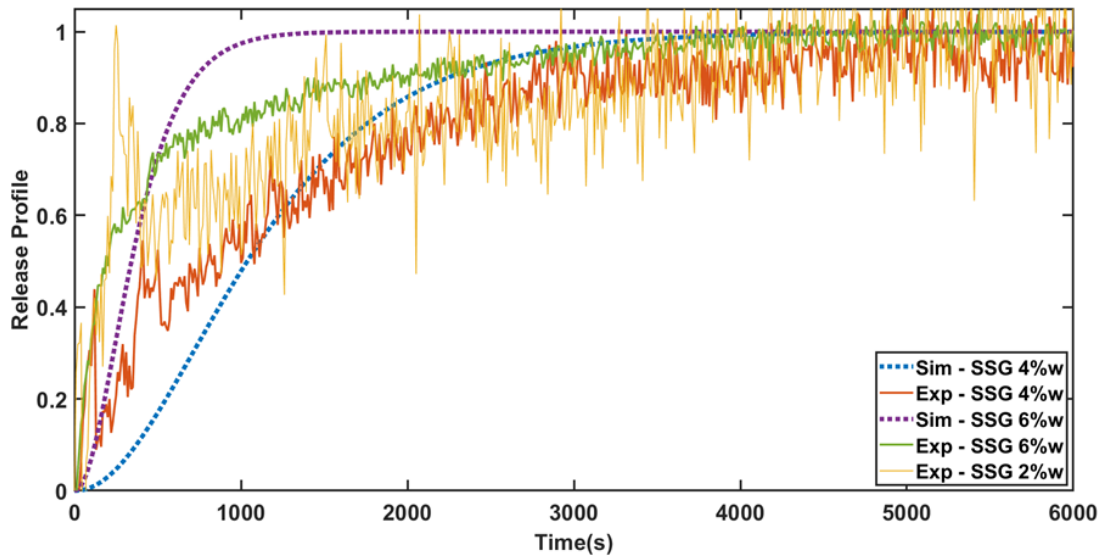


**Figure 7.9:** The experimental and simulation release profile (Eq. (6.38)) of MCC granules granulated with 5 %w HPMC binder

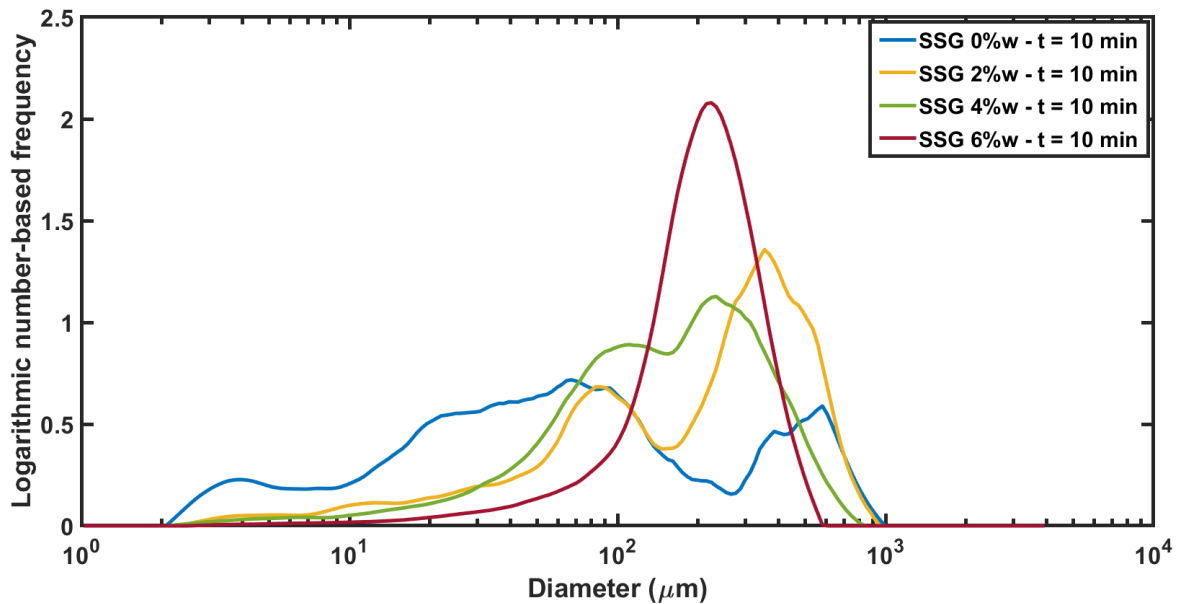


**Figure 7.10:** The particle size distribution of disintegrating MCC granules granulated with 5 %w HPMC binder at 10 minutes of disintegration

The model was fitted to the data to obtain the breakage time and the PSD. The data are shown in Figures 7.9 and 7.12 respectively. Unlike the granules made with high concentration of binder, in this case, they do not show a high level of accuracy. This is due to the assumption of no aggregate's formation in the granule, and the low level of strength in the granules. Within weaker granules, the forces generated by liquid bridging through water penetration into the granules appear to be on par with the forces created by solid bridges. This results in

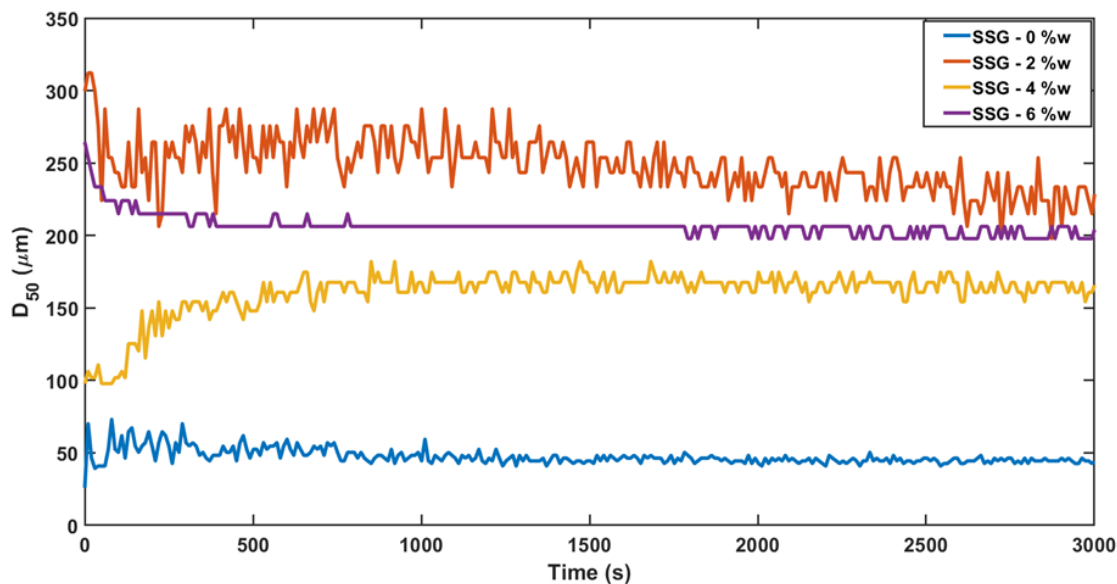


**Figure 7.11:**  $D_{50}$  value of disintegrating MCC granules granulated with 5 %w HPMC binder over the course of disintegration

an increased overall strength of the granules, thereby challenging the assumption that only solid bridges serve as the predominant bonding forces within them which is also supported the findings of (Rumpf 1962) that in smaller aggregates/granules, the liquid bridging force would be comparable to the forces stemming from the solid bridges. Despite this fact, the model can capture the disintegration behaviour accurately. Based on the results, it is important to perform more experiments to establish a robust equation between breakage time and SSG concentration. It also has to be noted the issue with determining the initial distribution of granules, like the data in section 7.2.1, still exists here and a log-normal distribution has been considered for the initial size distribution of granules.

### 7.2.3 DCPA granules

The particle counts data obtained from the FBRM for this type of formulation are shown in Figure 7.13. Based on the flow cell data, a fast disintegration was anticipated, and this has occurred here too, as depicted in Figure 7.14. The erosion part was omitted using the parameters obtained from the erosion only part of the data (Table 7.1). The Weibull exponent data obtained from the release profile, listed at Table 7.2, hints at the same type of swelling and layer detachment mechanism observed for MCC granules made with low concentration HPMC in the binder, a diffusive-like swelling, and an almost spontaneous release of the granules.

Just like the previous cases in section 7.2.1 and 7.2.2, the PSD data and average size of the distribution was obtained in order to analyse the impact of disintegrant loading on the data. The reason why a lower time (1 minute instead of 10 minutes) has been chosen for PSDs in Figure 7.15 is because of the lower release time of DCPA granules, attested by the values in Table 7.2.

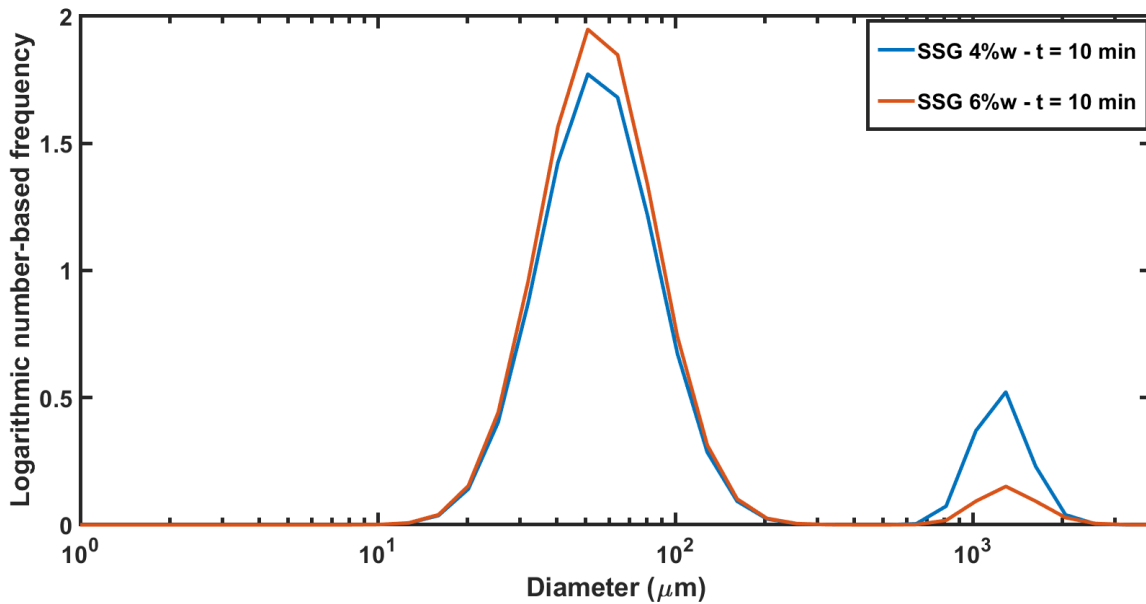


**Figure 7.12:** The simulated particle size distribution of MCC granules, granulated with 5 %w HPMC binder at 10 minutes of disintegration

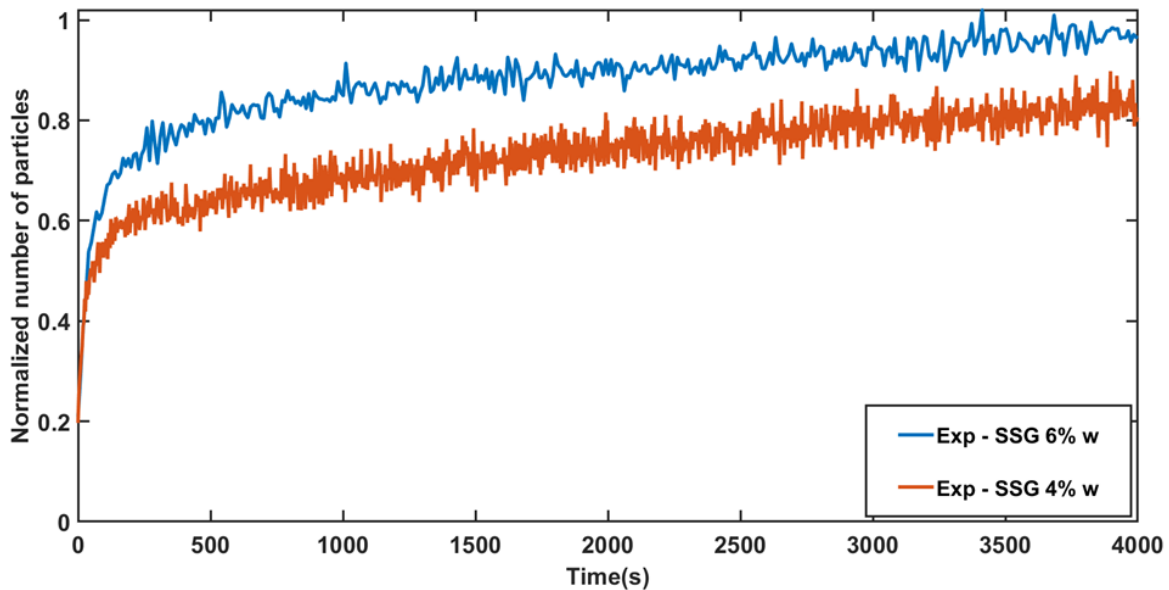


**Figure 7.13:** The profile of total number of particles released during disintegration of granules for DCPA granules. The data are normalized for better visualization

The data shown in Figure 7.14 clearly shows a much faster disintegration compared to MCC granules in Figures 7.2 and 7.9. Simultaneously, as it can be seen from Figure 7.15, there are much less aggregates observed after 1 minutes. This could be due to a combination of two factors, the first factor is low strength of granules as attested by their swelling behaviour (section 5.4.1) and the second factor is their microstructure which is possibly made of sub-

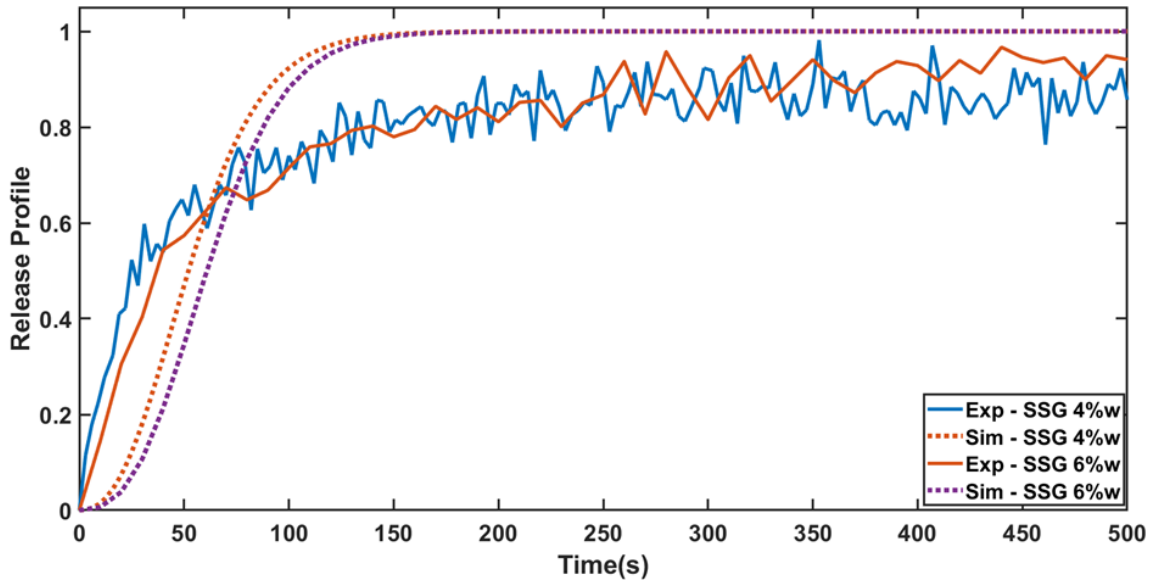


Figure 7.14: The experimental and simulation release profile (Eq. (6.38)) of DCPA granules

granules close to the size of primary particles. Therefore, not only the breakage rate of granules would be fast but also the new born particles would be much smaller leading to a fast decrease of particle size and the less amount of aggregates, as attested in both Figures 7.15 and 7.16.

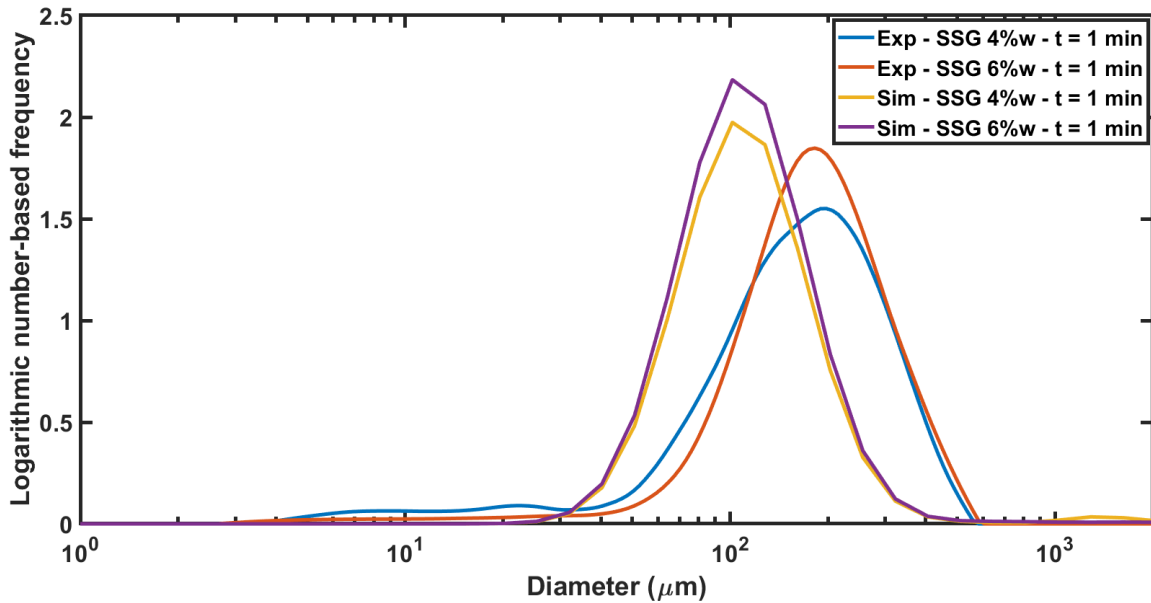
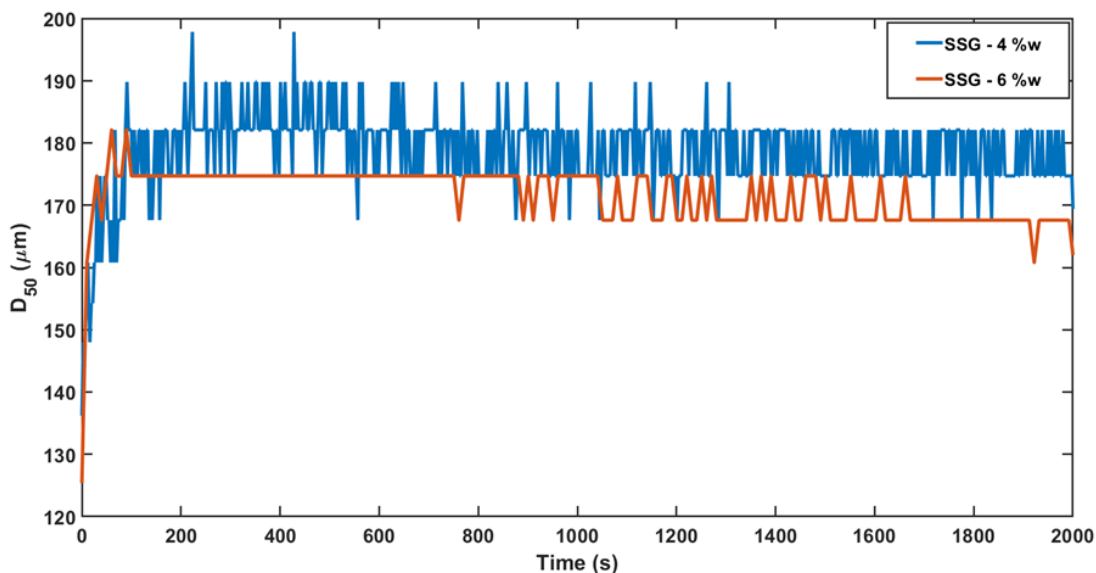


Figure 7.15: The experimental and simulated particle size distribution of disintegrating DCPA granules at 1 minutes of disintegration

The discrepancies between the experimental and simulated size distributions (Figure 7.15) could be due to two reasons:

- i. The first reason is the impact of size and opacity on chord length distribution in FBRM. In the method presented in Section 3.3.7, the relationship between size and chord length distributions is direct. However, as it is documented by (Yu et al. 2008, Kail et al. 2007), the particles with different size and opacity level have different impact on chord length distribution. This means equations (3.8) and (3.9) cannot capture the true relationship between size and chord length distribution, and therefore, a level of error is introduced in the inverse problem when the size distribution is obtained from the chord length distribution.
- ii. The second reason is related to the discrepancy between the size distribution data obtained from the malvern mastersizer for the powders and the FBRM data. In the malvern mastersizer, the obtained distribution is volume based which has to be converted to a number-based distribution for the fitting process. This conversion can create discrepancies, specifically in smaller sizes as in volume based distribution, the larger sizes have a more impact on the distribution compared to the smaller sizes. Thus, when the number-based distribution is obtained from the volume-based distribution, a certain level of error may be introduced in smaller sizes of the distribution.



**Figure 7.16:**  $D_{50}$  value of disintegrating DCPA granules over the course of disintegration

The obtained breakage times for each formulation through fitting of the model to release profile data (Eq. (6.38)) are listed in Table 7.3. The data clearly show a much faster disintegration time as the breakage time is around 20 s while the other formulations were in the range of hundreds. Based on these values, the model was tested against the experimental data. The model in the case of 4 %w SSG agrees to a greater extent with the data, while for 6 % w SSG, the data deviates from the release profile data. The reason for this deviation is the same as MCC granules with 6 % w SSG in section 7.2.2; the granule strength reinforcement due to liquid bridging stemming from the water penetration when the granules are weak. Further studies should be performed on evaluation of the granule strength, specifically the

impact of liquid bridging on the disintegration behaviour of the granules. The PSD data for DCPA granules with 4 and 6 %w was simulated using the obtained breakage time and the data from section 5.4.1. It was shown that the assumption of no aggregate formation is more reasonable here compared to MCC granules at section 7.2.1 and 7.2.2. This is related to a much higher disintegration rate and possibly lower granules strength which makes the lifespan of any formed aggregate smaller leading to a faster breakage rate of aggregates and higher accumulation rate of primary particles.

### 7.3 Effect of liquid to solid ratio

While effect to liquid to solid ratio was not the main purpose of the study but its impact of disintegration of granules was investigated using FBRM. The excipient was MCC, SSG loading was fixed at 4 %w, and the concentration of HPMC in the binder was 12.5 %w. Wet massing time was set at 5 minutes and the liquid to solid ratio was changed between 0.8, 0.9 and 1. The FBRM data are shown for the granules in Figure 7.17.

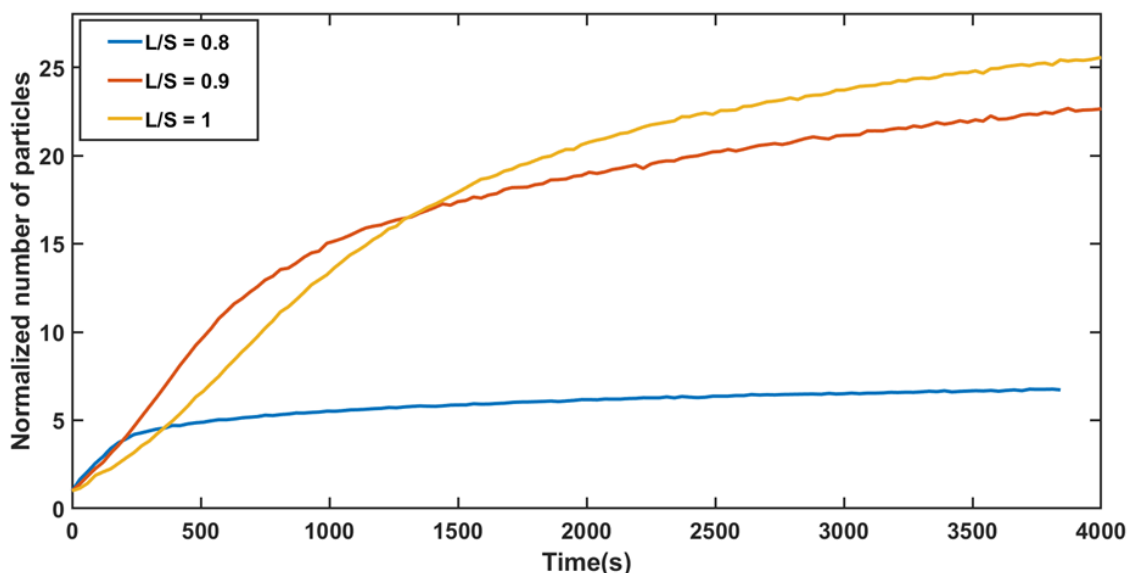


**Figure 7.17:** The profile of total number of primary particles released during disintegration of MCC granules with different liquid to solid ratio

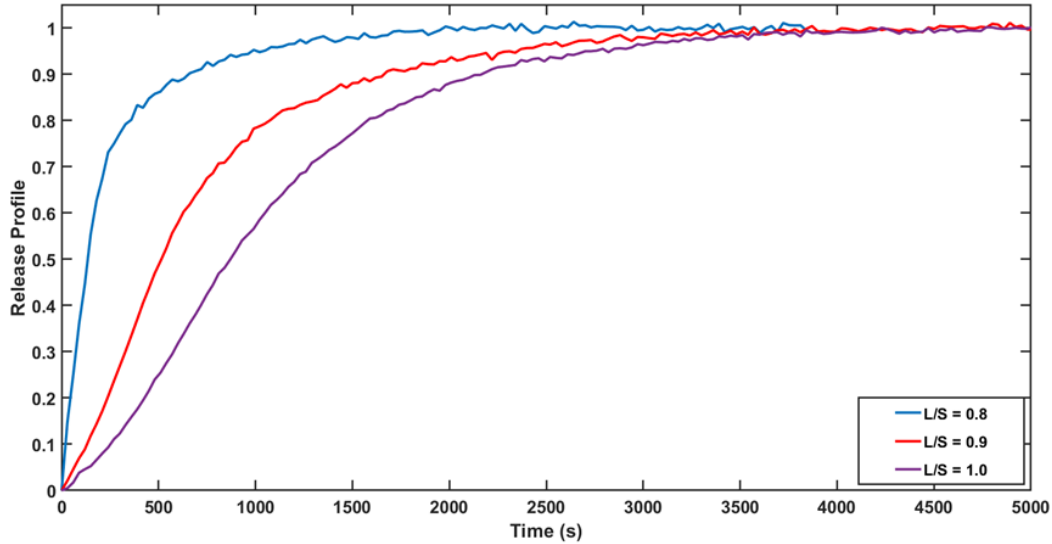
The data clearly showed a slower disintegration by increasing the liquid to solid ratio which leads to an increase in granule strength. To make sure, the erosion related parameters for each formulation were calculated, listed in Table 7.4, and the erosion process was omitted from the data and the release profile was obtained (Figure 7.18).

The release profile, shown in Figure 7.18, proves the theory of reduction in disintegration rate by increasing the liquid to solid ratio as MCC granules with 0.8 liquid to solid ratio are the fastest to reach the final state followed by granules with 0.9 and 1 liquid to solid ratio. Based on the release profile data, the Weibull distribution parameters were obtained and listed in Table 7.5.

An interesting fact about the formulation is the change in the release mechanism based on

**Table 7.4:** The erosion related parameters for MCC granules made with different liquid to solid ratio

Liquid to solid ratio	$a_1(1/s^2)$	$a_2(1/s)$	$\tau_s(s)$
0.8	-1.18e-05	1.08	13679
0.9	-2.77e-05	0.74	39845
0.1	-3.16e-5	0.83	39333

**Figure 7.18:** The release profile (Eq. (6.38)) of total number of primary particles released during disintegration of MCC granules with different liquid to solid ratio**Table 7.5:** The Weibull distribution related parameters for MCC granules made with different liquid to solid ratio

Liquid to solid ratio	$\tau_r(s)$	$n$
0.8	171	0.95
0.9	720	1.12
1.0	1174	1.38

the data in Table 7.5. The Weibull distribution exponent keeps increasing from values around 1 to 1.5 which means the swelling mechanism goes from convective to diffusive, most likely due to increasing gelling of HPMC blocking the pores to penetrated water. At the same time, the layer detachment rate goes from spontaneous to constant value. This inclines a change in disintegration mechanism as for granule with 0.8 liquid to solid ratio, with convective swelling and spontaneous layer detachment, the disintegration mechanism leans towards water uptake while in the case of granule with liquid to solid ratio of one, disintegration mechanism

leans towards swelling. Based on the data for MCC granules with different formulation (Table 7.2), liquid to solid ratio has the most impact on disintegration mechanism, more than disintegration loading or concentration of binder in the binder solution. An estimation of both release time and the exponent in Weibull distribution based on liquid to solid ratio has been given in Figures 7.19 and 7.20 respectively. The estimation could be used later for the sake of linking these parameters to a process model.

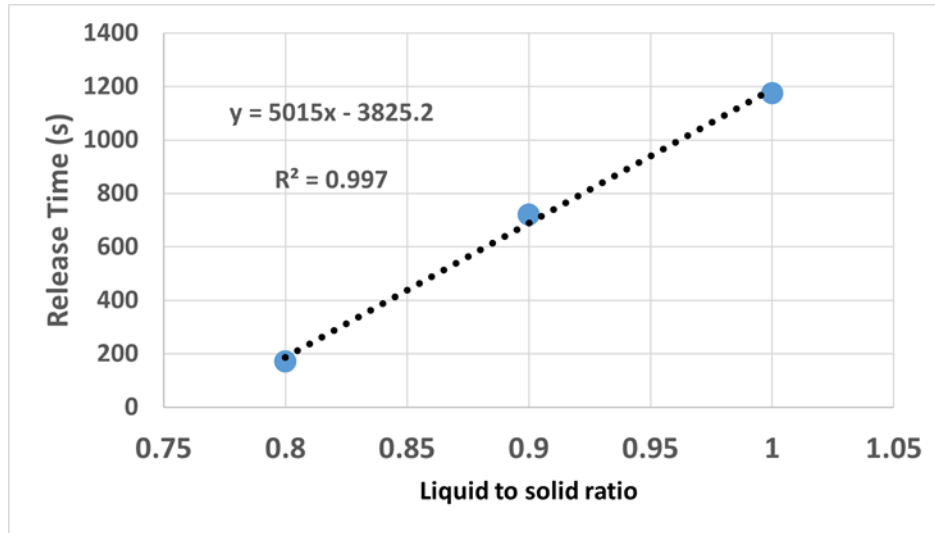


**Figure 7.19:** The release inherent time vs liquid to solid ratio and its estimation for MCC granules with different liquid to solid ratio

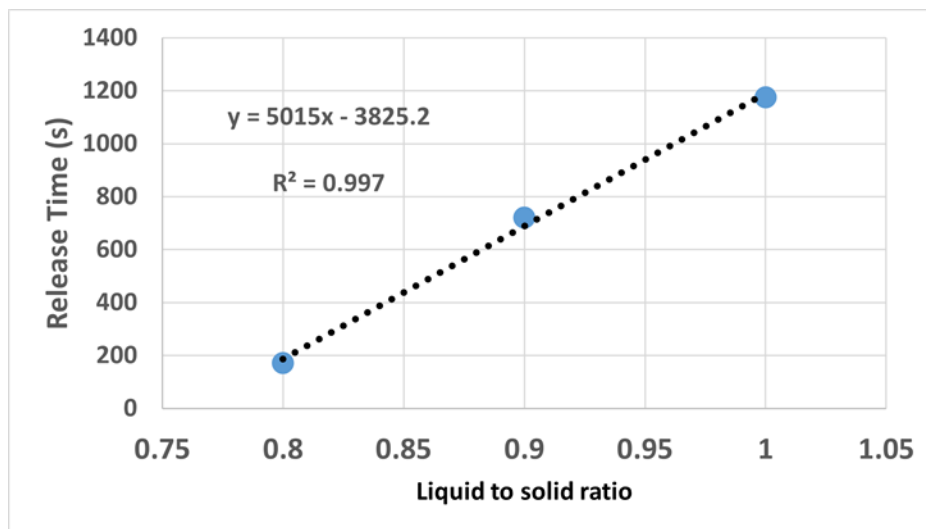


**Figure 7.20:** The Weibull distribution related exponent vs liquid to solid ratio and its estimation for MCC granules with different liquid to solid ratio

## 7.4 Conclusion

In this chapter, the population balance model developed for the disintegration of granules was tested against the data obtained from the focused beam reflectance measurement (FBRM) technique. A simple method was used to omit the impact of hydrodynamic forces on the data. Then, a new variable known as the release profile (Eq. (6.38)) was defined which is related to swelling performance of the granules.

The results showed that this variable obeys a cumulative Weibull distribution as it was speculated in the literature (Caramella et al. 1988). The parameters obtained from the model can indicate the speed of disintegration, the swelling mechanism and the detachment mechanism. For the MCC granules consisting of 12.5 %w HPMC in the binder, the disintegration was slowest. However, the value increased with SSG content in the granules. The swelling mechanism for all granules obeyed a diffusion mechanism. The detachment rate of the particle layer for MCC granules made of 12.5 %w HPMC is constant. However, the type of detachment mechanism changed for remaining granule formulations (MCC granules made with 5 %w HPMC and DCPA granules), as in those cases the detachment mechanism was almost spontaneous. The model for all formulations were fitted against the release profile data based on the assumption that no aggregate would be formed from the disintegration of granules and the granules would directly disintegrate to primary particles.

The model for MCC made of binder solution with 12.5 %w HPMC showed a great level of accuracy for the simulated release profile. Furthermore, a relationship was obtained between the SSG concentration in the granule and the breakage time. A drop in accuracy was seen for the granules made with 5 %w HPMC binder solution. However, the model was able to predict the behaviour of release profile accurately. One peculiar phenomenon here was the lack of swelling by granules containing 2 %w SSG. It was also shown that for MCC granules, there is a considerable number of aggregates formed from the disintegration of original granules with a long lifespan, not captured by the model. The breakage time obtained from DCPA granules showed a much lower value than the other type of granules, something that was anticipated based on the flow cell results.

The model for 4 %w SSG granules is still able to predict the release profile accurately but in the case of 6 %w granules, the accuracy drops dramatically. It is speculated that this is due to the impact of liquid bridging induced by water penetration in weak granules such as the ones seen here. The predicted particle size distribution of DCPA granules match with the experimental data which supports the assumption that granules immediately disintegrate to their primary particles.

Lastly, the impact of liquid to solid ratio on the disintegration mechanism was investigated. It was shown that liquid to solid ratio can affect both swelling and particle layer detachment mechanism. As this ratio increases, the swelling process transitions from a convective type to a diffusion-based mechanism. Simultaneously, the detachment mechanism shifts from spontaneous release to a more consistent, constant rate of release. This highlights the sensitivity of these mechanisms to variations in the liquid-to-solid ratio.

## Chapter 8

# Conclusions and Recommendations

### 8.1 Conclusions

The aim of this thesis was to generate and validate a mechanistic model for the swelling driven disintegration and dispersion of granules. Two mechanistic models were developed for a single granule case, the first assuming all constituent particles are mono-sized, and the second assuming the constituent particles are distributed in size. It was found that the diffusivity of disintegrant, granule composition and the initial size of the primary particles all play an important role in the performance of the mono-sized single granule swelling model while in the case of distributed model, the structural and intrinsic parameters also affect the model.

The mono-sized single granule swelling model was then validated using the experimental data obtained from the flow cell experiments. The data showed that by increasing the disintegration concentration, the swelling rate increases. However, factors such as the water absorbance during granulation, storage conditions and especially the gelling effect of the binder should be considered in the disintegration performance.

Following validation of the single granule model, a mechanistic population balance model for the disintegration of the granules was presented. This is the first time a population balance has been applied to the swelling driven disintegration of granules. The model uses a series of assumptions alongside the mono-sized single granule swelling model to describe the terms in the population balance model. A GSA of the model showed a clear impact of disintegrant diffusivity on the disintegration performance, followed by initial size of disintegrant and porosity difference at infinite, a structural parameter.

The population balance model was validated by examining the experimental disintegration of granules with varying formulations. It was observed experimentally that granules underwent erosion in the disintegration vessel, a mechanism not included in the model, and a novel method to account for the impact of erosion on the FBRM data was developed. Initially it was observed that the swelling release profile obeyed a Weibull distribution, as expected from the literature. Based on the parameters of the Weibull distribution, the release time, detachment mechanism of the particle layer from the surface of the granules and swelling mechanism can be determined. It was found out that the granules with the binder containing 12.5 %w HPMC in the binder solution showed a constant detachment rate of the surface particle layer while the other two type of formulations (MCC granules made with 5 %w HPMC

and DCPA granules) showed a spontaneous type of detachment. All the aforementioned granules showed a diffusion type of swelling.

Furthermore, the effect of liquid to solid ratio on the disintegration mechanism was investigated. The data showed a clear impact of liquid to solid ratio on changing the mechanism as by increasing it, the mechanism shifted from convective linear swelling with spontaneous release to a diffusion type of swelling with constant rate of release. The model showed a high level of accuracy for release profile of granules made with a high concentration of HPMC in the binder. This accuracy decreased for other formulations, specifically DCPA granules containing 6 %w SSG. In contrast, the predicted particle size distribution of DCPA showed more accuracy compared to granules made with MCC. It was speculated that because of the low strength of the granules, the liquid bridge induced by the water penetration could interfere in the disintegration, increasing the strength of the granules and decreasing the breakage rate of the granules.

In short, the novelties of this thesis are:

- The development of a mechanistic macro model for the swelling of granules that considers the particles size distribution of primary particles and is capable of predicting important parameters such as size, porosity, saturation and size of primary particles.
- The development of the first mechanistic population balance model for the swelling driven disintegration of granules.
- Introduction of a new methodology for modelling and validation of product performance modelling of granules.

Both single granules swelling model and population balance model developed here have the capability to be combined with other types of mechanism involved in the disintegration of granules, especially dissolution. Furthermore, the single granule swelling model can be easily modified for the tablets, as they are one of the most used products in pharmaceutical industry and the prediction of their disintegration behaviour is very important. Finally, a new methodology has been developed to relate the product model parameters to process parameters. This can lead to the design of disintegrating products, something of utmost interest in the industry.

## 8.2 Future works

For the future works, it is recommended that:

- i. Any work should be shifted from the granules to tablets. Due to the higher degree of variability and the irregularity in shape and smaller sizes, granules pose greater challenges for experimental investigation when compared to tablets. Tablet processing also makes it less susceptible to variability. The models for processing the tablets are already robust making it easier to link up the product performance model to tableting models.
- ii. Investigating the formation and impacts of micro cracks on the strength of granules.
- iii. Further works on determining the impact of liquid bridging in the case of fast release. By doing this, the PBM model can be modified to include the impact of liquid in the strength of the granules increasing the confidence of the model.

- iv. Developing models that can describe the particle size distribution of aggregates created from the disintegration of tablets.
- v. Calibrating some of the parameters in the single granule swelling model using detailed models such as DEM based models (Sweijen, Chareyre, Hassanizadeh & Karadimitriou 2017, Sweijen et al. 2018, 2020, Kalný et al. 2021, Braile et al. 2022, Soundaranathan et al. 2023) which can be combined with other techniques such as finite element method (FEM) (Nguyen et al. 2014, Amoddeo & Giovine 2019, Atrian et al. 2021), lattice boltzmann method (LBM) (Jia & Williams 2007, Mohamad 2019, Boschetti et al. 2020, 2022) and material point method (MPM) (Więckowski 2004, Zhang et al. 2008, Yerro et al. 2015, Fern et al. 2019, de Vaucorbeil et al. 2020). Particularly, the MPM can capture many features of a disintegrating granule, such as swelling, fracture and breakage in a multiphase domain (Nairn 1970, Zhang et al. 2008, Sadeghirad et al. 2011).
- vi. To use the model in conjunction with other product performance models, specifically a dissolution model, to test the impact of the disintegration on API release profile.
- vii. Link the model to a process model such as high shear wet granulation in order to optimize the process model based on desired disintegration attributes of the granules such as release profile or disintegration time.

# Bibliography

- Abbott, D. D., Packman, E. W., Rees, E. W. & Harrison, J. W. E. (1959), ‘A preliminary report of the effect of gastric mucous upon tablet disintegration’, *Journal of the American Pharmaceutical Association* **48**(1), 19–21.
- Adolfsson, Å. & Nyström, C. (1996), ‘Tablet strength, porosity, elasticity and solid state structure of tablets compressed at high loads’, *International Journal of Pharmaceutics* **132**(1), 95–106.
- Akseli, I., Hancock, B. C. & Cetinkaya, C. (2009), ‘Non-destructive determination of anisotropic mechanical properties of pharmaceutical solid dosage forms’, *International Journal of Pharmaceutics* **377**(1), 35–44.
- Akseli, I., Ladyzhynsky, N., Katz, J. & He, X. (2013), ‘Development of predictive tools to assess capping tendency of tablet formulations’, *Powder Technology* **236**, 139–148.
- Akseli, I., Xie, J., Schultz, L., Ladyzhynsky, N., Bramante, T., He, X., Deanne, R., Horspool, K. R. & Schwabe, R. (2017), ‘A practical framework toward prediction of breaking force and disintegration of tablet formulations using machine learning tools’, *Journal of Pharmaceutical Sciences* **106**(1), 234–247.
- Al-Raoush, R. I. (2002), Extraction of Physically-Realistic Pore Network Properties from Three-Dimensional Synchrotron Microtomography Images of Unconsolidated Porous Media, PhD thesis, Louisiana State University.
- Am Ende, M. T., Bell, C. L., Peppas, N. A., Massimo, G. & Colombo, P. (1995), ‘Measurement of the swelling force in ionic polymeric networks: Ii. swelling force and disintegration of controlled release dosage formulations using ph-sensitive components’, *International Journal of Pharmaceutics* **120**(1), 33–40.
- Amoddeo, A. & Giovine, P. (2019), ‘Micromechanical modelling of granular materials and fem simulations’, *Meccanica* **54**(4-5), 609–630.
- Antheunis, H., van der Meer, J.-C., de Geus, M., Heise, A. & Koning, C. E. (2010), ‘Autocatalytic equation describing the change in molecular weight during hydrolytic degradation of aliphatic polyesters’, *Biomacromolecules* **11**(4), 1118–1124.
- Antheunis, H., van der Meer, J.-C., de Geus, M., Kingma, W. & Koning, C. E. (2009), ‘Improved mathematical model for the hydrolytic degradation of aliphatic polyesters’, *Macromolecules* **42**(7), 2462–2471.

- Anwar, S., Fell, J. & Dickinson, P. (2005), 'An investigation of the disintegration of tablets in biorelevant media', *International Journal of Pharmaceutics* **290**(1-2), 121–127.
- Arndt, O.-R., Baggio, R., Adam, A. K., Harting, J., Franceschinis, E. & Kleinebudde, P. (2018), 'Impact of different dry and wet granulation techniques on granule and tablet properties: A comparative study', *Journal of Pharmaceutical Sciences* **107**(12), 3143–3152.
- Arndt, O.-R. & Kleinebudde, P. (2018), 'Influence of binder properties on dry granules and tablets', *Powder Technology* **337**, 68–77.
- Atrian, A., Lund, J., Radtke, L., Skorych, V., Dosta, M. & Düster, A. (2021), 'A partitioned scheme for coupling of fem and dem simulations of granular materials', *PAMM* **21**(1), e202100134.
- Augsburger, L. L., Brzezczko, A. W., Shah, U. V. & Hahm, H. A. (2013), Super disintegrants: Characterization and function, in J. Swarbrick, ed., 'Encyclopedia of Pharmaceutical Technology : Volume 6', 3rd edn, Vol. 6, CRC Press, pp. 3553–3582.
- AutoChem, M. T. (2016), 'Particletrack with fbrm method of measurement – technology introduction – mettler toledo – en'.
- Balankin, A. S., Paredes, R. G., Susarrey, O., Morales, D. & Vacio, F. C. (2006), 'Kinetic roughening and pinning of two coupled interfaces in disordered media', *Physical Review Letters* **96**(5), 056101.
- Bawuah, P., Evans, M., Lura, A., Farrell, D. J., Barrie, P. J., Kleinebudde, P., Markl, D. & Zeitler, J. A. (2023), 'At-line porosity sensing for non-destructive disintegration testing in immediate release tablets', *International Journal of Pharmaceutics: X* **5**, 100186.
- Bawuah, P., Silfsten, P., Ervasti, T., Ketolainen, J., Zeitler, J. A. & Peiponen, K.-E. (2014), 'Non-contact weight measurement of flat-faced pharmaceutical tablets using terahertz transmission pulse delay measurements', *International Journal of Pharmaceutics* **476**(1-2), 16–22.
- Bear, J. (2018), *Modeling Phenomena of Flow and Transport in Porous Media*, Vol. 31 of *Theory and Applications of Transport in Porous Media*, Springer International Publishing.
- Bele, M. H. & Derle, D. V. (2012), 'Effect of sorbed water on disintegrant performance of four brands of polacrillin potassium nf', *AAPS PharmSciTech* **13**(1), 24–34.
- Bell, C. & Peppas, N. A. (1996), 'An apparatus to measure polymer swelling under load', *International Journal of Pharmaceutics* **134**(1-2), 167–172.
- Berardi, A., Bisharat, L., Blaibleh, A., Pavoni, L. & Cespi, M. (2018), 'A simple and inexpensive image analysis technique to study the effect of disintegrants concentration and diluents type on disintegration', *Journal of Pharmaceutical Sciences* **107**(10), 2643–2652.
- Berg, C. F. (2014), 'Permeability description by characteristic length, tortuosity, constriction and porosity', *Transport in Porous Media* **103**(3), 381–400.

- Bi, Y. X., Sunada, H., Yonezawa, Y. & Danjo, K. (1999), 'Evaluation of rapidly disintegrating tablets prepared by a direct compression method', *Drug Development and Industrial Pharmacy* **25**(5), 571–581.
- Bika, D. G., Gentzler, M. & Michaels, J. N. (2001), 'Mechanical properties of agglomerates', *Powder Technology* **117**(1-2), 98–112.
- Bika, D., Tardos, G., Panmai, S., Farber, L. & Michaels, J. (2005), 'Strength and morphology of solid bridges in dry granules of pharmaceutical powders', *Powder Technology* **150**(2), 104–116.
- Borgonovo, E. & Plischke, E. (2016), 'Sensitivity analysis: A review of recent advances', *European Journal of Operational Research* **248**(3), 869–887.
- Boschetti, P. J., Pelliccioni, O., Sabino, M. A., Vera, N. & Pappaterra, M. F. (2020), 'Lattice boltzmann simulation of swelling behavior of cylindrical ipn hydrogel tablets', *Fluid Phase Equilibria* **508**, 112449.
- Boschetti, P. J., Toro, D. J., Ontiveros, A., Pelliccioni, O. & Sabino, M. A. (2022), 'Lattice boltzmann method simulations of swelling of cuboid-shaped ipn hydrogel tablets with experimental validation', *Heat and Mass Transfer* **58**(5), 763–777.
- Boyle, J. F., Manas-Zloczower, I. & Feke, D. L. (2005), 'Hydrodynamic analysis of the mechanisms of agglomerate dispersion', *Powder Technology* **153**(2), 127–133.
- Braile, D., Hare, C. & Wu, C.-Y. (2022), 'Dem analysis of swelling behaviour in granular media', *Advanced Powder Technology* **33**(11), 103806.
- Brivadis, L. & Sacchelli, L. (2022), 'New inversion methods for the single/multi-shape cld-to-psd problem with spheroid particles', *Journal of Process Control* **109**, 1–12.
- Brú, A. & Pastor, J. M. (2006), 'Experimental characterization of hydration and pinning in bentonite clay, a swelling, heterogeneous, porous medium', *Geoderma* **134**(3), 295–305.
- Buchholz, J., Clausen, U. & Vastag, A. (1998), Grundlagen der verkehrslogistik, *in* J. Buchholz, U. Clausen & A. Vastag, eds, 'Handbuch der Verkehrslogistik', Logistik in Industrie, Handel und Dienstleistungen, Springer, pp. 1–25.
- Burdine, N. (1953), 'Relative permeability calculations from pore size distribution data', *Journal of Petroleum Technology* **5**(03), 71–78.
- Cai, J. & Yu, B. (2011), 'A discussion of the effect of tortuosity on the capillary imbibition in porous media', *Transport in Porous Media* **89**(2), 251–263.
- Caramella, C., Colombo, P., Conte, U., Ferrari, F., Gazzaniga, A., LaManna, A. & Peppas, N. A. (1988), 'A physical analysis of the phenomenon of tablet disintegration', *International Journal of Pharmaceutics* **44**(1), 177–186.
- Caramella, C., Ferrari, F., Bonferoni, M. C. & Ronchi, M. (1990), 'Disintegrants in solid dosage forms', *Drug Development and Industrial Pharmacy* **16**(17), 2561–2577.

- Caramella, C., Ferrari, F., Bonferoni, M. C., Ronchi, M. & Colombo, P. (1989), 'Rheological properties and diffusion dissolution behaviour of hydrophilic polymers.', *Bollettino Chimico Farmaceutico* **128**(10), 298–302.
- Caramella, C., Ferrari, F., Ubaldo, C., Gazzaniga, A., LaManna, A. & Colombo, P. (1989), 'Experimental evidence of disintegration mechanisms', *Acta pharmaceutica tecnologica* **35**(1), 30–33.
- Cardona, J., Ferreira, C., McGinty, J., Hamilton, A., Agimelen, O. S., Cleary, A., Atkinson, R., Michie, C., Marshall, S., Chen, Y.-C., Sefcik, J., Andonovic, I. & Tachtatzis, C. (2018), 'Image analysis framework with focus evaluation for in situ characterisation of particle size and shape attributes', *Chemical Engineering Science* **191**, 208–231.
- Carstensen, J. T. & Chan, P.-C. (n.d.), 'Relation between particle size and repose angles of powders', **15**(1), 129–131.
- Catellani, P., Predella, P., Bellotti, A. & Colombo, P. (1989), 'Tablet water uptake and disintegration force measurements', *International Journal of Pharmaceutics* **51**(1), 63–66.
- Chen, C. R., Lin, Y. H., Cho, S. L., Yen, S. Y. & Wu, H. L. S. (1997), 'Investigation of the dissolution difference between acidic and neutral media of acetaminophen tablets containing a super disintegrant and a soluble excipient', *Chemical & Pharmaceutical Bulletin* **45**(3), 509–512.
- Chen, J., Park, H. & Park, K. (1999), 'Synthesis of superporous hydrogels: Hydrogels with fast swelling and superabsorbent properties', *Journal of Biomedical Materials Research* **44**(1), 53–62.
- Chen, Y. Y., Hughes, L. P., Gladden, L. F. & Mantle, M. D. (2010), 'Quantitative ultra-fast mri of hpmc swelling and dissolution', *Journal of Pharmaceutical Sciences* **99**(8), 3462–3472.
- Christopher Frey, H. & Patil, S. R. (2002), 'Identification and review of sensitivity analysis methods', *Risk Analysis* **22**(3), 553–578.
- Colombo, P., Conte, U., Caramella, C., Manna, A. L. & Geddo, M. (1984), 'Disintegrating force as a new formulation parameter', *Journal of Pharmaceutical Sciences* **73**(5), 701–705.
- Colombo, P., Ferrari, F., Gazzaniga, A., Caramella, C., Conte, U., La Manna, A. & Pappas, N. A. (1988), 'Simulation of the disintegration process of pharmaceutical tablets', *Pharmaceutica Acta Helvetiae* **63**(8), 221–223.
- Cooper, B. F. & Brecht, E. A. (1957), 'Surfactants in tablets to improve disintegration', *Journal of the American Pharmaceutical Association* **46**(9), 520–524.
- Coutant, C. A., Skibic, M. J., Doddridge, G. D., Kemp, C. A. & Sperry, D. C. (2010), 'In vitro monitoring of dissolution of an immediate release tablet by focused beam reflectance measurement', *Molecular Pharmaceutics* **7**(5), 1508–1515.
- Curlin, L. C. (1955), 'A note on tablet disintegration with starch', *Journal of the American Pharmaceutical Association (Scientific Edition)* **44**(1), 16.

- da Silva, C. A. M. & Taranto, O. P. (2015), 'Real-time monitoring of gas–solid fluidized-bed granulation and coating process: Evolution of particle size, fluidization regime transitions, and psychometric parameters', *Drying Technology* **33**(15-16), 1929–1948.
- Davies, A. J. (2011), *The Finite Element Method: An Introduction with Partial Differential Equations*, 2nd ed edn, Oxford University Press, Oxford ; New York.
- Davies, W. L. & Gloor, W. T. (1972), 'Batch production of pharmaceutical granulations in a fluidized bed ii: Effects of various binders and their concentrations on granulations and compressed tablets', *Journal of Pharmaceutical Sciences* **61**(4), 618–622.
- De Boer, J. (1980), 'The wettability of scoured and dried cotton fabrics', *Textile Research Journal* **50**(10), 624–631.
- de Vaucorbeil, A., Nguyen, V. P., Sinaie, S. & Wu, J. Y. (2020), Material point method after 25 years: Theory, implementation, and applications, in S. P. A. Bordas & D. S. Balint, eds, 'Advances in Applied Mechanics', Vol. 53, Elsevier, pp. 185–398.
- Dees, P. (1980), The Mechanisms of Tablet Disintegration, PhD thesis, University Leiden.
- Delker, T., Pengra, D. B. & Wong, P.-z. (1996), 'Interface pinning and the dynamics of capillary rise in porous media', *Physical Review Letters* **76**(16), 2902–2905.
- Desai, P. M., Liew, C. V. & Heng, P. W. S. (2012), 'Understanding disintegrant action by visualization', *Journal of Pharmaceutical Sciences* **101**(6), 2155–2164.
- Desai, P. M., Liew, C. V. & Heng, P. W. S. (2016), 'Review of disintegrants and the disintegration phenomena', *Journal of Pharmaceutical Sciences* **105**(9), 2545–2555.
- Diersch, H.-J. G., Clausnitzer, V., Myrnyy, V., Rosati, R., Schmidt, M., Beruda, H., Ehrnsperger, B. J. & Virgilio, R. (2010), 'Modeling unsaturated flow in absorbent swelling porous media: Part 1. theory', *Transport in Porous Media* **83**(3), 437–464.
- Diersch, H.-J. G., Clausnitzer, V., Myrnyy, V., Rosati, R., Schmidt, M., Beruda, H., Ehrnsperger, B. J. & Virgilio, R. (2011), 'Modeling unsaturated flow in absorbent swelling porous media: Part 2. numerical simulation', *Transport in Porous Media* **86**(3), 753–776.
- Dieter, P., Stefan, D., Günter, E. & Michael, K. (2011), 'In-line particle sizing for real-time process control by fibre-optical spatial filtering technique (sft)', *Advanced Powder Technology* **22**(2), 203–208.
- Djemai, A. & Sinka, I. (2006), 'Nmr imaging of density distributions in tablets', *International Journal of Pharmaceutics* **319**(1-2), 55–62.
- Dorkoosh, F. A., Verhoef, J. C., Borchard, G., Rafiee-Tehrani, M., Verheijden, J. H. M. & Junginger, H. E. (2002), 'Intestinal absorption of human insulin in pigs using delivery systems based on superporous hydrogel polymers', *International Journal of Pharmaceutics* **247**(1), 47–55.

- Dubé, M., Rost, M., Elder, K. R., Alava, M., Majaniemi, S. & Ala-Nissila, T. (1999), ‘Liquid conservation and nonlocal interface dynamics in imbibition’, *Physical Review Letters* **83**(8), 1628–1631.
- Eklund, D. E. & Salminen, P. J. (1986), ‘Water transport in the blade coating process’, *TAPPI journal* **69**, 116–119.
- El-Barghouthi, M., Eftaiha, A., Rashid, I., Al-Remawi, M. & Badwan, A. (2008), ‘A novel superdisintegrating agent made from physically modified chitosan with silicon dioxide’, *Drug Development and Industrial Pharmacy* **34**(4), 373–383.
- Ellison, C. D., Ennis, B. J., Hamad, M. L. & Lyon, R. C. (2008), ‘Measuring the distribution of density and tableting force in pharmaceutical tablets by chemical imaging’, *Journal of Pharmaceutical and Biomedical Analysis* **48**(1), 1–7.
- Erdos, S. & Bezegh, A. (1977), ‘Studies on the mechanism of disintegration.’, *Pharmaceutical Industry* **11**, 1130–113.
- Fern, J., Rohe, A., Soga, K. & Alonso, E., eds (2019), *The Material Point Method for Geotechnical Engineering: A Practical Guide*, 1 edn, CRC Press, Boca Raton : CRC Press, Taylor & Francis Group, [2019].
- Ferry, J. D. (1980), *Viscoelastic Properties of Polymers*, John Wiley & Sons.
- Florence, A. T. & Attwood, D. (2015), *Physicochemical Principles of Pharmacy: In Manufacture, Formulation and Clinical Use*, Pharmaceutical Press.
- Fox, R. O., Laurent, F. & Passalacqua, A. (2023), ‘The generalized quadrature method of moments’, *Journal of Aerosol Science* **167**, 106096.
- Fu, Y., Yang, S., Jeong, S. H., Kimura, S. & Park, K. (2004), ‘Orally fast disintegrating tablets: Developments, technologies, taste-masking and clinical studies’, *Critical Reviews & Trade; in Therapeutic Drug Carrier Systems* **21**(6).
- Gabbott, I. P., Al Husban, F. & Reynolds, G. K. (2016), ‘The combined effect of wet granulation process parameters and dried granule moisture content on tablet quality attributes’, *European Journal of Pharmaceutics and Biopharmaceutics* **106**, 70–78.
- Ganderton, D. & Fraser, D. R. (1970), ‘Some observations of the penetration and disruption of tablets by water’, *Journal of Pharmacy and Pharmacology* **22**(S1), 95S–103S.
- Ganji, F., Vasheghani-Farahani, S. & Vasheghani-Farahani, E. (2010), ‘Theoretical description of hydrogel swelling: A review’, *Iranian Polymer Journal* **19**, 375–398.
- Gasmi, H., Danede, F., Siepmann, J. & Siepmann, F. (2015), ‘Does plga microparticle swelling control drug release? new insight based on single particle swelling studies’, *Journal of Controlled Release* **213**, 120–127.
- Gautschi, W. (2004), *Orthogonal Polynomials: Computation and Approximation*, Numerical Mathematics and Scientific Computation, Oxford University Press.

- Gissinger, D. & Stamm, A. (1980), 'A comparative evaluation of the properties of some tablet disintegrants', *Drug Development and Industrial Pharmacy* **6**(5), 511–536.
- Gohel, M. C. & Jogani, P. D. (2005), 'A review of co-processed directly compressible excipients', *Journal of Pharmacy & Pharmaceutical Sciences: A Publication of the Canadian Society for Pharmaceutical Sciences, Societe Canadienne Des Sciences Pharmaceutiques* **8**(1), 76–93.
- Gordon, M. S., Chatterjee, B. & Chowhan, Z. T. (1990), 'Effect of the mode of croscarmellose sodium incorporation on tablet dissolution and friability', *Journal of Pharmaceutical Sciences* **79**(1), 43–47.
- Grassi, M., Colombo, I. & Lapasin, R. (2000), 'Drug release from an ensemble of swellable crosslinked polymer particles', *Journal of Controlled Release* **68**(1), 97–113.
- Handy, L. L. (1960), 'Determination of effective capillary pressures for porous media from imbibition data', *Transactions of the AIME* **219**(01), 75–80.
- Hansen, S. & Ottino, J. M. (1996), 'Agglomerate erosion: A nonscaling solution to the fragmentation equation', *Physical Review E* **53**(4), 4209–4212.
- He, X., Barone, M. R., Marsac, P. J. & Sperry, D. C. (2008), 'Development of a rapidly dispersing tablet of a poorly wetttable compound—formulation doe and mechanistic study of effect of formulation excipients on wetting of celecoxib', *International Journal of Pharmaceutics* **353**(1), 176–186.
- Hong, W., Zhao, X., Zhou, J. & Suo, Z. (2008), 'A theory of coupled diffusion and large deformation in polymeric gels', *Journal of the Mechanics and Physics of Solids* **56**(5), 1779–1793.
- Horváth, V. K. & Stanley, H. E. (1995), 'Temporal scaling of interfaces propagating in porous media', *Physical Review E* **52**(5), 5166–5169.
- Hounslow, M. J., Pearson, J. M. K. & Instone, T. (2001), 'Tracer studies of high-shear granulation: Ii. population balance modeling', *AIChE Journal* **47**(9), 1984–1999.
- Huang, J., Goolcharran, C., Utz, J., Hernandez-Abad, P., Ghosh, K. & Nagi, A. (2010), 'A pat approach to enhance process understanding of fluid bed granulation using in-line particle size characterization and multivariate analysis', *Journal of Pharmaceutical Innovation* **5**(1-2), 58–68.
- Hui, C.-Y. & Muralidharan, V. (2005), 'Gel mechanics: A comparison of the theories of biot and tanaka, hocker, and benedek', *The Journal of Chemical Physics* **123**(15), 154905.
- Hulburt, H. & Katz, S. (1964), 'Some problems in particle technology: A statistical mechanical formulation', *Chemical Engineering Science* **19**(8), 555–574.
- Jenkins, L. M. & Donald, A. M. (1997), 'Use of the environmental scanning electron microscope for the observation of the swelling behaviour of cellulosic fibres', *Scanning* **19**(2), 92–97.

- Jia, X. & Williams, R. (2007), 'A hybrid mesoscale modelling approach to dissolution of granules and tablets', *Chemical Engineering Research and Design* **85**(7), 1027–1038.
- Jivraj, M., Martini, L. G. & Thomson, C. M. (2000), 'An overview of the different excipients useful for the direct compression of tablets', *Pharmaceutical Science & Technology Today* **3**(2), 58–63.
- Joekar-Niasar, V. (2011), 'Effect of fluids properties on non-equilibrium capillarity effects: Dynamic pore-network modeling', *International Journal of Multiphase Flow* p. 17.
- Kabiri, K., Omidian, H., Hashemi, S. & Zohuriaan-Mehr, M. (2003), 'Synthesis of fast-swelling superabsorbent hydrogels: Effect of crosslinker type and concentration on porosity and absorption rate', *European Polymer Journal* **39**(7), 1341–1348.
- Kail, N., Briesen, H. & Marquardt, W. (2007), 'Advanced geometrical modeling of focused beam reflectance measurements (fbrm)', *Particle & Particle Systems Characterization* **24**(3), 184–192.
- Kalný, M., Grof, Z. & Štěpánek, F. (2021), 'Microstructure based simulation of the disintegration and dissolution of immediate release pharmaceutical tablets', *Powder Technology* **377**, 257–268.
- Kariuki, W. I., Freireich, B., Smith, R. M., Rhodes, M. & Hapgood, K. P. (2013), 'Distribution nucleation: Quantifying liquid distribution on the particle surface using the dimensionless particle coating number', *Chemical Engineering Science* **92**, 134–145.
- Kaunisto, E., Rasmuson, A., Bergenholtz, J., Rimmelgas, J., Lindfors, L. & Folestad, S. (2013), 'Fundamental mechanisms for tablet dissolution: Simulation of particle deaggregation via brownian dynamics', *Journal of Pharmaceutical Sciences* **102**(5), 1569–1577.
- Khan, K. & Rhodes, C. (1975), 'Water-sorption properties of tablet disintegrants', *Journal of Pharmaceutical Sciences* **64**(3), 447–451.
- Khare, A. R., Peppas, N. A., Massimo, G. & Colombo, P. (1992), 'Measurement of the swelling force in ionic polymeric networks i. effect of ph and ionic content', *Journal of Controlled Release* **22**(3), 239–244.
- Khattab, I., Menon, A. & Sakr, A. (1993), 'Effect of mode of incorporation of disintegrants on the characteristics of fluid-bed wet-granulated tablets', *Journal of Pharmacy and Pharmacology* **45**(8), 687–691.
- Kipper, M. J. & Narasimhan, B. (2005), 'Molecular description of erosion phenomena in biodegradable polymers', *Macromolecules* **38**(5), 1989–1999.
- Kissa, E. (1996), 'Wetting and wicking', *Textile Research Journal* **66**(10), 660–668.
- Koponen, A., Kataja, M. & Timonen, J. (1997), 'Permeability and effective porosity of porous media', *Physical Review E* **56**(3), 3319–3325.
- Kottke, Mary J, K. & Rudnic, E. M. (2002), Tablet dosage forms, in G. S. Banker & C. T. Rhodes, eds, 'Modern Pharmaceutics', 4th edn, Marcel Dekker, pp. 287–333.

- Kwan, K. C., Swart, F. O. & Mattocks, A. M. (1957), 'Factors affecting tablet disintegration', *Journal of the American Pharmaceutical Association* **46**(4), 236–239.
- Kwon, T. H., Hopkins, A. E. & O'Donnell, S. E. (1996), 'Dynamic scaling behavior of a growing self-affine fractal interface in a paper-towel-wetting experiment', *Physical Review E* **54**(1), 685–690.
- Laity, P. R. & Cameron, R. E. (2010), 'Synchrotron x-ray microtomographic study of tablet swelling', *European Journal of Pharmaceutics and Biopharmaceutics* **75**(2), 263–276.
- Lam, C. & Horvath, V. K. (2000), 'Pipe network model for scaling of dynamic interfaces in porous media', *Physical Review Letters* **85**(6), 1238–1241.
- Larobina, D., Mensitieri, G., Kipper, M. J. & Narasimhan, B. (2002), 'Mechanistic understanding of degradation in bioerodible polymers for drug delivery', *AIChE Journal* **48**(12), 2960–2970.
- Laughlin, R. D. & Davies, J. E. (1961), 'Some aspects of capillary absorption in fibrous textile wicking', *Textile Research Journal* **31**(10), 904–910.
- Lendlein, A. & Kelch, S. (2002), 'Shape-memory polymers', *Angewandte Chemie International Edition* **41**(12), 2034–2057.
- Lenz, J., Bunjes, H., Kwade, A. & Juhnke, M. (2021), 'An improved method for the simultaneous determination of water uptake and swelling of tablets', *International Journal of Pharmaceutics* **595**, 120229.
- Leskinen, J. T. T., Simonaho, S.-P., Hakulinen, M. & Ketolainen, J. (2010), 'In-line ultrasound measurement system for detecting tablet integrity', *International Journal of Pharmaceutics* **400**(1), 104–113.
- Li, J., Tao, L., Dali, M., Buckley, D., Gao, J. & Hubert, M. (2011), 'The effect of the physical states of binders on high-shear wet granulation and granule properties: A mechanistic approach toward understanding high-shear wet granulation process. part ii. granulation and granule properties', *Journal of Pharmaceutical Sciences* **100**(1), 294–310.
- Li, K. & Horne, R. N. (2004), 'An analytical scaling method for spontaneous imbibition in gas/water/rock systems', *SPE Journal* **9**(03), 322–329.
- Li, Z., Qiao, Z. & Tang, T. (2017), *Numerical Solution of Differential Equations: Introduction to Finite Difference and Finite Element Methods*, 1st ed edn, Cambridge University Press.
- Lieberman, H. A., Lachman, L. & Schwartz, J. B., eds (1989), *Pharmaceutical Dosage Forms-Tablets*, 2nd ed., rev. and expanded edn, Dekker, New York.
- List, P. & Muazzam, U. (1979), 'Swelling force allowing the disintegration of tablets', *Pharmaceutical Industry* **41**, 459–464.
- Litster, J. (2016), *Design and Processing of Particulate Products*, Cambridge University Press.

- Lowenthal, W. (1972), 'Disintegration of tablets', *Journal of Pharmaceutical Sciences* **61**(11), 1695–1711.
- Lowenthal, W. & Burruss, R. A. (1971), 'Mechanism of action of starch as a tablet disintegrant iv: Effect of medicaments and disintegrants on mean pore diameter and porosity', *Journal of Pharmaceutical Sciences* **60**(9), 1325–1332.
- Luginbühl, R. & Leuenberger, H. (1994), 'Use of percolation theory to interpret water uptake, disintegration time and intrinsic dissolution rate of tablets consisting of binary mixtures', *Pharmaceutica Acta Helveticae* **69**(3), 127–134.
- Macleán, N., Walsh, E., Soundaranathan, M., Khadra, I., Mann, J., Williams, H. & Markl, D. (2021), 'Exploring the performance-controlling tablet disintegration mechanisms for direct compression formulations', *International Journal of Pharmaceutics* **599**, 120221.
- Markl, D., Hanneschläger, G., Sacher, S., Leitner, M. & Khinast, J. G. (2014), 'Optical coherence tomography as a novel tool for in-line monitoring of a pharmaceutical film-coating process', *European Journal of Pharmaceutical Sciences* **55**, 58–67.
- Markl, D., Strobel, A., Schlossnikl, R., Botker, J., Bawuah, P., Ridgway, C., Rantanen, J., Rades, T., Gane, P., Peiponen, K.-E. & Zeitler, J. A. (2018), 'Characterisation of pore structures of pharmaceutical tablets: A review', *International Journal of Pharmaceutics* **538**(1-2), 188–214.
- Markl, D., Wang, P., Ridgway, C., Karttunen, A.-P., Chakraborty, M., Bawuah, P., Pääkkönen, P., Gane, P., Ketolainen, J., Peiponen, K.-E. & Zeitler, J. A. (2017), 'Characterization of the pore structure of functionalized calcium carbonate tablets by terahertz time-domain spectroscopy and x-ray computed microtomography', *Journal of Pharmaceutical Sciences* **106**(6), 1586–1595.
- Markl, D., Yassin, S., Wilson, D. I., Goodwin, D. J., Anderson, A. & Zeitler, J. A. (2017), 'Mathematical modelling of liquid transport in swelling pharmaceutical immediate release tablets', *International Journal of Pharmaceutics* **526**(1-2), 1–10.
- Markl, D. & Zeitler, J. A. (2017), 'A review of disintegration mechanisms and measurement techniques', *Pharmaceutical Research* **34**(5), 890–917.
- Marshall, P. V., Pope, D. G. & Carstensen, J. T. (1991), 'Methods for the assessment of the stability of tablet disintegrants', *Journal of Pharmaceutical Sciences* **80**(9), 899–903.
- Marucci, M., Ragnarsson, G., von Corswant, C., Welinder, A., Jarke, A., Iselau, F. & Axelsson, A. (2011), 'Polymer leaching from film coating: Effects on the coating transport properties', *International Journal of Pharmaceutics* **411**(1-2), 43–48.
- Masoodi, R. & Pillai, K. M. (2010), 'Darcy's law-based model for wicking in paper-like swelling porous media', *AIChE Journal* **56**(9), 2257–2267.
- Mohamad, A. A. (2019), *Lattice Boltzmann Method: Fundamentals and Engineering Applications with Computer Codes*, Springer London, London.

- Mohanachandran, P. S., Sindhumol, P. G. & Kiran, T. S. (n.d.), 'Superdisintegrants: An overview', **6**(1), 105–109.
- Morel-Seytoux, H. J., Meyer, P. D., Nachabe, M., Tourna, J., van Genuchten, M. T. & Lenhard, R. J. (1996), 'Parameter equivalence for the brooks-corey and van genuchten soil characteristics: Preserving the effective capillary drive', *Water Resources Research* **32**(5), 1251–1258.
- Moreton, R. C. (2008), Disintegrants in tableting, in L. L. Augsburger & S. W. Hoag, eds, 'Pharmaceutical Dosage Forms: Tablets, Vol. 2: Rational Design and Formulation, 3rd Edition', 3rd edition edn, Vol. 2, CRC Press, pp. 217–250.
- Mualem, Y. (1976), 'A new model for predicting the hydraulic conductivity of unsaturated porous media', *Water Resources Research* **12**(3), 513–522.
- Myers, D. (n.d.), *Surfaces Interfaces and Colloids: Principles and Applications*, 1 edn, Wiley.
- Nairn, J. (1970), 'Material point method calculations with explicit cracks', *Computer Modeling in Engineering & Sciences* **4**(6), 649–664.
- Narasimhan, B. & Peppas, N. A. (1996), 'On the importance of chain reptation in models of dissolution of glassy polymers', *Macromolecules* **29**(9), 3283–3291.
- Nguyen, T. K., Combe, G., Caillerie, D. & Desrues, J. (2014), 'Fem  $\times$  dem modelling of cohesive granular materials: Numerical homogenisation and multi-scale simulations', *Acta Geophysica* **62**(5), 1109–1126.
- Nichols, G., Byard, S., Bloxham, M. J., Botterill, J., Dawson, N. J., Dennis, A., Diart, V., North, N. C. & Sherwood, J. D. (2002), 'A review of the terms agglomerate and aggregate with a recommendation for nomenclature used in powder and particle characterization', *Journal of Pharmaceutical Sciences* **91**(10), 2103–2109.
- Nogami, H., Hasegawa, J. & Miyamoto, M. (1967), 'Studies on powdered preparations. xx. disintegration of the aspirin tablets containing starches as disintegrating agent', *Chemical & Pharmaceutical Bulletin* **15**(3), 279–289.
- Nogami, H., Nagai, T., Fukuoka, E. & Sonobe, T. (1969), 'Disintegration of the aspirin tablets containing potato starch and microcrystalline cellulose in various concentrations'.
- Nott, K. P. (2010), 'Magnetic resonance imaging of tablet dissolution', *European Journal of Pharmaceutics and Biopharmaceutics* **74**(1), 78–83.
- Nyström, C., Alderborn, Gör., Duberg, M. & Karehill, P.-G. (1993), 'Bonding surface area and bonding mechanism—two important factors for the understanding of powder comparability', *Drug Development and Industrial Pharmacy* **19**(17-18), 2143–2196.
- Odian, G. (2004), *Principles of Polymerization*, 4 edition edn, Wiley.
- Omidian, H., Hashemi, S., Sammes, P. & Meldrum, I. (1998), 'A model for the swelling of superabsorbent polymers', *Polymer* **39**(26), 6697–6704.

- Omidian, H., Park, K. & Rocca, J. G. (2007), 'Recent developments in superporous hydrogels', *Journal of Pharmacy and Pharmacology* **59**(3), 317–327.
- Omidian, H., Rocca, J. G. & Park, K. (2005), 'Advances in superporous hydrogels', *Journal of Controlled Release* **102**(1), 3–12.
- Ottino, J. M., DeRoussel, P., Hansen, S. & Khakhar, D. V. (1999), Mixing and dispersion of viscous liquids and powdered solids, in J. Wei, ed., 'Advances in Chemical Engineering', Vol. 25, Academic Press, pp. 105–204.
- Patel, N. R. & Hopponet, R. E. (1966), 'Mechanism of action of starch as a disintegrating agent in aspirin tablets', *Journal of Pharmaceutical Sciences* **55**(10), 1065–1068.
- Patel, S., Kaushal, A. M. & Bansal, A. K. (2007), 'Effect of particle size and compression force on compaction behavior and derived mathematical parameters of compressibility', *Pharmaceutical Research* **24**(1), 111–124.
- Peppas, N. A. & Colombo, P. (1989), 'Development of disintegration forces during water penetration in porous pharmaceutical systems', *Journal of Controlled Release* **10**(3), 245–250.
- Peppas, N. A., Colombo, P., Conte, U., Gazzaniga, A., Caramella, C. & Ferrari, F. (1989), 'Energetics of tablet disintegration', *International Journal of Pharmaceutics* **51**(1), 77–83.
- Pierrat, P. & Caram, H. S. (1997), 'Tensile strength of wet granular materials', p. 11.
- Purcell, W. (1949), 'Capillary pressures - their measurement using mercury and the calculation of permeability therefrom', *Journal of Petroleum Technology* **1**(02), 39–48.
- Qiu, G., Jiang, T., Li, H. & Wang, D. (2003), 'Functions and molecular structure of organic binders for iron ore pelletization', *Colloids and Surfaces A: Physicochemical and Engineering Aspects* **224**(1-3), 11–22.
- Quodbach, J. & Kleinebudde, P. (2014a), 'A new apparatus for real-time assessment of the particle size distribution of disintegrating tablets', *Journal of Pharmaceutical Sciences* **103**(11), 3657–3665.
- Quodbach, J. & Kleinebudde, P. (2014b), 'Systematic classification of tablet disintegrants by water uptake and force development kinetics', *Journal of Pharmacy and Pharmacology* **66**(10), 1429–1438.
- Quodbach, J. & Kleinebudde, P. (2015), 'Performance of tablet disintegrants: Impact of storage conditions and relative tablet density', *Pharmaceutical Development and Technology* **20**(6), 762–768.
- Quodbach, J. & Kleinebudde, P. (2016), 'A critical review on tablet disintegration', *Pharmaceutical Development and Technology* **21**(6), 763–774.
- Quodbach, J., Moussavi, A., Tammer, R., Frahm, J. & Kleinebudde, P. (2014), 'Tablet disintegration studied by high-resolution real-time magnetic resonance imaging', *Journal of Pharmaceutical Sciences* **103**(1), 249–255.

- Rudnic, E. M., Rhodes, C. T., Welch, S. & Bernardo, P. (1982), 'Evaluations of the mechanism of disintegrant action', *Drug Development and Industrial Pharmacy* **8**(1), 87–109.
- Ruegger, C. E. & Çelick, M. (2000), 'The effect of compression and decompression speed on the mechanical strength of compacts', *Pharmaceutical Development and Technology* **5**(4), 485–494.
- Rumpf, H. (1962), 'The strength of granules and agglomerates', *Agglomeration* pp. 379–418.
- Rwei, S., Manas-Zloczower, I. & Feke, D. (1991), 'Characterization of agglomerate dispersion by erosion in simple shear flows', *Polymer Engineering and Science* **31**(8), 558–562.
- Rwei, S. P., Manas-Zloczower, I. & Feke, D. L. (1990), 'Observation of carbon black agglomerate dispersion in simple shear flows', *Polymer Engineering and Science* **30**(12), 701–706.
- Sackett, C. K. & Narasimhan, B. (2011), 'Mathematical modeling of polymer erosion: Consequences for drug delivery', *International Journal of Pharmaceutics* **418**(1), 104–114.
- Sadeghirad, A., Brannon, R. M. & Burghardt, J. (2011), 'A convected particle domain interpolation technique to extend applicability of the material point method for problems involving massive deformations', *International Journal for Numerical Methods in Engineering* **86**(12), 1435–1456.
- Saltelli, A., ed. (2008), *Global Sensitivity Analysis: The Primer*, Wiley.
- Saripella, K. K., Mallipeddi, R. & Neau, S. H. (2014a), 'Crosppovidone interactions with water. i. calorimetric study of the effect of polyplasdone particle size on its uptake and distribution of water', *Journal of Pharmaceutical Sciences* **103**(2), 669–675.
- Saripella, K. K., Mallipeddi, R. & Neau, S. H. (2014b), 'Crosppovidone interactions with water. ii. dynamic vapor sorption analysis of the effect of polyplasdone particle size on its uptake and distribution of water', *International Journal of Pharmaceutics* **475**(1), 174–180.
- Schindwein, W. S. & Gibson, M., eds (2018), *Pharmaceutical Quality by Design: A Practical Approach*, 1 edn, Wiley.
- Schlumberger, C. & Thommes, M. (2021), 'Characterization of hierarchically ordered porous materials by physisorption and mercury porosimetry—a tutorial review', *Advanced Materials Interfaces* **8**(4), 2002181.
- Schoenmaker, B. D., der Schueren, L. V., Vrieze, S. D., Westbroek, P. & Clerck, K. D. (2011), 'Wicking properties of various polyamide nanofibrous structures with an optimized method', *Journal of Applied Polymer Science* **120**(1), 305–310.
- Schott, H. (1992a), 'Kinetics of swelling of polymers and their gels', *Journal of Pharmaceutical Sciences* **81**(5), 467–470.
- Schott, H. (1992b), 'Swelling kinetics of polymers', *Journal of Macromolecular Science, Part B* **31**(1), 1–9.

- Schuchard, D. R. & Berg, J. C. (1991), 'Liquid transport in composite cellulose - superabsorbent fiber networks', *Wood and Fiber Science* **23**(3), 342–357.
- Scurati, A., Feke, D. & Manas-Zloczower, I. (2005), 'Analysis of the kinetics of agglomerate erosion in simple shear flows', *Chemical Engineering Science* **60**(23), 6564–6573.
- Shampine, L. F., Gladwell, I. & Thompson, S. (2003), *Solving ODEs with MATLAB*, illustrated edition edn, Cambridge University Press, Cambridge ; New York.
- Shampine, L. F. & Reichelt, M. W. (1997), 'The matlab ode suite: Bdf and ndf', *SIAM Journal on Scientific Computing* **18**(1), 1–22.
- Shen, E., Kipper, M. J., Dziadul, B., Lim, M.-K. & Narasimhan, B. (2002), 'Mechanistic relationships between polymer microstructure and drug release kinetics in bioerodible polyanhydrides', *Journal of Controlled Release* **82**(1), 115–125.
- Shen, E., Pizszczek, R., Dziadul, B. & Narasimhan, B. (2001), 'Microphase separation in bioerodible copolymers for drug delivery', *Biomaterials* **22**(3), 201–210.
- Shi, S. Q. & Gardner, D. J. (2000), 'A new model to determine contact angles on swelling polymer particles by the column wicking method', *Journal of Adhesion Science and Technology* **14**(2), 301–314.
- Shotton, E. & Leonard, G. S. (1972), 'The effect of intra- and extragranular maize starch on the disintegration of compressed tablets', *Journal of Pharmacy and Pharmacology* **24**(10), 798–803.
- Shotton, E. & Leonard, G. S. (1976), 'Effect of intragranular and extragranular disintegrating agents on particle size of disintegrated tablets', *Journal of Pharmaceutical Sciences* **65**(8), 1170–1174.
- Siepmann, J. & Göpferich, A. (2001), 'Mathematical modeling of bioerodible, polymeric drug delivery systems', *Advanced Drug Delivery Reviews* **48**(2), 229–247.
- Siepmann, J. & Peppas, N. (2012), 'Modeling of drug release from delivery systems based on hydroxypropyl methylcellulose (hpmc)', *Advanced Drug Delivery Reviews* **64**, 163–174.
- Siepmann, J. & Siepmann, F. (2013), 'Mathematical modeling of drug dissolution', *International Journal of Pharmaceutics* **453**(1), 12–24.
- Smallenbroek, A. J., Bolhuis, G. K. & Lerk, C. F. (1981), 'The effect of particle size of disintegrants on the disintegration of tablets', *Pharmaceutisch weekblad* **3**(1), 1048–1051.
- Sobol, I. (2001), 'Global sensitivity indices for nonlinear mathematical models and their monte carlo estimates', *Mathematics and Computers in Simulation* **55**(1-3), 271–280.
- Sohi, H., Sultana, Y. & Khar, R. K. (2004), 'Taste masking technologies in oral pharmaceuticals: Recent developments and approaches', *Drug Development and Industrial Pharmacy* **30**(5), 429–448.

- Soundaranathan, M., Al-Sharabi, M., Sweijen, T., Bawuah, P., Zeitler, J. A., Hassanizadeh, S. M., Pitt, K., Johnston, B. F. & Markl, D. (2023), 'Modelling the evolution of pore structure during the disintegration of pharmaceutical tablets', *Pharmaceutics* **15**(2), 489.
- Soundaranathan, M., Vivattanaseth, P., Walsh, E., Pitt, K., Johnston, B. & Markl, D. (2020), 'Quantification of swelling characteristics of pharmaceutical particles', *International Journal of Pharmaceutics* **590**, 119903.
- Sultan, T., Hasan Rozin, E., Dave, V. S. & Cetinkaya, C. (2023), 'Non-destructive detection of disintegrant levels in compressed oral solid dosage forms', *International Journal of Pharmaceutics* **642**, 123171.
- Sweijen, T., Chareyre, B., Hassanizadeh, S. & Karadimitriou, N. (2017), 'Grain-scale modelling of swelling granular materials; application to super absorbent polymers', *Powder Technology* **318**, 411–422.
- Sweijen, T., Hassanizadeh, S. M. & Chareyre, B. (2020), 'Unsaturated flow in a packing of swelling particles; a grain-scale model', *Advances in Water Resources* **142**, 103642.
- Sweijen, T., Hassanizadeh, S. M., Chareyre, B. & Zhuang, L. (2018), 'Dynamic pore-scale model of drainage in granular porous media: The pore-unit assembly method', *Water Resources Research* **54**(6), 4193–4213.
- Sweijen, T., van Duijn, C. & Hassanizadeh, S. (2017), 'A model for diffusion of water into a swelling particle with a free boundary: Application to a super absorbent polymer particle', *Chemical Engineering Science* **172**, 407–413.
- Szymkiewicz, A. (2012), *Modelling Water Flow in Unsaturated Porous Media: Accounting for Nonlinear Permeability and Material Heterogeneity*, Springer Science & Business Media.
- Tajarobi, F., Abrahmsén-Alami, S., Carlsson, A. S. & Larsson, A. (2009), 'Simultaneous probing of swelling, erosion and dissolution by nmr-microimaging—effect of solubility of additives on hpmc matrix tablets', *European Journal of Pharmaceutical Sciences* **37**(2), 89–97.
- Thibert, R. & Hancock, B. C. (1996), 'Direct visualization of superdisintegrant hydration using environmental scanning electron microscopy', *Journal of Pharmaceutical Sciences* **85**(11), 1255–1258.
- Tritt-Goc, J. & Kowalczyk, J. (2002), 'In situ, real time observation of the disintegration of paracetamol tablets in aqueous solution by magnetic resonance imaging', *European Journal of Pharmaceutical Sciences* **15**(4), 341–346.
- Tye, C. K., Sun, C. C. & Amidon, G. E. (2005), 'Evaluation of the effects of tableting speed on the relationships between compaction pressure, tablet tensile strength, and tablet solid fraction', *Journal of Pharmaceutical Sciences* **94**(3), 465–472.
- Uecker, M., Zhang, S., Voit, D., Merboldt, K.-D. & Frahm, J. (2012), 'Real-time mri: Recent advances using radial flash', *Imaging in Medicine* **4**(4), 461–476.
- Uhrich, K. E., Cannizzaro, S. M., Langer, R. S. & Shakesheff, K. M. (1999), 'Polymeric systems for controlled drug release', *Chemical Reviews* **99**(11), 3181–3198.

- Versteeg, H. K. & Malalasekera, W. (2007), *An Introduction to Computational Fluid Dynamics: The Finite Volume Method*, 2nd ed edn, Pearson Education Ltd, Harlow, England ; New York.
- Więckowski, Z. (2004), ‘The material point method in large strain engineering problems’, *Computer Methods in Applied Mechanics and Engineering* **193**(39-41), 4417–4438.
- Wilson, D., Wren, S. & Reynolds, G. (2012), ‘Linking dissolution to disintegration in immediate release tablets using image analysis and a population balance modelling approach’, *Pharmaceutical Research* **29**(1), 198–208.
- Wollborn, T., Schwed, M. F. & Fritsching, U. (2017), ‘Direct tensile tests on particulate agglomerates for the determination of tensile strength and interparticle bond forces’, *Advanced Powder Technology* **28**(9), 2177–2185.
- Yang, X., Sun, Z., Shui, L. & Ji, Y. (2017), ‘Characterization of the absolute volume change of cement pastes in early-age hydration process based on helium pycnometry’, *Construction and Building Materials* **142**, 490–498.
- Yassin, S., Goodwin, D. J., Anderson, A., Sibik, J., Ian Wilson, D., Gladden, L. F. & Axel Zeitler, J. (2015), ‘The disintegration process in microcrystalline cellulose based tablets, part 1: Influence of temperature, porosity and superdisintegrants’, *Journal of Pharmaceutical Sciences* **104**(10), 3440–3450.
- Yassin, S., Su, K., Lin, H., Gladden, L. F. & Zeitler, J. A. (2015), ‘Diffusion and swelling measurements in pharmaceutical powder compacts using terahertz pulsed imaging’, *Journal of Pharmaceutical Sciences* **104**(5), 1658–1667.
- Yardley, A. S., Bellinghausen, S., Milton, R. A., Litster, J. D. & Brown, S. F. (2021), ‘Efficient global sensitivity-based model calibration of a high-shear wet granulation process’, *Chemical Engineering Science* **238**, 116569.
- Yerro, A., Alonso, E. & Pinyol, N. (2015), ‘The material point method for unsaturated soils’, *Géotechnique* **65**(3), 201–217.
- Yu, Z. Q., Chow, P. S. & Tan, R. B. H. (2008), ‘Interpretation of focused beam reflectance measurement (fbrm) data via simulated crystallization’, *Organic Process Research & Development* **12**(4), 646–654.
- Zeitler, J. A., Taday, P. F., Newnham, D. A., Pepper, M., Gordon, K. C. & Rades, T. (2007), ‘Terahertz pulsed spectroscopy and imaging in the pharmaceutical setting - a review’, *Journal of Pharmacy and Pharmacology* **59**(2), 209–223.
- Zhang, D. Z., Zou, Q., VanderHeyden, W. B. & Ma, X. (2008), ‘Material point method applied to multiphase flows’, *Journal of Computational Physics* **227**(6), 3159–3173.
- Zhang, X.-Y., Trame, M., Lesko, L. & Schmidt, S. (2015), ‘Sobol sensitivity analysis: A tool to guide the development and evaluation of systems pharmacology models’, *CPT: Pharmacometrics & Systems Pharmacology* **4**(2), 69–79.

# Appendices

## Appendix A

# Saturation distribution in a granule

To obtain the saturation distribution inside a non-absorbing spherical granule, meaning equation (4.26) with conditions listed in Eq. (4.27), finite volume method (FVM) has been used. In this method, the sphere is divided evenly to certain number of points ( $N_p$ ) connected to each other through their boundaries:

$$r_{c,i} = \frac{i-1}{N_p-1}, \quad i = 1, 2, \dots, N_p \quad (\text{A.1})$$

and the lower boundary of  $i^{\text{th}}$  point would be:

$$r_{c,i-\frac{1}{2}} = \begin{cases} 0, & i = 1 \\ \frac{r_{c,i} + r_{c,i-1}}{2} = \frac{i-\frac{3}{2}}{N_p-1}, & i = 2, \dots, N_p \end{cases} \quad (\text{A.2})$$

in which the first boundary is the centre of the granule while the rest are the arithmetic average of neighbouring points. In FVM, the properties between each neighbouring boundary points, known as cell, is constant and the changes only happens at the boundaries. However, in here unlike finite difference method (FDM) where partial differential equations are discretised using finite difference formulas (Li et al. 2017) or finite element method (FEM) where the function is reduced to its weaker form and approximated using a series of piecewise functions (Davies 2011), the properties are volume-averaged over each cell (Versteeg & Malalasekera 2007) leading to an inherent mass conservation in the equations. If the same procedure would be done to equation (4.26), the result would be:

$$\int_{r_{c,i-\frac{1}{2}}}^{r_{c,i+\frac{1}{2}}} \frac{\partial \hat{S}}{\partial t_c} r_c^2 dr_c = \int_{r_{c,i-\frac{1}{2}}}^{r_{c,i+\frac{1}{2}}} \frac{\partial}{\partial r_c} \left( r_c^2 \frac{\partial \hat{S}^{n+1}}{\partial r_c} \right) r_c^2 dr_c, \quad i = 1, \dots, N_p - 1 \quad (\text{A.3})$$

Due to definition of volume-averaged property and lack of deformation the medium, the integral in the left side can be replaced by the time derivative piecewise saturation multiplied

by the volume of the cell. In other words:

$$\int_{r_{c,i-\frac{1}{2}}}^{r_{c,i+\frac{1}{2}}} \frac{\partial \hat{S}}{\partial t_c} r_c^2 dr_c = \frac{d}{dt} \left( \int_{r_{c,i-\frac{1}{2}}}^{r_{c,i+\frac{1}{2}}} S r_c^2 dr_c \right) = \frac{d}{dt} \left( S_i \int_{r_{c,i-\frac{1}{2}}}^{r_{c,i+\frac{1}{2}}} r_c^2 dr_c \right) = \frac{d \hat{S}_i}{dt_c} \int_{r_{c,i-\frac{1}{2}}}^{r_{c,i+\frac{1}{2}}} r_c^2 dr_c = \frac{d \hat{S}_i}{dt_c} \left\{ \frac{r_{c,i+\frac{1}{2}}^3 - r_{c,i-\frac{1}{2}}^3}{3} \right\} = r_{c,i+\frac{1}{2}}^2 \frac{\partial \hat{S}^{n+1}}{\partial r_c} \Big|_{r_{c,i+\frac{1}{2}}} - r_{c,i-\frac{1}{2}}^2 \frac{\partial \hat{S}^{n+1}}{\partial r_c} \Big|_{r_{c,i-\frac{1}{2}}}, \quad i = 1, \dots, N_p - 1 \quad (\text{A.4})$$

It is worth mentioning that at the centre of the granule ( $i = 1$ ) the last term at the right side of Eq. (A.4) is equal to zero due to the boundary condition at that location. The only term that needs to be redefined is the position based derivatives for each boundary at the right side of Eq. (A.4). If a centre-based formula such as the ones presented at (Versteeg & Malalasekera 2007) is utilized here, the derivatives can be approximated using the following Eq. (A.5):

$$\frac{\partial \hat{S}^{n+1}}{\partial r_c} \Big|_{r_{c,i+\frac{1}{2}}} \approx \frac{\hat{S}_{i+1}^{n+1} - \hat{S}_i^{n+1}}{r_{c,i+1} - r_{c,i}} \quad (\text{A.5})$$

By taking into considerations the boundary conditions at Eq. (4.27), the discretised form of Eq. (4.26) based on Eq. (A.4) and (A.5) would be:

$$\frac{d \hat{S}_i}{dt_c} = \frac{3}{r_{c,i+\frac{1}{2}}^3 - r_{c,i-\frac{1}{2}}^3} \times \begin{cases} r_{c,i+\frac{1}{2}}^2 \left( \frac{\hat{S}_{i+1}^{n+1} - \hat{S}_i^{n+1}}{r_{c,i+1} - r_{c,i}} \right), & i = 1 \\ \left( r_{c,i+\frac{1}{2}}^2 \frac{\hat{S}_{i+1}^{n+1} - \hat{S}_i^{n+1}}{r_{c,i+1} - r_{c,i}} - r_{c,i-\frac{1}{2}}^2 \frac{\hat{S}_i^{n+1} - \hat{S}_{i-1}^{n+1}}{r_{c,i} - r_{c,i-1}} \right), & i = 2, \dots, N_p - 2 \\ \left( r_{c,i+\frac{1}{2}}^2 \frac{1 - \hat{S}_i^{n+1}}{r_{c,i+1} - r_{c,i}} - r_{c,i-\frac{1}{2}}^2 \frac{\hat{S}_i^{n+1} - \hat{S}_{i-1}^{n+1}}{r_{c,i} - r_{c,i-1}} \right), & i = N_p - 1 \end{cases} \quad (\text{A.6})$$

The series of ODEs at Eq. (A.6) are highly nonlinear. One of the best ODE solvers in our disposal is backward differentiation formula (BDF) which are a family of implicit linear multistep ordinary differential equation (ODE) solvers designed for stiff differential equations (Shampine et al. 2003). One of the best method of BDF family at our disposal is a method called *ode15s* which has been already implemented in MATLAB (Shampine & Reichelt 1997). In order to increase the stability of the method, the Jacobian matrix has been obtained explicitly (Eq. (A.7)) and given to the ODE solver *ode15s*:

$$\mathbf{J} = \frac{3(n+1)}{r_{c,i+\frac{1}{2}}^3 - r_{c,i-\frac{1}{2}}^3} \times \begin{cases} -r_{c,i+\frac{1}{2}}^2 \frac{\hat{S}_i^n}{r_{c,i+1} - r_{c,i}}, & i = j = 1 \\ -r_{c,i+\frac{1}{2}}^2 \frac{\hat{S}_i^n}{r_{c,i+1} - r_{c,i}} - r_{c,i-\frac{1}{2}}^2 \frac{\hat{S}_i^n}{r_{c,i} - r_{c,i-1}}, & i = j = 2, \dots, N_p - 1 \\ r_{c,i-\frac{1}{2}}^2 \frac{\hat{S}_{i-1}^n}{r_{c,i} - r_{c,i-1}}, & i = j + 1 = 2, \dots, N_p - 1 \\ r_{c,i+\frac{1}{2}}^2 \frac{\hat{S}_{i+1}^n}{r_{c,i+1} - r_{c,i}}, & i = j - 1 = 1, \dots, N_p - 2 \\ 0, & \text{otherwise} \end{cases} \quad (\text{A.7})$$

Finally, the MATLAB code for the solution of Eq. (4.26) is:

```
function [r_c,t_c,eff_sat] = saturation(n,N_p)

% n      : the exponent, ref to eq. (4.24)
% N_p    : number of points, ref to eq. (A.1)

% r_c    : cell points, ref to eq. (A.1)
% r_cb   : cell boundary points, ref to eq. (A.2)
% t_c    : normalized time domain, ref to eq. (4.26)
% eff_sat: (local) effective saturation, ref to eq. (4.6)

if nargin<2
    N_p = 51;
    if nargin<1
        n = 1;
    end
end

r_c = linspace(0,1,N_p)';
r_cb = [0;(r_c(1:N_p-1) + r_c(2:N_p))/2];

t_c = 0:1e-4:0.8;

opts = odeset('RelTol',1e-10,'AbsTol',1e-12,'MaxStep',1e-3,
    'BDF','on','Jacobian',@(t,S)Jacob(t,S,n,r_c,r_cb,N_p));

[~,eff_sat] = ode15s(@(t,S)discretised_fun(t,S,n,r_c,r_cb,
    N_p),t_c,zeros(N_p-1,1),opts);

eff_sat(:,N_p) = 1;      % boundary condition at the surface
eff_sat(1,N_p) = 0;     % initial condition at the surface

end

% ODE function, ref to eq. (A.6)
function Deff_sat = discretised_fun(t,S,n,r_c,r_cb,N_p)

Deff_sat = zeros(N_p-1,1);

for i=1:N_p-1
    switch i
        case 1
            Deff_sat(i) = 3 * r_cb(i+1)^2 * (S(i+1)^(n+1) - S(i)
```

```

      ^ $(n+1)$ )/(r_c(i+1) - r_c(i))/(r_cb(i+1)^3 - r_cb(i)
      ^3);

    case N_p-1
      Deff_sat(i) = 3 * ( r_cb(i+1)^2 * (1 - S(i)^ $(n+1)$ )/
        (r_c(i+1) - r_c(i)) - r_cb(i)^2 * (S(i)^ $(n+1)$  - S(i-1)^ $(n+1)$ )/
        (r_c(i) - r_c(i-1)))/(r_cb(i+1)^3 - r_cb(i)^3);

    otherwise
      Deff_sat(i) = 3 * ( r_cb(i+1)^2 * (S(i+1)^ $(n+1)$  - S(i)^ $(n+1)$ )/
        (r_c(i+1) - r_c(i)) - r_cb(i)^2 * (S(i)^ $(n+1)$  - S(i-1)^ $(n+1)$ )/
        (r_c(i) - r_c(i-1)))/(r_cb(i+1)^3 - r_cb(i)^3);

    end
  end

end

% Jacobian matrix, ref to eq. (A.7)
function J = Jacob(t,S,n,r_c,r_cb,N_p)

J = zeros(N_p-1);

for i=1:N_p-1
  switch i
    case 1
      J(i,i) = -3 * (n+1) * r_cb(i+1)^2 * S(i)^ $n$ /(r_c(i+1) - r_c(i))/(r_cb(i+1)^3 - r_cb(i)^3);
      J(i,i+1) = 3 * (n+1) * r_cb(i+1)^2 * S(i+1)^ $n$ /(r_c(i+1) - r_c(i))/(r_cb(i+1)^3 - r_cb(i)^3);

    case N_p-1
      J(i,i-1) = 3 * (n+1) * r_cb(i)^2 * S(i-1)^ $n$ /(r_c(i) - r_c(i-1))/(r_cb(i+1)^3 - r_cb(i)^3);
      J(i,i) = -3 * (n+1) * (r_cb(i+1)^2 * S(i)^ $n$ /(r_c(i+1) - r_c(i)) + r_cb(i)^2 * S(i)^ $n$ /(r_c(i) - r_c(i-1)))/(r_cb(i+1)^3 - r_cb(i)^3);

    otherwise
      J(i,i-1) = 3 * (n+1) * r_cb(i)^2 * S(i-1)^ $n$ /(r_c(i) - r_c(i-1))/(r_cb(i+1)^3 - r_cb(i)^3);
      J(i,i) = -3 * (n+1) * (r_cb(i+1)^2 * S(i)^ $n$ /(r_c(i+1) - r_c(i)) + r_cb(i)^2 * S(i)^ $n$ /(r_c(i) - r_c(i-1)))/(r_cb(i+1)^3 - r_cb(i)^3);
  end
end

```

```

+1) - r_c(i)) + r_cb(i)^2 * S(i)^n/(r_c(i) - r_c(i
-1)))/(r_cb(i+1)^3 - r_cb(i)^3);
J(i,i+1) = 3 * (n+1) * r_cb(i+1)^2 * S(i+1)^n/(r_c(
i+1) - r_c(i))/(r_cb(i+1)^3 - r_cb(i)^3);

end
end
end

```

A typical effective saturation profile for  $n = 2$  has been shown in Figure A.1:

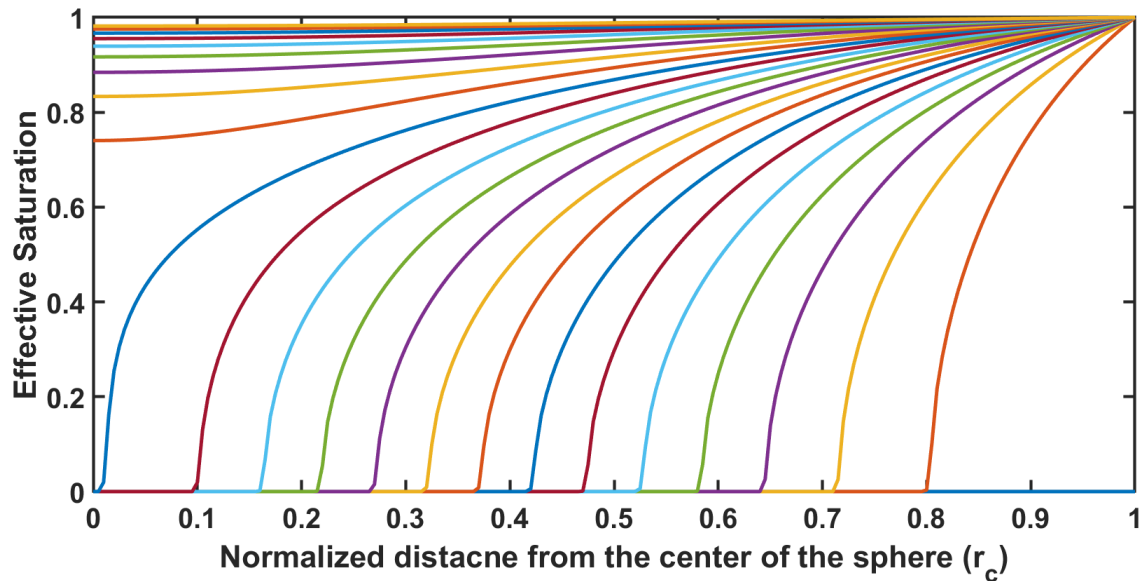


**Figure A.1:** The effective saturation profile versus  $r_c$  at different times ( $t_c$ ) for  $n = 2$  with  $\Delta t = 0.01$  and  $N_p = 201$ . The computation time was less than 3 s.

## Appendix B

# A PBM model for the hydrodynamic erosion

Physical erosion is a process by friction forces caused by velocity gradient around particles. In disintegration of granules, this process can be described as negative growth through population balance equation where due to friction a very small number of primary particles are detached from the surface of the granules. Therefore, in this process not only the granules shrink due to particles being taken away from their surface but the number of primary particles in the granule ( $n_p$ ) would decrease too. If it is assumed the decrease in rate of radius caused by erosion is  $G_{er}$ , based on the uniformity assumption in the structure of granules, the rate of primary particles separated from the surface of a granule with radius  $R$  would be:

$$G_{n_p}(R) = \frac{4\pi R^2 G_{er}(R)}{\frac{4\pi}{3} R^3} n_p(R) = \frac{3G_{er}(R)}{R} n_p(R) \quad (\text{B.1})$$

which means in a swelling driven disintegration involving erosion, Eq. (6.17) would not stand any more and should be replaced by the value at equation (B.1). Another function that needs to be changed is the growth rate of a granule which can be summarized in Eq. (B.2):

$$G_R(R) = G_R^{swe}(R) - G_{er}(R) \quad (\text{B.2})$$

in which  $G_R^{swe}(R)$  is the growth rate of radius caused by swelling, defined in Eq. (6.21) and  $G_R$  is the net growth rate. All the population balance equations in Chapter 6 that involve  $G_R$  should be redefined based the definition in Eq. (B.2). At the same time, because  $G_{n_p}$  is not zero any more due to involvement of erosion, equation (6.24) would change to equation (B.3):

$$\frac{\partial n_p(R, t)}{\partial t} = -G_R(R, t) \frac{\partial n_p(R, t)}{\partial R} - G_{n_p}(R) = -G_R(R, t) \frac{\partial n_p(R, t)}{\partial R} - \frac{3G_{er}(R)}{R} n_p(R) \quad (\text{B.3})$$

At the same time, the number of release primary particles would increase due to not only swelling but also erosion, releasing primary particles which means Eq. (6.34) would turn into Eq. (B.4):

$$\frac{\partial n_{f,i}(r, t)}{\partial t} = x_{n,i} \int_{R_{min}}^{\infty} \left( \psi(R, t) + \frac{3G_{er}(R)}{R} \right) n_g(R, t) n_p(R, t) f_i(R, r, t) dR \quad (\text{B.4})$$

and the rate of total number of released primary particles can be described by Eq. (B.5):

$$\frac{\partial}{\partial t} \left\{ \int_0^\infty n_{f,i}(r,t) \right\} = \int_{R_{min}}^\infty \left( \psi(R,t) + \frac{3G_{er}(R)}{R} \right) n_g(R,t) n_p(R,t) dR \quad (B.5)$$

Now, in the case of no swelling ( $\psi(R,t) = 0$ ) and linear relationship between erosion growth rate and radius of granule,  $G_{er}(R) = \frac{R}{\tau_s}$  where  $\tau_s$  is the designated as erosion time, Eq. (B.5) would be changed to the following form of Eq. (B.6):

$$\frac{\partial}{\partial t} \left\{ \int_0^\infty n_{f,i}(r,t) \right\} = \int_{R_{min}}^\infty \frac{3}{\tau_s} n_g(R,t) n_p(R,t) dR \quad (B.6)$$

At the same time, it is known that the total number of released primary particles would be the total number of primary particles leaving the granules. In other words:

$$\int_0^\infty n_{f,i}(r,t) = \int_{R_{min}}^\infty n_g(R,0) n_p(R,0) dR - \int_{R_{min}}^\infty n_g(R,t) n_p(R,t) dR \quad (B.7)$$

by putting Eq. (B.6) into Eq. (B.7), the final form of the equation can be reached:

$$-\frac{\partial}{\partial t} \left\{ \int_{R_{min}}^\infty n_g(R,t) n_p(R,t) dR \right\} = \frac{3}{\tau_s} \int_{R_{min}}^\infty n_g(R,t) n_p(R,t) dR \quad (B.8)$$

which the solution to the equation would be:

$$\int_{R_{min}}^\infty n_g(R,t) n_p(R,t) dR = \exp\left(-\frac{3t}{\tau_s}\right) \int_{R_{min}}^\infty n_g(R,0) n_p(R,0) dR \quad (B.9)$$

The total number of released primary particles at time t can be obtained from Eq. (B.10):

$$\int_0^\infty n_{f,i}(r,t) = \left\{ 1 - \exp\left(-\frac{3t}{\tau_s}\right) \right\} \int_{R_{min}}^\infty n_g(R,0) n_p(R,0) dR \quad (B.10)$$

and based on Eq. (6.38), the release profile would be:

$$X(t) = 1 - \exp\left(-\frac{3t}{\tau_s}\right) \quad (B.11)$$

If the erosion time is considerably larger than the experimental time ( $t \gg \tau_s$ ), then by using Taylor expansion series until second order, Eq. (B.10) would be reduced to Eq. (B.12):

$$\int_0^\infty n_{f,i}(r,t) \approx \left\{ \frac{3t}{\tau_s} - \frac{9t^2}{2\tau_s^2} \right\} \int_{R_{min}}^\infty n_g(R,0) n_p(R,0) dR \quad (B.12)$$

This equation has a striking resemblance to Eq. (7.1), which means the fitting parameters in Eq. (7.1) can be summarized in Eq. (B.13):

$$\begin{cases} a_1 = \frac{-9}{2\tau_s^2} \int_{R_{min}}^\infty n_g(R,0) n_p(R,0) dR \\ a_2 = \frac{3}{\tau_s} \int_{R_{min}}^\infty n_g(R,0) n_p(R,0) dR \end{cases} \quad (B.13)$$

and therefore, the erosion time can be obtained from the fitting parameters,  $a_1$  and  $a_2$ :

$$\tau_s = -\frac{3 a_2}{2 a_1} \quad (\text{B.14})$$

A list of erosion time has been given in Table 7.1 and 7.4 for the chosen formulations. All the erosion data for MCC granules and the estimation versus SSG loading and binder concentration has been shown in Figure B.1.

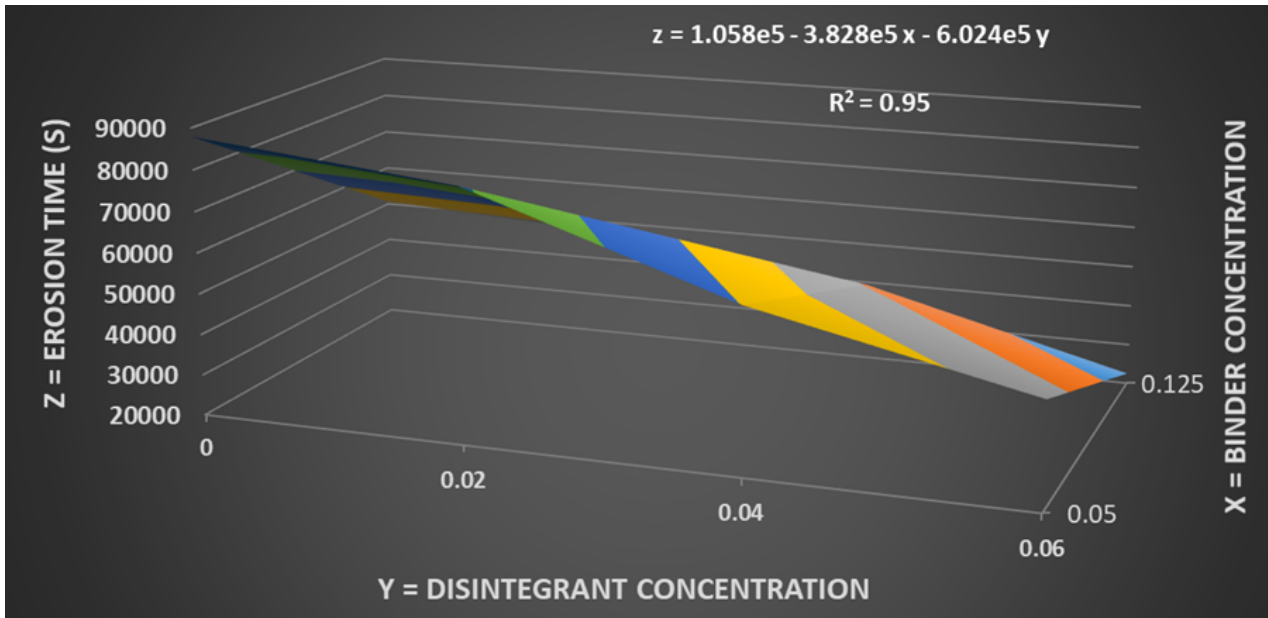


**Figure B.1:** The erosion time obtained from FBRM data for each MCC granules made with different SSG loading and binder concentration and its estimation